The expression and role of the immune checkpoint regulator Programmed Cell Death Protein 1-Ligand 1 in the tumor-stroma interplay of pancreatic ductal adenocarcinoma

Dissertation

Zur Erlangung des Doktorgrades

der Mathematisch-Naturwissenschaftlichen Fakultät

der Christian-Albrechts Universität zu Kiel

vorgelegt von

Tina Daunke

Kiel, 2023

First Reviewer: Prof. Dr. rer. nat. Susanne Sebens

Second Reviewer: Prof. Dr. rer. nat. Regina Scherließ

Date of disputation: 25.10.2023

Preface

Parts of this dissertation have been already published. The respective manuscripts are attached in the appendix.

Group Young Researchers in Inflammatory Carcinogenesis *, Wandmacher AM, Mehdorn A-S, Sebens S. The Heterogeneity of the Tumor Microenvironment as Essential Determinant of Development, Progression and Therapy Response of Pancreatic Cancer. *Cancers (Basel)*. 2021;13(19):4932. DOI:10.3390/cancers13194932

* Group members (in alphabetical order): Aldag L, Beckinger S, **Daunke T**, Philipp LM, Surrow A, Yesilyurt UU. These authors have contributed equally to this work and share first authorship.

Daunke T† , Beckinger S†, Rahn S, Krüger S, Heckl S, Schäfer H, Wesch D, Pilarsky C, Eckstein M, Hartmann A, Röcken C, Wandmacher AM, Sebens S. Expression and role of the immune checkpoint regulator PD-L1 in the tumor-stroma interplay of pancreatic ductal adenocarcinoma. *Front Immunol*. 2023; 14(6):1-19. DOI:10.3389/fimmu.2023.1157397

† These authors have contributed equally to this work and share first authorship.

Zusammenfassung

Das duktale Pankreasadenokarzinom (PDAC) ist die vierthäufigste krebsbedingte Todesursache in den westlichen Ländern und wird voraussichtlich bis 2030 zur zweithäufigsten krebsbedingten Todesursache aufsteigen. Diese hohe Sterblichkeitsrate hängt mit dem fortgeschrittenem Krankheitsstadium zum Diagnosezeitpunkt zusammen, da es keine spezifischen Symptome gibt und Tumormarker nur eine geringe Spezifität aufweisen. Zum Zeitpunkt der Diagnose haben die meisten Patienten daher bereits eine lokal fortgeschrittene Erkrankung oder Metastasen, insbesondere in der Leber, gebildet. Da die chirurgische Resektion die einzige kurative Behandlung bei lokal begrenzten PDAC-Tumoren darstellt, werden nur palliative chemotherapeutische Behandlungen als Standardtherapie für fortgeschrittene und metastasierte Erkrankungen eingesetzt. Daher werden dringend effizientere Behandlungsmöglichkeiten benötigt. Immun-Checkpoint-Inhibitoren (ICI), z. B. gegen den programmierte Zelltodprotein 1-Ligand 1 (PD-L1) oder seinen Rezeptor PD-1, haben die Therapie vieler Krebsarten deutlich verbessert, scheiterten aber bisher beim PDAC. Makrophagen sind eine der am häufigsten vorkommenden Immunzellpopulationen in der Tumormikroumgebung (TME) des PDAC, die je nach ihrem Phänotyp die Tumorprogression entweder fördern oder aufhalten können. Um das Versagen der Behandlung mit PD-L1/PD-1-Inhibitoren beim PDAC besser zu verstehen, wurde in dieser Arbeit die PD-L1-Expression im Kontext eines dynamischen TME beim PDAC und insbesondere die Auswirkungen von Makrophagen untersucht.

Immunhistochemische Analysen ergaben, dass PD-L1 hauptsächlich von Stromazellen, einschließlich Makrophagen, und nicht von PDAC-Zellen in primären PDAC-Geweben und zugehörigen Lebermetastasen exprimiert wird. Vor allem an den Invasionsfronten der Tumorläsionen zwischen CD8+ T-Zellen und Tumorzellen waren häufig Makrophagen in großer Zahl und eine starke PD-L1-Färbung zu finden. In 2D Experimenten konnte gezeigt werden, dass CD8+ T-Zellen die phänotypischen Unterschiede zwischen *in vitro* polarisierten M1- und M2-ähnlichen Makrophagen verringern, die PD-L1 Expression auf Makrophagen jedoch steigern. Beide Makrophagenpopulationen widerum führten trotz gesteigerter PD-L1 Expression zur Erhöhung des Aktivierungsstatus der CD8+ T-Zellen, was sich aber nicht in einem Rückgang der duktalen pankreatischen Epithelzellen Viabilität widerspiegelte. Um zu untersuchen, ob PD-L1 exprimierende Makrophagen das Ansprechen von PDAC-Zellen auf die Behandlung mit PD-L1/PD-1-Inhibitoren beeinflussen, wurde ein 3D Sphäroidmodell mit zwei verschiedenen PDAC-Zelllinien und unterschiedlichen Verhältnissen von *in vitro* differenzierten primären M1- oder M2-ähnlichen Makrophagen etabliert. In Übereinstimmung mit den *in situ* Ergebnissen wurde eine hohe PD-L1-Expression in Makrophagen und nicht in PDAC-Zellen beobachtet, die durch die Anwesenheit von PDAC-Zellen noch verstärkt wurde. Der Effektor-Phänotyp der co-kultivierten CD8+ T-Zellen, der sich in der Expression von Aktivierungsmarkern und der Freisetzung von

Effektormolekülen zeigt, wurde durch PDAC-Makrophagen-Sphäroide eher verstärkt, insbesondere durch M1-ähnliche Makrophagen im Vergleich zu Sphäroiden in Monokultur. Dies war jedoch nicht mit einem erhöhten PDAC-Zelltod verbunden. Die ICI-Behandlung mit Durvalumab oder Pembrolizumab allein oder in Kombination mit Gemcitabin beeinflusste den Effektor-Phänotyp der CD8+ T-Zellen und das Absterben von PDAC-Zellen kaum. Trotz der starken PD-L1-Expression in Makrophagen führte die ICI-Behandlung also nicht zu einer verstärkten Aktivierung und einem zytotoxischen Phänotyp von CD8+ T-Zellen. Insgesamt liefern die Ergebnisse dieser Arbeit neue Erkenntnisse über das Zusammenspiel von PDAC-Zellen und Makrophagen sowie deren Einfluss auf PD-L1 und die Immunabwehr des PDAC und bietet eine Erklärung für die schwache therapeutische Wirkung der ICI-Behandlung beim PDAC.

Summary

Pancreatic ductal adenocarcinoma (PDAC) is the 4th leading cause of cancer-related death in Western countries and is predicted to increase to the 2nd most common cause of cancer-related death by 2030. This high mortality is associated with the late stage of disease at diagnosis due to the lack of specific symptoms and poor specificity of tumor markers. When diagnosed, most of the patients already exhibit a locally advanced disease or formed metastases, especially in the liver. As surgical resection is the only curative therapy for locally restricted PDAC tumors, only palliative chemotherapeutic treatments are the standard-of-care therapy for advanced and metastasized disease stages. Thus, more efficient treatment options are urgently needed. Immune checkpoint inhibitors (ICI), e.g., targeting Programmed Cell Death Protein 1-Ligand 1 (PD-L1) or its receptor PD-1, have markedly improved the therapy of many cancers but so far failed in PDAC. Macrophages represent one of the most abundant immune cell populations within the tumor microenvironment (TME) of PDAC being able to either support or restrain tumor progression depending on their phenotype. To better understand the treatment failure of PD-L1/PD-1 inhibitors in PDAC, this thesis aimed to examine PD-L1 expression in the context of a dynamic TME in PDAC with a particular focus on the impact of macrophages.

Immunohistochemical analyses revealed that PD-L1 is mainly expressed by stroma cells, including macrophages and not PDAC cells in primary PDAC tissues and corresponding liver metastases. Notably, a high local abundance of macrophages and strong PD-L1 staining were commonly found at invasion fronts of tumoral lesions between CD8+ T cells and tumor cells. In 2D experiments, the phenotypic differences between *in vitro* polarized M1-like and M2-like were abolished, but the PD-L1 expression on macrophages was increased by CD8+ T cells co-culture. Despite the enhanced PD-L1 expression on macrophages, the activation stage of CD8+ T cells was enhanced by macrophage attendance which, however, was not reflected in decreased pancreatic ductal epithelial cell viability. In order to investigate whether PD-L1-expressing macrophages impact the response of PDAC cells to treatment with PD-L1/PD-1 inhibitors, a 3D spheroid model comprising two different PDAC cell lines and different ratios of *in vitro* differentiated primary M1- or M2-like macrophages was established. In line with the *in situ* findings, high PD-L1 expression was observed in macrophages rather than PDAC cells, which was further increased by the presence of PDAC cells. The effector phenotype of co-cultured CD8+ T cells exemplified by the expression of activation markers and release of effector molecules was rather enhanced by PDAC macrophage spheroids, particularly with M1-like macrophages compared to mono-culture spheroids. However, this was not associated with enhanced PDAC cell death. ICI treatment with either Durvalumab or Pembrolizumab alone or in combination with Gemcitabine hardly affected the effector phenotype of CD8+ T cells along with PDAC cell death. Thus, despite strong PD-L1 expression

in macrophages, ICI treatment did not result in an enhanced activation and cytotoxic phenotype of CD8+ T cells. Overall, the results of this thesis revealed novel insights into the interplay of PDAC cells and macrophages and its impact on PD-L1 and immune evasion of PDAC thereby explaining the poor therapeutic effects of ICI treatment in PDAC.

Abbreviations

µM	Mikromolar
2D	Two-dimensional
3D	Three-dimensional
AIB1/NCOA3	Amplified in breast cancer 1/nuclear receptor coactivator 3
APCs	Antigen-presenting cells
ARG1	Arginase 1
ATCC	American type culture collection
ATRA	All-*trans* retinoic acid
BPE	Bovine pituitary extract
BRCA	Breast cancer susceptibility gene
BSA	Bovine serum albumin
CAF(s)	Cancer-associated fibroblast(s)
CAR	Chimeric antigen receptor
CC	Cell culture
ccK18	Caspase-cleaved Keratin 18
CCL	C-C motif ligand
CD	Cluster of differentiation
CDA	Cytidine deaminase
CDKN2A	Cyclin-dependent kinase inhibitor 2A
cDNA	Complementary DNA
CH	Swiss
CHEK2	Checkpoint kinase 2
CO_2	Carbon dioxide
CRC	Colorectal cancer
CTC	Circulating tumor cell
CTLA-4	Cytotoxic T lymphocyte-associated antigen-4
CTLs	Cytotoxic T lymphocytes
CXCL	C-X-C motif ligand
DC(s)	Dendritic cell(s)
ddH_2O	Aqua distilled
DE	Germany
DMEM	Dulbecco´s Modified Eagle Medium

DMSO	Dimethylsulfoxide
DN	Double negative
ECM	Extracellular matrix
EDTA	Ethylenediaminetetraacetate
EGF	Epidermal Growth Factor
EGFR	Epidermal Growth Factor Receptor
ELC	Epstein–Barr virus-induced molecule-1 ligand chemokine
EMT	Epithelial-Mesenchymal Transition
FC	Flow cytometry
FCS	Fetal calf serum
FDA	Food and Drug Administration
FGF	Fibroblast Growth Factor
FoV	Fields of View
FOXP3	Forkhead-box-protein P3
FRA	France
FRβ	Folate receptor β
FSC	Forward scatter
g	Gram
GAPDH	Glycerinaldehyd-3-phosphate-dehydrogenase
GM-CSF	Granulocyte-macrophage colony stimulating factor
h	Hour(s)
HGF	Hepatocyte Growth Factor
HIF1	Hypoxia-inducible factor 1
HLA	Human leucocyte antigen
HMFs	Hepatic myofibroblasts
HSCs	Hepatic stellate cells
ICAM-1	Integrin ligands intercellular adhesion molecule 1
ICI(s)	Immune checkpoint inhibitor(s)
ICOS	Inducible T cell co-stimulator
IDO	Indoleamine 2,3-dioxygenase 1
IF	Immunofluorescence
IFN	Interferon
IgV	Variable immunoglobulin region

IHC	Immunohistochemistry
IL	Interleukine
iNOS	Inducible nitric oxide synthase
IPMN	Intraductal papillary mucinous neoplasms
IS	Immunological synapse
ITIM	Immunoreceptor tyrosine-based inhibitory motif
JPN	Japan
$KHCO_3$	Potassium hydrogen carbonate
KRAS	Kirsten rat sarcoma
l	liter
L1CAM	L1 cell adhesion molecule
LAG-3	Lymphocyte-activation gene 3
L-Gln	L-Glutamine
LN(s)	Lymph node(s)
LPS	Lipopolysaccharides
LRSC	Leukoreduction system chambers
MACS	Magnetic-activated cell sorting
MAPK	Mitogen-activated protein kinase
M-CSF	Macrophage colony stimulating factor
MDCS(s)	Myeloid-derived suppressor cell(s)
MHC	Major histocompatibility complex
min	Minute(s)
ml	Milliliter
mM	Millimolar
mm	Millimeter
MMp	Matrix metalloproteinase
MCN	Mucinous cystic neoplasms
mTOR	Mammalian target of rapamycin
ng	Nanogram
NH_4Cl	Ammonium chloride
NK	Natural killer
NSCLC	Non-small cell lung cancer
PALB2	Partner and localizer of BRCA2

PanIN(s)	Pancreatic intraepithelial neoplasia(s)
PBMCs	Peripheral blood mononuclear cells
PBS	Phosphate-buffered saline
PD-1	Programmed Cell Death Protein 1
PDAC	Pancreatic ductal adenocacinoma
PDEC(s)	Pancreatic ductal epithelial cell(s)
PD-L1	Programmed Cell Death Protein 1-Ligand 1
Pen/Strep	Penicillin/Streptomycin
PFA	Paraformaldehyde
PGE	Prostaglandin E
PI	Propidium iodide
PI3K	Phosphatidylinositol 3-kinase
PSCs	Pancreatic stellate cells
RASGRP1	RAS guanyl-releasing protein 1
RNA	Ribonucleic acid
RNS	Reactive nitrogen species
ROS	Reactive oxygen species
RPMI	Roswell Park Memorial Institute
RT	Room temperature
SDF-1	Stromal Cell-derived Factor-1
sEVs	Small extracellular vesicles
SHP	Src homology region 2 domain-containing phosphatase
SLC	Secondary lymphoid organ chemokine
SMAD	Suppressor of mothers against decapentaplegic
SMAD4	Mothers against decapentaplegic homolog 4
SSC	Side scatter
TAM(s)	Tumor-associated macrophage(s)
TCR(s)	T cell receptor(s)
TGFβ	Transforming Growth Factor beta
TH	T helper
TIGIT	T cell immunoreceptor with Ig and ITIM domains
TILs	Tumor-infiltrating lymphocytes
TIM-3	T-cell immunoglobulin and mucin-domain 3

TMB	Tumor mutational burden
TME	Tumor microenvironment
TNF	Tumor Necrosis Factor
Treg(s)	Regulatory T cell(s)
Tris	Tris(hydroxymethyl)aminomethane
TSC	Tuberous sclerosis complex
UK	United Kingdom
UKSH	University Hospital Schleswig-Holstein
ULA	Ultra-low attachment
USA	United States of America
v/v	Volume per volume
VCAM-1	Vascular Cell Adhesion molecule 1
VEGF	Vascular Endothelial Growth Factor
VISTA	V-domain Ig suppressor of T cell activation
w/v	Weight per volume
Zeb	Zinc finger E-box-binding homeobox
αSMA	Alpha-smooth muscle actin

Table of contents

1. Introduction

1.1. Epidemiology and risk factors

In Western countries, pancreatic ductal adenocarcinoma (PDAC) is the 4th leading cause of cancer-related deaths, with a low 5-year survival rate of 10 % [1]. The incidences significantly differ between countries. Europe and North America show the highest age-standardized incidence, whereas Africa and South Central Asia have the lowest incidence (**Figure 1**) [2].

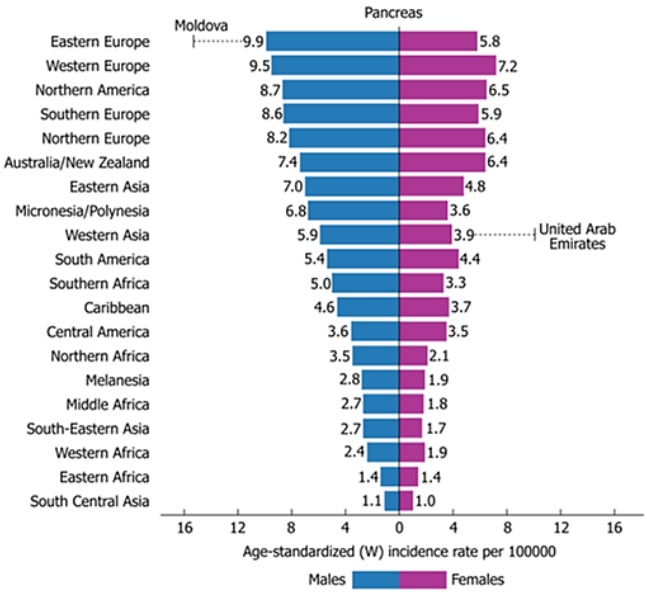

Figure 1: Diagram of pancreatic cancer incidence in both sexes worldwide [2].

The incidence of PDAC considerably rises in the Western world and is predicted to increase from the 4th to the 2nd most common cause of cancer-related deaths by 2030 in the United States [2]. The high mortality is associated with the late stage of the disease at diagnosis due to the lack of specific symptoms and poor specificity of tumor markers. Further, it often metastasizes to distant organs, including the liver (76-80 % of patients), the peritoneum (48 %), or the lung (45 %) [3]. To date, the only curative treatment option is resection, but most patients are not eligible due to the advanced disease stage at diagnosis or comorbidities. Even if the primary tumor has been successfully resected, the 5-year survival rate of these patients is only 27 % [2].

In Germany, around 19,000 new cases of PDAC were detected in 2018 (age-standardized incidence men vs. women: 15.1 % vs. 10.8 % per 100,000 persons). The median age at diagnosis is 76 years in men and 72 years in women. In Germany, PDAC is also the 4th most common cause of cancer-related deaths among both men (7.4 % of cancer-related deaths) and women (8.7 % of cancer-related deaths) [4].

For PDAC, several risk factors are known and can be divided into non-modifiable and modifiable risk factors [2]. A non-modifiable risk is the patients age, as it is known that over 90 % of cases at diagnosis are at least 55 years old and peak in the 7th and 8th decade [5,6]. Further, patients with an early stage of the disease are 2.3 years younger than those with advanced stage cancer, indicating that the cancer progression needs 1-2 years to develop from early to late stage of disease [7]. Other non-modifiable risk factors are the sex and ethnicity of patients. Men become 30 % more commonly diseased than women, and African-Americans and Caucasian people show higher incidences than Pacific Islanders and Asian-Americans [5]. Moreover, the blood group can play a crucial role in developing PDAC as patients with blood group 0 have a significantly lower risk than patients with blood group A, followed by AB and B [8]. Family history, genetic susceptibility, infections, and diabetes mellitus also belong to the group of non-modified risk factors [9,10]. Modifiable risk factors are smoking and alcohol abuse. Smoking shows a dose-responsive significantly increased risk for developing pancreatic cancer, and consumption of > 30 g alcohol per day demonstrated an increased risk of pancreatic cancer [2]. Likewise, obesity and chronic pancreatitis are associated with developing PDAC [2,9].

1.2. Pathology and Pathogenesis

PDAC is the most abundant disease of pancreatic cancer (>85 % of cancer cases) [11]. It is characterized by its ductal, glandular morphology and commonly originates from the head of the pancreas and infiltrates into surrounding tissue (e.g., lymph nodes, spleen, and peritoneal cavity) [11,12]. Tumors often show a variety of differentiation ranging from well-differentiated to poorly differentiated adenocarcinomas within one tumor and have significant intra- and inter-tumoral histological heterogeneity [13]. In PDAC, several aggressive histological patterns were observed, such as tumor invasion into peripancreatic soft tissue, large vessels, and adjacent structures, lymphovascular invasion, involvement of resection margins, and lymph node metastasis. Patients with these aggressive histological features are associated with an enhanced risk of post-operative tumor occurrence (distant metastases) and poor survival [13]. The disease arises through step-wise genetic mutations from normal mucosa to specific precursor lesions [2,14]. The three best-characterized precursor lesions include intraductal papillary mucinous neoplasms (IPMN), mucinous cystic neoplasms (MCN), and the best-studied lesion, pancreatic intraepithelial neoplasia (PanIN) [2,12,14]. PanINs often occur in the smaller pancreatic ducts (<0.5 cm) and are non-invasive lesions. They show divergent morphological alterations compared to normal ducts and can be graded into three stages [2,11,12]. The first-grade lesions comprise mucinous tall columnar epithelial cells with basally oriented nuclei [11] and can be divided into PanIN 1A, which forms flat duct architecture, and PanIN 1B, which are characterized by papillary

structure [15]. Lesions with moderate atypical structural alterations are characterized as PanIN grade 2, while PanIN grade 3 is recognized by wide nuclear atypia (Figure 2). During progression of grades 2 and 3, cells also express more supranuclear mucin and show papillary projections [11].

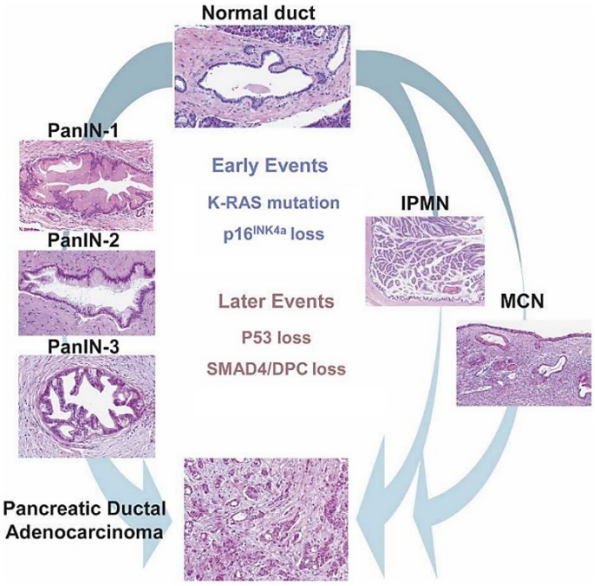

Figure 2: Pancreatic precursor lesions and their genetic events involved in progression of PDAC. Histological images of the precursor lesions IPMN and MCN, as well as the three PanIN lesions (grade 1 – 3), reflecting the progressing atypia which can lead to a PDAC. The genetic mutations are divided into early and late events and mostly occur in PanIN and, to a lesser extent, in IPMN and MCN. The figure is modified regarding reference [12].

PDAC is described by several inherited and recurring somatic mutations [13]. Main drivers for PanIN lesions and the formation of PDAC are four different genes: the oncogenic *Kirsten rat sarcoma* (*KRAS)* virus oncogene homolog gene mutation, acting as one of the first mutations, and mutations of the tumor suppressor genes *TP53*, the *cyclin-dependent kinase inhibitor 2A (CDKN2A)* and *mothers against decapentaplegic homolog 4 (SMAD4)* [12,13,16]. The *KRAS* gene is mutated mainly in PDAC and results in missense mutations in the codons 12 or 13. Besides G12V and G12R, the most common *KRAS* mutations is G12D which leads to a replacement of Gylcin by other amino acids resulting in the activation of *KRAS* [12,17]. Activating KRAS mutations cause enhanced cell proliferation, differentiation, and increased survival and migration of tumor cells. Further, KRAS mutations are found in over 90 % of low-grade PanIN and PDAC cases [16]. The mutated KRAS gene induces the stress response in cells resulting in oncogene-induced senescence and loss of the p16ink4a protein, encoded by the *CDKN2A* gene. When a loss of *CDKN2A* is also present, the blocking of entry into the cell cycle's S-phase is also lost. Furthermore, mutation of *TP53* impacts the ability to express genes responsible for cell cycle arrest or apoptosis after DNA damage or cellular stress. The final mutation to complete PDAC development is the loss of *SMAD4*, which results in abnormal Transforming Growth Factor beta (TGFβ)-dependent effects regarding proliferation. Additionally, the loss of *SMAD4* is associated with poorer

survival of PDAC patients [16]. Notably, higher grades of PanIN also obtain an increasing number of genetic alterations [12,14]. Further, less common oncogene mutations were identified in PDAC, such as *CMYC*, *MYB*, a*mplified in breast cancer 1/nuclear receptor coactivator 3 (AIB1/NCOA3)*, *Epidermal Growth Factor Receptor (EGFR)*, or *GATA6*, as well as recurrent chromosomal amplifications. Genes responsible for DNA damage repair were also found to be impaired in PDAC patients, e.g., *breast cancer susceptibility genes 1 and 2 (BRCA1 and BRCA2), ATM, partner and localizer of BRCA2 (PALB2), checkpoint kinase 2 (CHEK2), RAD51C, and RAD51D* [13].

Based on genetic and transcriptomic characterization, Moffitt *et al.* identified two subtypes of PDAC cells: the basal-like and classical subtypes. Here, two different stromal subtypes were also identified (normal and activated). The basal-like subtype or activated stroma showed a worse prognosis compared to the other subtypes [18]. Since a characteristic of PDAC is the presence of a dense stroma containing fibroblasts and immune cells [12,13], the impact of the stromal compartment is described in more detail in section 1.3.

1.3. Tumor-stroma in PDAC

Tumors are not composed of tumor cells alone, they instead are a complex ecosystem which comprises non-cellular factors and many non-neoplastic cell types, such as blood cells, fat cells, endothelial cells, immune cells, and cancer-associated fibroblasts (CAFs) [19]. In the physiological context, the stroma has a tumor-suppressing role, regulating the proliferation, motility, and infiltration of differentiated epithelial cells into the extracellular matrix [20,21]. These functions are regulated through the secretion of cytokines and growth factors [22].

PDAC is characterized by an extensive desmoplastic stroma which is mostly hypoxic and immunosuppressive, comprising among others CAFs, tumor-infiltrating B, T, and natural killer (NK) lymphocytes as well as myeloid cells like monocytes, macrophages, dendritic cells (DCs), and myeloid-derived suppressor cells (MDSCs) [13,16,23,24] (Figure 3). CAFs, as one of the most abundant stroma cell populations, can produce several soluble factors, including TGFβ, interleukins (IL), Stromal Cell-derived Factor-1 (SDF-1), Fibroblast Growth Factor (FGF), Hepatocyte Growth Factor (HGF), and Galectin-1, thereby regulating the pathogenesis and invasiveness of PDAC [13,16,24]. B lymphocytes, especially regulatory B cells, are a newly defined and, therefore, not well-characterized cell population in the context of the tumor microenvironment (TME). They can regulate disease development through the secretion of IL-10, IL-35, and IL-21, and thus, suppress the immune response against tumors, thereby contributing to carcinogenesis [16].

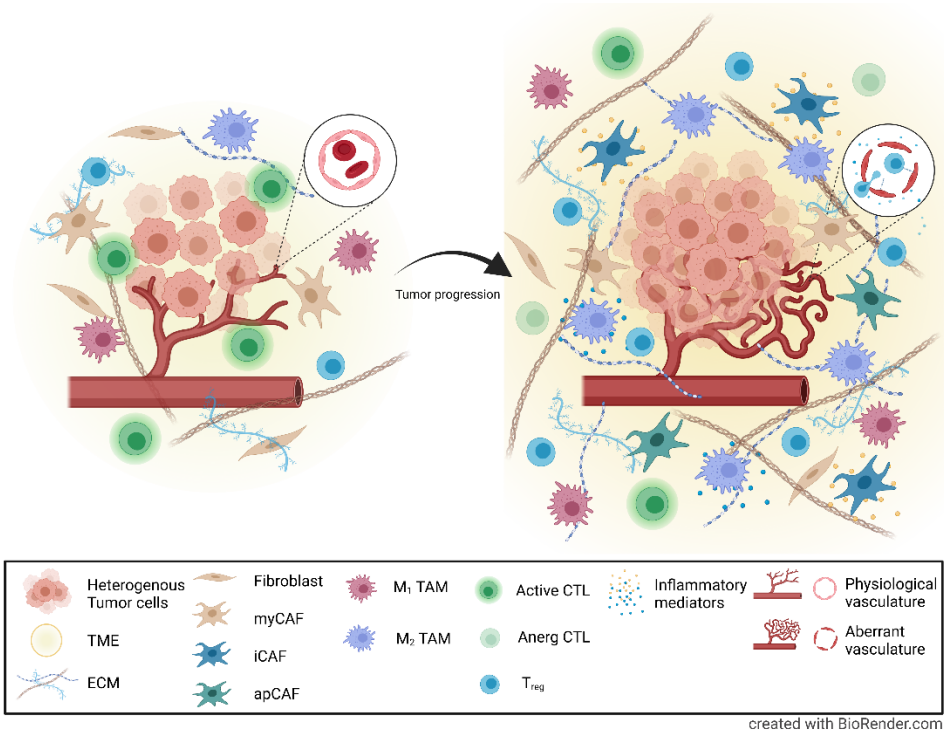

Figure 3: The tumor microenvironment TME of PDAC is characterized by a high tumor and stroma heterogeneity. The TME undergoes fundamental alterations, including the activation of fibroblasts and transdifferentiation into CAFs, alteration of ECM molecules, enrichment of immunosuppressive cell populations (tumor-associated macrophages (TAMs) and regulatory T cells), elevation of inflammatory mediators, and formation of new and modified blood vessels. The figure is revised regarding reference [24].

The dense acellular extracellular matrix (ECM) in PDAC acts as a physical barrier limiting the delivery and diffusion of oxygen, nutrients, and therapeutics into PDAC [25]. The ECM predominantly consists of collagens, fibronectin, and laminin produced by CAFs, developing a physically hard tumor with enhanced interstitial fluid pressure [24–26]. Different T cell populations can be found in the TME of primary PDAC. With their different effector phenotypes, T cells essentially affect the process of tumor and metastases formation in several ways. Increased numbers of immunosuppressive T cells can be detected during PDAC progression, whereas tumor-directed immune functions are inhibited and/or even lost. Accordingly, the attendance of CD8+ T cells, which are key players of anti-tumor immunity, is associated with prolonged overall survival of PDAC patients [24]. NK cells, identified as unspecific killer cells, can recognize and kill tumor and virus-infected cells without prior antigen stimulation. However, recent data indicate that NK cells can be polarized towards a tumor-promoting phenotype due to soluble factors and extracellular vesicles in the PDAC TME [27]. DCs are also found in the TME of PDAC and are associated with better survival of PDAC patients, however, most human specimens show low numbers of DCs, which are mostly located at the tumor margins and not inside the tumor [24]. MDSCs, as immunosuppressive cells, suppress CD4+ T cell and CD8+ T cell function through direct cell-cell contact with lymphocytes [24,27]. Monocytes and macrophages represent the most dominant immune

cell population and acquire different pro- or anti-tumor phenotypes dependent on environmental factors [16,24].

In the following sections, tumor associated macrophages (TAMs) (section 1.4) and CD8+ T cells (section 1.5) will be introduced in more detail, as both cell populations are found in PDAC tissues and were in the focus of this thesis.

1.4. Tumor-associated macrophages (TAMs)

1.4.1. Origin and polarization

Macrophages, as one of the innate immune cell populations, play a crucial role in first-line defense against pathogens, including effects of direct tumor cell killing through the release of cytolytic enzymes, secretion of cytotoxic factors, antibody-dependent cell-mediated cytotoxicity via Fc receptors and presentation of tumor antigens to activate T cell immune response [28,29]. Tissue-resident macrophages predominantly originate from embryonic precursor cells, which seed tissues during the prenatal and perinatal periods. This develops in at least two waves, including macrophage precursor cells from the fetal yolk sac or fetal liver progenitor cells [30]. These precursor cells settle distant tissues and emerge as locally proliferating, self-maintained tissue-resident macrophages that can endure into adulthood [31–34]. In some tissues, these macrophages are rapidly displaced by monocytes derived from hematopoietic stem cells. In the pancreas, the origin of macrophages is a mixture of embryonic precursor and hematopoietic stem cells [30]. In contrast to tissue-resident macrophages, infiltrated macrophages differentiate from monocytes to macrophages derived from bone marrow-derived myeloid progenitor cells [35,36]. Macrophages are able to switch their functional and phenotypic properties due to signals in the surrounding microenvironment during both physiological and pathological conditions [37]. Following a simplified model, monocytes can differentiate into classically activated, pro-inflammatory M1- or alternatively activated, anti-inflammatory M2-macrophages [38–40]. Monocytes activated by Interferon γ (IFNγ) or lipopolysaccharides (LPS) evolve into M1-type macrophages, while IL-4 leads to polarization into M2-like macrophages [41,42]. Additionally, the M2 subtype can be further divided into M2a (after exposure to IL-4 or IL-13), M2b after exposure to immune complexes in combination with LPS or IL-1β, or M2c macrophages after stimulation with IL-10, glucocorticoids or TGFβ [43,44]. The polarization of different macrophage types is also accompanied by specific alterations in cell morphology and phenotype [44–46]. Thus, the surrounding TME with its changing composition (e.g., oxygen level, type, and amount of other stromal or tumor cells) affects the phenotype and effector function of macrophages and promotes a switch of one macrophage type to

another. Detecting surface markers specific for M1- or M2-like macrophages are used to characterize macrophage infiltration in many diseases, e.g., cancer [47].

Table 1: Markers and cytokine secretion of M1- and M2-like macrophages. Characterization of macrophage subtypes by their function, expression of surface markers, and secretion of cytokines, chemokines, and other factors. Adapted from [29,47,48].

Macrophage subtype	Function	Human Markers	Secretion of
M1-like	Pro-inflammatory, Immunosupportive	CD80 CD86 HLA-DR iNOS CD64	IL1 TNFα IFNγ RNS ROS
M2-like	Anti-inflammatory, Immunosuppressive	CD206 CD204 CD163 ARG1 FRβ	IL-4 IL-10 TGFβ MMps VEGF CCL2

Besides the mentioned polarization stimuli, Granulocyte-Macrophage Colony Stimulating Factor (GM-CSF) and Macrophage Colony Stimulating Factor (M-CSF) are described to polarize *in vitro* cultured monocytes towards M1- and M2-like phenotype, respectively [47,49]. Although most of the human markers on *in vitro* polarized macrophages are similar for polarization with IFNγ or GM-CSF (M1) and IL-4, IL-10, and M-CSF (M2), respectively, the surface levels of macrophages polarized with GM-CSF in comparison with IFNγ showed differences in CD206 expression as GM-CSF seems to induce CD206 [47]. This again highlights the complexity of macrophage polarization in response to the surrounding microenvironment.

Hence, the plasticity of macrophages might have essential therapeutic and disease-driving implications [37], therefore playing a major role in this study.

1.4.2. TAMs in PDAC

In the tumor-stroma, macrophages are called TAMs and are one of the most abundant immune cell populations in the TME of PDAC. The most common source of tissue-resident macrophages in the pancreas are monocytes from the blood circulation derived from the bone marrow [50,51]. Most pancreas-resident macrophages are in a quiescent state, suggesting that these macrophages could persist in the pancreas over a long term. TAMs predominantly originate from tissue-resident

macrophages or monocytes of blood circulation, which infiltrate into injured tissue. Similarly, macrophages can be also recruited from blood monocytes [50,52]. Even at an early stage of pancreatic lesions, macrophages, as one of the first immune cell populations, are recruited and accumulate in the tissue [53]. The number of macrophages increases during disease progression [52,54].

Although the phenotype and frequency of macrophages are highly dynamic, TAMs in PDAC mostly exhibit M2-like characteristics as CD163+ macrophages were predominantly detected in primary PDAC [55–59]. The M2-phenotype is associated with pro-tumoral effects, including tumorigenesis, immunosuppression, angiogenesis, metastasis acceleration, and chemotherapeutic resistance [29,60–62]. Accordingly, patients with a high M2-like macrophage abundance show a poor prognosis and decreased survival [58,59,63]. Bidirectional signaling between macrophages and epithelial cells expressing mutant *KRAS* showed to promote a pro-tumorigenic phenotype of macrophages which intensified cancerous phenotypes of the epithelial cells [64]. One strategy by which TAMs promote tumor immune evasion is the release of immunosuppressive cytokines like IL-10, TGFβ, IL-6, Prostaglandin E (PGE), CCL2, CCL17, CCL20, and others, which inactivates CD8+ T cell response [29]. Further, the expression of immune checkpoint molecules, which refer to co-inhibitory signals of immune cells impeding the immune response, can be adopted by tumor cells to suppress the surrounding immune response [64]. TAMs strengthen the signaling of immune checkpoint molecules like Cytotoxic T Lymphocyte-associated Antigen-4 (CTLA-4) and Programmed Cell Death Protein 1-Ligand 1 (PD-L1), and they themselves express enhanced levels of PD-L1 which impede the immune recognition by T cells [65]. Another immunosuppressive strategy is the accumulation of MDSCs and M2-polarized TAMs in tumoral lesions accompanied by a decreased presence of cytotoxic T lymphocytes (CTLs) and T helper cells [53]. As PDAC growth depends on the delivery of oxygen and nutrients, angiogenesis is a crucial pathological process to ensure the influx of oxygen and nutrients into the tumor. Macrophages are aggregated in hypoxic areas of PDAC, and many surround intertumoral vessels indicating the association between TAMs and angiogenesis. The angiogenesis is induced by pro-angiogenic factors like Vascular Endothelial Growth Factor (VEGF), which is released by tumor and stroma cells, e.g., TAMs [65]. In PDAC, high levels of VEGF are associated with an increased risk of metastasis [65]. Further, as TAMs secrete a plethora of growth factors, chemokines, and cytokines, they efficiently induce Epithelial-Mesenchymal Transition (EMT) (section 1.6). In PDAC, TAMs also promote therapy resistance as macrophages can rapidly metabolize and inactivate the cytostatic drug Gemcitabine [66]. Moreover, the amount of M2-like macrophages increased after Gemcitabine treatment in a mouse model system, indicating another drug resistance mechanism caused by TAMs [53]. Further, cytidine deaminase (CDA), an enzyme, which transports chemotherapeutic drugs in cells and is responsible for their metabolization into inactive forms, is upregulated in PDAC cells in combination with TAMs and

Gemcitabine treatment [67]. Binenbaum *et al.* showed that TAMs communicate with cancer cells through so-called macrophage-derived exosomes, which are internalized by tumor cells. This leads to reduced Gemcitabine concentrations and upregulation of CDA in PDAC cells [68].

In summary, TAMs play an important role in PDAC progression and therapy resistance. Therefore, targeting macrophages is a major subject in several pre-clinical and clinical trials, e.g., addressing CD40 interaction (NCT03214250; NCT04536077; NCT04807972; NCT04888312), a combination of Gemcitabine and α-PD-1 antibody [69], or TAMs repolarization [70].

1.5. (Tumor-infiltrating) T lymphocytes

In PDAC patients, a higher density of CD8+ T cells in tumor areas was observed to be associated with a better survival outcome [71–73]. In contrast, an increased infiltration of regulatory T cells (Tregs) correlates with a poor clinical outcome in many cancer types, including PDAC [74,75]. Due to the different effector phenotypes, T cells can essentially impact tumor progression and metastasis formation in several ways. T cells generally originate from bone marrow-derived multipotent hematopoietic stem cells, which migrate through the blood circulation into the thymus to further undergo T cell maturation. T cells can be divided into different populations, including γδ T cells and αβ T cells, whereas the latter can be subdivided into CD4+ T cells and CD8+ T cells [36]. The population of CD4+ T cells is very heterogeneous, as they can differentiate into various subsets, including T helper (TH) cells TH1, TH2, TH17, T follicular helper cells, and Tregs according to the different cytokine composition in their microenvironment [36,76].

TH1 cells support bacterial infection elimination through recognition of bacterial antigens presented on major histocompatibility complex (MHC)-II of macrophages and secretion of IFNγ. Thus, macrophages are stimulated to destroy phagocytosed bacteria [36]. TH1 cells are characterized by their profound secretion of IFNγ, which furthermore promotes the recruitment of CD8+ T cells, M1-like macrophages, and NK cells, therefore capturing a tumor-suppressing phenotype [27,76,77]. IL-2 secreted by TH1 CD4+ T cells is crucial for proliferation and survival of CD8+ T cells [36].

TH2 cells secrete IL-4, IL-5, IL-10, and IL-13 [36,78] and eliminate infection of extracellular parasites [36]. In PDAC, tumor cells and the TME foster differentiation of TH2 cells and their secretion of IL-4 and IL-10, which act immune-suppressive and promote polarization of monocytes into M2-like macrophages [24]. Additionally, IL-4 and IL-13 contribute to ECM remodeling as they trigger collagen synthesis in myofibroblasts [24].

T regs, characterized by their expression of forkhead-box-protein P3 (FOXP3), recognize self-antigens to maintain self-tolerance, restore tissue homeostasis and regulate inflammatory response [36]. Tregs are considered as the most potent inhibitor of the anti-tumor immune response as they can inhibit the activity of CD4+, CD8+, and NK cells. They secrete cytokines like IL-10 and TGFβ, both known for their immunosuppressive function and compete with effector T cells to connect to antigen-presenting cells (APCs) [79].

γδ T cells can own phagocytic properties and recognize antigens in an MHC-independent way to present antigens to CD3+ αβ T cells. Therefore, this T cell subset acts as a promising tumor-suppressive T cell population [24] and is promising for novel immunotherapeutic strategies in cancer treatment.

CD8+ T cells represent the primary CTL subset that accomplishes lysis of virus-infected, neoplastic, and damaged cells. Thereby, CD8+ T cells recognize antigens presented on the MHC of APCs via their highly specific T cell receptor (TCR). After recognition, CD8+ T cells form an immunological synapse (IS) and release granules containing different cytotoxic molecules, including Perforin, Granzymes, and Granulysin. Perforin forms pores in the plasma membrane of the target cell, through which Granzymes and Granulyisn can be released into the target cell's cytosol. Granzymes activate apoptosis via caspase activation, and granulysin has anti-microbiotic properties and can induce apoptosis when released in high concentrations. Further, CD8+ T cells secrete cytokines, such as IFNγ and TNFα, that contribute to the immune response. In detail, IFNγ fosters the expression of MHC-class I molecules. It further activates macrophages and guides them to the center of infection, where they act as APCs or effector cells [36]. IFNγ is also able to induce cell cycle arrest, e.g., in tumor cells [80].

The attendance of CD8+ T cells in PDAC is associated with better survival outcomes [71–73]. PDAC is generally characterized as a "cold" tumor because of low T cell infiltration [75,81]. As outlined above, the complex TME of PDAC with its immunosuppressive cells contributes to the dysfunctionality or downregulation of anti-tumor immune response, including T cell exhaustion [82]. Further, PDAC cells secrete cytokines, such as CCL5, TGFβ, and IL-10, that are associated with Treg migration and accumulation. The presence of Tregs in turn is associated with several tumor-promoting effects, e.g., suppression of co-stimulatory ligands CD86 and CD40 on APCs, that are important for CD8+ T cell activation, thereby impairing activation of CD8+ T cells [75]. As the heterogeneity of T cell subsets is markedly high, first attempts have been undertaken to consider the T cell diversity for patient stratification and optimized treatment. Nevertheless, based on the non-T cell inflamed (cold) tumors of PDAC, immunotherapies targeting the effector phenotype of CD8+ T cells have been ineffective in PDAC so far [24].

1.5.1. T cell priming and maturation

T lymphocytes, produced in the bone marrow, migrate to the thymus to undergo a complete maturation process [83]. Double negative (DN) thymocytes (CD4- and CD8-) enter the thymus and pass through four DN stages (DN 1-4) [84]. Early-stage DN1 cells do not express CD25, while DN2 cells are characterized by elevated CD25 expression [36]. DN3 cells express a pre-TCR, proliferate and develop into DN4 cells [36,84]. Finally, DN4 cells express mature TCRs and co-receptors and begin to proliferate [36].

The TCR on the surface of thymocytes is a membrane protein containing different subunits and is responsible for the specific recognition of antigens. To reach the great diversity of highly specific TCRs, a process named V(D)J recombination occurs during T cell maturation in the thymus [85]. During V(D)J recombination, numerous variable (V), diversity (D), and joining (J) gene segments are assembled to create various TCRs on thymocytes [86]. Besides the genetic rearrangement of different TCR variants, this process simultaneously goes along with the formation of two different T cell lineages: T cells expressing subunit α and β to form TCRs (αβ T cells) and T cells that exhibit TCRs containing γ and δ subunit (γδ T cells). γδ T cells are typically CD4 and CD8 double negative, whereas αβ T cells express both co-receptors [87]. The two different TCR subunits respectively comprise a constant immunoglobulin-like domain and a variable region. Both variable regions of the subunits form the highly specific antigen binding site. The TCR alone is not sufficient to transfer signals intracellularly after antigen binding. Therefore, the CD3 complex comprising two ε-chains, one δ-chain, and one γ-chain is expressed to mediate signal transduction into the cell to induce T cell differentiation, proliferation, and cytokine secretion [36].

Afterwards, DN3 cells evolve through immature CD8-positive cells into double-positive CD4+ and CD8+ cells [36]. In the cortex of the thymus, double-positive thymocytes undergo a process of positive and negative selection to either progress into single positive CD4+ or CD8+ cells [88]. Positive selection is described as a process whereby double-positive cells recognize low-affinity self-peptide:self-MHC and mature to express profound amounts of TCR [36]. After positive selection, the reactivity to self-peptide:self-MHC is decreased [83]. At the end of the positive selection phase, the expression of one co-receptor is abandoned. CD4-expressing T cells produce receptors that recognize antigens presented on self-MHC class II molecules, while CD8-expressing T cells carry receptors that recognize peptides on self-MHC class I molecules. The decision of which co-receptor remains expressed depends on the binding site of constant areas of either MHC-class I or class II. Therefore, positive selection is only completed when TCR and co-receptor interact with the MHC molecule [36]. In contrast, the negative selection causes the deletion of self-reactive T cells by inducing apoptosis due to a high-affinity interaction with self-MHC molecules [36,89]. The process of negative selection addresses the high

recognition of auto-antigens on cortical or medullary epithelial cells or bone marrow-derived APCs [36]. After positive and negative selection, mature T cells exit the thymus and circulate in the peripheral lymphoid organs such as spleen and lymph nodes (LNs) [88].

1.5.2. T cell activation and inhibition

Naïve T cells that exit the thymus migrate into lymphoid organs and LNs through high endothelial venules in the paracortical T cell zone. Since the frequency of naïve T cells specific for a distinct antigen is very low, antigen-presenting DCs must easily meet various potential T cell suitors in the T zones [90]. The interaction of T cells and APCs like DCs is achieved by the LN stromal framework in order to enhance the probability of finding a cognate interaction which further results in the initiation of an immune response [91]. In contrast to T cells, DCs enter the LNs predominantly via afferent lymphatic vessels, but in the spleen, both cell populations enter from the blood. The chemokine receptor CCR7 and its ligands (e.g., Epstein–Barr virus-induced molecule-1 ligand chemokine (ELC) and secondary lymphoid organ chemokine (SLC)) are responsible for the recruitment of naïve T cells and DCs into lymphoid T zones [90].

When both cell populations arrive in the T zones, binding of TCR to a specific antigen on MHC class I or MHC class II is achieved. A huge peptide repertoire can be presented on the membrane surface via MHC class I or MHC class II molecules for recognition by CD4+ or CD8+ T cells [92]. Although intracellular antigens are presented on MHC class I molecules and endocytosed extracellular antigens are bound to MHC class II molecules, a process called cross-presentation enables the presentation of extracellular antigens on MHC class I and intracellular antigen peptides on MHC class II complexes [93,94].

As the first step of T cell activation is delivered by engagement of TCR with antigenic peptide on MHC molecules [89,95], the co-receptors CD4 or CD8 must interact with nonpolymorphic domains of the MHC molecules to participate actively in T cell activation [85] (Figure 4). Therefore, CD4 binds to MHC class II and co-receptor CD8 interacts with MHC class I molecules [36,85]. The TCR ligation alone is associated with T cell anergy or unresponsiveness, wherefore a co-stimulatory signal is necessary to prevent T cells from unresponsiveness [96]. Thus, the next signal is the interaction of co-stimulatory molecules such as CD28 on T cells with its primary ligands CD80 or CD86 on APCs [96,97]. The CD28 receptor family, including CD28, CTLA-4, ICOS, and PD-1, is best characterized and provides principal signals for optimal T cell function [97].

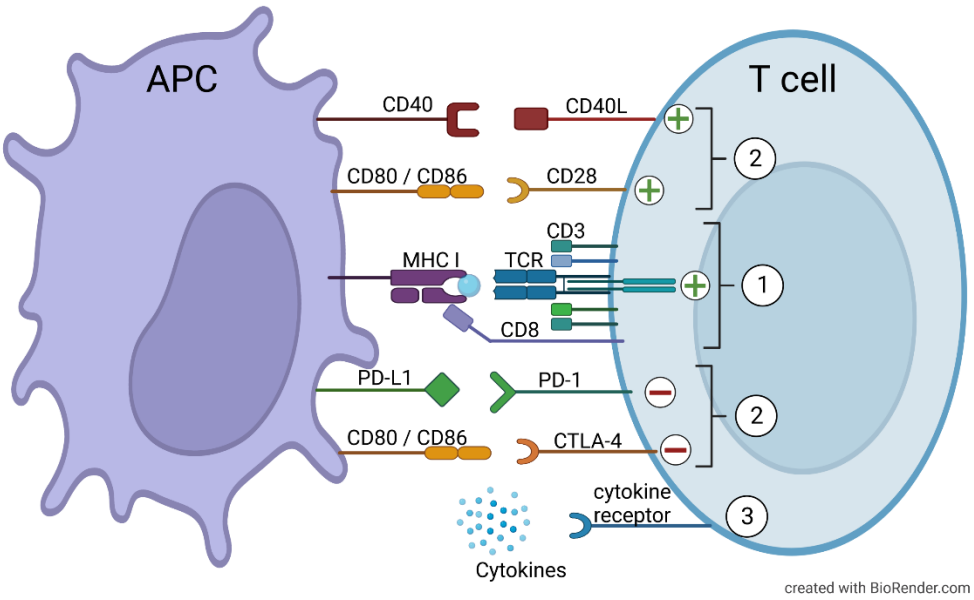

Figure 4: Main interactions between APCs and CD8+ T cells for complete T cell activation. Three signals are needed for T cell activation. 1) Engagement of specific antigen, presented on APC's MHC, and TCR-CD3 complex on T cells, and binding of co-receptor CD8 to constant region of MHC. 2) Co-stimulatory interaction of CD28 and CD80/CD86. To suppress T cell activation, co-inhibitory binding of PD-1 and PD-L1 or CTLA-4 and CD80/CD86 is required. 3) Cytokine signaling for regulation of T cell activation. Adapted from [98].

To regulate T cell activation, co-inhibitory molecule interaction is needed. One prominent example for suppression of T cell response is the binding of CTLA-4 to CD80 or CD86, both also ligands for CD28. Therefore, a competition between CD28 and CTLA-4 for their ligand binding exists and adds another layer of complexity to CD28 signaling regulation [96].

Table 2: Selection of co-stimulatory and co-inhibitory molecules involved in T cell activation. The symbol * represents molecules that are expressed on T cells. In the column "Effect", co-stimulatory effects are denoted as "+" and co-inhibitory effects are marked as "-".

Receptor	Ligand(s)	Effect	Reference(s)
?*	TIM1	-	99
CD137 (4-1BB)*	CD137L	+	100
CD27*	CD70	+	99,101
CD278 (ICOS)*	ICOSL	+	102,103
CD279 (PD-1)*	CD274 (PD-L1)*, CD273 (PD-L2)*	-	104,105
CD28*	CD80*, CD86*	+	96
CD30*	CD30L	+	99
CD40	CD40L*	+	99,101
CTLA-4*	CD80*, CD86*	-	96,106
GITR (CD357)*	GITRL	+	99
LAG-3 (CD223)*	MHC II	-	99,103
OX40*	OX40L	+	99
TIGIT*	CD155	-	103
TIM-3*	Galectin-9	-	24

The third signal is the regulation of T cell activation via different cytokines. CD28-mediated signals are demanded for IL-2 production and serve as survival factors of T cell proliferation [107], but also IFNα/β, IL-12, IL-15, and IL-21 regulate CD8+ T cell activation [108–111].

After successfully priming and maturation phase of T cells in the lymphoid organs, they start to differentiate and proliferate in order to migrate through the blood circulation into target tissues [36]. However, T cell activation is dependent on the duration and composition of signal availability [112]. Thus, the regulation of over- and under-stimulation is crucial for effective T cell function, as both results in induction of anergy and apoptosis [113,114].

1.5.3. Co-inhibitory interactions of PD-1/PD-L1 and CTLA-4/CD80

Since unimpeded T cell activity can result in T cell responses against self-antigens and autoimmune disease, it is important to maintain the homeostasis of T cell activity and inhibition [115]. The co-inhibitory receptor PD-1 consists of a single N-terminal variable immunoglobulin region (IgV) like domain, a stalk comprising approximately 20 amino acids separating the IgV domain from plasma membrane, a transmembrane domain, and a cytoplasmic tail with an immunoreceptor tyrosine-based inhibitory motif (ITIM) and an immunoreceptor tyrosine-based switch motif [116,117]. The engagement of PD-1 leads to the phosphorylation of both motifs and the recruitment of Src homology region 2 domain-containing phosphatase 1 (SHP-1) and SHP-2 [118]. In response to this, TCR/CD28-mediated activation of phosphatidylinositol 3-kinase (PI3K) is inhibited by dephosphorylation of CD3 ζ-chains. Therefore, PD-1 interaction directly inhibits effector T cell functions such as survival, proliferation, cytokine production, and cytotoxicity [117].

PD-1 is a member of the CD28 superfamily, however, it has distinct molecular features that differ from classical members of the CD28 family [116]. PD-1 is rather expressed on activated mature T cells, however, low amounts are also expressed on DN thymocytes (CD4- CD8-), as well as in activated NK T cells, B cells, monocytes, and immature Langerhans' cells [116]. During T cell activation, PD-1 expression is upregulated in about 6 hours and in tumors, it is highly expressed in dysfunctional/exhausted effector T cells (both CD4+ and CD8+) as well as Tregs [117]. The two ligands of PD-1 (PD-L1 and PD-L2) are constitutively expressed in low amounts on APCs, as well as non-hematopoietic cells, including pancreatic islet cells, vascular endothelial cells, and cells in tissue of immune privileges such as placenta, testes, and eyes. The PD-L1 expression is inducible by pro-inflammatory cytokines like type I and II interferons, TNFα, and VEGF. The PD-1 pathway plays an important role in suppression of effector T cells, whereby maintaining self-tolerance and promoting the resolution of inflammation during immune responses [118].

CTLA-4 is a structural homolog of CD28 and shares the same B7 ligands with CD28 (CD80, CD86), but CTLA-4 binds its ligands with greater avidity and affinity [119]. Based on the covalent homodimer structure, each CTLA-4 homodimer binds to two divalent B7 molecules resulting in a stable CTLA-4-B7 structure on the cell surface. In contrast, CD28 monovalent binds to B7 molecules [119]. Although CTLA-4 binds both B7 molecules, CD80 has a higher affinity to be bound by CTLA-4 compared to CD86 [120,121]. Various mechanisms have been reported for T cell inhibition by CTLA-4, including competition for CD28 by binding to CD80 and CD86 [122], modulation of TCR signaling by the SHP-2 and serine-threonine phosphatase PP2A [123,124], disruption of CD28 localization at the IS [125], and impairment of the expression or composition of lipid rafts at the T cell surface [126–128]. CTLA-4 expression is induced on conventional activated CD4+ and CD8+ T cells but is constitutively expressed on Tregs. Further, it can also be expressed by B cells, DCs, monocytes, placental fibroblasts, granulocytes, CD34+ stem cells, embryogenic mouse cells, pituitary glands, and embryoid bodies [119].

CD80 is a type-1 transmembrane glycoprotein and is expressed by macrophages, activated B cells, and activated T cells. CD80 bound by CD28 leads to co-stimulation of T cells, while CTLA-4/CD80 binding induces co-inhibitory signals [129] indicating the two faces of CD80.

Overall, the co-stimulatory and co-inhibitory interactions are very complex, as alterations in the dynamic expression of involved molecules can promote or interrupt distinct interactions. Thus, alteration of the expression patterns could have implications for the synergy observed in immunotherapy [130].

1.6. EMT and metastasis

The EMT is a reversible process that allows epithelial cells to aquire a mesenchymal-like phenotype by morphological and molecular alterations, which results in an enhancement of migratory capacity, invasiveness, increased production of ECM components, and elevated resistance to apoptosis. Physiologically, it is a central process during embryogenic development, wound healing, and tissue regeneration [25,131]. Besides, EMT is a key process in tumor progression and therapy resistance of many carcinomas, e.g., in PDAC [25,132]. On a functional level, epithelial cells lose their cell-cell adhesions and apical-basal polarity while gaining enhanced migratory, invasive, and metastatic properties [25,133]. During EMT, gene expression and post-translational mechanisms are changed, leading to the repression of epithelial characteristics and the adoption of mesenchymal properties [134]. On a molecular level, cells undergoing EMT express decreased levels of epithelial genes like E-cadherin, Occludin, and ZO-1 and increased levels of mesenchymal genes such as L1 cell adhesion molecule (L1CAM), N-cadherin, Vimentin, and Fibronectin [135–137]. This process is promoted by several transcription factors,

including Snai1 (Snail), Snai2 (Slug), Zinc finger E-box-binding homeobox (Zeb) 1 and 2, and Twist, especially in PDAC [134,138–140]. Once expressed and activated, each of these transcription factors can pleiotropically induce the complex EMT process by activating a series of intracellular signaling programs. The Mesenchymal-Epithelial Transition (MET) is its reverse process, where motile, multipolar mesenchymal cells undergo transition into polarized epithelial cells [131,133]. The TME plays an essential role in EMT and also its reversion. Chronic inflammation promotes EMT, as the altered TME secretes several cytokines and growth factors. In contrast, acellular fibrotic tissue enhances intertumoral pressure and formation of functionally and structurally aberrant blood vessels resulting in hypoxia [25]. These changes promote the process of EMT that fosters invasiveness and metastatic capabilities of tumor cells. Especially CAFs can induce EMT through secretion of TGFβ, IL-6, TNFα, and IL-1, but also M2-like macrophages promote EMT through secretion of IL-6, IL-10, TNFα, TGFβ, and chemokine CCL20 [25,57]. Additionally, the tumor-associated microbiome and hypoxia are known inducers of EMT [24]. Furthermore, the dense desmoplastic stroma of PDAC includes large amounts of fibrillar collagen, fibronectin, laminin, and proteoglycans, rather produced by CAFs than cancer cells. Besides the physical barrier of stiff ECM, these proteins also have a signaling function that contributes to EMT and thereby to metastasis of PDAC cells [25]. Metastasis formation is characterized by the invasion of carcinoma cells, which invade the basement membrane into the adjacent stroma, following the intravasation and survival in the blood or lymph circulation, followed by extravasation into the parenchyma of distant tissues, and lastly by the re-establishment of neoplastic cell properties at remote sites (even after a long period of dormancy) [137] (Figure 5).

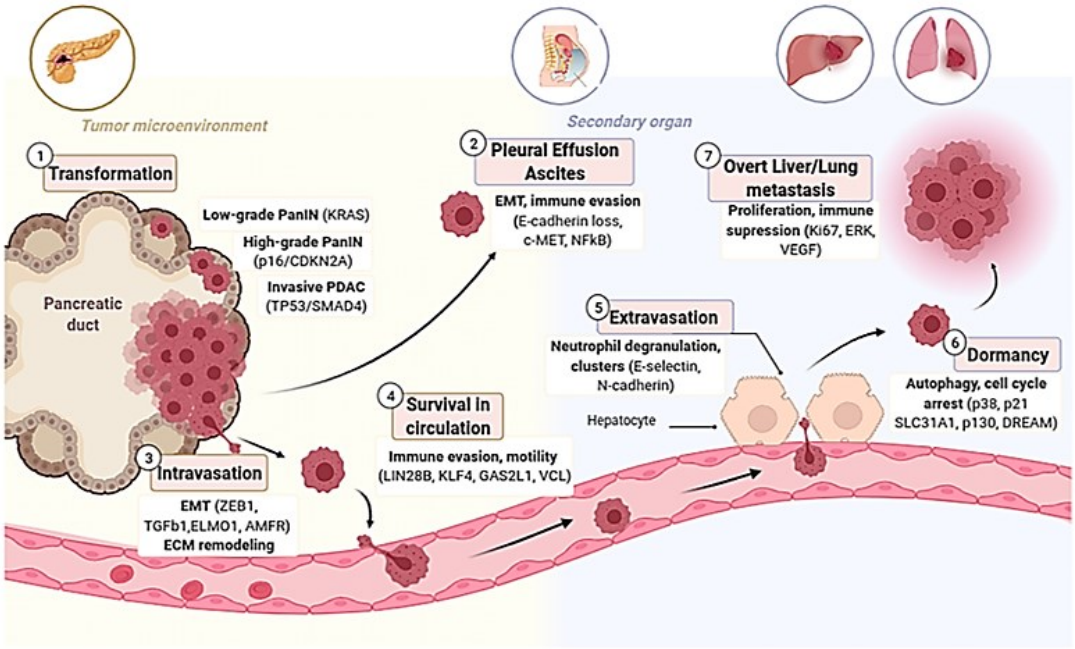

Figure 5: Epithelial-Mesenchymal-Transition (EMT) and metastasis (with responsible genes). (1) Normal pancreatic ductal epithelial cells transform into an invasive pancreatic ductal adenocarcinoma (PDAC) via several mutations (first, low-grade PanIN, high-grade PanIN). (2) Transformed cells undergo EMT and invade the surrounding tissue or can colonize into the peritoneum and form ascites or pleural effusion. **(3)** PDAC cells invade the blood or lymphatic vessels. **(4)** Circulating tumor cells (CTC) survive in the circulation. **(5)** CTC extravasate into secondary organs, **(6)** where they might remain in a dormant stage for several years and **(7)** eventually form metastases in the liver or lung [137].

Important drivers for metastasis formation in PDAC are abberant TP53 [24], SMAD4 [141], Wnt [142] signaling, and abnormal ECM gene expression [142]. Studies of a murine mouse model indicate that PDAC cell-derived small extracellular vesicles (sEVs) covered with Ezrin foster macrophage polarization to M2-like phenotype and support metastasis formation in the liver [143]. Further, the molecule Granulin secreted by circulating monocytes and hepatic metastasis-associated macrophages benefits the activation of hepatic stellate cells (HSCs) into hepatic myofibroblasts (HMFs), thereby promoting liver metastases [143]. Moreover, hypoxia selects the most malignant tumor cells, and through the Hypoxia-Inducible Factor 1 (HIF1), tumor suppressor genes are suppressed while fostering the metastatic cascade [144,145].

Overall, the TME with its altered composition of cytokines, chemokines, hypoxic conditions and ECM molecules, contributes to EMT accompanied by metastasis formation.

1.7. Cancer immunity and immunotherapy

The immune system preserves the defense against foreign, infected antigens and self-antigens by an appropriate balance between activation and inhibition of the immune response. A central role in this

process play receptor-ligand bindings between T cells which are activated by the presentation of antigens and various cells of the immune system. In carcinogenesis and anti-tumor immunity, the immune response plays also a crucial role [146]. A process called cancer immunoediting occurs in three phases: elimination, equilibrium, and escape. In elimination phase, the innate and adaptive immunity detect and destroy transformed cells. Sometimes, tumor cells are not completely eliminated and enter the equilibrium phase in which the immune system controls the tumor outgrowth. In the last phase, tumor cells overcome dormancy and leading to tumor progression [147]. This is achieved through strategies that prevent attacks from immune cells. The tumor cells start to build a microenvironment at the time of tumor occurrence to make it difficult for the immune system to eliminate cancer cells effectively [148]. The cancer immunity cycle involves multiple steps to obtain efficient control of cancer growth by the immune system. The process is started by releasing tumoral neo-antigens generated due to genomic instability. The uptake of these antigens by APCs and migration to LNs results in the priming and activation of naïve CD8+ T cells. The CD8+ T cells migrate via the bloodstream and infiltrate the tumor-stroma, where they possibly recognize and eliminate tumor cells. The cytotoxic immune response of CD8+ T cells releases additional antigens fueling the cancer immunity cycle [149–151]. All cancer immunity cycle steps must function properly to generate an effective cancer immune response. However, in cancer patients, this cycle might be impaired, resulting in the lack of anti-tumor immunity and thereby in cancer development and progression [150].

Several immune escape mechanisms are established by cancer cells to evade the immune response. First, the release of tumor-specific antigens can be impaired. Due to apoptosis or necrosis, antigens are released in the microenvironment and phagocytosed by APCs. The lack of dying tumor cells leads to an ineffective antigen release preventing antigen presentation of APCs and the further steps of the cancer immunity cycle [152,153]. The antigen processing and presentation can also be impaired. Soluble factors like cytokines (e.g., IL-6, IL-35), lipids, or tumor exosomes can inhibit DC maturation and lead to immune surveillance. In detail, IL-35 was found to decrease expression of HLA-DR, CD83, and co-stimulatory molecules such as CD40, CD80, and CD86 on DCs. IL-6 suppressed DC maturation by down-regulation of MHC class II molecules and CD86 expression via IL-6/STAT3 pathway [154]. Elevated levels of pro-angiogenic factors like VEGF can be another strategy for immune evasion as the formation of abnormal tumor blood vessels can act as a physical barrier to prevent infiltration of effector T cells [155,156]. Additionally, VEGF reduces the expression of Vascular Cell Adhesion Molecule 1 (VCAM-1) and Integrin Ligands Intercellular Adhesion Molecule 1 (ICAM-1) on endothelial cells, resulting in a diminished adhesion of CD8+ T cells to endothelial cells and thereby reduced tumor infiltration [157,158]. The overexpression of the endothelial B receptor also prevents T cells from migration into the tumor tissue, contributing to the low abundance of tumor-infiltrating lymphocytes (TILs) [154]. Next, tumor cells

can escape the T cell response by MHC class I downregulation. Only tumor cells presenting antigens on their MHC class I molecule can be recognized by activated T cells and, thus, be eliminated. Here, tumor cells can downregulate the surface expression of MHC class I molecules, express defective MHC class I molecules, or upregulate factors conferring resistance to cytotoxic activity of immune cells and/or local immunosuppression [117]. Even though T cells have made their way through the different impediments above, they can also face various immunosuppressive factors preventing their proper T cell activity. On the one hand, upregulation of immunosuppressive enzymes like Indoleamine-2,3-dioxygenase 1 (IDO 1), which is expressed by tumor cells and stroma cells, can suppress T cells [154]. On the other hand, the upregulation of inhibitory immune checkpoint molecules impairs T cells. In detail, PD-1 is upregulated on activated T cells, and tumor cells often express its ligand PD-L1, causing T cell inhibition and suppressed antitumor immunity [159,160]. PD-L1 is frequently expressed on tumor cells in several malignancies and correlates significantly with a poor prognosis, including renal, urothelial, gastric, ovarian, esophageal, hepatocellular, and PDAC [161]. PD-L1 on tumor cells can be induced by IFNγ [162–165], which is also expressed by T cells, creating a negative feedback mechanism due to the attendance of T cells in the TME [165]. Furthermore, PD-L1 on tumor cells can act as an immunosuppressive receptor in order to mediate anti-apoptotic signals causing resistance to the cytotoxicity of CD8+ T cells and Fas-mediated killing [166]. It was also demonstrated that PD-L1 could protect tumor cell toxicity by IFNγ [167], but also expression of Lymphocyte-activation gene 3 (LAG-3), T-cell immunoglobulin and mucin-domain 3 (TIM-3), T cell immunoreceptor with Ig and ITIM domains (TIGIT), and V-domain Ig suppressor of T cell activation (VISTA) on T cells can mediate the immune evasion of tumor cells [154]. Moreover, the attendance of immunosuppressive cell populations, including Tregs, TAMs, and MDSCs suppress the immune response against tumor cells through secretion of immunosuppressive cytokines (such as IL-10, TGFβ), chemokines (C-X-C motif ligand (CXCL) 8), expression of inhibitory enzymes (IDO and arginase-1), or expression of co-inhibitory molecules (PD-L1 on APCs or CTLA-4, PD-1, TIM-3 and LAG-3 on Tregs) [154].

Especially in PDAC, several immune escape mechanisms are crucial for disease progression. Several studies identified a correlation between PD-L1 expression and poor survival of patients [81,168,169], but 43.7 – 69.6 % of primary PDAC tissues exhibit no or only low PD-L1 expression [170,171]. Furthermore, the PD-L1 expression observed in PDAC is predominantly detected on stromal cells and the location of these cells is significantly associated with the presence of CD3, CD4, CD8, FOXP3, and CD68 positive cells [170,172]. Of note, CD8+ T cells and macrophages were associated with PD-L1-expressing areas in cancer [173] and most of these macrophages were CD163 positive in primary PDAC, indicating an anti-inflammatory phenotype [24,55,56,59] which is also associated with poor prognosis and reduced patient survival [58,59,174,175]. Further, the low tumor mutational burden (TMB), especially in PDAC, is associated

with the presentation of fewer antigens on MHC class I molecules resulting in impaired recognition as foreign antigens and preventing T cells from activation and cytotoxicity [154]. Moreover, cancer FOXP3 promotes PDAC immune evasion via recruitment of Tregs into PDAC tumors [176], but also CAFs, promote an immunosuppressive environment e.g., via CXCL12 and M-CSF secretion thereby recruiting monocytes and promoting the accumulation of M2-polarized macrophages. In a murine PDAC model, PDAC cell-derived sEVs covered with Ezrin were shown to foster a polarization towards an M2-phenotype and supporting metastasis formation in the liver [24]. In turn, M2-type TAMs in PDAC secrete immunosuppressive cytokines like IL-10, TGFβ, IL-6, PGE, CCL2, CCL17, and CCL20 and thereby inhibit the immune response of CD8+ T cells and switch an inflammatory response into calmness [54].

The interplay of tumor cells and the immune system is very complex, and tumor cells establish various escape mechanisms to evade the immune response. In order to overcome the immune escape mechanisms, different therapeutic approaches have been investigated. Cancer vaccines containing four key components, including tumor antigen-peptides, formulations, immune adjuvants, and delivery vehicles, have been designed to induce or amplify tumor-specific T cell response by active immunization [177]. Another therapeutic treatment is adoptive T cell therapy. Chimeric antigen receptor (CAR) T cell therapy has shown potent anti-cancer activity. The advantage of CAR T cell therapy is, that tumor-specific proteins are recognized more effectively due to the independent presentation of antigens on MHCs. Thus, CAR T cells overcome defects in antigen presentation and processing exploited by tumor cells [178]. Therapies targeting immunosuppressive cells can unleash anticancer immune responses, e.g., suppression of Tregs by monoclonal antibodies can stabilize cancer disease [154]. Further therapy options are immune checkpoint blockades and combination therapies. These are discussed in more detail in the next section.

1.8. Immune checkpoint inhibition of PD-1 and PD-L1

Immune checkpoint inhibition has emerged as an effective strategy in the field of immunotherapy. Monoclonal antibodies can significantly reduce solid tumor size, inhibit advanced tumors and metastases, and enhance overall survival in patients [179]. Antibodies against CTLA-4 (such as Ipilimumab) could increase the 10-year survival for patients with metastatic melanoma and were approved by the Food and Drug Administration (FDA) in 2011 [178,180]. The application of antibodies targeting the PD-1/PD-L1 axis has also shown advantages in survival of several malignancies by increasing the response rates and diminishing side effects compared to CTLA-4 treatment [180]. To date, the FDA has approved six monoclonal antibodies which target PD-1 or PD-L1 [179] (Table 3).

Table 3: FDA-approved PD-1 and PD-L1 targeting monoclonal antibodies for cancer immunotherapy.

Antibody (Trade name)	Target	Isotype	Company
Cemiplimab (Libtayo)	PD-1	human IgG4	Sanofi/Regeneron
Nivolumab (Opdivo)	PD-1	human IgG4	Bristol-Myers Squibb
Pembrolizumab (Keytruda)	PD-1	humanized IgG4	Merck/MSD
Atezolizumab (Tecentriq)	PD-L1	humanized IgG1	Genentech/Roche
Avelumab (Bavencio)	PD-L1	human IgG1	Merck/Pfizer
Durvalumab (Imfinzi)	PD-L1	human IgG1	Medimmune/Astra Zeneca

FDA approved Cemiplimab-rwlc in 2021 as first-line treatment in patients with non-small cell lung cancer (NSCLC) whose tumors have high PD-L1 expression [181]. Nivolumab and Pembrolizumab acquired the permission for therapy of NSCLC, terminal melanoma, and renal cell cancer [179]. Atezolizumab was approved by the FDA in 2022 for the treatment of unresectable or metastatic alveolar soft part sarcoma [182], Avelumab in 2020 for maintenance treatment of urothelial carcinoma [183], and Durvalumab was initially approved in 2017 for the treatment of stage III unresectable NSCLC and locally advanced or metastatic urothelial cancer [184]. Mono-therapeutic treatment with immune checkpoint inhibitors showed benefits in several cancer entities, while in other malignancies, monotherapy failed so far. Thus, promising clinical trials on combinational treatment approaches with surgery, radiation therapy, traditional chemotherapy, or ICI combinations that are used in first-line or subsequent treatment are ongoing [185]. In 2022, the FDA approved Durvalumab therapy in combination with Gemcitabine or Cisplatin for patients with locally advanced or metastatic biliary tract cancer [186], Avelumab plus Axitinib, a tyrosine kinase inhibitor for treatment of renal cell carcinoma or Cemiplimab-rwlc combination with Platinum-based chemotherapy for NSCLC with no EGFR, anaplastic lymphoma kinase, or Proto-oncogene tyrosine-protein kinase ROS1 aberrations in 2022 [187]. Already in 2018, Atelizumab was approved in combination with Bevacizumab (an α-VEGF monoclonal antibody), Paclitaxel, and Carboplatin for first-line treatment of metastatic non-squamous NSCLC patients [188]. The ongoing phase Ib clinical trial investigates the effect of Nivolumab and stereotactic radiosurgery in metastatic breast cancer and brain metastases (NCT03807765).

Interfering this inhibitory PD-1/PD-L1 axis by treatment with ICI monotherapy revolutionized the therapeutic regimens for multiple cancer entities [189–191], but so far failed in PDAC [192,193], although considerable PD-L1 expression levels in PDAC cell lines have been reported in PDAC [81,171,176]. Therefore, numerous clinical trials are ongoing to investigate the beneficial impact of combinational therapies,

e.g., in PDAC. A randomized multicenter phase Ib/II clinical trial study examines the efficacy of combinational treatment of neoadjuvant chemoradiation therapy with Pembrolizumab in PDAC patients (NCT02305186). An open label, single arm, multicenter clinical trial investigates the combination of AZD0171 (a monoclonal antibody against leukemia inhibitory factor) and Durvalumab as well as standard-of-care chemotherapy in metastatic PDAC (NCT04999969).

Overall, ICI therapy harbor great potential for treatment of different cancer entities that were beforehand endowed with poor prognoses. However, some patients do not show anticipated responses. Thus, the consideration and identification of predictive biomarkers for ICI treatment must be included. To date, the PD-L1 expression and amplification, as well as a high TMB, microsatellite instability, and CD8 infiltration, are considered as primary predictive markers for ICI response rates [194]. Moreover, combinational treatments of ICI with surgery, radiation therapy, traditional chemotherapy, or ICI combinations might reveal beneficial responses to cancer therapy.

In the present study, Pembrolizumab and Durvalumab were utilized to investigate the effects of blocking the PD-1/PD-L1 axis on the activity, effector phenotype, and PDAC cell killing properties of CD8+ T cells in different microenvironmental conditions.

1.9. Aim of the study

Cancer immunotherapy has emerged as an effective strategy since 2014 when immune checkpoint inhibition of PD-1 was approved for melanoma [195]. Monoclonal antibodies against immune checkpoint molecules can significantly reduce solid tumor size, inhibit advanced tumors and metastases, and enhance overall survival in patients [179]. Treatment with ICI, e.g., targeting PD-L1 or its receptor PD-1, have markedly improved the therapy of many cancers but so far failed in PDAC [192,193]. TAMs represent one of the most abundant immune cell populations within the TME of PDAC being able to either support or restrain tumor progression depending on their phenotype [50,51]. Although the phenotype and frequency of macrophages are highly dynamic, TAMs in PDAC mostly exhibit M2-like characteristics and are associated with pro-tumoral effects, including tumorigenesis, immunosuppression, metastasis acceleration, and chemotherapeutic resistance [29,55–62]. Of note, PDAC-derived TAMs exhibit properties of both M2- and M1-like polarization and have been shown to promote EMT, a process that fosters invasion of PDAC and premalignant pancreatic ductal epithelial cells (PDECs) [57]. As EMT is also associated with the acquisition of a drug resistant phenotype and immune evasive properties, TAMs are potent drivers of drug resistance as well as immune escape and suppression at all stages of tumor development [196]. Still, it is poorly understood whether PD-L1-expressing TAMs with different polarization phenotypes contribute to immune evasion of PDAC cells, particularly when the latter themselves do not or only hardly express PD-L1.

Thus, to obtain further insight into PD-L1-mediated immune evasion during PDAC progression and the reasons for anti-PD-L1 treatment failure in this tumor entity, this study examined the PD-L1 expression and its spatial distribution as well as the as the stromal composition in primary PDAC tissues and corresponding liver metastases. Based on these findings and to mimic the dynamic TME comprising different amounts and phenotypes of macrophages during PDAC progression, the next aim was to establish a stroma-enriched spheroid model with two different PDAC cell lines and different ratios of M1- or M2-like macrophages. Here, phenotype and PD-L1 expression of macrophages and PDAC cells as well as the PDAC killing activity of CD8+ T cells were examined. Finally, the last aim of the study was to elucidate how these distinct stromal conditions impact treatment efficacy of ICI in monotherapy as well as in combination with Gemcitabine.

2. Material

2.1. Chemicals and reagents

Compound	**Manufacturer**
4-(2-hydroxyethyl)-1-piperazineethansulfonic acid (HEPES)	Pan-Biotech GmbH, Aidenbach, DE
Accutase solution	Pan-Biotech GmbH, Aidenbach, DE
Ammonium chloride (NH_4Cl)	Merck Millipore, Billerica, USA
Bovine pituitary extract (BPE)	Life Technologies, Carlsbad, USA
Bovine serum albumin (BSA)	Biomol, Hamburg, DE
CellTrace™ Violet Cell Proliferation Kit	ThermoFisher Scientific, Waltham, USA
CellTracker™ Green CMFDA Dye	ThermoFisher Scientific, Waltham, USA
Dimethylsulfoxide (DMSO)	Sigma Aldrich via Merck, St. Louis, USA
Dulbecco´s Modified Eagle Medium (DMEM)	Pan-Biotech GmbH, Aidenbach, DE
Acetic acid, 10 %	Merck Millipore, Billerica, USA
Ethanol	Merck Millipore, Billerica, USA
Ethylenediaminetetraacetate (EDTA)	Carl Roth GmbH, Karslruhe, DE
FcR blocking reagent, human	BioLegend, San Diego, USA
Fetal calf serum (FCS)	Pan-Biotech GmbH, Aidenbach, DE
Fluoro-Gel	Electron Microscopy Science, Hatfield, UK
Hoechst	Thermo Fisher Scientific, Waltham, USA
Keratinocyte serum-free medium	Life Technologies, Carlsbad, USA
L-Glutamine (L-Gln)	Biochrom via Merck Millipore, Billerica, USA
Natriumchlorid	Carl Roth GmbH, Karslruhe, DE
Pancoll, 1.077 g/l	Pan-Biotech GmbH, Aidenbach, DE
Paraformaldehyde (PFA) 4.0 %	Thermo Fisher Scientific, Waltham, USA
Penicillin/Streptomycin (Pen/Strep)	Biochrom via Merck Millipore, Billerica, USA
Phosphate-buffered saline (PBS) Dulbecco	Biochrom via Merck Millipore, Billerica, USA
Potassium hydrogen carbonate ($KHCO_3$)	Merck Millipore, Billerica, USA
Propidium Iodide (PI)	Sigma Aldrich via Merck, St. Louis, USA
Puromycin (10 mg/ml)	Invivo Gen, San Diego, USA

Compound	Manufacturer
Roswell Park Memorial Institute (RPMI) 1640 Medium	Biochrom via Merck Millipore, Billerica, USA
Sodium pyruvate	Biochrom, via Merck Millipore, Billerica, USA
Solution 555	Beckman Coulter, Brea, USA
Tris(hydroxymethyl)aminomethane (Tris)	Carl Roth GmbH, Karslruhe, DE
Trypsin-EDTA	Biowest, Nuaillé, FRA

2.2. Buffer

Density gradient & counterflow centrifugation

Buffer	Formulation
Elutriation buffer	0,1 % (v/v) FCS 10 mM EDTA in PBS pH 7,4
Erythrocyte lysis buffer	NH_4Cl 10 M $KHCO_3$ 0,1 mM EDTA in ddH_2O

Flow cytometry

Buffer	Formulation
Cyto-Fast Fix perm solution	
Cyto-Fast perm wash solution 10X	Diluted to 1X using ddH_2O
Fixation solution	1 % (v/v) PFA in MACS buffer
Magnetic-activated cell sorting (MACS) buffer	0.5 % (w/v) BSA 2 mM EDTA in PBS pH 7,4 sterile-filtered and vacuum-degassed

2.3. Cell culture material

2.3.1. Cell lines

Cell line	Information
A818-6	A818 cells were isolated from ascites of a 75-year-old female with differentiated PDAC in the head of pancreas [197]. The subclone A818-6 was obtained by limited dilution of original cell population, is highly differentiated, and harbor *kras* and *p53* mutations [197]. A818-6 cells were kindly provided by H. Kalthoff (Kiel, DE).
BxPc3	Moderately differentiated BxPc3 cells were isolated from the primary tumor of a 61-year-old Caucasian female with PDAC [198,199]. These cells exhibit *p53* mutations but wildtype *kras* gene [200]. BxPc3 cells were purchased from American Type Culture Collection (ATCC) (Manassas, USA).
Colo357	Colo357 cells were isolated from a lymph node metastasis of a 77-year-old woman with pancreatic adenosquamous carcinoma. Colo357 cells exhibit single *kras* gene mutation (G12V) but wildtype *p53* and are moderately differentiated [198,200].
(H6c7eR-KR) H6c7-KRAS	H6c7-KRAS cells, originating from human PDECs, were immortalized by retroviral infection containing E6/E7 genes of human papillomavirus 16. Further, H6c7-KRAS cells harbor a retroviral vector containing a mutation of the *kras* gene at G12V [201,202]. These cells were used as a premalignant human PDEC model, which only carries G12V *kras* gene mutation. H6c7-KRAS cells were kindly provided by M.-S. Tsao (Ontario Cancer Institute, Toronto, Canada).
Panc1	Poorly differentiated Panc1 cells were isolated from a primary PDAC of a 56-year-old Caucasian male [198,203]. Panc1 cells show driver mutations in *kras*, *p53,* and *p16* genes [204,205]. Panc1 cells were purchased from ATCC (Manassas, USA).

Panc89	Panc89 cells were isolated from a lymph node metastasis of a 64-year-old Caucasian male with PDAC. These cells have Q61H *kras* mutation and Y220C *p53* mutation [200]. Panc89 cells are moderately differentiated [198] and kindly provided by K. Keiichi (Kyoto Prefectural University of Medicine, JPN).
PancTu1	PancTu1 cells originate from a Caucasian female with PDAC. These cells contain G12D *kras, p53* and *p16* mutations [200,204]. PancTu1 cells are poorly differentiated [198,204] and were kindly provided from M. v. Bülow (University of Mainz, DE).
PT45 (PT45P1)	Poorly differentiated PT45 cells were derived from primary tumor of PDAC and harbor *kras* and *p53* mutations [198,204]. They were kindly provided by H. Kalthoff (Kiel, DE).

2.3.2. Primary cells

Primary cell population	**Information**
Human T-lymphocytes	Human T-lymphocytes were isolated from leucocyte-retaining systems of different healthy blood donors and selected for CD8+ T cells. The leucocyte retaining systems were provided by the Institute of Transfusion Medicine in Kiel.
Human macrophages	Human monocytes were isolated from leucocyte-retaining systems of different blood donors and were *in vitro* polarized into M1- or M2-like macrophages. The leucocyte retaining systems were provided by the Institute of Transfusion Medicine in Kiel.

The study project was approved by the Ethics committee of the Medical Faculty of Kiel University (reference number: A110/99 and D490/17). Written informed consent was obtained from all blood donors.

2.3.3. Cell culture media

Cell culture-routine

Cell line/primary cells	Formulation of medium
CD8+ T cells	RPMI 1640 medium 10 % (v/v) FCS 20 mM HEPES 1 % (v/v) L-Gln 1 % (v/v) Sodium pyruvate 1 % (v/v) Pen/Strep
H6c7-KRAS	50 % (v/v) Keratinocyte serum-free medium 50 % (v/v) RPMI 1640 10 % (v/v) FCS 1 % (v/v) L-Gln 50 µg/ml BPE 5 ng/ml Epidermal Growth Factor (EGF) 4 µg/ml Puromycin
M1-like macrophages	RPMI 1640 medium 5 % (v/v) FCS 1 % (v/v) L-Gln 1 % (v/v) Pen/Strep
M2-like macrophages	RPMI 1640 medium 1 % (v/v) FCS 1 % (v/v) L-Gln 1 % (v/v) Pen/Strep
PancTu1, Panc1, Panc89, A818-8, BxPc3, Colo357	RPMI 1640 medium 10 % (v/v) FCS 1 % (v/v) L-Gln 1 % (v/v) Sodium pyruvate
PT-45	RPMI 1640 medium 5 % (v/v) FCS 1 % (v/v) L-Gln

Co-culture

Cell line/primary cells	**Formulation of medium**
All co-cultures	RPMI 1640 Medium 10 % (v/v) FCS 20 mM HEPES 1 % (v/v) L-Gln 1 % (v/v) Sodium pyruvate 1 % (v/v) Pen/Strep

2.3.4. Growth factors and cytokines

Compound	Final concentration [ng/ml]	Manufacturer
EGF, human recombinant	20	ThermoFisher Scientific, Waltham, USA
GM-CSF, human recombinant	2.4	BioLegend, San Diego, USA
IFNγ, human recombinant	10	BioLegend, San Diego, USA
IL-2, human recombinant	60	BioLegend, San Diego, USA
M-CSF, human recombinant	50	BioLegend, San Diego, USA

2.4. Patient-derived material

2.4.1. Ethics statement

The research project containing serial tissue section from primary tumors and liver metastases of PDAC was approved by the Ethics committee of the Friedrich-Alexander Universität Erlangen-Nürnberg (reference number: 4607) and the Ethics committee of the Medical Faculty of Kiel University (reference number: A110/99). Written informed consent was obtained from all patients.

2.4.2. Histopathology and study cohort

Four patients with primary tumor of PDAC and corresponding liver metastases were included in this study cohort. Tissues from primary PDAC tumors were obtained either from one patient during oncological surgery at the University Hospital Schleswig-Holstein (UKSH) Campus Kiel and from 3 patients during oncological surgery at the University Hospital Erlangen. Corresponding liver metastases tissues were acquired by excision (one patient) or resection. Tissue sections were sectioned, fixed in

formalin, and embedded in paraffin. Tumor grade and stage were classified according to the 7th edition of the UICC guidelines by board-certified surgical pathologists in the Institute of Pathology, UKSH Campus Kiel, or the Institute of Pathology at the University Hospital Erlangen. Clinic-pathological data were obtained from the hospital records of UKSH Kiel and University Hospital Erlangen. Before study inclusion, all patient data were pseudonymized.

2.5. Molecular biological material

2.5.1. Antibodies

2.5.1.1. Antibodies for immunofluorescence staining (IF), immunohistochemistry (IHC), cell culture (CC) and flow cytometry (FC)

Isotype controls

Target (-Conjugate) (Clone)	**Host (Isotype)**	**Concentration in µg/ml**	**Manufacturer**
Isotype-AF647 (MOPC-173)	Mouse (IgG2a, κ)	25	Biolegend, San Diego, USA
Isotype-APC (MOPC-21)	Mouse (IgG1, κ)	200	BioLegend, San Diego, USA
Isotype-APC (MPC-11)	Mouse (IgG2b, κ)	100	Biolegend, San Diego, USA
Isotype-FITC (MOPC-21)	Mouse (IgG1, κ)	500	BioLegend, San Diego, USA
Isotype-PE (MOPC-21)	Mouse (IgG1, κ)	200	BioLegend, San Diego, USA
Isotype-PE (MOPC-173)	Mouse (IgG2a, κ)	200	BioLegend, San Diego, USA
Isotype-PE/Cy7 (MOPC-21)	Mouse (IgG1, κ)	200	BioLegend, San Diego, USA

Antibodies

Antibody (Clone)	**Host (Isotype)**	**Concentration in µg/ml (Dilution)**	**Manufacturer**
CD3 (LN10)	Mouse (IgG1)	32 (IHC 1:100)	Leica Biosystems, Wetzlar, DE
CD3 (UltraLEAF) (OKT3)	Mouse (IgG2a, κ)	1000 (CC 1:666.67)	BioLegend, San Diego, USA
CD4-APC (RPA-T4)	Mouse (IgG1, κ)	50 (FC 1:25)	BioLegend, San Diego, USA
CD8 (4B11)	Mouse (IgG2b)	28.5 (IHC 1:100)	Leica Biosystems, Wetzlar, DE
CD8a-FITC (RPA-T8)	Mouse (IgG1, κ)	200 (FC 1:20)	BioLegend, San Diego, USA
CD14-PE (M5E2)	Mouse (IgG2a, κ)	200 (FC 1:20)	BioLegend, San Diego, USA
CD25-APC (BC96)	Mouse (IgG1, κ)	100 (FC 1:20)	BioLegend, San Diego, USA
CD28 (UltraLEAF) (CD28.2)	Mouse (IgG1, κ)	1000 (CC 1:666.67)	BioLegend, San Diego, USA
CD68 (514H12)	Mouse (IgG2a)	37 (IHC 1:100)	Leica Biosystems, Wetzlar, DE
CD80-APC (2D10)	Mouse (IgG1, κ)	200 (FC 1:20)	BioLegend, San Diego, USA
CD163 (10D6)	Mouse (IgG1)	49 (IHC 1:100)	Leica Biosystems, Wetzlar, DE
CD163-FITC (GHI/61)	Mouse (IgG1, κ)	400 (FC 1:20)	BioLegend, San Diego, USA
CD206-FITC (15-2)	Mouse (IgG1, κ)	200 (FC 1:20)	BioLegend, San Diego, USA
CD274 (PD-L1) (E1L3N)	Rabbit (IgG)	874 (IF 1:200 / IHC 1:100)	Cell signaling Technologies, Danvers, USA

Antibody (Clone)	**Host (Isotype)**	**Concentration in µg/ml (Dilution)**	**Manufacturer**
CD274-PE/Cy7 (MIH3)	Mouse (IgG_1, κ)	200 (FC 1:20)	BioLegend, San Diego, USA
CD279-APC (EH12.2H7)	Mouse (IgG_1, κ)	50 (CC 1:10)	BioLegend, San Diego, USA
CD279-PE (EH12.2H7)	Mouse (IgG_1, κ)	100 (CC 1:10)	BioLegend, San Diego, USA
CTLA-4-PerCP/Cy5.5 (BNI3)	Mouse (IgG_{2a})	100 (FC 1:20)	BioLegend, San Diego, USA
EpCAM-APC (9c4)	Mouse (IgG_{2b})	12 (FC 1:20)	BioLegend, San Diego, USA
PanCK (AE1/AE3)	Mouse (IgG_1)	200 (IHC 1:200)	NeoMarkers via Thermo Fisher Scientific, Waltham, USA
α/β TCR-FITC (IP26)	Mouse (IgG_1, κ)	400 (FC 1:20)	BioLegend, San Diego, USA
αSMA (1A4)	Mouse (IgG_{2a}, κ)	50 (IHC 1:400)	NeoMarkers via Thermo Fisher Scientific, Waltham, USA

2.5.1.2. Blocking antibodies and Isotype controls

Antibody (Clone)	**Host (Isotype)**	**Concentration in µg/ml (Dilution)**	**Manufacturer**
IgG1	Human (IgG1)	5000 (CC: 1:500)	AstraZeneca, Cambridge, UK
Durvalumab	Human (IgG1, κ)	5000 (CC: 1:500)	AstraZeneca, Cambridge, UK
IgG4	Human (IgG4, κ)	1000 (CC: 1:100)	Sigma Aldrich via Merck, St. Louis, USA
Pembrolizumab	Human (IgG4)	1000 (CC: 1:100)	Merck Sharp & Dohme, Kenilworth, USA

2.6. Consumables

Consumable	**Manufacturer**
0.1-10 µl, 10-200 µl, 100-1000 µl pipette tips	Sarstedt, Nümbrecht, DE
1.25 ml, 5.0 ml Dispenser tips	Labsolute via Th. Geyer GmbH & Co. KG, Renningen, DE
1.5 ml, 2.0 ml Eppendorf tubes	Sarstedt, Nümbrecht, DE
12-/24-/96-well plates, flat-bottom	Sarstedt, Nümbrecht, DE
15 ml, 50 ml centrifuge tubes	Sarstedt, Nümbrecht, DE
18 mm coverslips	Menzel, Braunschweig, DE
25 cm^2 cell culture flasks	Sarstedt, Nümbrecht, DE
5 ml, 10 ml, 50 ml serological pipettes	Sarstedt, Nümbrecht, DE
75 cm^2 cell culture flasks	Sarstedt, Nümbrecht, DE
96-*well* plate, V-bottom	Greiner Bio-One GmbH, Frickenhausen, DE
Cell scraper, 25 cm	Sarstedt, Nümbrecht, DE
CryoPure tube, 1.0 ml, white	Sarstedt, Nümbrecht, DE
Eclipse Needle cannula, 30 gauche x 1/2	Becton Dickinson AG, Allschwill, CH
MACS LD columns	Miltenyi Biotec GmbH, Bergisch Gladbach, DE
Micro-Touch nitrile examination gloves	Ansell GmbH, München, DE
Parafilm M sealing film	Brand GmbH & Co. KG, Wertheim, DE
Scalpel	Feather, Osaka, JPN
SuperFrost Plus object slide 76x26 mm	Menzel, Braunschweig, DE
Syringe, 1 ml	Becton Dickinson AG, Allschwill, CH
Transfer pipettes 3.5 ml	Sarstedt, Nümbrecht, DE
Ultra-low attachment (ULA) plates, 96-well, U-bottom	faCellitate, Mannheim, DE
VueLife Closed Culture System, 32 ml	Süd-Laborbedarf, Gauting, DE

2.7. Kit systems

Kit	Manufacturer
Alexa Fluor 488 Tyramide SuperBoost Kit	Thermo Fisher Scientific, Waltham, USA
CD8+ T cell isolation kit, human	Miltenyi Biotec GmbH, Bergisch Gladbach, DE
LEGENDplex, custom human panel	BioLegend, San Diego, USA
M30 CytoDeath™ (PEVIVA®)	TECOmedical AG, Sissach, CH
MojoSort human CD14+ monocytes isolation kit	BioLegend, San Diego, USA
peqGOLD Total RNA Kit	PeqLab, Erlangen, DE
PEVIVA M30 CytoDeath Kit	Diapharma, West Chester, USA
RevertAid First Strand cDNA Synthesis Kit	Thermo Fisher Scientific, Waltham, USA

2.8. Laboratory Devices

Incubators

Device	Manufacturer
BBD 6220 CO_2 incubator	Thermo Fisher Scientific, Waltham, USA
HERA Cell 240 incubator	Thermo Fisher Scientific, Waltham, USA

Measuring devices

Device	Manufacturer
BD FACSCalibur flow cytometer	Beckton, Dickinson and Company, Franklin Lakes, USA
BD FACSymphony flow cytometer	Beckton, Dickinson and Company, Franklin Lakes, USA
Infinite 200 Pro microplate reader	Tecan Group, Männedorf, CH
LightCycler 480 II	Roche, Basel, CH
MACSQuant X Flow cytometer	Miltenyi Biotec GmbH, Bergisch Gladbach, DE
Neubauer counting chamber	Marienfeld Superior GmbH & Co. KG, Lauda-Königshofen, DE
pH meter 7110	inoLab, Weilheim, DE

Microscopes

Device	Manufacturer
AE2000	Motic, Wetzlar, DE
Lionheart FX Automated Microscope	BioTek, Bad Friedrichshall, DE
NyOne	SYNENTEC, Elmshorn, DE

Pipettes

Device	Manufacturer
Finnpipette F1 0.2 – 2 µl	Thermo Fisher Scientific, Waltham, USA
Finnpipette F1 1 – 10 µl	Thermo Fisher Scientific, Waltham, USA
Finnpipette F1 2 – 20 µl	Thermo Fisher Scientific, Waltham, USA
Finnpipette F1 20 – 200 µl	Thermo Fisher Scientific, Waltham, USA
Finnpipette F1 100 – 1000 µl	Thermo Fisher Scientific, Waltham, USA
Finnpipette F1 multi-channel 30 – 300 µl	Thermo Fisher Scientific, Waltham, USA
PIPETBOY acu	Integra Biosciences, Fernwald, DE
Ripette	Ritter, Schwabmünchen, DE

Sterile benches

Device	Manufacturer
HERA Safe	Thermo Fisher Scientific, Waltham, USA
HERA Safe KS	Thermo Fisher Scientific, Waltham, USA

Scales

Device	Manufacturer
Precisa BJ 2100D	Precisa Gravimetrics AG, Dietikon, CH
Precisa XB120A	Precisa Gravimetrics AG, Dietikon, CH

Centrifuges

Device	Manufacturer
Heraeus Fresco 17	Thermo Fisher Scientific, Waltham, USA
Heraeus Multifuge X1	Thermo Fisher Scientific, Waltham, USA
JE-5.0 Elutriator Rotor	Beckmann Coulter GmbH, Krefeld, DE
Rotino 420 R	Hettich, Tuttlingen, DE
Sunlab Mini Centrifuges	Labdiscount GmbH, Mannheim, DE

Other Devices

Device	Manufacturer
ARPEGE 110, liquid nitrogen tank	Air Liquide GmbH, Düsseldorf, DE
BOND-MAX Autostainer	Leica Biosystems, Wetzlar, DE
Freezer (-20 °C)	Liebherr, Ochsenhausen, DE
Fridge (4 °C)	Liebherr, Ochsenhausen, DE
HERAfreeze Basic freezer (-80 °C)	Thermo Fisher Scientific, Waltham, USA
Laboport vacuum pump	KNF Neuberger, Freiburg, DE
MACS MultiStand	Miltenyi Biotec GmbH, Bergisch Gladbach, DE
Masterflex L/S tubing pump	Cole Parmer Instruments, Novodirect GmbH, Kehl/Rhein, DE
MILLI-Q Reagent Water System	Merck Millipore, Billerica, US
NanoZoomer S60	Hamamatsu photonics, Hamamatsu, JPN
PMS 1000i microplate shaker	Grant bio, Essex, UK
VORTEX Genius 3 vortex shaker	IKA-Werke, Staufen, DE
Water bath	STÖRK-TRONIC, Störk GmbH & Co. KG, Stuttgart, DE

2.9. Software

Software	Manufacturer
BD FACSDiva Software	Beckton Dickinson, Heidelberg, DE
FACSCalibur CellQuest Pro	BD Bioscience, San Jose, USA
FlowJo 10.7.1	FlowJo, LCC, Oregon, USA
Gen5 Data Analysis Software	BioTek, Bad Friedrichshall, DE
GraphPad Prism 9.3.1	GraphPad Software, Boston, USA
LEGENDplex Data Analysis software v8	VigeneTech Inc., Carlisle, USA
MACSQuantify Version 2.13.0.	Miltenyi Biotec GmbH, Bergisch Gladbach, DE
Microsoft Office 365	Microsoft Corporation, Redmond, USA
NDP.view2	Hamamatsu photonics, Hamamatsu, JPN

3. Methods

3.1. Cell biological methods

3.1.1. Cultivation of human PDECs and PDAC cells

Human PDECs and PDAC cells were cultured in 75 cm^2 cell culture flasks in 10 ml of their respective medium (section 2.3.3) to a cell confluence of 80 - 90%. For further cultivation, cells were split at ratios of 1:5 to 1:10 twice a week. To detach adherent cells, the supernatant was discarded, 5 ml of pre-warmed Trypsin/EDTA were added followed by incubation at 37 °C for 10 - 15 min. When the cell layer was detached completely, the proteolytic reaction was stopped by adding 5 ml of their pre-warmed FCS-containing medium. Afterwards, cell suspension was transferred into a 50 ml tube and centrifuged at 300xg for 5 min at room temperature (RT). Next, supernatant was aspirated and cell sediment was resuspended in 10 ml of its respective culture medium according to the respective dilution ratios. Finally, cells were seeded in 75 cm^2 cell culture flasks and cultured for maintenance, expansion, and experiments at 37 °C, 5 % CO_2, and 86 % humidity.

3.1.2. Long-term storage of PDEC and PDAC cell lines and primary human lymphocytes in liquid nitrogen

All PDEC and PDAC cell lines as well as isolated human primary lymphocytes were long-term stored in liquid nitrogen. A cell number of $30x10^6$ lymphocytes or a full cultivation flask of PDEC or PDAC cell lines per cryo tube were used for long-term storage. First, cells were centrifuged at 300xg, 8 min at RT, and supernatant was discarded. Thereafter, cell sediment was resuspended in 1 ml FCS supplemented with 10 % (v/v) DMSO. Next, the cell suspension was transferred into cryotubes and stored at -80 °C for 24 h. After one day, the cryotubes were transferred into an ARPEGE 110 tank filled with liquid nitrogen.

3.1.3. Thawing of frozen cells

Frozen cells were rapidly thawed by adding their respective pre-warmed culture medium (37 °C) into the cryo tube. Already liquified cell suspension was placed in a 50 ml tube with 10 ml of fresh pre-warmed culture medium. For PDEC and PDAC cell lines 10 ml of culture medium were used per cryotube, for primary human lymphocytes 3 cryo tubes were diluted in 10 ml culture medium. Afterward, diluted cell suspension was centrifuged at 200xg, 5 min at RT to remove dead cells. Cell sediments of PDEC and PDAC cell lines were resuspended in their respective culture medium and

further cultivated (section 3.1.1) and cell sediments of human lymphocytes were resuspended in cold MACS buffer for following isolation of naïve CD8+ T cells (section 3.1.7).

3.1.4. Cell counting

To ensure of seeding appropriate cell numbers in experiments, the cell count was manually determined using a Neubauer counting chamber. After resuspension of the cell suspension, 10 µl of cell suspension were used to completely fill the counting chamber. Only light-breaking cells in 2 opposing quadrants were counted, their mean value was calculated and the chamber factor of 10^4 was added. The vital cell number was calculated by the following formula:

$$\frac{counted\ cell\ number}{counted\ squares} \cdot 10^4 = \frac{counted\ cells}{ml}$$

3.1.5. Isolation peripheral blood mononuclear cells (PBMCs)

Lymphocytes and monocytes were isolated from leukoreduction system chambers (LRSC) of healthy blood donors. These donors gave their informed consent. The LRSC comprises leukocyte concentrate composing numerous blood cell populations including lymphocytes and monocytes. For separation of PBMCs from other blood components like erythrocytes, granulocytes and debris, a density gradient centrifugation with pancoll was performed. For that purpose, two 50 ml tubes were filled with 10 ml of pancoll and slowly overlayed with 40 ml of leukocyte concentrate/PBS mixture (1:11) to generate two separate phases. Next, the 50 ml tubes were centrifuged for 25 min, 350xg at RT with slow acceleration and without mechanical deceleration. After centrifugation, the upper PBS phase was discarded and the two interphases containing PBMCs were collected in another 50 ml tube and filled up with MACS buffer to 50 ml. Afterwards, the mixture was centrifuged for 8 min, 300xg at 4 °C followed by supernatant discard and resuspension in 10 ml erythrocyte lysis buffer for elimination of remaining erythrocytes. The erythrocyte lysis buffer was incubated for 6 min at RT in the dark, subsequently filled up with elutriation buffer to 50 ml, and centrifuged at previous conditions. Next, the cell sediment was resuspended in 50 ml elutriation buffer and counted. A cell number of $8x10^8$ to $1.2x10^9$/50 ml was used for the following counterflow centrifugation (elutriation).

3.1.6. Counterflow centrifugation (elutriation)

Counterflow centrifugation was performed to separate lymphocytes from monocytes according to their differential sedimentation potential (Figure 6). For this purpose, the tubing system and the

elutriation chamber were washed with 70 % ethanol in ddH_2O, followed by water and cold elutriation buffer. The determined cell number of PBMCs was loaded into the system at 3500 rpm and 4 °C. The pumping flowrate was started at 26 ml/min and the system was washed with 200 ml elutriation buffer.

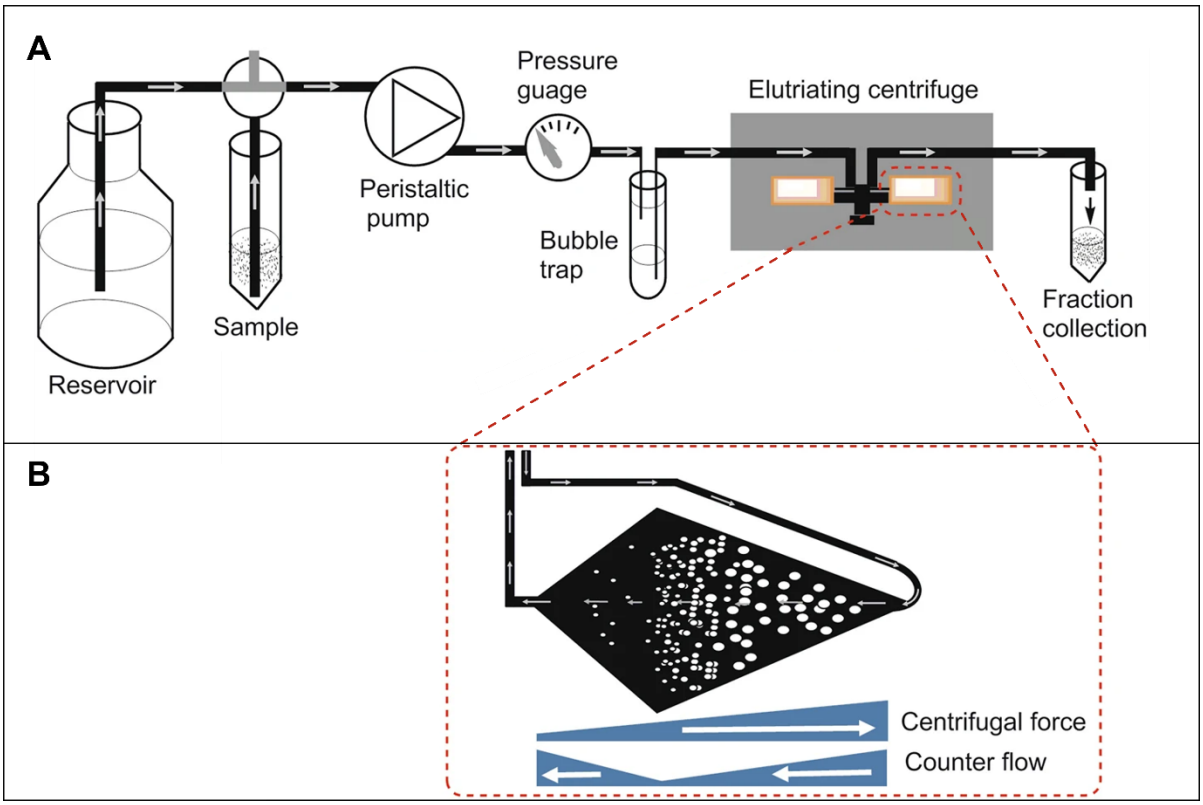

Figure 6: Schematic illustration of counterflow centrifugation (A) and principle of separation (B). PBMCs acquired from density gradient centrifugation are loaded into the elutriation system. The different cell populations are separated according to their different sedimentation potentials. The constant centrifugal force and the increasing counter flow, created by the peristaltic pump, separate different cell populations [206].

The first 3 fractions of 50 ml cell suspension were saved at flowrate of 26 ml/min. Then, the different fractions were collected by increasing the flow rate in 2 ml/min steps until fraction of 32 ml/min was reached. Next, flow rate was enhanced by 1 ml/min steps until the last fraction of 43 ml/min was acquired, the centrifugation was stopped, and the stop fraction was collected. The fractions 26 to 34 ml/min mostly contained lymphocytes, whereas fractions 35 to 40 ml/min comprised a lymphocyte/monocytes mixture and fractions above 41 ml/min yielded monocytes. The purity of fractions was determined by flow cytometric analysis via forward/side scatter. Next, all fractions with a higher purity than 85 % were centrifuged for 8 min, 200xg, and 4 °C to remove dead cells and were washed with PBS. The lymphocyte-enriched cell sediments were prepared for long-term storage in liquid nitrogen (section 3.1.2). The monocyte-enriched fractions above 85 % were used for following macrophage polarization (section 3.1.10).

3.1.7. Isolation of primary human CD8+ T cells

After counterflow centrifugation, frozen lymphocytes were thawed (section 3.1.3) and the cell number was determined, including dead cells to load a proper cell number to the LD columns in the following step. For the isolation of human CD8+ T cells the MACS isolation kit from Miltenyi was used, following modified manufacturer's instructions with reduced antibody and bead concentrations (50 %) and extended incubation times (1.5-fold). The advantage of negatively isolated cells is that the cell population to be isolated stayed unaffected whereas all other cell populations remained in the magnetic column due to antibody and bead binding. Cold and degassed MACS buffer was used for CD8+ T cell isolation and equilibration of columns was performed by preventing air bubbles in the system ensuring an optimal isolation. Thawed lymphocytes, whose total cell number was previously determined, were centrifuged at 300xg for 8 min and 4 °C. Cell sediment was resuspended in MACS buffer resulting in a concentration of 10^7 cells per 40 µl MAC buffer. Subsequently, 5 µl of biotin-antibody cocktail per 10^7 cells were added and incubated for 8 min at 4 °C. Afterwards, 30 µl MACS buffer and 10 µl of MicroBead cocktail per 10^7 cells were added, mixed thoroughly without forming air bubbles, and incubated for 15 min at 4 °C. During this incubation, MACS LD columns were equilibrated. For this purpose, LD columns were placed in a MACS MultiStand and 5 ml of MACS buffer were added to ensure equilibration of all LD columns. After MicroBead cocktail incubation, suspension was added evenly to the equilibrated columns. In order to collect the isolated CD8+ T cells, new 50 ml tubes filled with 5 ml of fresh MACS buffer were placed under the columns. After cell suspension had entered the LD columns, additional 5 ml of MACS buffer were added to the columns to isolate all unbound CD8+ T cells. Finally, all isolated CD8+ T cells were pooled, the cell number of living cells was determined and used for further activation culture (section 3.1.8). The purity of the isolated cells was checked by immunofluorescence staining of αβ T cell receptor (αβTCR), CD4 and CD8, and measured by a flow cytometer (section 3.2.1.1).

3.1.8. Activation and cultivation of primary human CD8+ T cells

The activation of primary human CD8+ T cells was conducted with a purified immobilized α-CD3 and soluble α-CD28 targeting antibody to create an artificial but physiological-like situation of T cell activation resulting in T cell proliferation and cytokine production [207]. For this purpose, a 24-well polystyrene plate was incubated for 2 h at 37 °C with 200 µl of 1.5 µg/ml α-CD3 antibody in PBS to allow a proper binding of the antibodies to the polystyrene surface of the plate. After 2 h, unbound antibody was discarded and all wells were washed twice with PBS. Then, 1.3 – 1.8 x 10^6 CD8+ T cells

were cultivated in 1 ml TCM per well. Additionally, 1.5 µg/ml α-CD28 antibody and 60 ng/ml IL-2 were added to the medium and cultured for 3 to 4 days at 37 °C, 5 % CO_2, and 86 % humidity.

3.1.9. Negative isolation of CD14+ primary human monocytes

For all 3D experiments, where a lower cell number of macrophages was needed, a negative isolation of CD14+ monocytes was performed by using a human CD14+ monocytes isolation kit from Biolegend according to a modified protocol of the manufacturer. All following information refers to a cell number of 10^7 cells. Briefly, PBMCs were resuspended in 100 µl MACS buffer, 1.25 µl Fc receptor blocking solution were added and incubated for 15 min at RT. Next, 2.5 µl of Biotin-antibody cocktail were added and incubated at 4 °C for 25 min. Afterwards, Streptavidin nanobeads were resuspended by vortexing, and 2.5 µl were added to the cell-antibody solution and incubated again for 25 min at 4 °C. Then, cell-antibody suspension was filled up to 4 ml with MACS buffer and centrifuged for 5 min at 300xg at 4 °C. The supernatant was discarded, and cell sediment was resuspended in 2.5 ml MACS buffer. The 4 ml tube was inserted into the magnet and negative selection was performed for 10 min. Afterwards, the remaining solution containing monocytes was collected in a fresh 50 ml tube. The remaining cells were washed with 2.5 ml MACS buffer and again inserted into the magnet for 10 min. Finally, the monocyte solution was collected in 50 ml, and purity measuring the forward scatter/side scatter (FSC/SSC) by a flow cytometer was performed.

3.1.10. Polarization and cultivation of primary human macrophages

Macrophages can arise as pro-inflammatory M1- or anti-inflammatory M2-macrophages. For *in vitro* experiments, polarization of isolated monocytes (sections 3.1.6) into M1- and M2-like macrophages was performed by stimulation with GM-CSF and M-CSF, respectively.

Counter flow fractions with a purity over 85 % were resuspended in M2 medium, collected in one 50 ml tube, and counted. For all 2D experiments, $15x10^6$ monocytes were transferred into a 50 ml tube. Afterwards, the cell suspension was filled up to 27 ml with either M1 medium or M2 medium, and either 2.4 ng/ml GM-CSF or 50 ng/ml M-CSF were added. Then, monocytes were transferred in VueLife culture bags and cultivated for 6 to 7 days at 37 °C, 5 % CO_2, and 86 % humidity. To isolate macrophages after their polarization culture, the VueLife bags were kept on ice for 30 min, macrophages were carefully detached by mechanical action, and the cell suspension was transferred into 50 ml tubes. To ensure that most of the macrophages were detached from the bags, the cultivation bags were rinsed with 20 ml of pre-warmed PBS. Then, cells were centrifuged at 300xg for 8 min at RT and cell sediments

were resuspended in the respective culture medium. Next, the cell number was determined (section 3.1.4) to obtain the required cell numbers for further experiments.

If the purity of monocyte fractions was too low, an intermediate step was performed to ensure a higher purity. In this case, the monocyte fractions were pooled, counted, and seeded in 10 cm petri dishes overnight. The seeded cell number was dependent on the purity of monocytes so that a final cell number of $10x10^6$ monocytes were allowed to adhere to the petri dish surface. The next day, the supernatant was discarded and the cells were rinsed with warm PBS to eliminate remaining lymphocytes. Afterward, monocytes were detached with 5 ml accutase for 15 min at 37 °C, scratched from the petri dish surface, filled up with 5 ml M2 medium, and centrifuged at 300xg, 8 min at RT. The cell sediment was resuspended in M2 medium and the cell number was determined.

The polarization of monocytes into M1- and M2-like macrophages for all 3D experiments was done in 12-well plates for 6 to 7 days at 37 °C, 5 % CO_2, and 86 % humidity. For this purpose, $2x10^6$ monocytes were seeded per 12-well and stimulated either with 2.4 ng/ml GM-CSF for M1-like macrophage polarization or 50 ng/ml M-CSF for M2-like macrophage polarization.

3.1.11. CD8+ T cell kinetic during and after activation culture

$1.3 – 1.8 \times 10^6$ CD8+ T cells were cultured in 24 well plates, where α-CD3, α-CD28 antibodies and IL-2 were added for T cell activation (section 3.1.8). Every day during activation culture, supernatants were collected and two wells of CD8+ T cells were washed twice with 1 ml PBS and centrifuged at 300xg and RT for 8 min to remove activation stimuli. Then, immunofluorescence staining (section 3.2.1.1) was conducted. After 4 days of activation culture, remaining CD8+ T cells were also washed twice with PBS and re-seeded in 24 well plates (in the absence of stimuli) until day 7 after start of activation culture. Again, during the entire culturing period cell culture supernatants were daily collected, and immunofluorescence staining was performed.

3.1.12. Mono- and co-culture 2D experimental settings

3.1.12.1. Durvalumab pre-treatment of CD8+ T cells in 2D

For 2D Durvalumab pre-treatment experiments, the following steps were performed (Figure 7):

Day 0: CD8+ T cell isolation and activation of T cells were performed.

Day 3: Restimulation of CD8+ T cells with IL-2.

Day 4: CD8+ T cells were mono-cultured in 12-well plates for 72 h. Additionally, either IgG1 or Durvalumab was applied to the CD8+ T cell culture.

Day 7: Characterization of pre-treated CD8+ T cells was performed by immunofluorescence staining for flow cytometric analysis. Further, CD8+ T cells were used for following PDAC viability assay (section 3.1.12.4) at day 7.

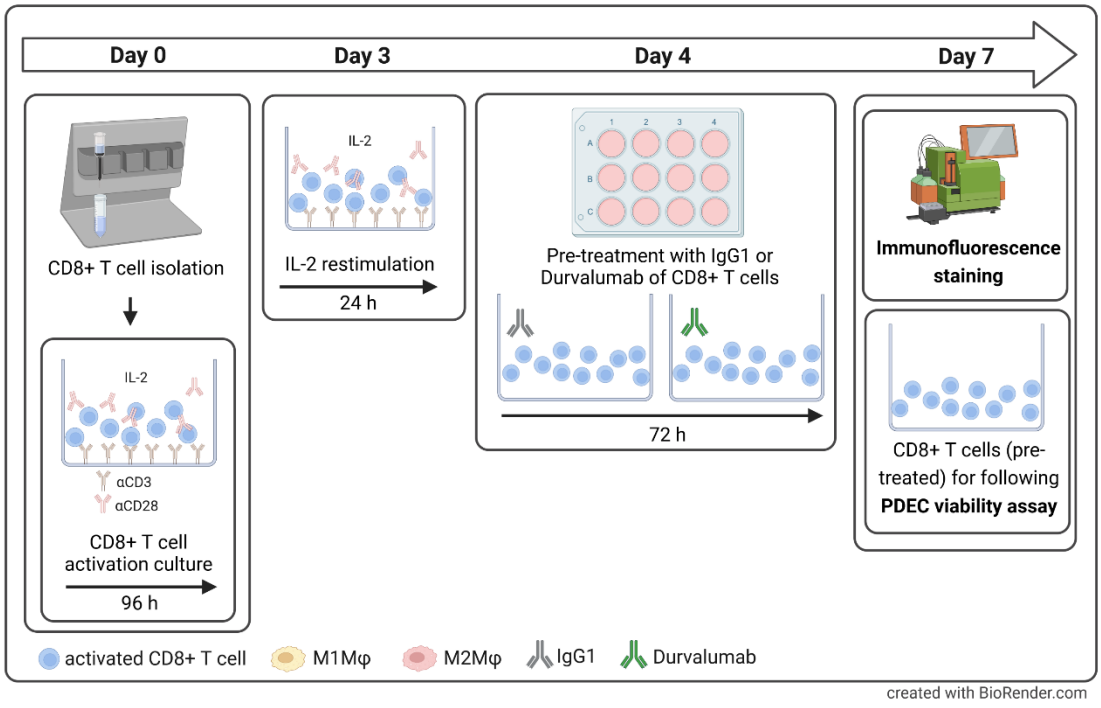

Figure 7: Experimental setting of Durvalumab pre-treatment of CD8+ T cells. Human CD8+ T cells were isolated out of human lymphocytes and activated via αCD3 antibody, αCD28 antibody, and IL-2 for 4 days. On day 3, IL-2 was applied again. Mono-culture of CD8+ T cells and treatment with either IgG1 or Durvalumab (10 µg/ml) were performed on day 4 for 72 h. Finally, immunofluorescence staining of activation markers and PD-1, PD-L1, and CD80 on CD8+ T cells was conducted on day 7. Additionally, CD8+ T cells were used for following PDAC viability assay.

3.1.12.2. Durvalumab treatment in direct co-culture of CD8+ T cells and PDEC in 2D

For 2D Durvalumab treatment in direct co-culture of CD8+ T cells and PDEC experiments, the following steps were performed (Figure 8):

Day 0: CD8+ T cell isolation and activation of T cells was performed.

Day 3: Restimulation of CD8+ T cells with IL-2. PDEC were labeled with CellTracker green (section 3.1.14) and seeded in 96-well plates ($5x10^4$ cells per 96 well).

Day 4: CD8+ T cells ($1x10^6$ cells per 96 well) were co-cultured with CellTracker green labeled PDEC for 24 h. Additionally, either IgG1 or Durvalumab was applied to the co-culture.

Day 5: PDEC viability assay was performed (section 3.1.12.4).

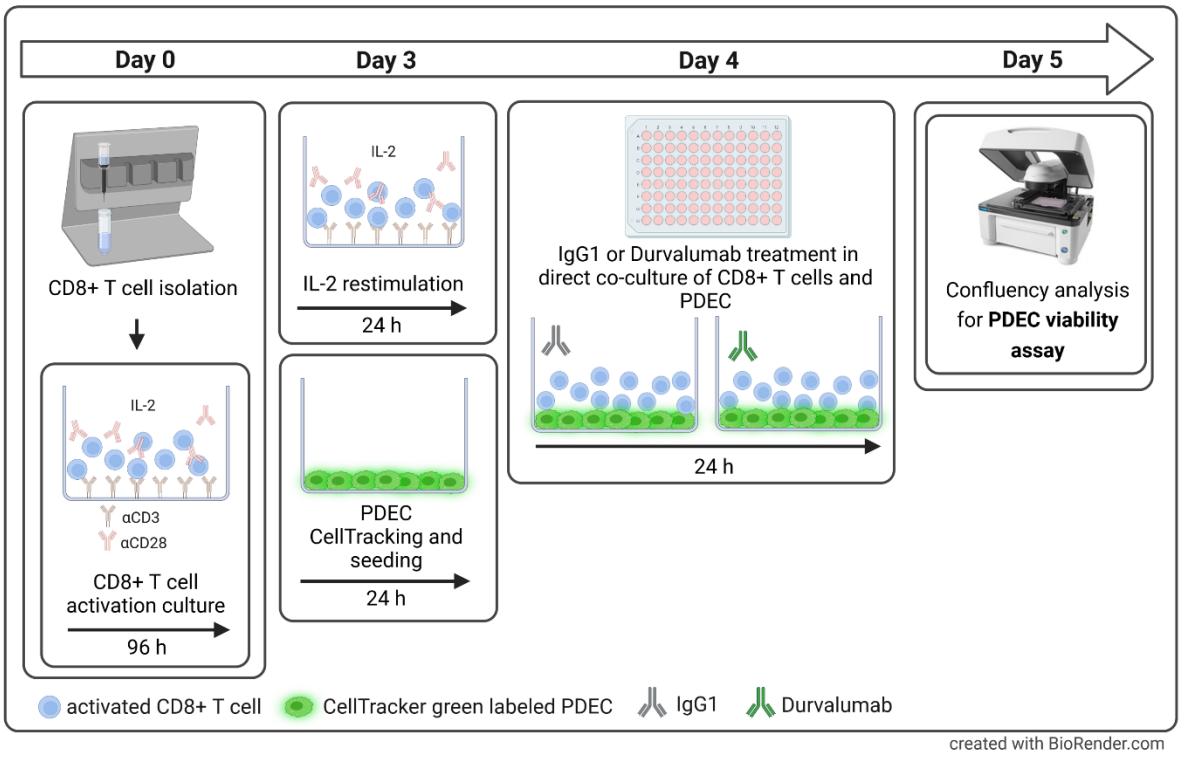

Figure 8: Experimental setting of Durvalumab treatment in direct co-culture of CD8+ T cells and PDECs. Human CD8+ T cells were isolated out of human lymphocytes and activated via αCD3 antibody, αCD28 antibody, and IL-2 or 4 days. On day 3, IL-2 was applied again to the T cells. In parallel, PDEC were labeled with CellTracker green and seeded in 96-well plates. On day 4, CD8+ T cells were co-cultured and treatment with either IgG1 or Durvalumab (10 µg/ml) was performed on day 4 for 24 h. Finally, fluorescence confluence analysis was assessed for PDEC viability assay.

3.1.12.3. Mono- and co-culture of macrophages and CD8+ T cells in 2D

For 2D mono- and co-culture experiments, polarized M1- or M2-like macrophages and pre-activated CD8+ T cells were seeded in 12-well plates. Culture occurred according to the following schedule (Figure 9).

Day 0: Macrophages were isolated and polarized for 7 days.

Day 3: CD8+ T cell isolation and activation of T cells was performed.

Day 6: Restimulation of CD8+ T cells with IL-2.

Day 7: M1- and M2-like macrophages were detached from polarization cultures and seeded ($1x10^6$ cells per well). After 3 h when macrophages had attached to the plate surface, pre-activated CD8+ T cells ($1x10^6$ cells) were co-cultured with macrophages in TCM. In parallel, macrophages and CD8+ T cells were cultured in mono-culture under identical conditions. To maintain the polarization of mono-

and co-cultured macrophages, either GM-CSF or M-CSF was added. Mono- and co-cultures of macrophages and CD8+ T cells were conducted for 48 h.

Day 9: Characterization of CD8+ T cells and macrophages was performed by immunofluorescence staining for flow cytometric analysis. Mono- or co-cultured CD8+ T cells were also used for following PDAC viability assay (section 3.1.12.4) at day 9.

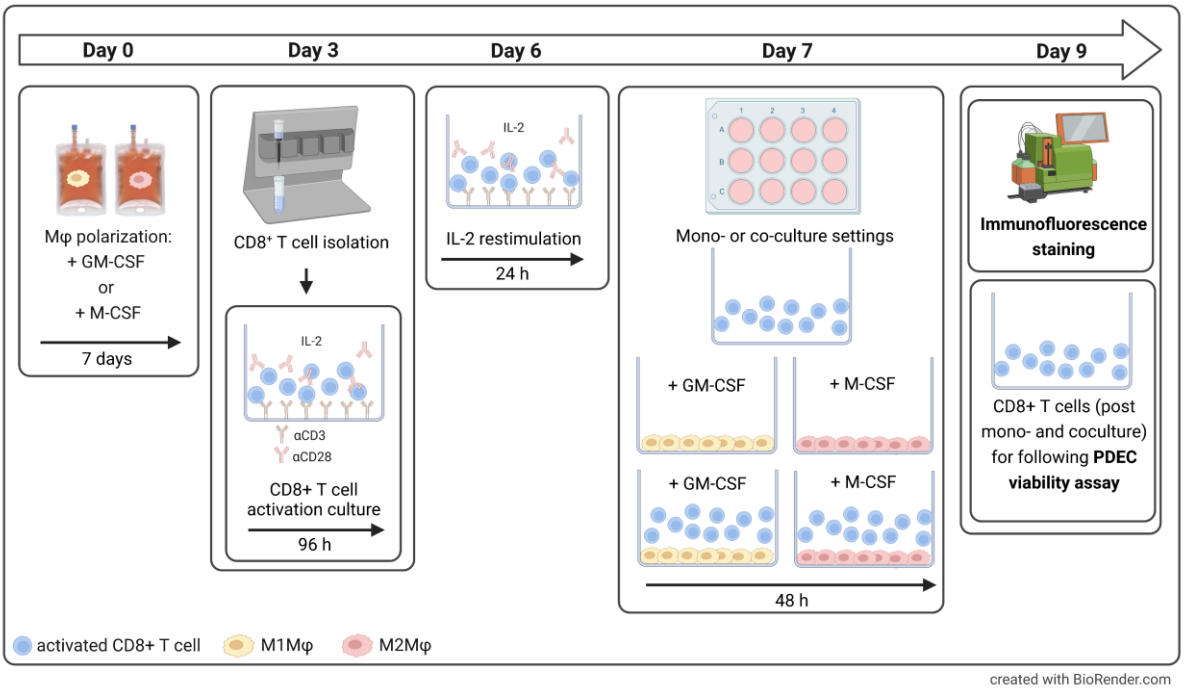

Figure 9: Experimental setting of CD8+ T cells and M1- or M2-like macrophage co-cultures. Isolated human monocytes were polarized for 7 days into M1- or M2-like macrophages by stimulation with Granulocyte-Macrophage Colony Stimulating Factor (GM-CSF) or Macrophage Colony Stimulating Factor (M-CSF). Human CD8+ T cells were isolated out of human lymphocytes and activated via αCD3 antibody, αCD28 antibody, and IL-2 for 4 days. On day 6, IL-2 was applied again to the T cells. Mono- and co-cultures of CD8+ T cells and M1- or M2-like macrophages were performed on day 7 for additional 48 h. Finally, Immunofluorescence staining of activation markers and PD-1, PD-L1, and CD80 on CD8+ T cells as well as polarization status of macrophages was conducted on day 9. Additionally, after 48 h mono- or co-culture with different macrophages, CD8+ T cells were used for following PDAC viability assay.

3.1.12.4. PDEC viability assay in 2D

Pre-activated CD8+ T cells (either pre-cultured with macrophages for 48 h, pre-treated with IgG1 or Durvalumab, or directly after 4-day activation culture and additional IgG1 or Durvalumab treatment) and CellTracker green labeled H6c7-KRAS and PancTu1 cells (section 3.1.14) were co-cultured to asses PDEC viability based on fluorescence confluence analysis. Mono-cultured PDECs were cultured as a control in parallel. All cultures were conducted according to the following schedule (Figure 10):

Day 0: CellTracker green labeling of PDECs and seeding in 96-well plate ($5x10^4$ cells per 96-well).

Day 1: PDECs were cultured alone (mono) or together with CD8+ T cells ($1x10^6$ CD8+ T cells per well) and PDEC fluorescence confluence was measured at timepoint 0 h.

Day 2: CD8+ T cells were discarded and PDECs were washed with PBS. Then, the fluorescence confluence of PDEC was measured at timepoint 24 h.

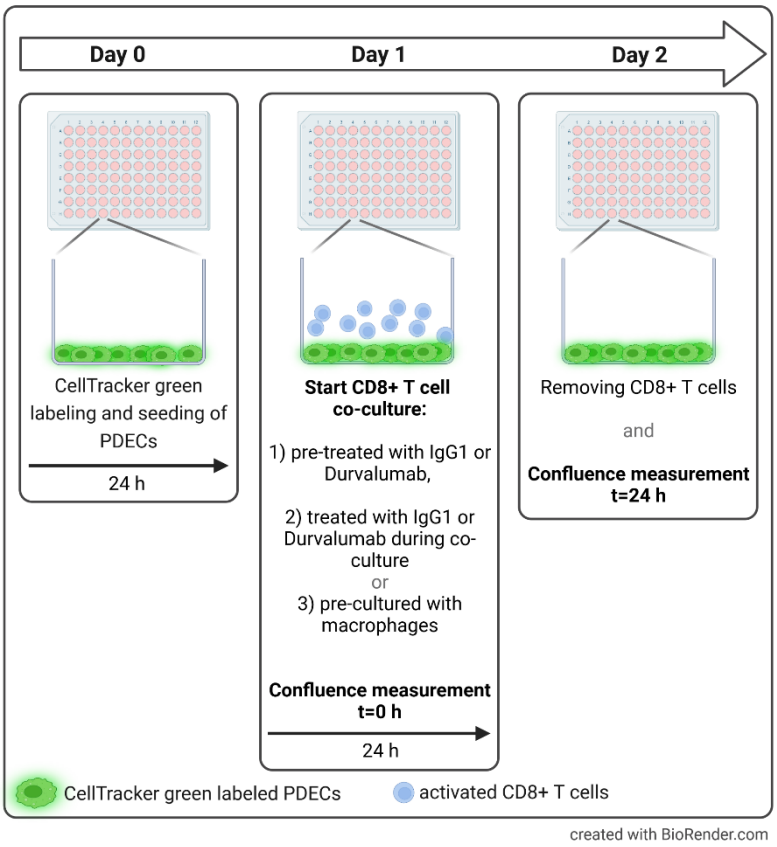

Figure 10: Schematic illustration of 2D PDEC viability assay. H6c7-KRAS or PancTu1 cells were labeled with CellTracker green and seeded in 96-well plates to adhere to the plate bottom. After 24 h, co-culture with CD8+ T cells was started and fluorescence confluence was measured at timepoint 0 h. PDEC viability was assessed after 1) CD8+ T cell pre-treatment with either IgG1 or Durvalumab for 3 days, 2) IgG1 or Durvalumab treatment during direct co-culture of pre-activated CD8+ T cells and PDECs, or 3) pre-culture of CD8+ T cells with both macrophage populations. On day 2, CD8+ T cells were discarded, PDECs were washed and fluorescence confluence was determined at timepoint 24 h.

In order to evaluate the PDEC viability, the ratio of confluence of timepoint 0 h and 24 h was calculated for respective co-culture or treatment conditions. Next, these ratios were normalized to PDEC mono-cultured samples to visualize specifically effects of co-cultures or treatment. Further, when treatment was applied, the normalized confluence ratio was normalized to respective IgG1 control ratios to picture only effects of specific treatment. Ratios >1 reflect increased PDEC viability, while ratios <1 indicate decreased PDEC viability.

3.1.13. Mono- and co-culture 3D experimental settings

3.1.13.1. Co-culture of PDAC spheroids and macrophages

PDAC cell lines and macrophages were detached as described in sections 3.1.1 and 3.1.10. The cell sediments were resuspended in TCM and the cell number was determined.

The following spheroid seeding was performed in 96-well ultra-low attachment (ULA) plates. For spheroid seeding, a final cell number of $2x10^4$ cells per well was used. To generate mono-cultured spheroids, $2x10^4$ PDAC cells were seeded. The PDAC/macrophage ratio 1:1 consisted of $1x10^4$ PDAC cells and $1x10^4$ macrophages, whereas the ratio 3:1 comprised $1.5x10^4$ PDAC cells and $0.5x10^4$ macrophages. All different culture conditions were seeded at the same timepoint in 150 µl TCM and incubated for 24 h or 72 h at 37 °C, 5 % CO_2, and 86 % humidity to allow spheroid formation.

To characterize the localization of cell populations and the PD-L1 status of tumor cells and macrophages as well as macrophage polarization in spheroid co-culture, the following experimental approach was conducted (Figure 11):

Day 0: Monocytes were isolated and polarized into M1- or M2-like macrophages for 7 days.

Day 7: Seeding of mono- or co-cultured PDAC spheroids was conducted.

Day 10: Characterization of macrophage polarization and PD-L1 status of macrophages and PDAC cells was performed via immunofluorescence staining and measured by a flow cytometer.

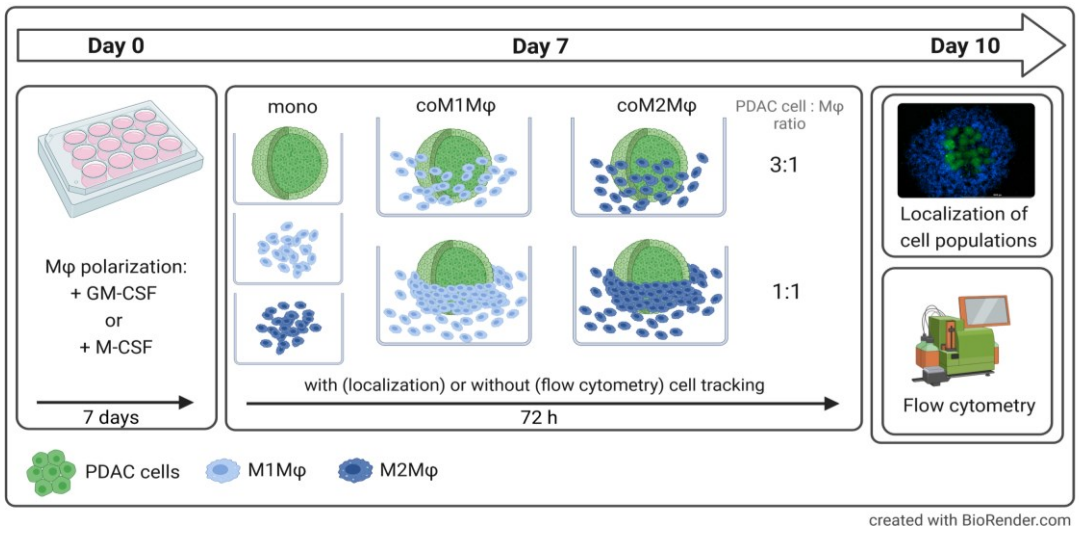

Figure 11: Schematic illustration of 3D co-culture setting with PDAC cells and M1- or M2-like macrophages. Isolated monocytes were polarized for 7 days into M1- or M2-like macrophages by stimulation with Granulocyte-Macrophage Colony Stimulating Factor (GM-CSF) or Macrophage Colony Stimulating Factor (M-CSF). Seeding of polarized macrophages and PDAC cells in different cell ratios was performed in ultra-low attachment plates on day 7. To analyze the localization of cell populations, PDAC cells were labeled with CellTracker green and macrophages with CellTrace violet. To examine PD-L1 expression by flow cytometry, unlabeled cells were used. After 3 days of spheroid formation and cultivation, analysis of localization, PD-L1 status, and macrophage polarization was conducted.

3.1.13.2. Co-culture of PDAC spheroids, macrophages and CD8+ T cells in the absence or presence of additional treatment

For the analysis of PDAC cell death and CD8+ T cell activation stage and effector phenotype, the experimental setup was conducted as followed (Figure 12):

Day 0: Monocytes were isolated and polarized into M1- or M2-like macrophages for 7 days.

Day 6: Isolation and activation of CD8+ T cells were performed.

Day 7: Seeding of mono- or co-cultured PDAC macrophage spheroids was conducted.

Day 8: Treatment with 10 µg/ml Gemcitabine or spheroids were left untreated.

Day 9: Medium was changed and CD8+ T cells were added at a 1:10 target cell/effector cell ratio. Either treatment with 10 µg/ml Durvalumab or Pembrolizumab or their respective isotype control was started or spheroid cultures were left untreated.

Day 10: Collection of supernatants and characterization of CD8+ T cells via immunofluorescence staining and flow cytometry analysis was performed.

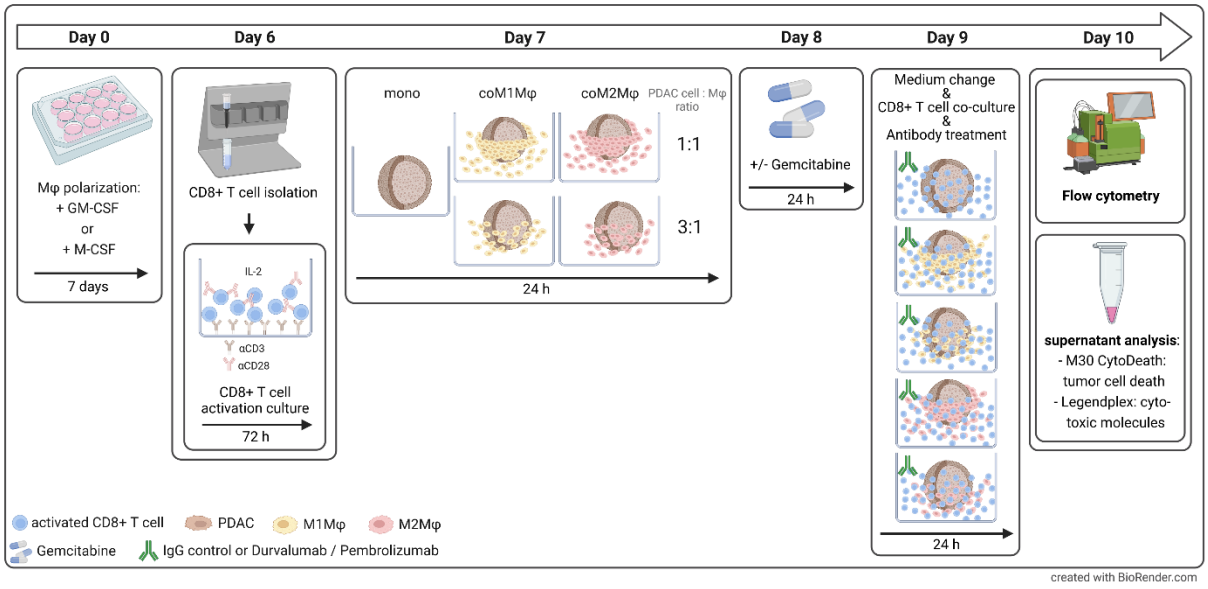

Figure 12: Schematic illustration of 3D co-culture experiments comprising PDAC cells, M1- or M2-like macrophages, and CD8+ T cells. Isolated monocytes were polarized into M1- or M2-macrophages for 7 days. After 6 days, separated and frozen lymphocytes were used for magnetic-activated cell sorting to isolate CD8+ T cells. CD8+ T cells were activated by stimulation with α-CD3 antibody, α-CD28 antibody, and IL-2 for 3 days. On day 7, the start of mono- or co-culture spheroid formation was conducted with M1- or M2-like macrophages and PDAC cells. One day later, either treatment with Gemcitabine (10 µg/ml) was started, or spheroids remained untreated for 24 h. On day 9, the medium was changed, and activated CD8+ T cells were added or spheroids were cultured in the absence of CD8+ T cells. Additionally, some experiments included treatment with immune checkpoint inhibitor Durvalumab or Pembrolizumab or their respective IgG isotype controls on day 9 for 24 h. On day 10, supernatants were collected following epithelial cell death analysis and cytotoxic molecule examination. Furthermore, CD8+ T cells were analyzed concerning their activation stage and expression of PD-1 and PD-L1 by immunofluorescence staining and flow cytometric analysis.

3.1.14. Cell tracking via fluorescent probes

In order to assess the PDEC viability in 2D cultures (section 3.1.12.4) and to discriminate different cell populations in 3D co-cultures (section 3.1.13.1), two fluorescent dyes were used to specifically label different cell populations. PDECs were labeled with the fluorescent dye 5-Chlormethylfluoresceindiacetat (CellTacker™ Green CMFDA) in 2D as well as 3D culture experiments, whereas macrophages in 3D cultures were labeled by CellTrace™ Violet. Briefly, the respective number of cells was centrifuged at 300xg and RT for 5 min. Afterwards, supernatants were discarded, and cell sediments were resuspended in the staining solution with the diluted dye and incubated at indicated temperature and time (Table 4). If necessary, the staining reaction was quenched with respective medium. Next, cells were centrifuged again at 300xg, RT for 5 min and subsequently counted and seeded. The evaluation of fluorescent confluence and visualization of different cell populations was conducted by a Lionheart FX Automated Microscope.

Table 4: Staining requirements for fluorescent dyes CellTrackerTM Green CMFDA and CellTraceTM Violet

Tracker/Tracer	Cell population	Cell number	Dilution	Dilution vehicle	Label conditions	Quench with medium
CellTracker™ Green CMFDA	PDEC	$5x10^5$/ml	1:2000	FCS-free medium	30 min, 37 °C	no
CellTrace™ Violet	macrophages	$2x10^5$/ml	1:2000	PBS	20 min, 37 °C	5X staining volume

3.2. Immunobiological methods

3.2.1. Immunofluorescence staining

3.2.1.1. Flow cytometry

The immunofluorescence staining was performed to study the expression of cell surface molecules on different cell populations. In the beginning, cells were counted (section 3.1.4), and 1.5 – $2x10^5$ cells were used for stainings (except 3D experiments where all cells were used). Then, cells were washed with PBS and blocked with 2.5 µl FcR and 25 µl MACS buffer. All following steps were conducted on ice. After FcR blocking, the cells were centrifuged in a V-bottom plate at 300xg, 4 °C for 8 min. The supernatant was discarded, and the cell sediment was resuspended in 25 µl of fluorescent dye-linked antibody staining solution. The staining solution was incubated for 30 min. Next, 175 µl MACS buffer were added and the plate was centrifuged again to discard the staining solution. The cell sediments were resuspended in 200 µl MACS buffer and centrifuged. As a last step, the cell sediments were fixed

in 150 µl 1 % PFA in MACS buffer. The measurement was conducted by a MACSQuant X and analyzed by FlowJo software.

3.2.1.2. Immunofluorescence staining for PD-L1 on cover-slip-seeded macrophages

To visualize PD-L1 expression on macrophages, the Alexa Fluor 488 Tyramide SuperBoost Kit (Thermo Fisher Scientific) was used according to the manufacturer's instructions. For this purpose, $1x10^6$ M1-like or M2-like macrophages were seeded on 18 mm coverslips in 12-well flat bottom plates. After 3 h of attachment, either activated CD8+ T cells ($1x10^6$ per 12-well) were added or macrophages were further mono-cultured for 48 h. Mono- or co-cultures with M1-like macrophages were stimulated with GM-CSF and cultures with M2-like macrophages with M-CSF for the culturing period. After 48 h, CD8+ T cells were discarded and macrophages were washed twice with PBS to eliminate remaining CD8+ T cells. Next, cells were fixed with 4 % PFA solution for 10 min and washed trice with PBS for 5 min. Then, macrophages were incubated with 3 % Hydrogen Peroxide Solution (Compound C2) for 1 h at RT in a humidified chamber. Afterwards, coverslips were rinsed trice with PBS and incubation with α-rabbit-PD-L1 antibody (clone E1L3N, Cell Signaling) diluted 1:200 in 1 % BSA/PBS was performed overnight in a humidified chamber. Next, the cells were washed again trice with PBS for 5 min and incubated with goat anti-rabbit poly-HRP-conjugated secondary antibody (Compound B) for 1 h at RT in a humidified chamber. Subsequently, cells were washed again trice with PBS for 5 min, and nuclei staining with Hoechst (1:500 in PBS) was performed for 30 min at RT in a humidified chamber. Afterwards, coverslips were washed again three times with PBS for 5 min, and Tyramide solution was added. After 10 min in the dark, reaction was stopped by aspirating the Tyramide solution and adding an equal amount of Reaction Stop Reagent to the coverslips. Then, cells were washed again three times with PBS and once with ddH_2O. Finally, coverslips were sealed upside-down in a drop of Fluoro Gel onto an object slide with clear nail polish. The dried and sealed object slides were stored at 4 °C and PD-L1 immunofluorescence staining was detected by a Lionheart FX Automated Microscope.

3.2.1.3. Propidium Iodide (PI) staining

To test the cell viability of 3D cultured PDEC, a PI staining was performed as PI intercalate into nucleic acids and display red fluorescence only in dead cells without intact plasma membrane [208]. The cell culture medium of PDEC spheroids was discarded, the PI staining solution (1:400 dilution in TCM) was added to spheroids and incubated for 1.5 h to allow PI to penetrate the spheroids. Afterwards, PI staining of spheroids were examined by a Lionheart FX Automated Microscope.

3.2.2. Immunohistochemistry

Immunohistochemical (IHC) stainings of whole mount serial sections from primary tumor and corresponding liver metastases of 4 PDAC patients were kindly performed by Sandra Krüger and Steffen Heckl by an autostainer Bond™ RX System in the Institute of Pathology at the UKSH in Kiel. Stained tissue sections were scanned using a Hamamatsu NanoZoomer 2.0 RS scanner at 400 times magnification and viewed with NDP.view2 software. The research was approved by the ethics committee of the Friedrich-Alexander Universität Erlangen-Nürnberg (reference number: 4607) and the Ethics committee of the Medical Faculty of Kiel University (reference number: A110/99). Written consent was obtained from all patients.

3.2.2.1. IHC single staining

For single IHC stainings, the following antibodies were used: PanCK (clone: AE1/AE3, NeoMarkers via Thermo Fisher Scientific), PD-L1 (clone: E1L3N, Cell Signaling), CD68 (clone: 514H12, Leica Biosystems), CD163 (clone: 10D6, Leica Biosystems), CD3 (clone: LN10, Leica Biosystems), and CD8 (clone: C8144B, Leica Biosystems)

3.2.2.2. IHC double staining

Further, immunohistochemical double stainings of liver metastases were performed. The first step involved the staining of PD-L1 (clone: E1L3N, Cell Signaling). Antigen retrieval was achieved with ER2 (EDTA-buffer Bond pH 9.0; 20 minutes). The antigen retrieval step was modified for the PD-L1 staining of those slides, which were to be combined with an alpha-smooth muscle actin (αSMA) (clone: 1A4, NeoMarkers via Thermo Fisher Scientific) staining in the second step: In those cases, PD-L1 visualization was enhanced in relation to the more intense αSMA signal by prolonging ER2 antigen retrieval to 30 minutes. The immunoreaction was visualized with the Bond™ Polymer Refine Detection Kit resulting in a brown color. The second step involved the staining of either αSMA, CD68, or PanCK. Antigen retrieval was carried out with ER1 (citrate buffer Bond pH 6.0; 20 minutes for αSMA), or ER2 (EDTA-buffer Bond pH 9.0; 20 minutes for CD68). The immunoreaction was visualized with the BOND™ Polymer Refine Red Detection Kit resulting in a red color.

3.2.2.3. IHC evaluation

Analyses of the single IHC stainings were performed in two steps. To analyze the cellular and histoanatomical distribution of different stained markers, an overall evaluation of the tissue sections was performed first: the entire tissue section was screened at low magnification (10-fold magnification) and the predominant distribution of immunopositive cells (tumor center and/or invasion front of primary tumor or liver metastases) was documented. In order to investigate more precisely the distribution and frequency of staining, 10 representative fields of view (FoV) at the invasion front and tumor center of the primary tumor or metastasis were investigated. All tissue sections were studied with regard to the predominant areas of stained cells at 200-fold magnification (FoV: 0.48x0.85 mm), except those stained for PD-L1 which were analyzed at 400-fold magnification (FoV: 0.42x0.24 mm). Every tissue section was assessed by their predominant localization of immunopositive cells (at the invasion front, tumor/metastasis center, or evenly distributed between invasion front and tumor center). For staining evaluation, a scoring system was established which rates the percentage of immunopositive cells in the FoV. The scoring system for tissue sections stained for PD-L1 and CD8 graded FoV into 0 % (negative), ≤1 %, and > 1% cells stained, whereas FoV in tissue sections stained for CD163 and CD68 were scored as 0 %, ≤10 %, 11-50 %, and >50 % cells stained. The PD-L1 staining intensity was graded as none, low and high. For each tissue section, areas with the highest frequency of immunopositive cells were documented to evaluate the main localization of cells stained for the respective markers within the tumor tissue.

3.2.3. Multiplex analysis of cell culture supernatants

LEGENDplex Human CD8/NK, mix and match panel from Biolegend, was used to determine different human cytotoxic molecules and cytokines (Granzyme A, Granzyme B, Perforin, Granulysin, IFN-γ) in the supernatants of CD8+ T cell mono- and co-culture with PDAC spheroids following manufacturer's instructions. The supernatants were centrifuged at 15000xg and 4 °C for 8 min to remove cell debris and stored at -80 °C. Prior to assay procedure, all reagents were pre-warmed to RT, the bead-containing vials were vortexed for 1 min and the 20X wash buffer was diluted with ddH_20. The lyophilized standard was solved in 250 µl assay buffer and a 1:4 serial dilution of the standard was performed with assay buffer. Overall, 7 different standard concentrations were prepared containing standard stock (C7), 1:4 dilution (C6), 1:16 dilution (C5), 1:64 dilution (C4), 1:256 dilution (C3), 1:1024 dilution (C2) and 1:4096 dilution (C1). Assay buffer (C0) was used as a blank sample. Next, 62.5 µl assay buffer were added into a 96-well V-bottom plate and either 12.5 µl of standard solutions or supernatants were included in the respective wells. Then, the beads were again vortexed for 30 sec

and 12.5 µl of bead solution were added. The plate was sealed with a plate sealer, covered with aluminum foil to protect from light, and incubated on a shaker at 800 rpm and RT for 2 h. Afterwards, the plate was centrifuged at 250xg at RT for 5 min to allow sedimentation of bead-bound analytes. The supernatants were immediately discarded after centrifugation by one continuous and forceful movement. Thereafter, the wells were washed by adding and resuspending 200 µl of wash buffer, followed by centrifugation at the same condition previously mentioned and supernatant discard. Then, 12.5 µl of detection antibody cocktail were added and the plate was sealed and foiled again for the following incubation on the plate shaker at 800 rpm and RT for 1 h. Afterwards, 12.5 µl SA-PE cocktail were added directly to each well and the plate was incubated as mentioned before for 30 min. Then, all wells were washed twice with wash buffer and after the last centrifugation step, all standard wells were resuspended in 150 µl wash buffer while all supernatant wells were diluted in 50 µl wash buffer. Data acquisition was carried out with a BD FACSymphony flow cytometer (Beckton Dickinson), and the evaluation was conducted with the LEGENDplex-data analysis software v8 according to the provided manual.

3.2.4. M30 CytoDeath

To specifically analyze cell death of PDAC cells, the M30 CytoDeath ELISA was used. The procedure is based on the accumulation of caspase-cleaved Keratin 18 (ccK18) in supernatants which is only released by apoptotic epithelial/carcinoma cells. Shortly, 25 µl of standard solutions or supernatant samples were added to pre-coated plates. Next, 75 µl of pre-diluted HRP conjugate solution were added per well and incubated for 4 h at RT on a plate shaker (600 U/ml). Afterwards, wells were washed 5-times with 200 µl wash buffer, 200 µl TMB substrate were added, and the plate was incubated for 20 min at RT in the dark. Then, the reaction was stopped by adding 50 µl of stop solution and mixed on a plate shaker for 5-10 min. Lastly, the plate was incubated for 5 minutes in the dark and then measured by Tecan Infinite® 200 PRO Microplate Reader. All samples were normalized to PDAC cell count seeded.

3.3. Statistics

Statistical analysis was performed using GraphPad Prism Version 9.4.1 (GraphPad Software Inc., La Jolla, USA). Normality was tested by using the Shapiro-Wilk normality test. If the samples passed the normality test, an ordinary one-way ANOVA using either Turkey's multiple comparisons or when comparing with control, Dunnett's multiple comparison tests were performed. To test grouped

samples, two way-ANOVA and followed multiple comparison was tested by Tukey test or comparing all samples with control, Dunnett's multiple comparison test was performed. Non-parametric data were analyzed by Kruskal-Wallis Test with Dunn's multiple comparison test comparing all samples with control. Normally distributed data is presented by column bar graph with mean and standard deviation, not normally distributed data is depicted by bar graphs with median and interquartile range in both directions. Results were considered as statistically significant for p-values < 0.05. Significance of results is indicated as follows: * = $p < 0.05$, **= $p < 0.01$, *** = $p < 0.001$, ****= $p < 0.0001$.

4. Results

4.1. *In situ* characterization of PD-L1 expression and immune cell attendance in primary tumors of PDAC patients and their corresponding liver metastases

In PDAC patients, several studies identified PD-L1 expression in pancreatic tumor tissues, but most of these studies only investigated cohorts of PDAC patients at AJCC Stages I – III [170–172,176]. The knowledge about an alteration of PD-L1 expression during disease progression and metastasis formation is missing. Therefore, the first aim of this study was to investigate primary tumors of PDAC patients and their corresponding liver metastases concerning PD-L1 expression. Furthermore, the attendance of immune cell populations which are highly relevant for tumor immunity was analyzed. For this purpose, immunohistochemical stainings of serial sections from primary tumors and corresponding liver metastases of four PDAC patients was performed. Patient characteristics are listed in Table 5.

Table 5: Clinico-pathological characteristics of PDAC patients in the analyzed cohort of this study.

Parameter	Number of cases
Patients	4
Median age (range)	71 (68-74)
Sex (male/female)	3/1
Tumor stage T1/T2/T3/T4	0/2/2/0
Nodal stage N0/N1	1/3
Metastasis stage M0/M1	0/4
Tumor grade 1 (well differentiated)	1
Tumor grade 2 (moderately differentiated)	0
Tumor grade 3 (poorly differentiated)	3

4.1.1. PD-L1 is expressed in all primary tumors and corresponding liver metastases and associated with the presence of macrophages and CD8+ T cells

Previous studies revealed that PD-L1 is expressed only in one-third to half of the cases at primary PDAC and is predominantly expressed by stromal cells [170,171,176]. One of the most abundant stroma cell populations are tumor-associated macrophages, which mostly exhibit anti-inflammatory M2-like characteristics [24,54]. In order to investigate PD-L1 expression in primary tumors and liver metastases and examine whether abundant macrophages are a source of PD-L1 expression, serial tissue sections of PDAC patients' primary tumors and corresponding liver metastases were immunohistochemically

stained for PD-L1 as well as the attendance of macrophages and CD8+ T cells. Figure 13 depicts representative images of a PDAC patient's primary tumor. To discriminate tumor cells from stroma cells, PanCK was stained (Figure 13A-C). PD-L1 expression is shown in Figure 13 D-F. General macrophage marker CD68 (Figure 13G-I) and M2-like macrophage marker CD163 (Figure 13J-L) were used to mark macrophages. T cells were stained with an α-CD3 antibody (Figure 13M-O) and CD8+ T cells were analyzed by CD8 staining (Figure 13P-R). In order to get evidence about the spatial distribution of tumor and immune cell populations as well as PD-L1 expression, an overview picture for the respective staining is shown (Figure 13A, D, G, J, M, and P). To differentiate areas at the tumor center (Figure 13B, E, H, K, N, and Q) from regions at the tumor invasion front (Figure 13C, F, I, L, O, and R), representative images of a higher magnification are also presented. Within the tumor as well as at the tumor invasion front, PD-L1 levels were found in all four cases (Figure 13 E and F). Macrophages, especially CD163+ macrophages, were located in PD-L1-expressing areas. Likewise, T cells (CD8+ T cells in particular) were found in these areas.

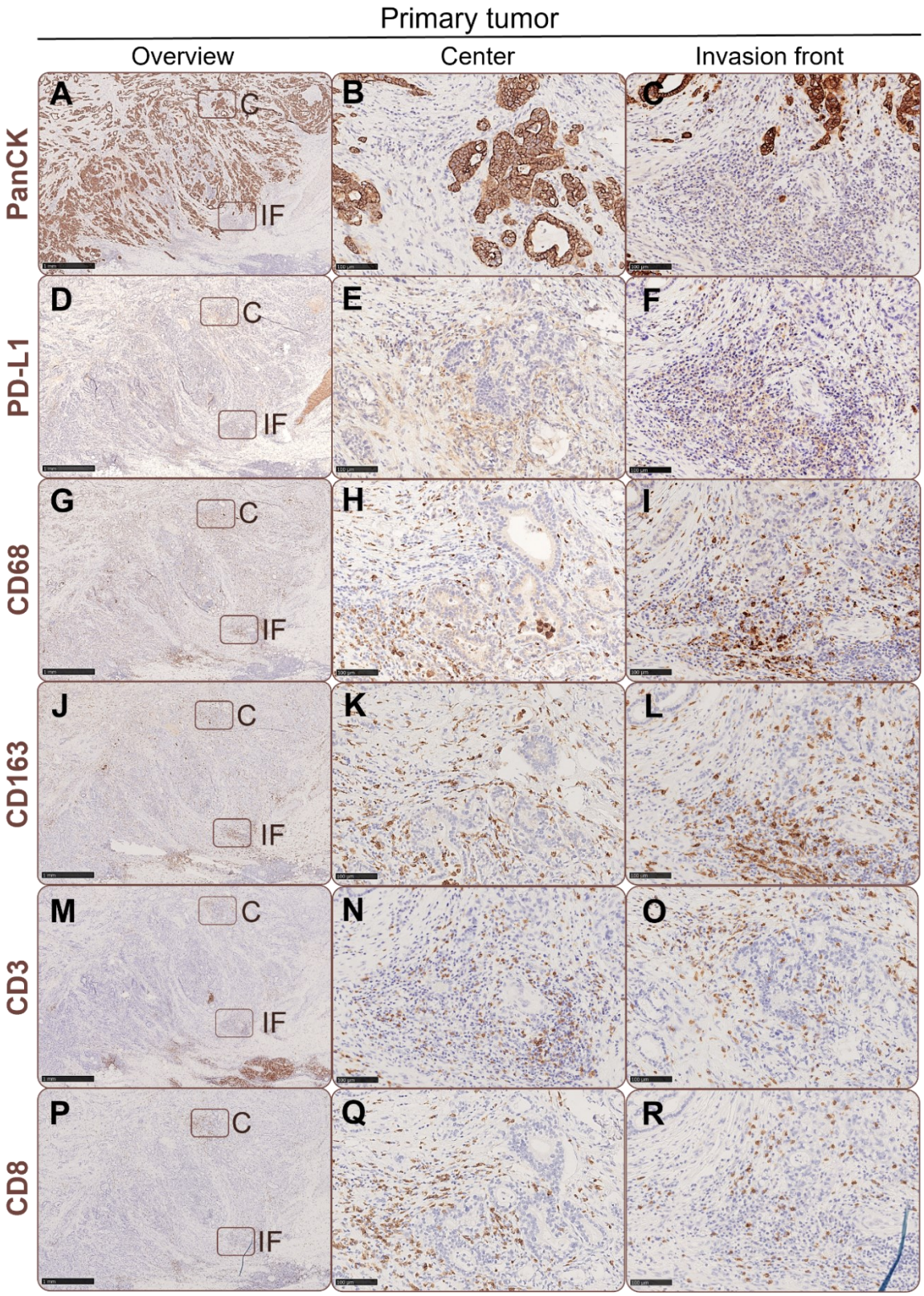

Figure 13: PD-L1 expression and localization of macrophages and T cells in serial tissue sections of primary tumors of PDAC patients. Representative images of immunohistochemical stainings of primary tumors of PDAC patients at different localizations. The following markers were stained: **(A-C)** PanCK (epithelial/tumor cells), **(D-F)** PD-L1, **(G-I)** CD68 (macrophages), **(J-L)** CD163 (M2-like macrophages), **(M-O)** CD3 (T cells), and **(P-R)** CD8 **(**CD8+ T cells). **A**, **D**, **G**, **J**, **M,** and **P** show an overview of the tissue sections, **B, E, H, K, N,** and **Q** depict areas in the tumor center. **C**, **F**, **I**, **L, O,** and **R** show areas at the tumor invasion front. Scale bar overview pictures: 1000 µm, tumor center and invasion front: 100 µm. C = Center, IF = Invasion front. (partially published data [209])

Similar results were observed in corresponding liver metastasis of these PDAC patients (Figure 14). Overview images of PanCK (Figure 14A-C), PD-L1 (Figure 14D-F), CD68 (Figure 14G-I), CD163 (Figure 14J-L), CD3 (Figure 14M-O) and CD8 (Figure 14P-R) are depicted in Figure 14. A clear border of PD-L1, CD68, and CD163 expression separates the metastasis from surrounding liver tissue. Within the metastasis, expression of CD68 and CD163 as well as CD3 and CD8 was clearly seen coinciding with PD-L1-expressing areas (Figure 14E+F). Interestingly, in contrast to non-metastasized patients [55], all investigated cases of this study showed PD-L1 expression in primary tumors and their corresponding liver metastases.

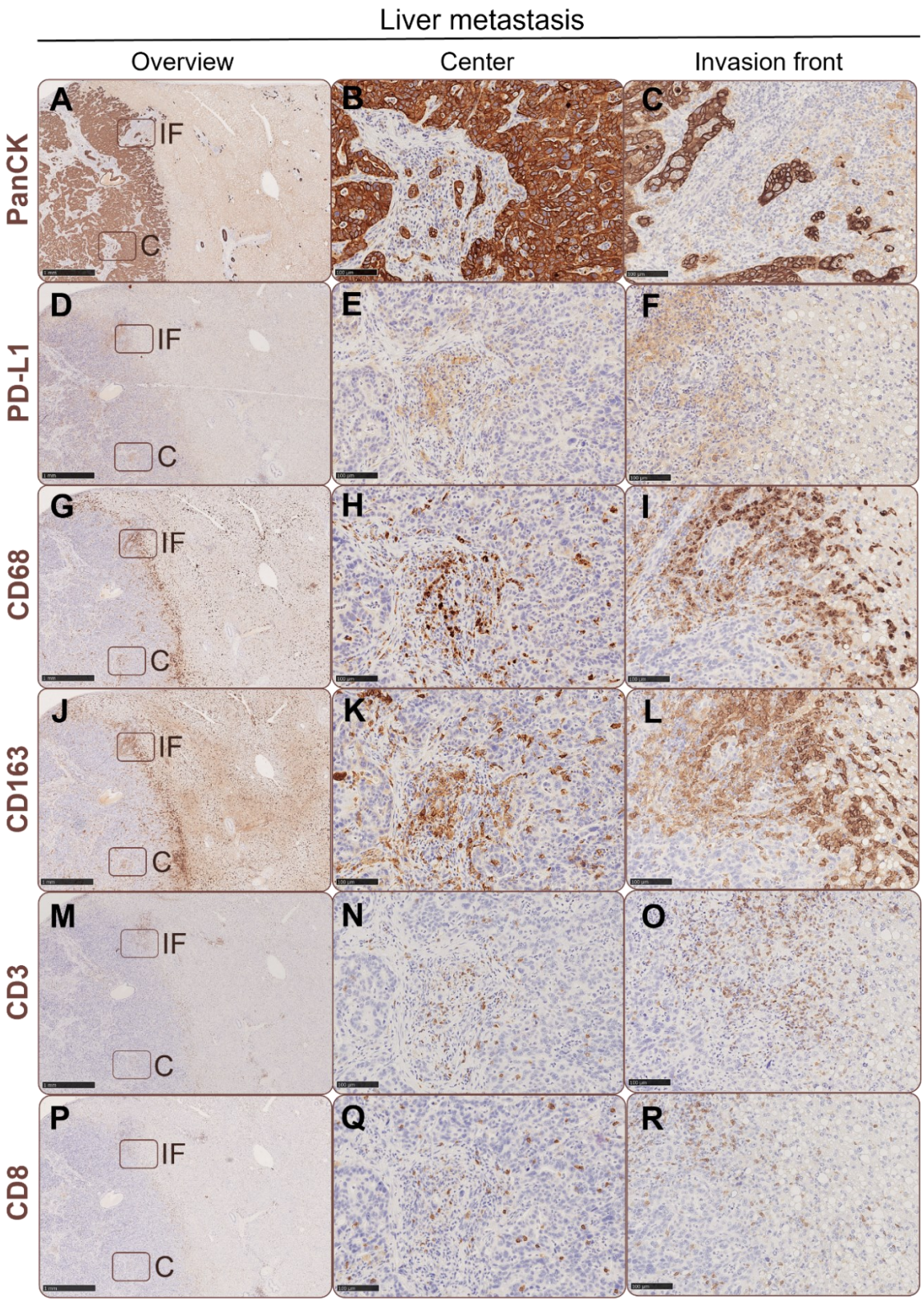

Figure 14: PD-L1 expression and localization of macrophages and T cells in serial tissue sections of corresponding liver metastases of PDAC patients. Representative images of immunohistochemical stainings of liver metastases of PDAC patients at different localizations of the metastasis. The following markers were stained: **(A-C)** PanCK (Epithelial/tumor cells), **(D-F)** PD-L1, **(G-I)** CD68 (macrophages), **(J-L)** CD163 (M2-like macrophages), **(M-O)** CD3 (T cells), and **(P-R)** CD8 **(**CD8+ T cells). **A**, **D**, **G**, **J**, **M,** and **P** show an overview of the tissue sections, **B, E, H, K, N,** and **Q** show areas in the tumor center. **C**, **F**, **I**, **L, O,** and **R** depict areas at metastasis invasion front. Scale bar overview pictures: 1000 µm, areas within tumor and invasion front: 100 µm. C = Center, IF = Invasion front. (partially published data [209]).

Next, all tissues from the PDAC patients were investigated regarding their localization of PD-L1, CD68, CD163, CD3, and CD8 expression. For this purpose, each stained marker was evaluated according to its predominant staining localization (center of primary tumor/metastasis, at the invasion front, or evenly distributed throughout the tumor/metastasis). PD-L1 expression in the primary tumor (white) was predominantly evenly distributed (75 % of cases) between the tumor center and invasion front, whereas PD-L1 expression in liver metastases (grey) was evenly distributed for all cases (Figure 15A). The expression of CD68 and CD163 was evenly distributed for both primary and secondary sites (Figure 15B+C). In contrast, CD3 expression in primary PDAC was mainly located at the invasion front, but in liver metastases, it was located at the invasion front and evenly distributed in 50 % of cases, respectively (Figure 15D). CD8 expression in liver metastases was mainly located at the invasion front but uniformly distributed at the primary site (Figure 15E).

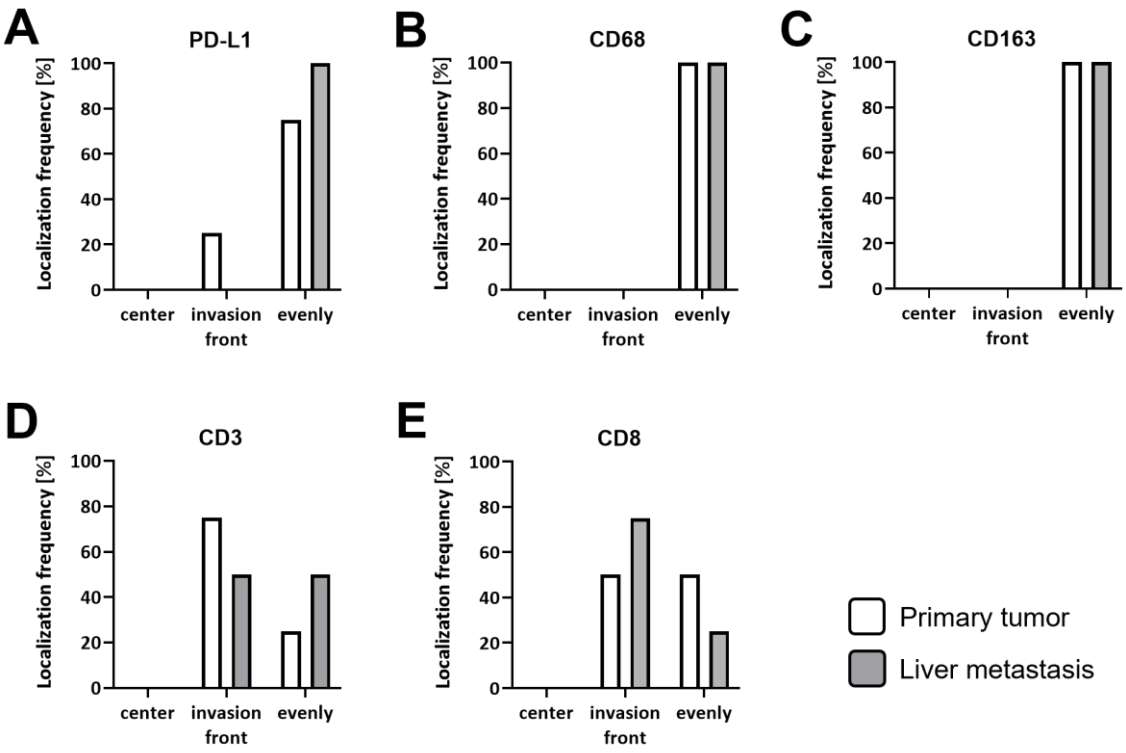

Figure 15: Localization of PD-L1 expression and attendance of macrophages and T cells in primary tumors and corresponding liver metastases of PDAC patients. Quantitative localization analysis of **(A)** PD-L1, **(B)** CD68, **(C)** CD163, **(D)** CD3, and **(E)** CD8 in primary tumors (white) or corresponding liver metastases (grey). Overviews of tissue slices were scored according to their predominant location of immunopositive cells. Three scores were used to determine location either in the center, at the invasion front, or evenly distributed between center and invasion front of respective primary tumors and liver metastases. Localization frequency denotes the percentage of immunopositive cells' predominant location in all cases. n=4. (partially published data [209]).

Overall, PD-L1-expressing areas were associated with the presence of macrophages (especially M2-like) and T cells (particularly CD8+) in primary tumors and corresponding liver metastases. Furthermore, all analyzed cases showed PD-L1 expression in both primary and secondary sites,

indicating that PD-L1-mediated immune evasion might operate during PDAC progression in these patients.

4.1.2. Macrophages are highly frequent at the primary and secondary site and PD-L1 is even more expressed in liver metastases than primary tumors

As the overview of serial tissue sections of primary tumors and corresponding liver metastases of PDAC patients showed an association of PD-L1 expression areas with the location of macrophages and CD8+ T cells, verification of these results was performed. Therefore, every staining was scored according to different staining frequencies to gain profound insight into distribution and frequency of each marker within the tissue sections. For this purpose, 10 Fields of View (FoV) were analyzed within the primary PDAC tumor (white) or liver metastases (grey) and at the invasion front (altogether 20 FoV for every staining) (Figure 16A). Since PD-L1, CD3, and CD8 showed only low numbers of positively stained cells, FoV were scored from 0 % (negative), ≤ 1 %, and > 1 % (Figure 16A, E, and F). In contrast, CD68 and CD163 showed higher numbers of positively stained cells and were scored from 0 % (negative), ≤ 10 %, 11-50 %, and > 50 % (Figure 16 C+D). Furthermore, for PD-L1 also the staining intensity was investigated and scored from none, low, and high staining (Figure 16B).

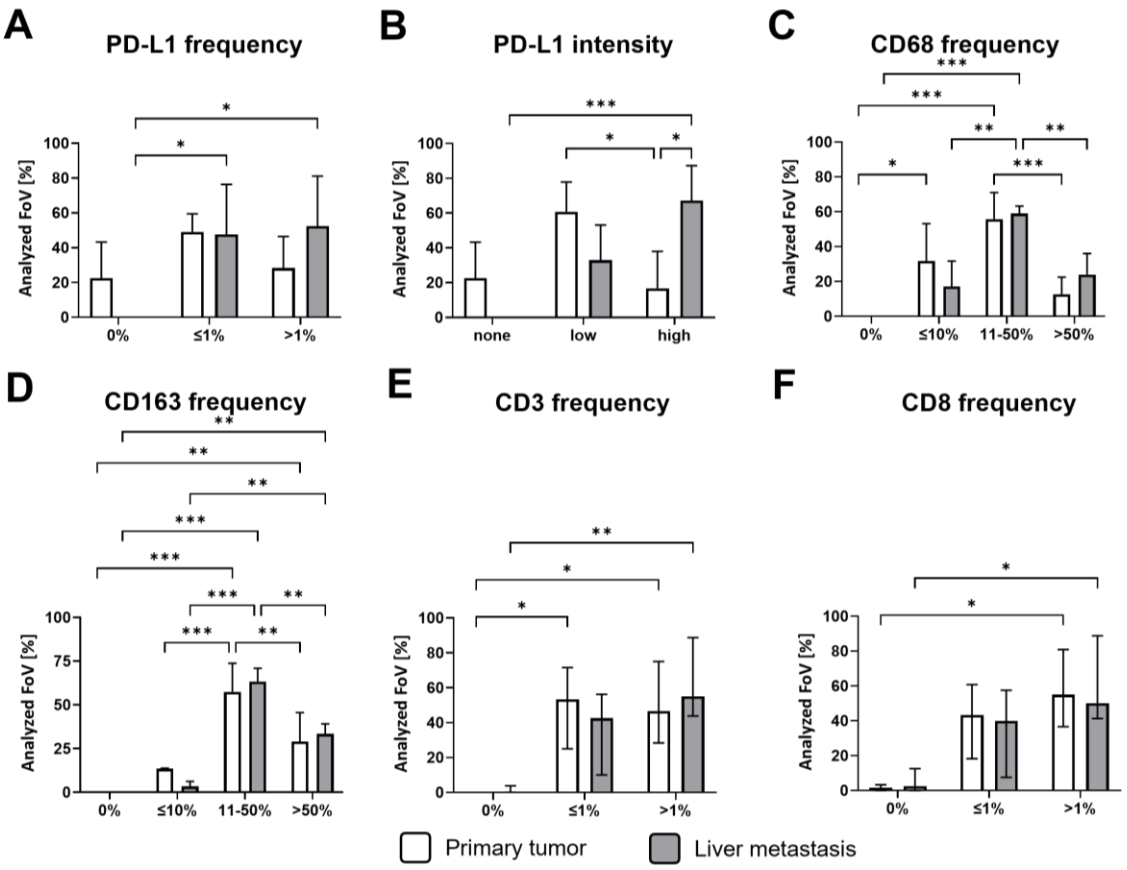

Figure 16: PD-L1 is expressed in primary PDAC tissues and even more in corresponding liver metastases. Classification of staining frequencies for respective markers in primary tumors (white) or corresponding liver metastases (grey). To analyze staining frequencies, 10 fields of view (FoV) at the invasion front and center of the primary tumor or metastasis were investigated according to their score classification. **(A)** PD-L1 frequency, **(B)** PD-L1 intensity, **(C)** CD68 frequency, **(D)** CD163 frequency, **(E)** CD3 frequency, and **(F)** CD8 frequency. Scores for **A**, **E**, and **F**: 0 %, ≤ 1 %, and > 1 %, **B**: none, low, high, and **C** and **D**: 0 %, ≤ 10 %, 11-50 %, or > 50 %. Parametric data are depicted as mean with standard deviation in one direction and non-parametric data are depicted as median with interquartile range in both directions. Two-way ANOVA with Tukey's multiple comparison test. n=4. * = $p < 0.05$. (partially published data [209]).

The frequency of PD-L1 positively stained cells was different in primary tumors and liver metastases (Figure 16A). Only in primary tumors, FoV without positive PD-L1 staining were observable, whereas all FoV in liver metastases had PD-L1 expression with 52 % of analyzed FoV presenting a PD-L1 frequency of > 1 %. In contrast, primary tumors had the highest amount of FoV ≤ 1 % positively stained cells. Similar results were observable for PD-L1 staining intensity (Figure 16B). In contrast to liver metastases, primary tumors showed FoV with no staining intensity and the highest amounts of analyzed FoV at low intensity (60 %), whereas liver metastases showed 67 % of analyzed FoV with high staining intensity. The frequencies of general macrophage marker CD68 and M2-like marker CD163 showed similar results for primary tumor and liver metastases (Figure 16C+D). The highest amount of analyzed FoV were seen with 11-50 % positively stained cells for both primary tumors (56 % CD68 and 57 % CD163) and liver metastases (59 % CD68 and 63 % CD163). Of note, FoV with more than 50 % positively stained cells were found for CD68 and CD163 at both tumor sites, underscoring the high attendance of macrophages in PDAC patient tissues. The CD3 and CD8 stainings also showed similar

results (Figure 16E+F) compared to macrophage stainings. The highest amounts of analyzed FoV were found with > 1 % positively stained cells in liver metastases (CD3 55 % and CD8 50 %). Attendance of CD3 T cells in primary tumors was evenly distributed between ≤ 1 and > 1 %, but stronger for CD8 positively stained cells (55 %).

Taken together, these results showed that liver metastases exhibit a higher PD-L1 expression frequency and staining intensity compared to primary tumors. Furthermore, macrophages were present at high frequencies in tissues of PDAC patients at primary and secondary sites in contrast to CD3 and CD8 T cells.

4.1.3. PD-L1-expressing cells as well as macrophages and CD8+ T cells were predominantly present at the invasion front of primary tumors and liver metastases

As described in section 4.1.1, the PD-L1 expression of primary tumors and corresponding liver metastases was associated with the attendance of macrophages and CD8+ T cells. In section 4.1.2, the results showed that macrophages were highly abundant, while CD8+ T cells were only present at low frequencies in PDAC tumors and liver metastases. Next, it was investigated whether PD-L1-expressing areas might be associated with the presence of macrophages and CD8+ T cells. For this purpose, an evaluation of the respective highest scores (PD-L1, CD3, and CD8: > 1 %; CD68 and CD163: > 50 %, PD-L1 intensity: high) was performed by investigation of 10 FoV in the center (plain) of primary tumor (beige) or liver metastases (brown) and 10 FoV at their invasion fronts (shaded). Then, percentages of the highest frequencies were calculated for both locations (center and invasion front) to get an insight into the localization of immunopositive cells. PD-L1 frequency of the highest score category showed that PD-L1-expressing cells were mainly located at the invasion front of both tissues (primary tumor vs. liver metastasis: 74.2 % vs. 62.2 %) (Figure 17A). This corresponded with the PD-L1 staining intensity which was also predominantly detected at the invasion fronts of both lesions (Figure 17B). CD68+ cells were almost exclusively visible at the invasion front of primary tumors and in 100 % of analyzed FoV in liver metastases (Figure 17C). The same results were seen for CD163+ stained cells (Figure 17D). Likewise, CD3 immunopositive cells were mostly located at the invasion fronts of primary tumors and liver metastases (CD3 primary tumor vs. liver metastasis: 72.3 vs. 74.4 %), and the highest frequency of CD8+ stained cells was similarly detected at the invasion fronts of both lesions (CD8 primary tumor vs. liver metastasis: 73.4 vs. 76.2 %) (Figure 17E+F).

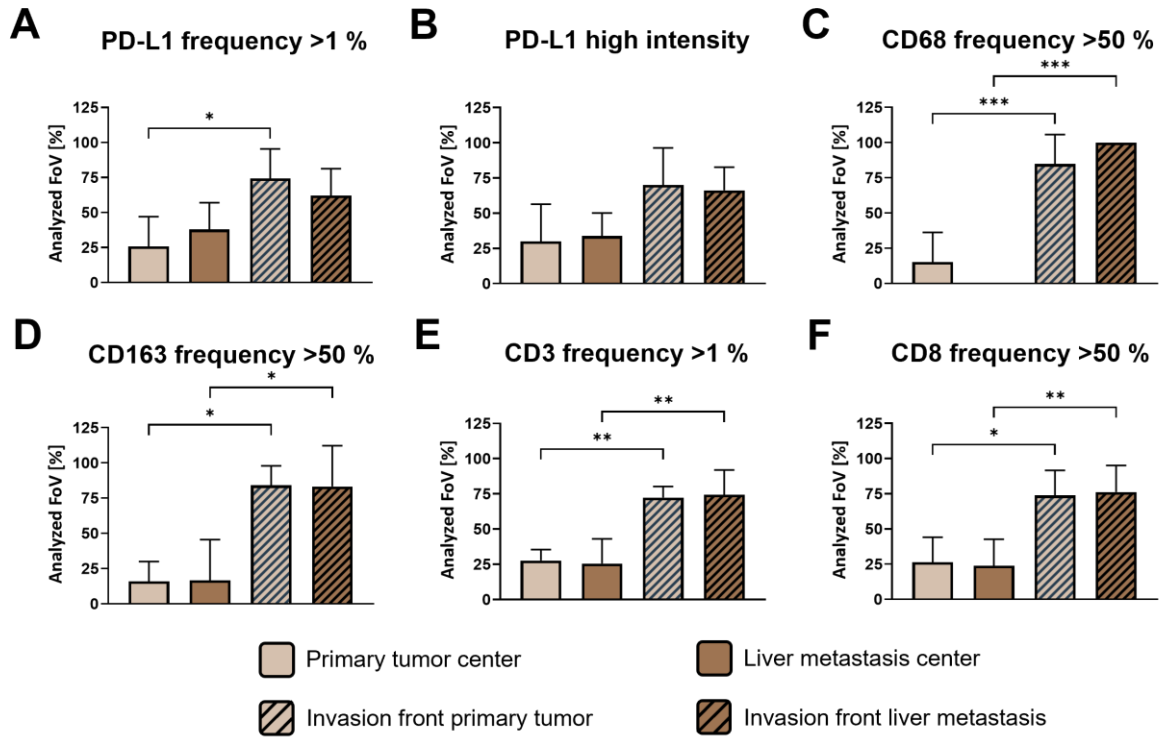

Figure 17: PD-L1 expression is predominantly localized at the invasion front of primary tumors and liver metastases and associated with high infiltration of macrophages and CD8+ T cells. Localization of immunopositive cells was investigated within the **(A)** highest frequency of PD-L1, **(B)** highest PD-L1 intensity, **(C)** highest CD68 frequency, **(D)** highest CD163 frequency, **(E)** highest CD3 frequency, and **(F)** highest CD8 frequency. For analysis of location, 10 fields of view (FoV) at the lesion center (plain) and at the invasion front (shaded) of primary tumors (light brown) or liver metastases (dark brown) were evaluated. Parametric data are depicted as mean with standard deviation in one direction. One-way ANOVA with Tukey's multiple comparison test. n=4. * = $p < 0.05$; ** = $p < 0.01$; *** = $p < 0.001$. (partially published data [209]).

As the immunohistological single stainings of serial tissues revealed a high co-localization of PD-L1 expression and CD163+ and CD8+ cells, double IHC stainings of PD-L1, CD68, CD8, and PanCK were performed to check whether PD-L1 is predominantly expressed by stroma cells. As hepatic myofibroblasts represent an important stromal population in liver metastases, too, αSMA was also stained. Representative images of a PDAC patient's liver metastasis are shown in Figure 18:.

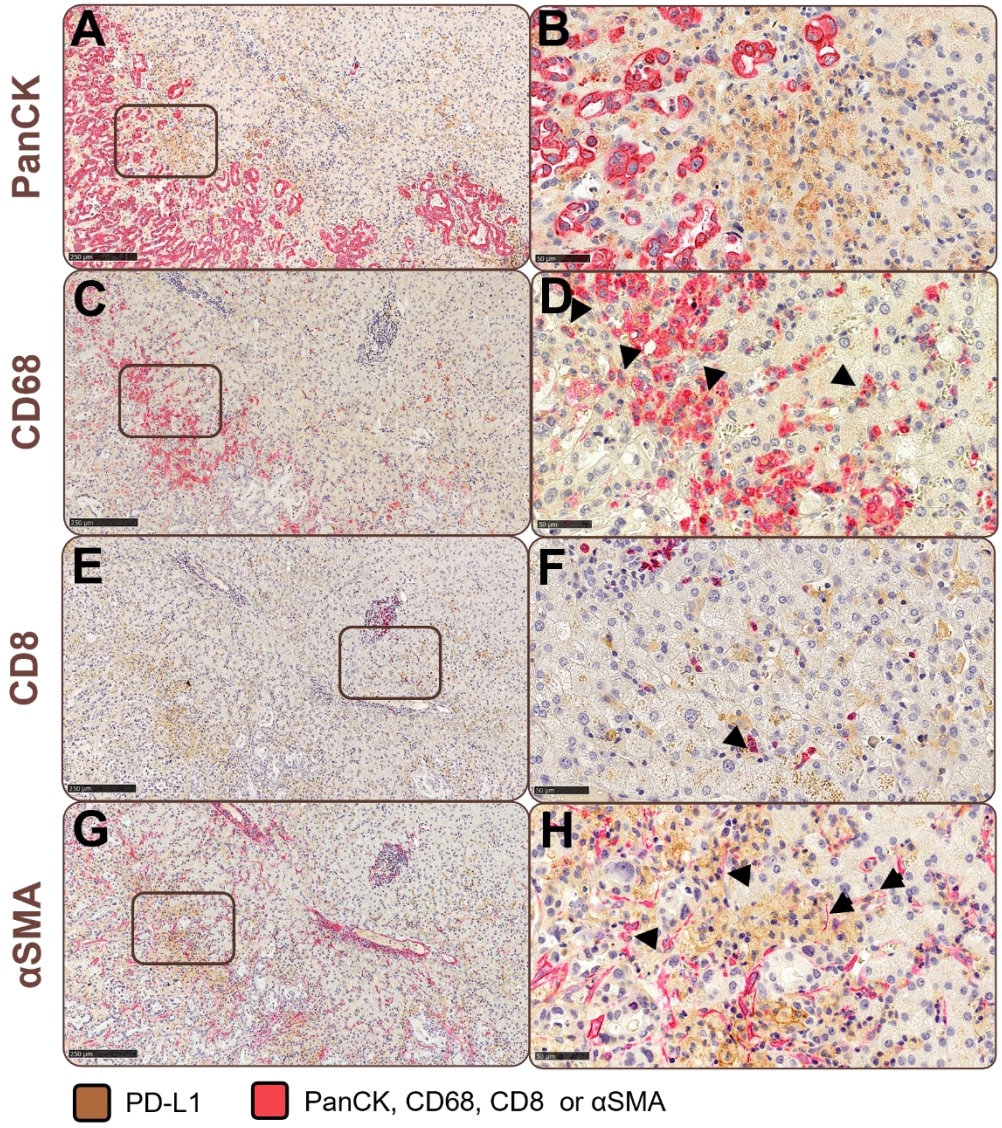

Figure 18: PD-L1 expression is predominantly co-localized with macrophages and hepatic myofibroblasts. Representative images of immunohistochemical double stainings for **(A+B)** PD-L1/PanCK, **(C+D)** PD-L1/CD68, **(E+F)** PD-L1/CD8, and **(G+H)** PD-L1/αSMA in the tissue of a liver metastasis of a PDAC patient. Brown staining represents PD-L1 immunopositive cells, and red staining represents either PanCK, CD68, CD8, or αSMA immunopositive cells. Scale bar left: 250 µm, right: 50 µm. Arrows represent double immunopositive cells. (partially published data [209]).

PanCK+ PDAC cells did not express PD-L1, as no PanCK and PD-L1 double immunopositive cells were detectable, while clear PD-L1 stainings were present in the surrounding cells (Figure 18A+B). Here, CD68+ macrophages co-localized with PD-L1-expressing cells (Figure 18C) indicating that macrophages express PD-L1 (Figure 18D, indicated by arrows). Similar to the lower frequency of CD8+ T cells in single IHC staining, only a few CD8+ T cells were detected at the invasion front and only one CD8+ cell showed PD-L1 expression (Figure 18E+F). Finally, hepatic myofibroblasts as another abundant cell population in liver metastases (represented by αSMA staining), were also found along with PD-L1-expressing cells (Figure 18G), showing that also αSMA+ and PD-L1+ cells were present in liver metastases. In summary, these data indicate that not PDAC cells but macrophages and hepatic myofibroblasts, as the most abundant stroma cell populations in liver metastases, are the main source of PD-L1 expression.

Altogether, these data showed that PD-L1, CD68, CD163, and CD8 can be found predominantly at the invasion front of primary tumor tissues and liver metastases, indicating that PD-L1 is associated with the attendance of macrophages (especially M2-like phenotype) and CD8+ T cells. Furthermore, the fact that both immune cell populations are predominantly found at the invasion fronts and not in the center of primary tumors or metastases, suggests that they are not able to infiltrate the tumor or metastasis properly. Further, macrophages and hepatic myofibroblasts were identified as the main source of PD-L1-expressing cells.

4.2. PD-L1 and its blockade in the CD8+ T cell/PDEC interplay

As the *in situ* results revealed that PD-L1 is predominantly expressed at the invasion fronts of primary tumors and metastases of PDAC patients where tumor cells and CD8+ T cells were present, the next aim of the study was to examine whether blocking of PD-L1 impacts the activation status and PDEC viability in the *in vitro* CD8+ T cell/PDEC interplay.

4.2.1. Expression of PD-1, PD-L1, and CD80 were enhanced during activation culture and is dependent on the activation stage of CD8+ T cells

T cells often found in the TME of PDAC exhibit an exhausted phenotype [73,210–212]. To investigate the CD8+ T cell/PDEC interplay *in vitro*, CD8+ T cells were needed, which mimic the exhausted phenotype of T cells in the tumor. The exhausted phenotype is characterized by elevated expression of PD-1 and early activation marker CD69 [210–212]. For this purpose, human lymphocytes were isolated from leukocyte retaining systems of healthy blood donors and separated from other cell populations via magnetic-activated cell separation by negative selection (section 3.1.7). Next, the CD8+ T cells were activated by stimulation with immobilized α-CD3- and soluble CD28-targeting antibodies as well as human IL-2. The activation culture was performed for 4 days. Afterwards, CD8+ T cells were seeded for additional 3 days. Analysis of activation status and expression of PD-1 was done daily via immunofluorescence staining and flow cytometric analysis. Additionally, the surface expression of the PD-1 ligand PD-L1 and CD80 was assessed on CD8+ T cells, as CD8+ T cells are also able to express both molecules [213–215], which might be involved in regulation of T cell activation or inhibition. As *cis*-binding of PD-L1 and CD80 was reported in the literature to potentially inhibit *trans*-binding of PD-1 and PD-L1 and foster co-stimulatory CD28-CD80 interaction [130], CD80 expression on T cells was also examined.

During activation culture, the size and granularity of CD8+ T cells increased seen by FSC/SSC plots, but after four days of activation culture, the size and granularity of CD8+ T cells decreased again (Figure

19A). The cell surface levels of early activation marker CD69 increased since day one in activation culture and peaked at day 3 (MFI ratio 0d vs. 3d: 1.67 vs. 79.4). At day 6, CD69 levels were reduced to levels of freshly isolated CD8+ T cells before activation culture (Figure 19B). Expression of late activation marker CD25 was also elevated during activation culture, but the increase only started on day 2. Similar to CD69, the highest peak of CD25 surface levels was measured on day 3 (MFI ratio 0d vs. 3d: 1.93 vs. 199.0) and dropped the next 4 days (Figure 19C). The expression of immune checkpoint receptor PD-1 was also enhanced during activation conditions until day 4 (MFI ratio 0d vs. 4d: 3 vs. 9.5), while when further cultured in the absence of activation stimuli, PD-1 levels rapidly decreased again (Figure 19D). Of note, cell surface levels of PD-L1 (Figure 19E), and CD80 levels (Figure 19F) were also found on CD8+ T cells. Cell surface expression of PD-L1 was also enhanced until day 2 (MFI ratio PD-L1: 5.5) and decreased at all following days to the level of freshly isolated T cells (MFI ratio 0d vs. 6d: 1.45 vs. 1.57). The enhancement of PD-1 and PD-L1 cell surface levels on CD8+ T cells might play a role in autoregulation against overactivation in the activation culture. In contrast, cell surface levels of CD80 did not increase until day 3, which was also their peak (MFI ratio 0d vs. 3d: 2.26 vs. 5.31). Afterwards, CD80 levels decreased until day 7 (Figure 19F). *Trans*-interaction of PD-L1/CD80 was also reported which results in suppressed T cell activation and cytokine production [118] enabling potential inhibitory mechanism against overactivation. The engagement of CD80 and CTLA-4, the latter being also expressed on CD8+ T cells but only in small amounts (Supplementary figure 1) [216], may result in inhibition of T cell activation and proliferation [217]. However, the low amounts of CTLA-4 on activated CD8+ T cells suggest that the CTLA-4/CD80 axis plays not a central role in co-inhibition of CD8+ T cells in this setting.

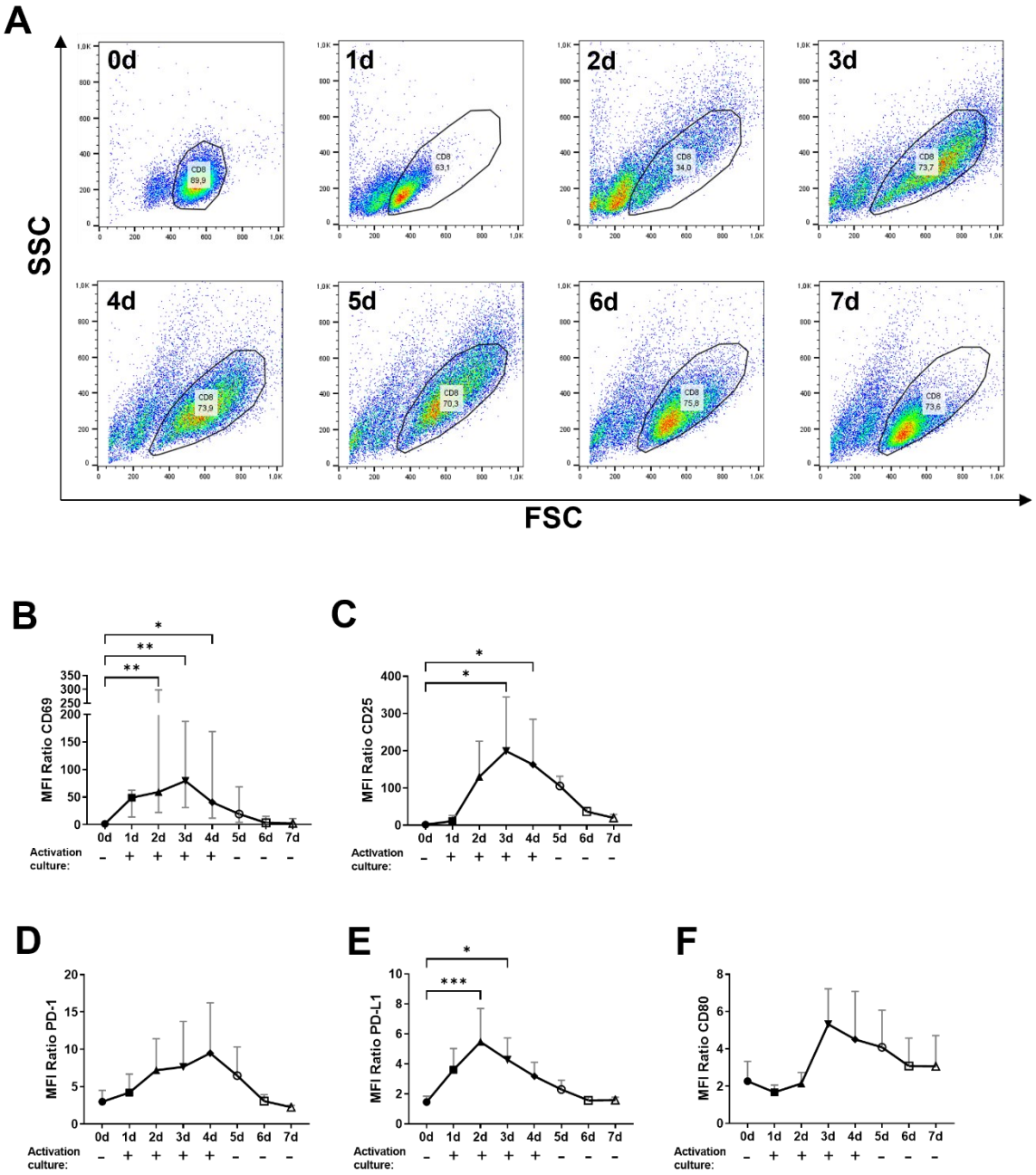

Figure 19: Cell surface level enhancement of activation markers CD69, CD25, and CD80 as well as immune checkpoint molecules PD-1 and PD-L1 during CD8+ T cell activation culture. Isolation of primary human lymphocytes from leucocyte retaining systems was performed by density gradient centrifugation followed by counter flow centrifugation. To isolate CD8+ T cells from human lymphocytes, a magnetic-activated cell sorting (MACS) system was used. Afterwards, untouched CD8+ T cells were stimulated with immobilized α-CD3 and soluble CD28-targeting antibodies as well as IL-2 for 4 days. At day 3, CD8+ T cells were again stimulated with IL-2. After 4 days, T cells were pooled, washed with PBS, and re-seeded for additional 3 days. **(A)** FSC/SSC dot plots during and after activation culture. CD8+ T cells were investigated daily during activation culture and subsequent seeding period concerning their surface levels of activation markers **(B)** CD69, and **(C)** CD25 as well as immune checkpoint molecules **(D)** PD-1, **(E)** PD-L1, and **(F)** CD80 via flow cytometric analysis. Data are presented as MFI ratio and denotes median fluorescence intensity ratio of specific staining antibody and its isotype control ($MFI^{specific}/MFI^{isotype}$). Parametric data are depicted as mean with standard deviation in one direction and non-parametric data are depicted as median with interquartile range in both directions. One-way ANOVA with Dunnett's multiple comparison test comparing all samples with 0d samples was used for parametric data and non-parametric data were analyzed by Kruskal-Wallis Test with Dunn's multiple comparison test comparing all samples with 0d. Not normally distributed data are depicted as median with interquartile range in both directions. Naive and 3d: n= 3, 1 and 2d: n=4 and 4 to 7d: n=5. * = $p < 0.05$, ** = $p < 0.01$, *** = $p < 0.001$.

Notably, after activation culture, CD8+ T cells exhibited high cell surface expression levels of CD25 and the early activation marker CD69 along with considerable cell surface levels of PD-1, pointing to an exhausted T cell phenotype often found in PDAC tissues [210–212]. The increase of PD-L1 in the activation culture also indicates an exhausted phenotype of CD8+ T cells because PD-1/PD-L1 interaction seems to play a major role as an inhibitory receptor pathway, which is involved in T cell exhaustion [211]. Furthermore, CD80 surface level enhancement during activation culture implies potential co-inhibitory axes, as PD-L1/CD80 *trans* binding and CTLA-4/CD80 interaction can result in T cell inhibition.

4.2.2. Increased concentrations of Granzyme A and B, Perforin, and IFNγ by CD8+ T cells during activation culture

In order to characterize CD8+ T cells during and after activation culture, analysis of supernatants concerning the concentration of cytotoxic molecules Granzyme A, Granzyme B, Granulysin, Perforin, and the effector cytokine IFNγ was performed. After 4 days of activation culture, CD8+ T cells were washed with PBS and cultured in fresh medium in the absence of activation stimuli for further 3 days. Supernatant concentrations of Granzyme A (Figure 20A), Granzyme B (Figure 20B), Perforin (Figure 20D), and IFNγ (Figure 20E) showed similar results as their concentrations were enhanced during the activation culture (1d – 4d), reaching a peak at the end (day 4). After seeding in the absence of activation stimuli, the concentration of mentioned molecules was either not altered (Granzyme A and IFNγ), slightly decreased (Granzyme B), or slightly increased (Perforin) from day 5 to 7. In contrast, Granulysin concentration increase started on day four and remained at a constant level for the following days (Figure 20C).

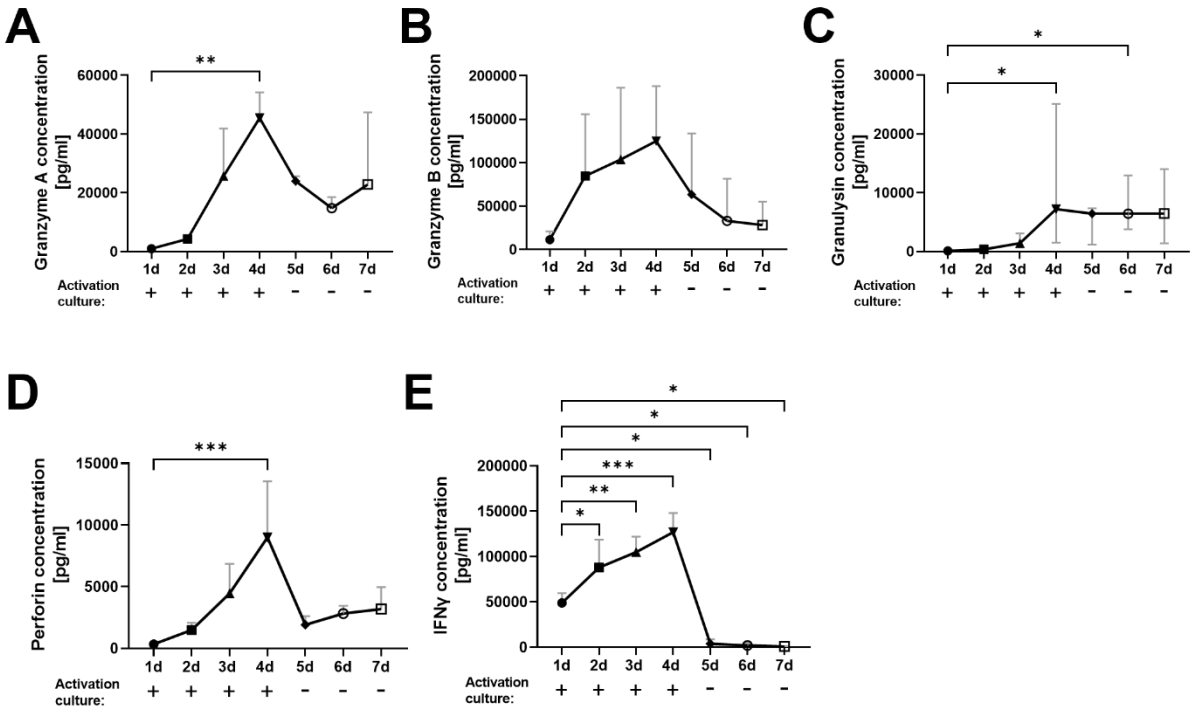

Figure 20: Supernatant concentration of cytotoxic molecules and IFNγ is dependent on activation stimuli during activation culture. Isolation of primary human lymphocytes from leucocyte retaining systems was performed by density gradient centrifugation followed by counter flow centrifugation. To isolate CD8+ T cells from human lymphocytes, a magnetic-activated cell sorting (MACS) system was used. Afterwards, untouched CD8+ T cells were stimulated with immobilized α-CD3 and soluble CD28-targeting antibodies as well as IL-2 for 4 days. At day 3, CD8+ T cells were again stimulated with IL-2. After 4 days, T cells were pooled, washed with PBS and re-seeded in the absence of activation stimuli for additional 3 days. CD8+ T cells were investigated daily concerning their supernatant concentration of **(A)** Granzyme A, **(B)** Granzyme B, **(C)** Granulysin, **(D)** Perforin, and **(E)** IFNγ. Parametric data are depicted as mean with standard deviation in one direction and non-parametric data are depicted as median with interquartile range in both directions. One-way ANOVA with Dunnett's multiple comparison test comparing all samples with 1d was used for parametric data and non-parametric data were analyzed by Kruskal-Wallis Test with Dunn's multiple comparison test comparing all samples with 1d. n= 3. * = $p < 0.05$, ** = $p < 0.01$, *** = $p < 0.001$.

Overall, supernatants of CD8+ T cells showed increased concentrations of Granzyme A/B, Perforin, and IFNγ during activation culture. However, after elimination of activation stimuli, the concentration of all investigated molecules was rapidly decreased (despite Granulyisn).

In summary, CD69 and CD25 expression of CD8+ T cells had its peak after three days of activation culture along with elevated PD-1 expression, representing an exhausted phenotype of CD8+ T cells. Further, the release of cytotoxic molecules was diminished after 4 days of activation culture, wherefore 4 day activated T cells were used for further experiments.

4.2.3. Blocking PD-L1 on CD8+ T cells did not affect activation stage of CD8+ T cells and PDEC viability

Having identified that CD8+ T cells also express PD-L1 on their surface (section 4.2.1), the next aim was to investigate the role of PD-L1 on CD8+ T cells by blocking PD-L1 on T cells. For this purpose, PD-L1 was blocked by application of Durvalumab in the following experiments.

In order to investigate whether and how blocking of PD-L1 on CD8+ T cells impairs the activation stage along with PD-1, PD-L1, and CD80 expression as well as PDEC viability after co-culture with CD8+ T cells, pre-activated CD8+ T cells were mono-cultured and treated with either hIgG1 or Durvalumab for 3 days. The cell surface levels of CD69 and CD25 (Figure 21A) were not affected by application of Durvalumab. Likewise, the expression of PD-1 and CD80 were not altered by Durvalumab treatment (Figure 21B). However, PD-L1 expression on CD8+ T cells was diminished when Durvalumab was applied (Figure 21B) indicating that Durvalumab blocks the binding epitope of immunofluorescence staining antibody used for flow cytometry, confirming successful inhibition of PD-L1.

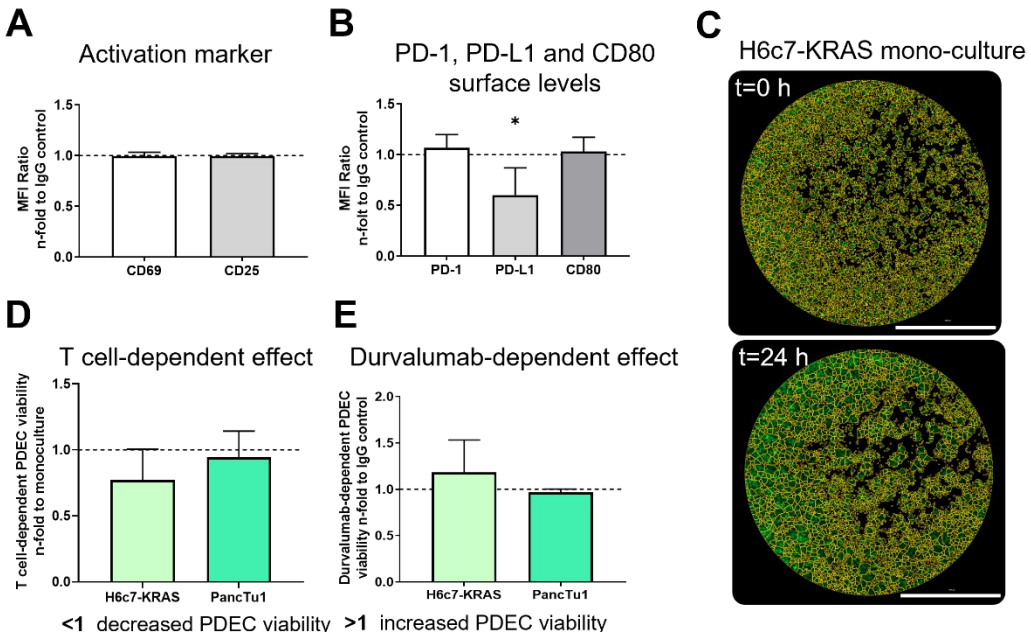

Figure 21: Blocking of PD-L1 on CD8+ T cells has no impact on activation stage and PDEC viability. Pre-activated CD8+ T cells were mono-cultured and treated with either hIgG1 or Durvalumab for 3 days. CD8+ T cells were investigated after 3 days concerning their surface levels of **(A)** activation marker CD69 (white) and CD25 (light grey) and **(B)** PD-1 (white), PD-L1 (light grey), and CD80 (dark grey) by flow cytometric analysis. Data are normalized to isotype control and the dashed lines mark an MFI ratio of "1". Data are presented as MFI ratio and denotes median fluorescence intensity ratio of specific staining antibody and its isotype control ($MFI^{specific}/MFI^{isotype}$). n=3. Afterwards, CD8+ T cells were co-cultured with CellTracker green labeled H6c7-KRAS or PancTu1 cells. Confluence at the beginning of PDEC/T cell co-culture was measured by detecting green fluorescence confluence. After 24 h, CD8+ T cells were discarded, PDEC were washed with PBS and again, fluorescent-dependent confluence was measured. **(C)** Representative images of fluorescence-based confluence analysis at timepoints t=0 h (above) and t=24 h (below). (Scale bar: 2000 µm). **(D+E)** Quantitative analysis of PDEC viability of H6c7-KRAS and PancTu1 cells. The ratio of confluence at t=24 h and t=0 h was calculated to obtain the confluence ratio. Then, this ratio was normalized to PDEC mono ratio to visualize the T cell-dependent effect **(D)**. To visualize the Durvalumab-dependent effect confluence ratio was normalized to the IgG1 isotype control **(E)**. The dashed lines mark a PDEC viability ratio of "1". Parametric data are depicted as mean with standard deviation in one direction. H6c7-KRAS n=4, PancTu1 n=3. * = $p < 0.05$.

The PDEC viability was assessed by a confluence analysis of CellTracker green labeled pre-malignant H6c7-KRAS or malignant PancTu1 cells at the start (t=0 h) and the end (t=24 h) of the culture period (Figure 21C). First, the effect of CD8+ T cell co-culture revealed a reduced PDEC viability especially in H6c7-KRAS cells (Figure 21D). Next, the effect of PD-L1 blocking via Durvalumab treatment on CD8+ T cells was investigated. Although PD-L1 was effectively blocked after application of Durvalumab, Durvalumab-dependent viability of either H6c7-KRAS or PancTu1 cells was not affected (Figure 21E).

Overall, Durvalumab effectively blocked PD-L1 on the cell surface of CD8+ T cells, but neither the activation status of CD8+ T cells nor PDEC viability were affected.

4.2.4. Blocking PD-L1 in direct co-culture of CD8+ T cells and PDEC cells decreased PDEC viability

Having identified that activation stage of CD8+ T cells and PDEC viability was not impaired when CD8+ T cells were pre-treated with Durvalumab, it was next elucidated whether blocking of PD-L1 is more effective in direct co-culture of CD8+ T cells and PDECs. Since pre-malignant H6c7-KRAS and malignant PancTu1 cells exhibit considerable PD-L1 expression [218] (Figure 27B), blocking this molecule with Durvalumab in direct co-culture with PD-L1-expressing CD8+ T cells was done for 24 h. Of note, fluorescent confluence analysis revealed that application of Durvalumab led to a decreased PDEC viability of both PDEC lines H6c7-KRAS and PancTu1 (H6c7-KRAS vs. PancTu1: 0.72 vs. 0.79) (Figure 22).

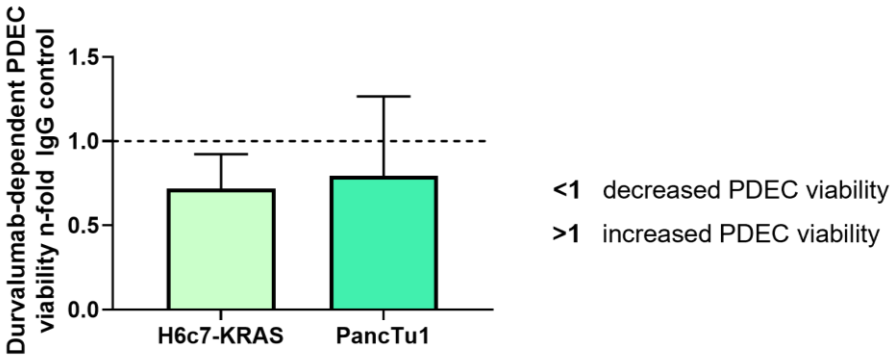

Figure 22: Blocking of PD-L1 in co-culture of CD8+ T cells and PDECs decreases PDEC viability of H6c7-KRAS and PancTu1 cells. Pre-activated CD8+ T cells were co-cultured with CellTracker green labeled PDECs and incubated with either hIgG1 or Durvalumab for 24 h. Confluence at the beginning of co-culture was measured by detecting green fluorescence confluence. After 24 h, CD8+ T cells were discarded, PDECs were washed with PBS and again fluorescent-dependent confluence was measured. The ratio of confluence at t=24 h and t=0 h was calculated. This ratio was normalized to the respective isotype control. Quantitative analysis of Durvalumab-dependent PDEC viability of H6c7-KRAS cells and PancTu1 cells. The dashed lines mark a Durvalumab-dependent PDEC viability ratio of "1". Parametric data are depicted as mean with standard deviation in one direction. H6c7-KRAS: n=4; PancTu1: n=3.

Altogether, Durvalumab led to a reduced viability in H6c7-KRAS and PancTu1 cells when the PD-L1 blocking antibody was applied directly in co-culture of tumor cells with CD8+ T cells, indicating an inhibiting role of PD-L1 expressed by PDECs.

4.3. *In vitro* characterization of PD-L1 and its blockade in CD8+ T cell/macrophage interplay with PDEC

The *in situ* results revealed that the expression of PD-L1 is associated with the attendance of macrophages and CD8+ T cells, predominantly seen at the invasion fronts of primary tumors and liver metastases. As these data also showed that CD8+ T cells and macrophages were in close proximity to each other, the next aim was to examine *in vitro,* whether and how CD8+ T cells were impacted by the presence of PD-L1-expressing macrophages and *vice versa*. Further, the effect of CD8+ T cells pre-cultured with different types of macrophages on PDEC viability was examined.

4.3.1. Phenotypic differences of M1-like and M2-like macrophages are abolished by co-culture with CD8+ T cells

In order to examine, whether and how the phenotypes of *in vitro* polarized pro-inflammatory M1-like and anti-inflammatory M2-like macrophages are altered due to the presence of CD8+ T cells, the cell morphology and expression of different polarization markers were analyzed. For this purpose, human monocytes were cultured for seven days in teflon-bags either with GM-CSF for polarization into pro-inflammatory M1-like macrophages or M-CSF for polarization into anti-inflammatory M2-like macrophages. As macrophage polarization is dependent on environmental factors, they can switch their phenotype due to changing microenvironment [24]. Knowing that CD8+ T cells express various cytokines like IFNγ [24,219], and the latter is responsible for polarization switch into M1-like macrophages [220], M-CSF was added to co-culture of CD8+ T cells and M2-like macrophages to maintain their anti-inflammatory polarization. To accomplish comparable culture conditions, GM-CSF was added to co-cultures of CD8+ T cells and M1-like macrophages. Monocultured macrophages were also seeded with their respective polarization stimulus.

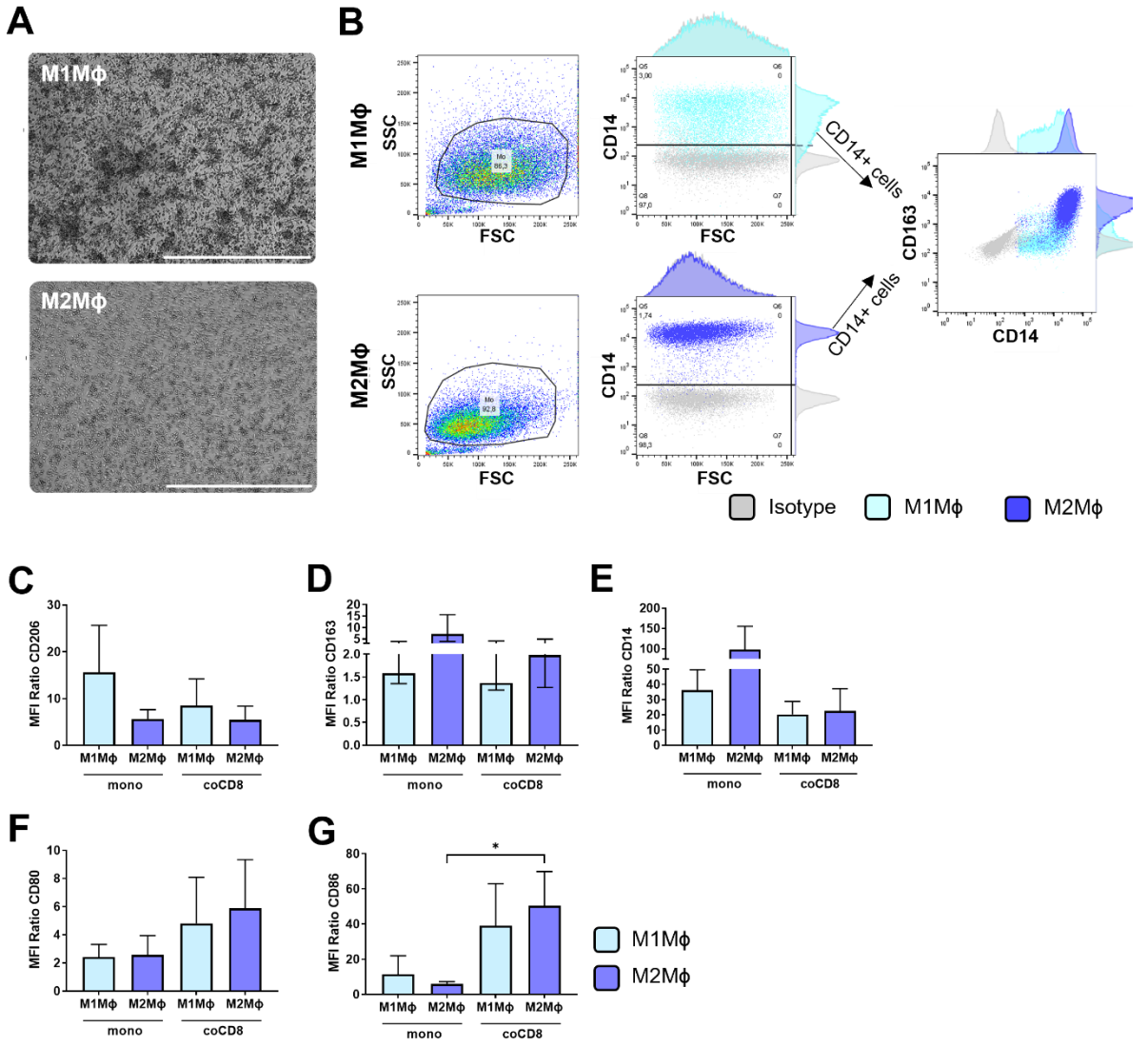

Figure 23: The polarization stage of M1-like or M2-like macrophages is altered due to CD8+ T cell co-culture. Isolation of primary human lymphocytes and monocytes from leucocyte retaining systems was performed by density gradient centrifugation followed by counter flow centrifugation. To isolate CD8+ T cells from human lymphocytes, a magnetic-activated cell sorting (MACS) system was used. Afterwards, untouched CD8+ T cells were stimulated with immobilized αCD3 and soluble CD28-targeting antibodies as well as IL-2 for 4 days. At day 3, CD8 T cells were again stimulated with IL-2. Human monocytes were cultured in teflon-bags for 7 days either with GM-CSF for polarization into pro-inflammatory M1-like macrophages (M1Mϕ) or M-CSF into anti-inflammatory M2 macrophages (M2Mϕ). Macrophages and CD8+ T cells were directly co-cultured for 48 h. During co-culture, GM-CSF or M-CSF was added to ensure M1- and M2-like phenotype of macrophages. **(A)** Representative phase contrast images of polarized human M1- or M2-like macrophages (Scale bar: 1000 µm). **(B)** Exemplary gating strategy of M1-like and M2-like macrophages. Shown are the FSC/SSC dot plots (left) and discrimination of CD14+ cells (light and dark blue) to exclude other cell populations in grey (middle). An exemplary double positive staining of CD14 and CD163 is depicted right (light blue: M1Mϕ, dark blue: M2Mϕ). Polarization of macrophages was investigated concerning their expression of **(C)** M1 marker CD206, **(D)** M2 marker CD163, **(E)** CD14 as well as co-stimulatory molecules **(F)** CD80 and **(G)** CD86 by flow cytometric analysis (light blue: M1Mϕ, dark blue: M2Mϕ). Data are presented as MFI ratio and denotes median fluorescence intensity ratio of specific staining antibody and its isotype control ($MFI^{specific}/MFI^{isotype}$). Parametric data are depicted as mean with standard deviation in one direction and non-parametric data are depicted as median with interquartile range in both directions. One-way ANOVA with Tukey's multiple comparison test, * = $p < 0.05$. n=4.

Representative images of macrophages revealed that M1-like macrophages form small cell clusters, whereas M2-like macrophages were scattered in mono-culture (Figure 23A). In order to analyze exclusively macrophages and no other blood cells, CD14 was stained as a general macrophage marker.

Only CD14+ macrophages were gated and further analyzed. The gating strategy for CD14+ macrophages is depicted in Figure 23B. To discriminate M1-like from M2-like macrophages, the expression of CD206 (Figure 23C), CD163 (Figure 23D), CD14 (Figure 23E), CD80 (Figure 23F), and CD86 (Figure 23G) were investigated. CD206 levels were higher in mono-cultured and co-cultured M1-like macrophages compared to respective M2-like macrophages. (MFI ratio mono M1 vs. mono M2: 15.6 vs. 5.6 and coM1 vs. coM2: 8.53 vs. 5.44) (Figure 23C). Although CD8+ T cells release IFNγ, which can induce an M1-phenotype switch [220], the application of M-CSF in M2-like macrophage mono- and co-culture stabilized the anti-inflammatory phenotype as CD163 surface levels were higher in both culture conditions compared to M1-like macrophages (Figure 23D). CD14 levels were highest in mono-cultured M2-like macrophages but were only slightly higher in co-cultured M2-like macrophages than M1-like macrophages (Figure 23E). Cell surface levels of CD80 and CD86 were enhanced in both macrophage populations after CD8+ T cell co-culture, but interestingly more pronounced in co-cultured M2-like macrophages (MFI ratio CD86 mono M2 vs. coM2: 5.91 vs. 50.34, $p = 0.01$) (Figure 23F+G).

Overall, the *in vitro* polarization of human monocytes into pro-inflammatory M1-like and anti-inflammatory M2-like macrophages clearly differed between both macrophage populations in mono-culture as well as in co-culture with CD8+ T cells, albeit to a lesser extent under the latter conditions. The presence of CD8+ T cells led to decreased cell surface levels of CD206 and CD14 on both macrophage types and diminished CD163 levels on M2-like macrophages. However, CD80 and CD86 levels were enhanced when both macrophage populations were co-cultured with CD8+ T cells.

4.3.2. PD-L1 surface levels on M1-like and M2-like macrophages were considerably enhanced in the presence of CD8+ T cells

As a next step, it was examined whether PD-L1 surface levels on M1-like macrophages differed from M2-like macrophages and whether the attendance of CD8+ T cells alter this expression pattern. Therefore, polarized macrophages were either mono- or co-cultured with pre-activated CD8+ T cells for 48 h. To maintain the polarization of M1-like or M2-like macrophages, GM-CSF or M-CSF was added to mono- or co-cultures and PD-L1 levels were investigated by immunofluorescence staining on coverslip-seeded macrophages (Figure 24A+B) or by flow cytometric analysis (Figure 24C+D). Representative images of M1-like macrophages mono-cultured and co-cultured with CD8+ T cells are depicted in Figure 24A. A considerable enhancement of PD-L1 levels was seen after co-culture with CD8+ T cells. Likewise, co-cultured M2-like macrophages with CD8+ T cells showed an increased PD-L1 expression compared to their mono-culture. In Figure 24C, a representative image of macrophages' immunofluorescence double staining (CD14 and PD-L1 by flow cytometric analysis) is depicted as a dot

plot with histograms. In line with the immunofluorescence staining on coverslips, increased PD-L1 surface levels as well as clearly enhanced levels in both macrophage populations after co-culture with CD8+ T cells were also detected by flow cytometric evaluation (MFI ratio M1 mono vs. M1co: 8.90 vs. 58.91; M2 mono vs. M2co: 2.96 vs. 72.72, p = 0,04).

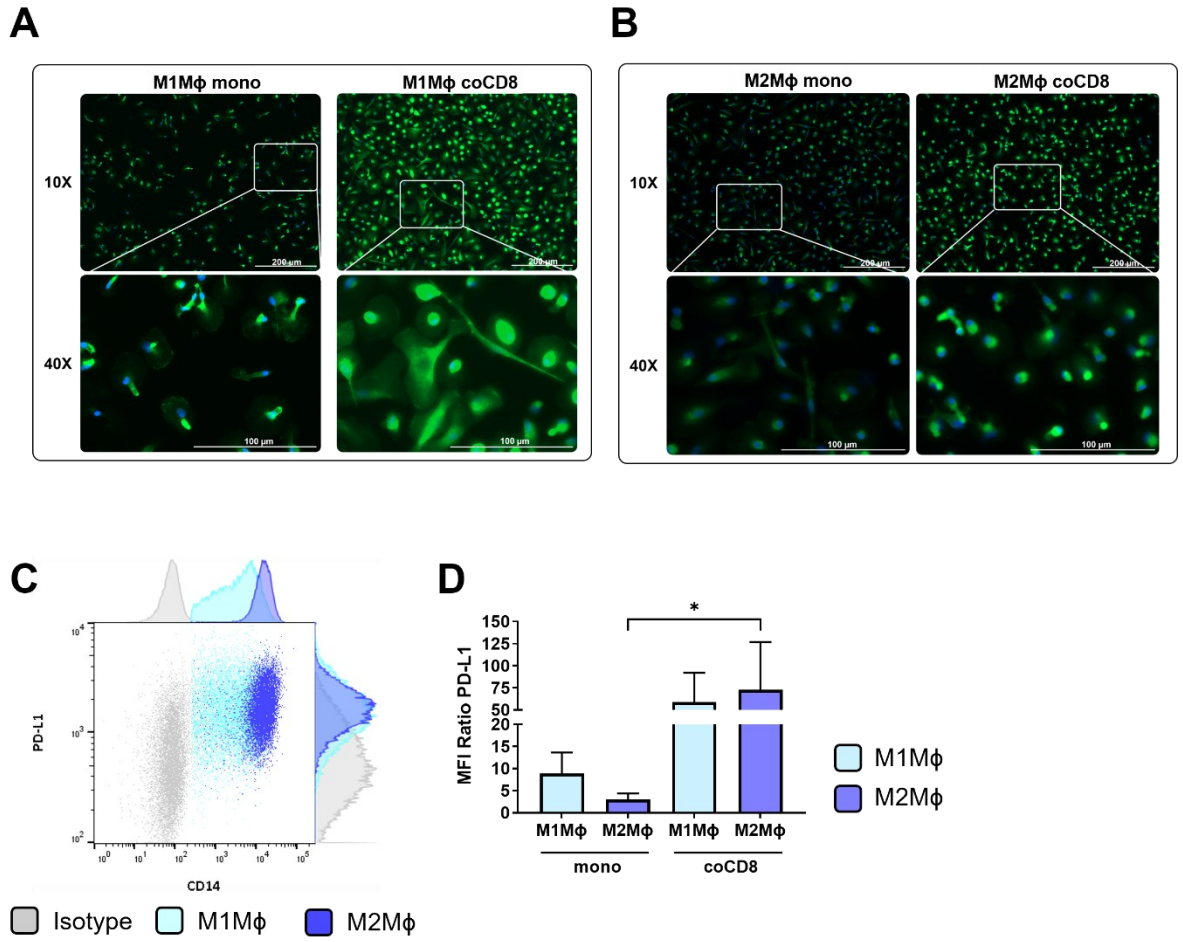

Figure 24: Cell surface levels of PD-L1 on M1-like or M2-like macrophages are markedly enhanced after CD8+ T cell co-culture. Isolation of primary human lymphocytes and monocytes from leucocyte retaining systems was performed by density gradient centrifugation followed by counter flow centrifugation. To isolate CD8+ T cells from human lymphocytes, a magnetic-activated cell sorting (MACS) system was used. Afterwards, untouched CD8+ T cells were stimulated with immobilized αCD3 and soluble CD28-targeting antibodies as well as IL-2 for 4 days. At day 3, CD8+ T cells were again stimulated with IL-2. Human monocytes were cultured in teflon-bags for 7 days either with GM-CSF for polarization into pro-inflammatory M1-like macrophages (M1Mϕ) or M-CSF for polarization into anti-inflammatory M2-like macrophages (M2Mϕ). Macrophages and CD8+ T cells were directly co-cultured for 48 h. During co-culture, GM-CSF or M-CSF was added to ensure M1-like and M2-like phenotype of macrophages. Representative fluorescence microscopy images of polarized human **(A)** M1-like macrophages or **(B)** M2-like macrophages either in mono-culture (mono) or co-culture with CD8+ T (coCD8) (Scale bar 10X: 200 µm, 40X: 100 µm). **(C)** Exemplary dot plot of double positive macrophages stained for CD14 and PD-L1 (light blue: M1Mϕ, dark blue: M2Mϕ, grey: isotype). **(D)** Quantitative analysis of CD14+ and PD-L1+ macrophages by flow cytometric analysis. Data are presented as MFI ratio and denotes median fluorescence intensity ratio of specific staining antibody and its isotype control ($MFI^{specific}/MFI^{isotype}$). Parametric data are depicted as mean with standard deviation in one direction. One-way ANOVA with Tukey's multiple comparison test, * = $p < 0.05$. n=4.

Altogether, both macrophage types enhanced their PD-L1 expression when co-cultured with CD8+ T cells, whereby co-cultured M2-like macrophages showed a higher PD-L1 increase compared to co-cultured M1-like macrophages.

4.3.3. Expression of immune checkpoint molecules is increased in CD8+ T cell co-culture with macrophages of different phenotypes

In order to investigate whether and how exhausted CD8+ T cells are impacted by the presence of pro-inflammatory M1-like or anti-inflammatory M2-like macrophages, analysis of activation stage as well as expression of CD80 and immune checkpoint molecules PD-1 and PD-L1 was performed. Pre-activated CD8+ T cells and polarized macrophages were directly co-cultured for 48 h. Knowing that the different phenotypes of macrophages are reduced but discriminable due to CD8+ T cell co-culture (section 4.3.1), the following surface expression levels of CD8+ T cells did not exhibit major differences between co-culture with both macrophage types. In detail, analyzing CD69 cell surface levels of CD8+ T cells, it was noticeable that co-culture with both M1-like as well as M2-like macrophages clearly enhanced CD69 levels (MFI ratio mono vs. coM1 vs. coM2: 1.52 vs. 9.52 vs. 7.30) (Figure 25A). In line with these results, higher CD25 surface levels in co-cultured CD8+ T cells with both macrophage populations were observed compared to mono-cultured CD8+ T cells (MFI ratio mono vs. coM1 vs. coM2: 9.08 vs. 30.34 vs. 23.70) (Figure 25B). Although the macrophage phenotypes were equalized to each other (section 4.3.1), co-culture with pro-inflammatory macrophages resulted in higher expression of both activation markers compared to co-culture with M2-like macrophages. The expression of PD-1 (Figure 25C) and its ligand PD-L1 (Figure 25D) was very similar since both molecules were enhanced after co-culture with either macrophage population. CD80 expression showed similar results, although the expression level of CD80 was generally very low (MFI ratio mono vs. coM1 vs. coM2: 1.27 vs. 1.59 vs. 1.51) (Figure 25E). Interestingly, CD8+ T cells co-cultured with M2-like macrophages showed lower cell surface levels for both immune checkpoint molecules compared to M1-like macrophage co-cultured CD8+ T cells. Furthermore, unpublished data from my master thesis showed elevated levels of all cytotoxic molecules (Granzyme A/B, Granulysin, Perforin) and IFNγ in CD8+ T cells after co-culture with both macrophage populations, but even higher concentrations after co-culture with M1-like macrophages, underscoring the pro-inflammatory property of M1-like macrophages [221].

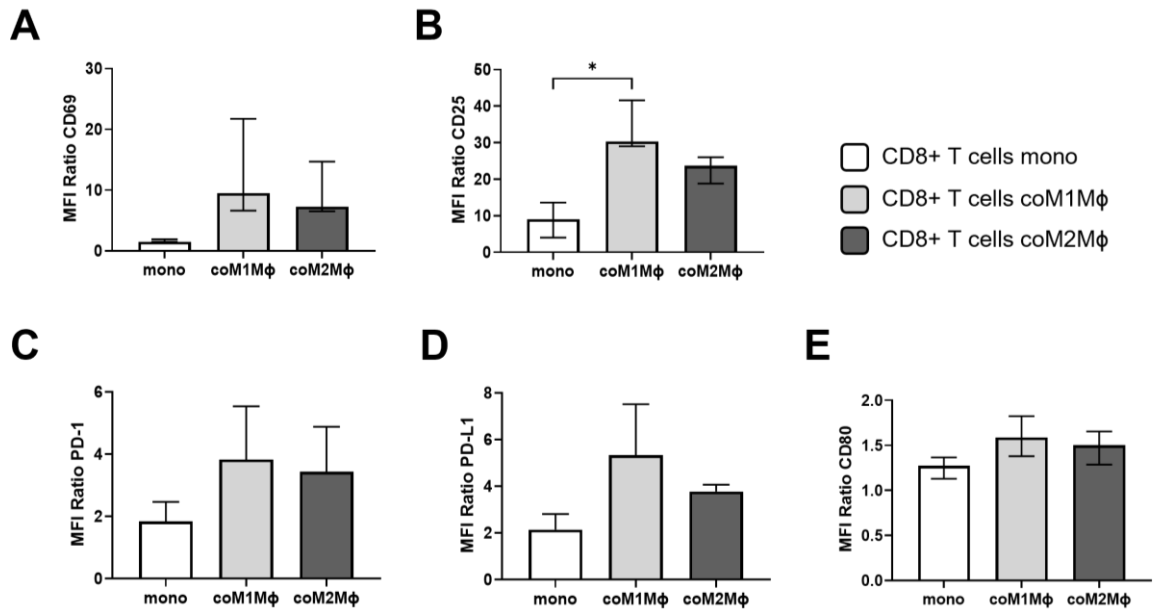

Figure 25: Elevated cell surface level of activation markers CD69 and CD25 as well as immune checkpoint molecules PD-1 and PD-L1 on CD8+ T cells after co-culture with M1-like or M2-like macrophages. Isolation of primary human lymphocytes and monocytes from leucocyte retaining systems was done by density gradient centrifugation followed by counter flow centrifugation. To isolate CD8+ T cells from human lymphocytes, a magnetic-activated cell sorting (MACS) system was used. Afterwards, untouched CD8+ T cells were stimulated with immobilized αCD3 and soluble CD28-targeting antibodies as well as IL-2 for 4 days. At day 3, CD8+ T cells were again stimulated with IL-2. Human monocytes were polarized for 7 days either with GM-CSF into pro-inflammatory M1-like macrophages (M1Mϕ) or M-CSF into anti-inflammatory M2-like macrophages (M2Mϕ). CD8+ T cells and macrophages were directly co-cultured for 48 h. During co-culture, GM-CSF or M-CSF was added to maintain the M1- and M2-like phenotype of macrophages. CD8+ T cells were investigated concerning their surface levels of activation markers **(A)** CD69 and **(B)** CD25 as well as immune checkpoint molecules **(C)** PD-1, **(D)** PD-L1, and **(E)** CD80 by flow cytometric analysis. Data are presented as MFI ratio and denotes median fluorescence intensity ratio of specific staining antibody and its isotype control ($MFI^{specific}/MFI^{isotype}$). Parametric data are depicted as mean with standard deviation in one direction and non-parametric data are depicted as median with interquartile range in both directions. Kruskal-Wallis test with Dunn's multiple comparison test, * = $p < 0.05$. n=3.

In summary, co-culture with both macrophage populations increased levels of activation molecules CD69 and CD25 as well as immune checkpoint molecules PD-1 and PD-L1 on CD8+ T cells, which was more pronounced after co-culture with M1-like macrophages. Although PD-L1 was highly expressed on CD8+ T cells and both macrophage populations, an increase of activation markers and concentration of cytotoxic molecules (data not shown, Master thesis [221]) was detected, pointing out that the PD-1/PD-L1 axis does not impede CD8+ T cell effector function, when PD-L1 is expressed by CD8+ T cells or macrophages.

4.3.4. Pre-culture of CD8+ T cells with macrophages does not alter PDEC viability

As the activation stage and release of cytotoxic molecules of CD8+ T cells were enhanced by co-culture with both macrophage populations, the next step was to examine the PDEC viability after co-culture with CD8+ T cells pre-cultured with macrophages. For this purpose, two different PDEC lines

(premalignant and high PD-L1-expressing H6c7-KRAS cells and malignant and moderate PD-L1-expressing PancTu1 cells) were used. First, pre-activated CD8+ T cells were either mono-cultured (CD8 post mono) or co-cultured with M1- or M2-like macrophages (CD8 post M1Mϕ or CD8 post M2Mϕ) for 48 h. Afterwards, CD8+ T cells were co-cultured with CellTracker green labeled H6c7-KRAS or PancTu1 cells for 24 h. The PDEC cell viability was assessed by confluence analysis of CellTracker green labeled H6c7-KRAS or PancTu1 cells. The ratio of confluence at t=24 h and t=0 h was calculated and then normalized to the ratio of PDEC mono-culture to focus on the T cell-dependent effect (Figure 26A+B). A T cell-dependent PDEC viability < 1 denotes a reduction of PDEC confluence compared to mono-cultured PDEC. Confluence analysis revealed no or negligible reduction of viability in H6c7-KRAS cells in the presence of CD8+ T cells (Figure 26A). In PancTu1 cells, only a negligible decrease of PDEC viability was detected after CD8+ T cell co-culture. Neither the pre-culture of CD8+ T cells with M1-like nor M2-like macrophages resulted in an enhanced reduction of PancTu1 cell viability.

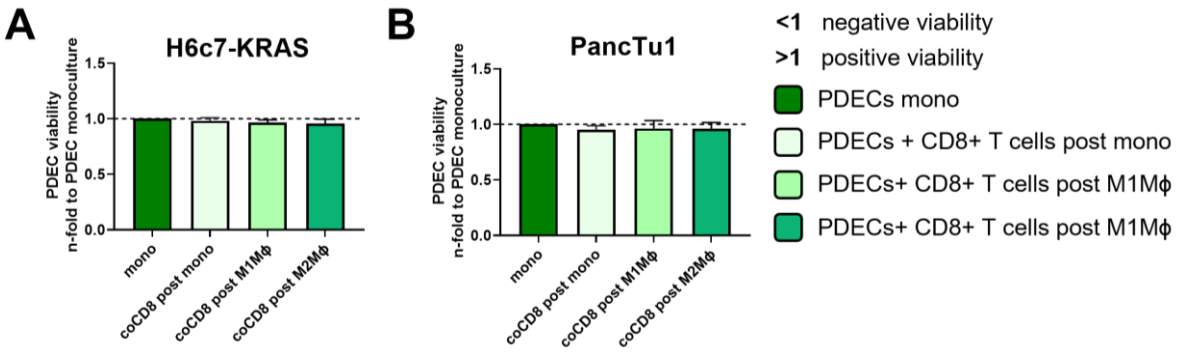

Figure 26: Negligible reduction of PDEC viability after co-culture with different pre-treated CD8+ T cells. Pre-activated CD8+ T cells (4 days) were either mono-cultured (CD8 post mono) or co-cultured with M1- or M2-like macrophages (CD8 post M1Mϕ or CD8 post M2Mϕ) for 48 h. Afterwards, CD8+ T cells were co-cultured with CellTracker green labeled H6c7-KRAS or PancTu1 cells. In parallel, PDECs were mono-cultured, too. Confluence at the beginning of PDEC / T cell co-culture was measured by detecting the green fluorescence confluence via microscope. After 24 h, CD8+ T cells were discarded, PDEC were washed with PBS and again fluorescence confluence was measured. The ratio of confluence at t=24 h and t=0 h was calculated and then normalized to ratio of mono-cultured PDEC. **(A)** Quantitative analysis of PDEC viability at indicated culture conditions of H6c7-KRAS cells. n=3. **(C)** Quantitative analysis of PDEC viability at indicated culture conditions of PancTu1 cells. Parametric data are depicted as mean with standard deviation in one direction. n=3.

Altogether, although CD8+ T cells showed an enhanced activation stage (section 4.3.3) and release of cytotoxic molecules and IFNγ (data not shown, Master thesis [221]) after co-culture with both macrophage types, this did not affect PDEC viability.

4.4. *In vitro* analysis of PD-L1 in the interplay of macrophages, T cells and PDEC in a 3D co-culture model

Since 2D cell culture on a flat bottom cannot fully represent pathophysiological conditions, 3D stroma-enriched culture systems better mimic the TME with different stromal cell populations. Therefore, the

next aim was to establish a 3D co-culture model of PDECs, macrophages, and CD8+ T cells to better mimic the dynamic TME in PDAC.

4.4.1. Analysis of PDEC lines concerning their spheroid formation ability and PD-L1 status

In order to investigate the immune-regulatory role of PD-L1 in a 3D cell-cell interaction context, it was first clarified which PDEC lines have the ability to form dense spheroids and express different levels of PD-L1, which can be further induced. For this purpose, eight different PDEC lines were seeded into ultra-low attachment plates to force the formation of spheroids (Figure 27A). Demonstrated in representative phase contrast images, only pre-malignant H6c7-KRAS as well as malignant PancTu1, Panc89, and A818-6 cells could form dense spheroids (Figure 27, upper row). Panc1 cells did not form spheroids at all, rather a loose aggregation of cells was observed. BxPc3 cells formed spheroids, but a considerable amount of single cells were found outside the spheroid. Finally, Colo357 and PT-45 cells both formed only loose spheroids (Figure 27). Next, the PD-L1 expression levels of all PDEC lines were investigated by immunofluorescence staining and subsequent flow cytometric analysis. H6c7-KRAS cells expressed the highest amounts of PD-L1 (MFI ratio PD-L1: 21.4), followed by PT-45 cells (MFI ratio PD-L1: 11,8), PancTu1 cells (MFI ratio PD-L1: 7.1) and A818-6 cells (MFI ratio PD-L1: 5.1). In contrast, Panc89, BxPc3, and Colo 357 cells only expressed low levels of PD-L1 (MFI ratio PD-L1: 1.75 – 3.56), and in Panc1 cells, almost no PD-L1 levels were detectable (MFI ratio PD-L1: 1,32) (Figure 27B). As co-culture experiments were planned with different stroma cell types and these cells release various cytokines which could affect PD-L1 expression, it was tested whether PD-L1 expression can be induced by treatment with IFNγ, as IFNγ is a well-known inducer of PD-L1 expression [164,222,223]. Indeed, IFNγ treatment improved PD-L1 expression on H6c7-KRAS, PancTu1, Panc89, BxPc3, Colo357 and A818-6 cells. The highest increase was detected on Colo357 and BxPc3 cells (n-fold MFI ratio PD-L1: 5.49 and 4.13). PancTu1 and Panc89 cells showed a similar moderate increase (n-fold MFI ratio PD-L1: 3.18 and 2.88) and H6c7-KRAS and A818-6 cells showed the lowest enhancement (n-fold MFI ratio PD-L1: 1.89 and 1.80). In contrast, IFNγ treatment did not result in PD-L1 induction on Panc1 and PT-45 cells (Figure 27C). Based on the ability to form dense spheroids as well as different amounts of basal and inducible PD-L1 expression, H6c7-KRAS, PancTu1, and Panc89 cells were chosen for further experiments.

Moreover, H6c7-KRAS cells were used as a model of high, PancTu1 cells as a model for moderate and Panc89 cells as a model for low PD-L1-expressing PDECs. To evaluate the viability of the spheroids, Celltracker green labeled PDECs were stained with PI, to investigate the presence of a potential necrotic core (Figure 27D). In H6c7-KRAS spheroids, a high PI staining was observed all over the

spheroid. In contrast, PancTu1 and Panc89 only showed low numbers of PI+ cells, indicating a good viability in 3D culture. Due to the poor viability of H6c7-KRAS spheroids, these cells were not considered for further usage as a 3D model.

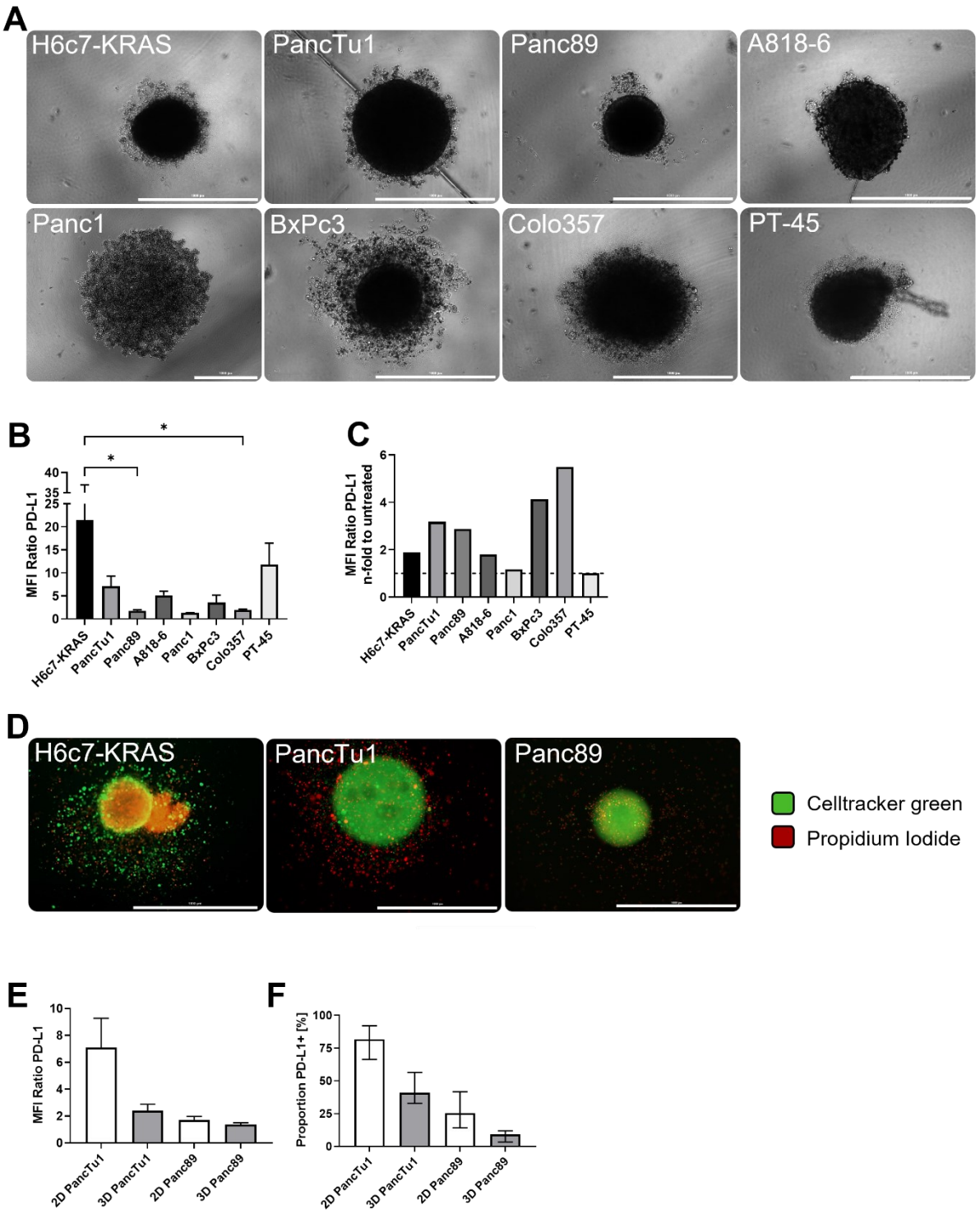

Figure 27: Analysis of different PDEC lines concerning their spheroid formation ability and PD-L1 status. Different PDEC lines were seeded into ultra-low attachment (ULA) plates for 3 days to investigate their spheroid formation ability. **(A)** Representative phase contrast images of 8 different PDEC lines (upper row: H6c7-KRAS, PancTu1, Panc89 and A818-6 cells, lower row: Panc1, BxPc3, Colo357, and PT-45 cells). (Scale bar: 1000 µm). **(B)** PD-L1 cell surface levels of 8 different PDEC lines measured by flow cytometric analysis. Data are presented as MFI ratio and denotes median fluorescence intensity ratio

of specific staining antibody and its isotype control ($MFI^{specific}/MFI^{isotype}$. One-way ANOVA with Tukey's multiple comparison test. KRAS+PancTu1: n=5, Panc89+Colo357: n=4, Panc1+BxPc3+A818-6+PT45: n=2. **(C)** PD-L1 cell surface levels after 72 h IFNγ treatment (10 ng/ml). **(D)** Representative fluorescent microscopy images of CellTracker green labeled H6c7-KRAS (left), PancTu1 (middle), and Panc89 cells (right). Red cells are Propidium Iodide + cells. (Scale bar: 1000 µm). **(E)** Flow cytometry analysis to compare PD-L1 MFI ratio of 2D (white) or 3D (grey) cultured PancTu1 and Panc89 cells. One-way ANOVA with Tukey's multiple comparison test. n=3. **(F)** Flow cytometry analysis to compare PD-L1+ proportions of 2D or 3D cultured PancTu1 and Panc89 cells. Kruskal-Wallis test with Dunn's multiple comparison test was performed. Parametric data are depicted as mean with standard deviation in one direction and non-parametric data are depicted as median with interquartile range in both directions. 2D PancTu1: n=4; others: n=3. * = $p < 0.05$.

Finally, the PD-L1 expression of PancTu1 and Panc89 cells in 2D and 3D cultures was examined in order to see whether 3D culture conditions might impact the PD-L1 expression of both cell lines. Under both culture conditions, PancTu1 cells showed a higher PD-L1 expression compared to Panc89 cells (Figure 27E). Moreover, PD-L1 expression in 3D cultured PancTu1 cells and Panc89 cells was lower compared to respective 2D cultured cells. Similar trends were seen for the proportion of PD-L1+ cells (Figure 27F).

Overall, as PancTu1 and Panc89 cells had the ability to form dense, viable spheroids and PancTu1 cells had moderate and Panc89 cells low basal PD-L1 expression, which was further inducible, they were used to establish a stroma-enriched 3D co-culture model.

4.4.2. Co-culture spheroids of PDAC cells and macrophages mimic PD-L1 expression and tumor-stroma conditions in primary PDAC and liver metastases

It is still poorly understood whether and how PD-L1-expressing macrophages with different inflammatory phenotypes contribute to immune evasion of PDAC cells, especially when PDAC cells express no or low PD-L1 expression. In order to simulate the tumor-stroma conditions identified *in situ* in primary PDAC and liver metastases, examination of the localization and phenotype of macrophages as well as PD-L1 expression in PDAC co-culture spheroids with different ratios and types of macrophages was performed. During PDAC progression, the number of macrophages increases with the stage of disease [52] and a higher attendance of CD163+ macrophages correlates with shorter 5-year overall and recurrence-free survival [224]. Therefore, a PDAC cell-to-macrophage ratio of 3:1 was used to mimic an earlier stage of PDAC with lower infiltration of macrophages (primary PDAC), whereas a 1:1 ratio served as a model for late-stage disease (liver metastasis). To obtain further insights into the localization of different macrophage populations in co-culture with tumor cells, macrophages were labeled violet, and tumor cells were labeled green by different fluorescent dyes. The representative images of fluorescent tumor cell mono-culture revealed that after 72 h of incubation, PancTu1 spheroids were bigger in size than Panc89 spheroids. Mono-cultures of both tumor cell lines containing $2x10^4$ tumor cells showed the biggest spheroid size, followed by 3:1 ratio ($1.5x10^4$ tumor cells) and 1:1

ratio (1 x10^4 tumor cells). Macrophages were mostly located at the margin, being more pronounced in spheroids with higher amounts of macrophages (1 x10^4 macrophages in 1:1 ratio) (Figure 28A).

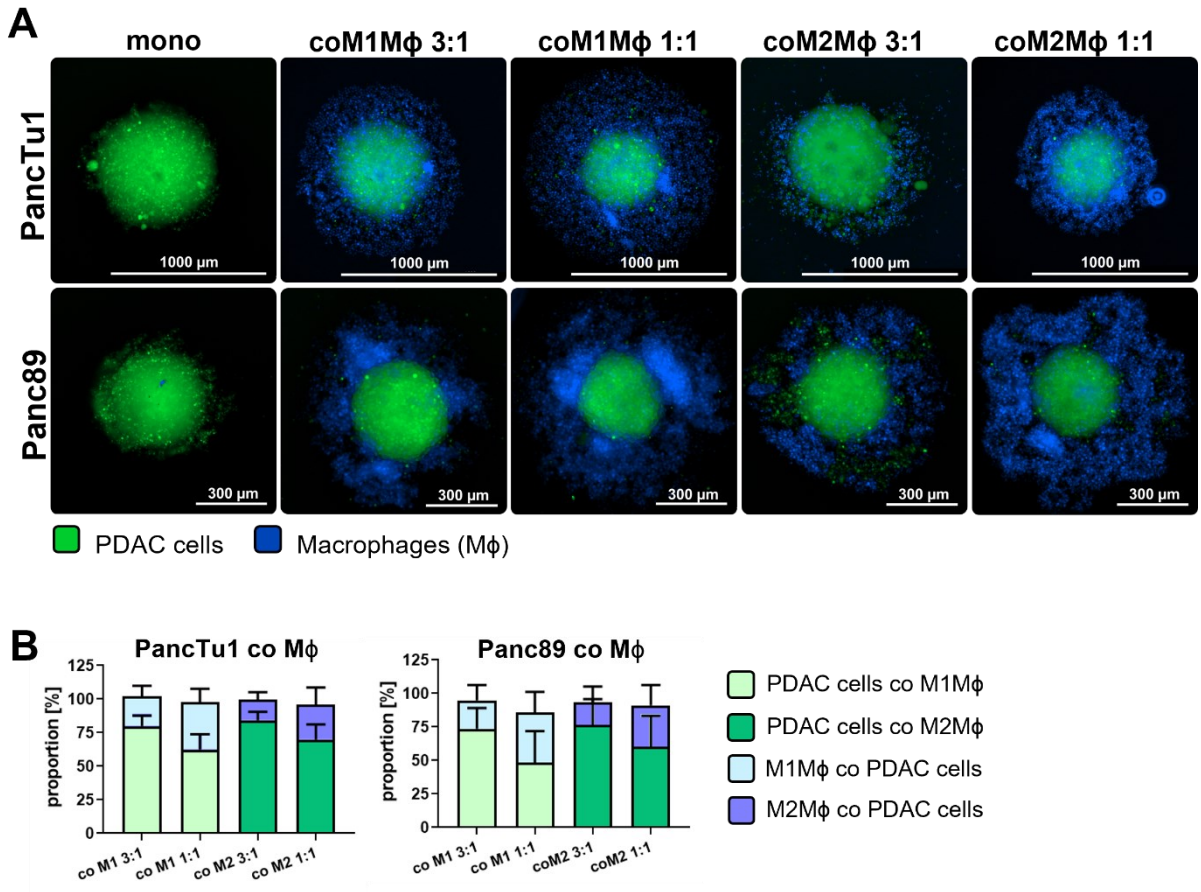

Figure 28: Co-culture spheroids containing PDAC cells and macrophages are stable for 72 h. Isolation of primary human monocytes from leucocyte retaining systems was performed by density gradient centrifugation followed by negative isolation of CD14+ monocytes. Human monocytes were cultured in 12-well plates for 6 to 7 days either with GM-CSF for polarization into pro-inflammatory M1-like macrophages (M1Mϕ) or M-CSF for polarization into anti-inflammatory M2-like macrophages (M2Mϕ). PancTu1 and Panc89 cell were either mono-cultured or co-cultured with M1-like or M2-like macrophages at 3:1 or 1:1 ratio for 72 h in ultra-low attachment plates to form spheroids. **(A)** Representative fluorescence microscopy images of CellTracker green labeled PancTu1 cells (upper row, green) or Panc89 cells (lower row, green) and CellTrace violet labeled macrophages (violet) at indicated co-culture conditions. (Scale bar PancTu1: 1000 µm; Panc89: 300 µm). **(B)** Proportions of PDAC cells and macrophages in co-culture 72 h after seeding. To discriminate PDAC cells from macrophages, single cell suspension of spheroids was stained with EpCAM and CD14-targeting antibodies for flow cytometric analysis (light green: PDAC cells co-cultured with M1-like macrophages, dark green: PDAC cells co-cultured with M2-like macrophages, light blue: M1-like macrophages co-cultured with PDAC cells, dark blue: M2-like macrophages co-cultured with PDAC cells). Ratio 3:1: 1.5x10^4 PDAC cells and 0.5x10^4 macrophages; ratio 1:1: 1x10^4 PDAC cells and 1x10^4 macrophages. Parametric data are depicted as mean with standard deviation in one direction. n=4. (published data [209]).

Next, it was elucidated whether the tumor cell-to-macrophage ratio is stable during 72 h of co-culture. Therefore, spheroids were dissociated and stained with immunofluorescence antibodies α-EpCAM (for tumor cell detection) and α-CD14 (for macrophage detection). The subsequent flow cytometric analysis revealed that the proportion of PDAC cells and macrophages remained almost stable after 72 h of co-culture (Figure 28B). PancTu1 cell and macrophage proportions in 3:1 co-culture were stable, whereas in the 1:1 ratio proportions of PancTu1 cells were slightly increased (PancTu1 co M1:

62.6 % and coM2: 69.8 %). Importantly, the proportions of Panc89 cells and macrophages still clearly differed between 3:1 and 1:1 ratios in co-cultures with both macrophage population co-cultures (coM1Mϕ 3:1: 73.7 %; coM1Mϕ 1:1: 48.3 %; coM2Mϕ 3:1: 76.3 %; coM2Mϕ 1:1: 60.4 %).

Next, it was investigated whether the presence of PDAC cells impacts macrophage polarization as macrophages exhibit a high plasticity and can change their phenotype in response to the surrounding microenvironment [24,37,225]. Therefore, macrophages were analyzed after 72 h co-culture with PDAC cells. Analysis of CD206 levels revealed higher surface expression on M1-like macrophages than on M2-like macrophages (MFI ratio CD206 M1 vs. M2: 9.1 vs. 1.8). The co-culture with PancTu1 cells led to higher expression levels in both macrophage populations (Figure 29A). Attendance of Panc89 cells did not alter the expression of CD206 on M1-like macrophages but slightly enhanced those on M2-like macrophages (Figure 29B). Expression of CD163 was slightly higher in mono-cultured M2-like than in M1-like macrophages (MFI ratio CD163 M1 vs. M2: 3.0 vs. 4.0) and the presence of either PDAC cell population considerably increased CD163 expression, especially on M2-like macrophages (Figure 29C+D). Analysis of CD14 revealed that M2-like macrophages had higher expression levels than M1-like macrophages (MFI ratio CD14 M1 vs. M2: 42.6 vs. 79.8) and both macrophage populations co-cultured with PancTu1 cells increased their CD14 surface expression in co-culture of both ratios. In contrast, only a slightly enhanced CD14 expression was detected on M2-like macrophages co-cultured with Panc89 spheroids (Figure 29E+F). CD80 levels were only slightly higher in mono-cultured M1-like compared to M2-like macrophages (MFI ratio CD80 M1 vs. M2: 1.7 vs. 1.2). Only marginal enhancement of CD80 levels were observed on M1-like macrophages co-cultured with Panc89 cells in 1:1 ratio. CD80 expression on M2-like macrophages co-cultured with both PDAC cell spheroids was only slightly increased in both ratios (Figure 29G+H).

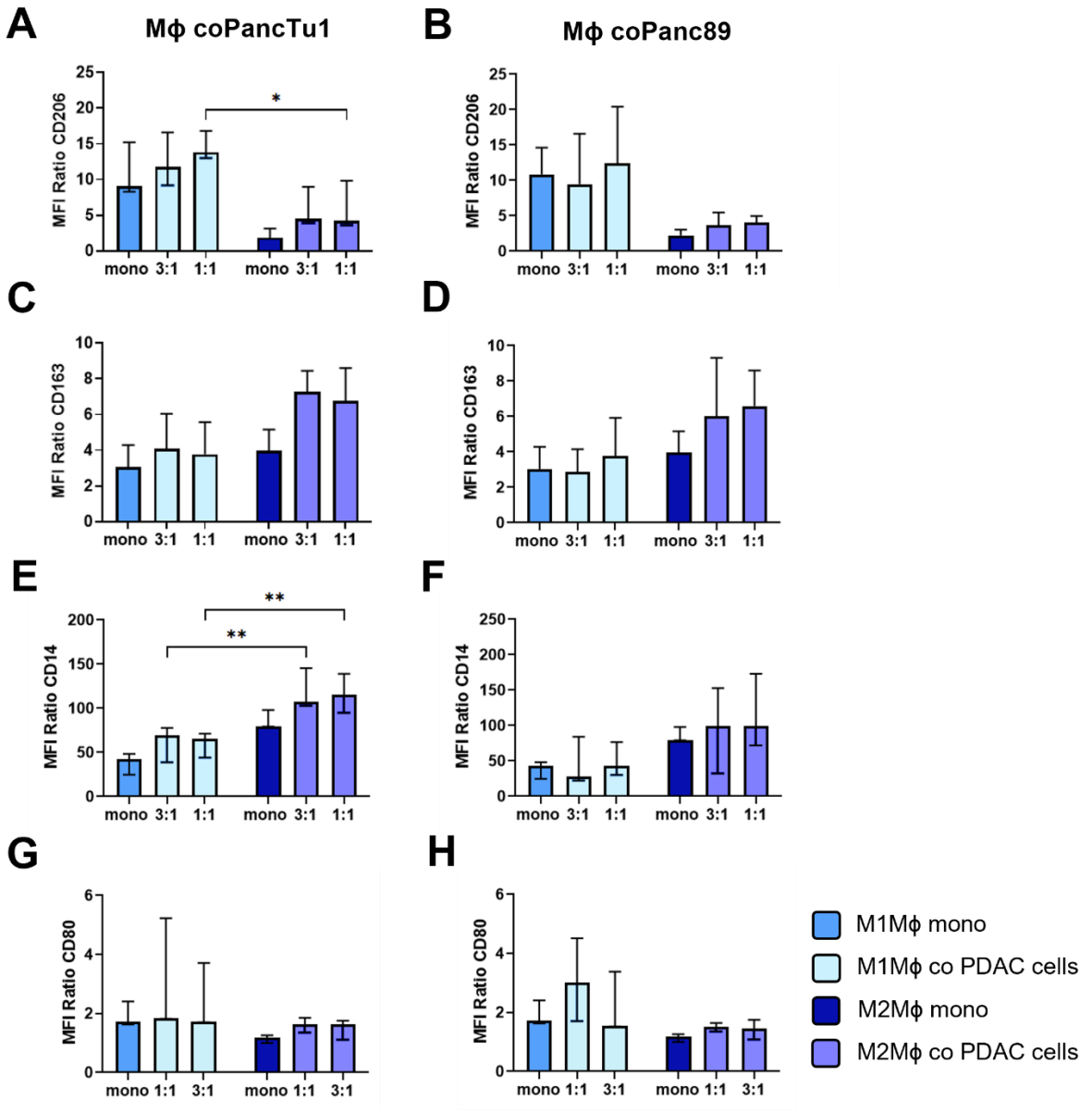

Figure 29: Co-cultured PDAC cell spheroids impact CD163 and CD14 expression on macrophages. Isolation of primary human monocytes from leucocyte retaining systems was performed by density gradient centrifugation followed by negative isolation of CD14+ monocytes. Human monocytes were cultured in 12-well plates for 6 to 7 days either with GM-CSF for polarization into pro-inflammatory M1-like macrophages (M1Mϕ) or M-CSF for polarization into anti-inflammatory M2-like macrophages (M2Mϕ). Macrophages were mono- or co-cultured with either PancTu1 or Panc89 cells for 72 h in ultra-low attachment plates to form spheroids. Macrophages were stained with antibodies against **(A+B)** CD206, **(C+D)** CD163, **(E+F)** CD14, and **(G+H)** CD80 and analyzed by flow cytometric analysis. Mono: $2x10^4$ macrophages; ratio 3:1: $1.5x10^4$ PDAC cells and $0.5x10^4$ macrophages; ratio 1:1: $1x10^4$ PDAC cells and $1x10^4$ macrophages. Data are presented as MFI ratio and denotes median fluorescence intensity ratio of specific staining antibody and its isotype control ($MFI^{specific}/MFI^{isotype}$). Parametric data are depicted as mean with standard deviation in one direction and non-parametric data are depicted as median with interquartile range in both directions. Two-way ANOVA with Tukey's multiple comparison test. * = $p < 0.05$; ** = $p < 0.01$. mono: n=3, coPDAC: n=5. (partially published data [209]).

It was further analyzed whether and how the attendance of the two different PDAC cell lines impacts PD-L1 expression on macrophages and *vice versa*. Mono-cultured M1-like macrophages had a higher PD-L1 expression than M2-like macrophages (MFI ratio PD-L1 M1 vs. M2: 4.2 vs. 2.1). Interestingly, PD-L1 expression on both macrophage populations was significantly enhanced when co-cultured with

PancTu1 spheroids and in low-expressing M2-like macrophages PD-L1 expression was elevated to similar levels of M1-like co-cultured macrophages (Figure 30A). The same trends were observed for macrophages co-cultured with Panc89 cells (Figure 30B). Mono-cultured PancTu1 cells were characterized by considerable PD-L1 surface levels which, however, were not further increased by macrophages in either co-culture setting (Figure 30 C). As described before, mono-cultured Panc89 cells exhibited hardly any PD-L1 surface expression (MFI ratio PD-L1 mono-cultured PancTu1 vs. Panc89: 4.1 vs. 1.2), and which was also almost not affected by either co-culture with macrophages (green bars, MFI ratio PD-L1: 1.2-1.69) (Figure 30D).

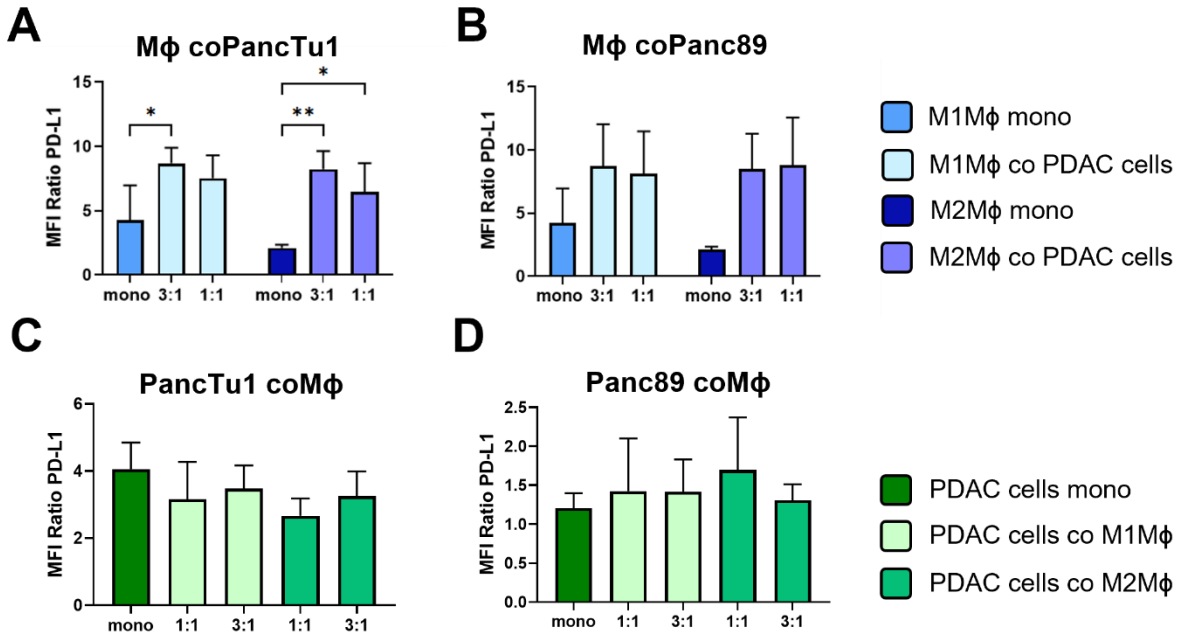

Figure 30: PD-L1 expression on macrophages, but not on PDAC cells, is enhanced by co-culture spheroids. Macrophages were mono-cultured or co-cultured with either PancTu1 or Panc89 cells for 72 h in ultra-low attachment plates to form spheroids. PD-L1 expression on **(A+B)** macrophages and **(C+D)** PDAC cells was assessed with targeting antibody for PD-L1 and examined via flow cytometric analysis. Mono: $2x10^4$ PDAC cells or macrophages; ratio 3:1: $1.5x10^4$ PDAC cells and $0.5x10^4$ macrophages; ratio 1:1: $1x10^4$ PDAC cells and $1x10^4$ macrophages. Data are presented as MFI ratio and denotes median fluorescence intensity ratio of specific staining antibody and its isotype control ($MFI^{specific}/MFI^{isotype}$). Parametric data are depicted as mean with standard deviation in one direction. Two-way ANOVA with Tukey's multiple comparison test. * = $p < 0.05$; ** = $p < 0.01$. mono: n=3, co-cultures: n=5. (published data [209]).

In summary, the results demonstrate a stable 3D co-culture system of PancTu1 and Panc89 with M1-like or M2-like macrophages in both cell ratios, well reflecting the TME of primary tumor and liver metastasis of PDAC. Moreover, the polarization of M2-like macrophages was stabilized by attendance of both PDAC cell lines, supporting the predominant presence of the M2 phenotype in TME of PDAC. Furthermore, in line with the *in situ* results, higher PD-L1 levels were detected on both macrophage populations rather than on PDAC cells, which was further intensified by PDAC cells.

4.4.3. PDAC spheroids containing macrophages impact the effector phenotype of CD8+ T cells but which does not result in enhanced PDAC cell death

As the 3D co-culture model of PDAC spheroids with M1- or M2-like macrophages well reflected the stroma-enriched TME in PDAC, the next step was to examine whether and how different stroma conditions might impact the activation stage, cytotoxic phenotype of CD8+ T cells and PDAC cell death. For this purpose, pre-activated CD8+ T cells were used after 3 days of activation culture, since their CD69 and CD25 expression as well as PD-1 and PD-L1 expression were considerably high (Figure 19).

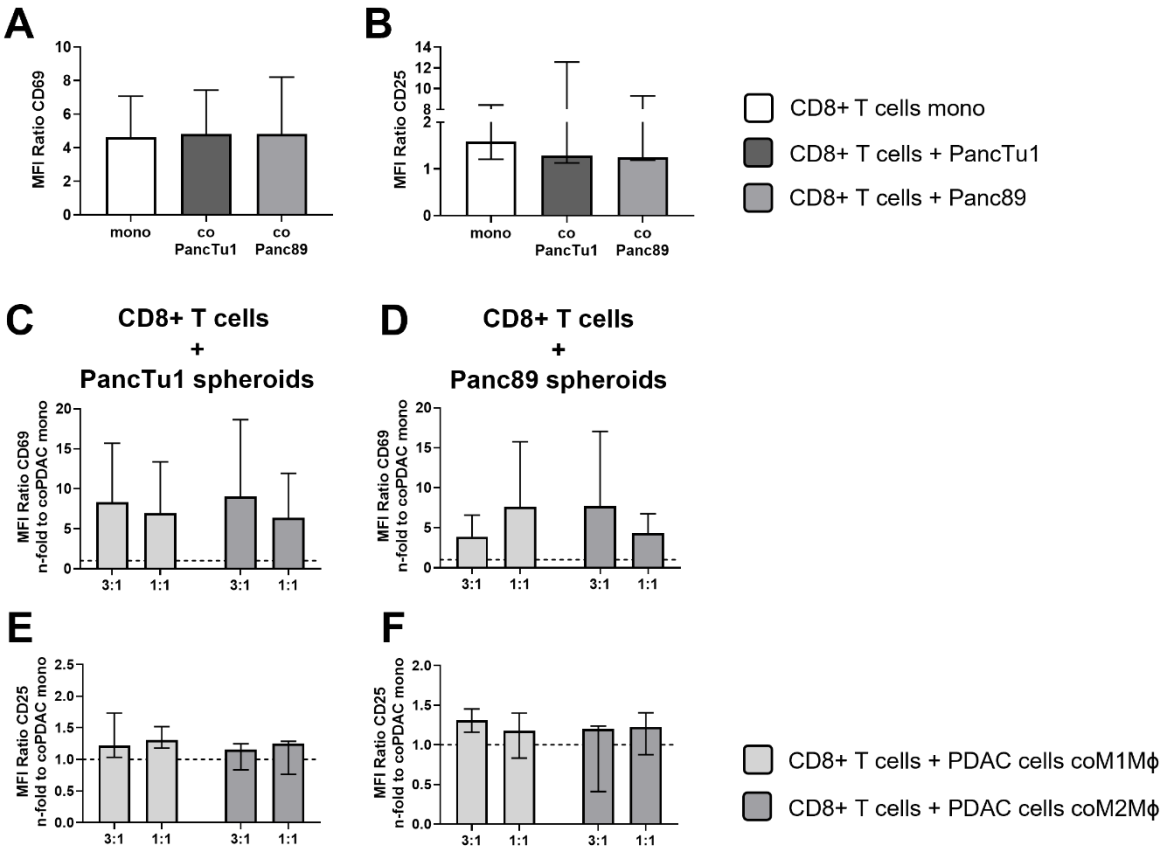

Figure 31: Activation status of CD8+ T cells is not altered by co-culture with PDAC cells but is clearly enhanced by macrophage-enriched PDAC spheroids. PancTu1 or Panc89 cells were mono-cultured or co-cultured with either M1- or M2-like macrophages in ultra-low attachment plates to form spheroids. After 48 h, pre-activated CD8+ T cells were added to spheroid culture for 24 h. Cell surface expression of activation markers **(A)** CD69 and **(B)** CD25 were analyzed on mono-cultured CD8+ T cells (white), or CD8+ T cells co-cultured with PancTu1 (dark grey) or Panc89 (light grey) spheroids by flow cytometric analysis. Not normally distributed data are depicted as median with interquartile range. n=4. Effect of M1-like (light grey) or M2-like macrophages (dark grey) enriched PDAC spheroids on **(C+D)** CD69 and **(E+F)** CD25 levels of CD8+ T cells. Data are normalized to CD8+ T cell co-culture with PDAC cell mono spheroids. Ratio 3:1: $1.5x10^4$ PDAC cells and $0.5x10^4$ macrophages; ratio 1:1: $1x10^4$ PDAC cells and $1x10^4$ macrophages. Data are presented as MFI ratio and denotes median fluorescence intensity ratio of specific staining antibody and its isotype control ($MFI^{specific}/MFI^{isotype}$). Parametric data are depicted as mean with standard deviation in one direction and non-parametric data are depicted as median with interquartile range in both directions. The dashed lines mark an MFI ratio of "1". n=4. (partially published data [209]).

First, it was investigated whether the attendance of mono-cultured PancTu1 or Panc89 spheroids alters the activation status of CD8+ T cells. However, neither PancTu1 nor Panc89 spheroids affected CD69 expression levels on CD8+ T cells, whereas CD25 levels were slightly reduced after co-culture with both

PDAC cell lines (MFI Ratio CD25 mono vs. coPancTu1 vs. coPanc89: 1.58 vs. 1.29 vs. 1.25) (Figure **31**A+B). Next, the effect of macrophage-enriched PDAC spheroids in different cell ratios on activation stage of CD8+ T cells was examined. For this purpose, CD69 and CD25 levels of CD8+ T cells cultured with co-culture spheroids were normalized to respective mono-cultured PDAC spheroids in order to specifically outline the effects of PDAC cell primed macrophages on CD8+ T cells. In contrast to Figure 31A and B, co-culture of both PDAC spheroids with M1- and M2-like macrophages led to a marked increase of CD69 expression on CD8+ T cells (Figure 31C+D). In detail, especially CD69 surface levels were enhanced on CD8+ T cells co-cultured with PancTu1 spheroids at a 3:1 ratio with both macrophage types (Figure 31C). Panc89 co-culture spheroids with M1-like macrophages at 3:1 ratio and M2-like macrophages at 1:1 ratio led to the highest expression of CD69 on CD8+ T cells (Figure **31**D). However, CD25 expression on CD8+ T cells was only slightly affected by co-culture spheroids comprising PDAC cells and macrophages (MFI Ratio CD25 CD8+ T cells coPancTu1 coMϕ: 1.15 – 1.3; coPanc89 coMϕ: 1.31 – 1.17) (Figure 31E+F).

Further, it was elucidated whether and how PD-1 and PD-L1 levels were altered by the presence of mono-cultured PDAC cell spheroids and co-culture spheroids with both macrophage types and ratios (Figure 32A+B). Since the surface levels of CD80 on CD8+ T cells were very low and not altered by the presence of PDAC spheroids or even lowered the by attendance of macrophages (Supplementary figure 2), they were not further investigated. The expression of PD-1 and PD-L1 was not impacted by mono-cultured PDAC spheroids. Similarly, PD-1 expression on CD8+ T cells was not altered due to any macrophage-enriched PDAC spheroids (Figure 32D+E). In contrast, PD-L1 levels were slightly enhanced by trend on CD8+ T cells cultured with macrophage-enriched PancTu1 spheroids (MFI Ratio PD-L1 CD8+ T cells coPancTu1 coM1Mϕ 3:1 vs. 1:1: 1.24 vs. 1.22 and coM2Mϕ 3:1 vs. 1:1: 1.22 vs. 0.99). PD-L1 levels were even significantly enhanced when cultured with Panc89 co-culture spheroids with M1-like macrophages at an 1:1 ratio and at both ratios with M2-like macrophages (MFI Ratio PD-L1 CD8+ T cells coPanc89 coM1Mϕ 3:1 vs. 1:1: 1,04 vs. 1,28 and coM2Mϕ 3:1 vs. 1:1: 1.36 vs. 1.27) (Figure 32F+G).

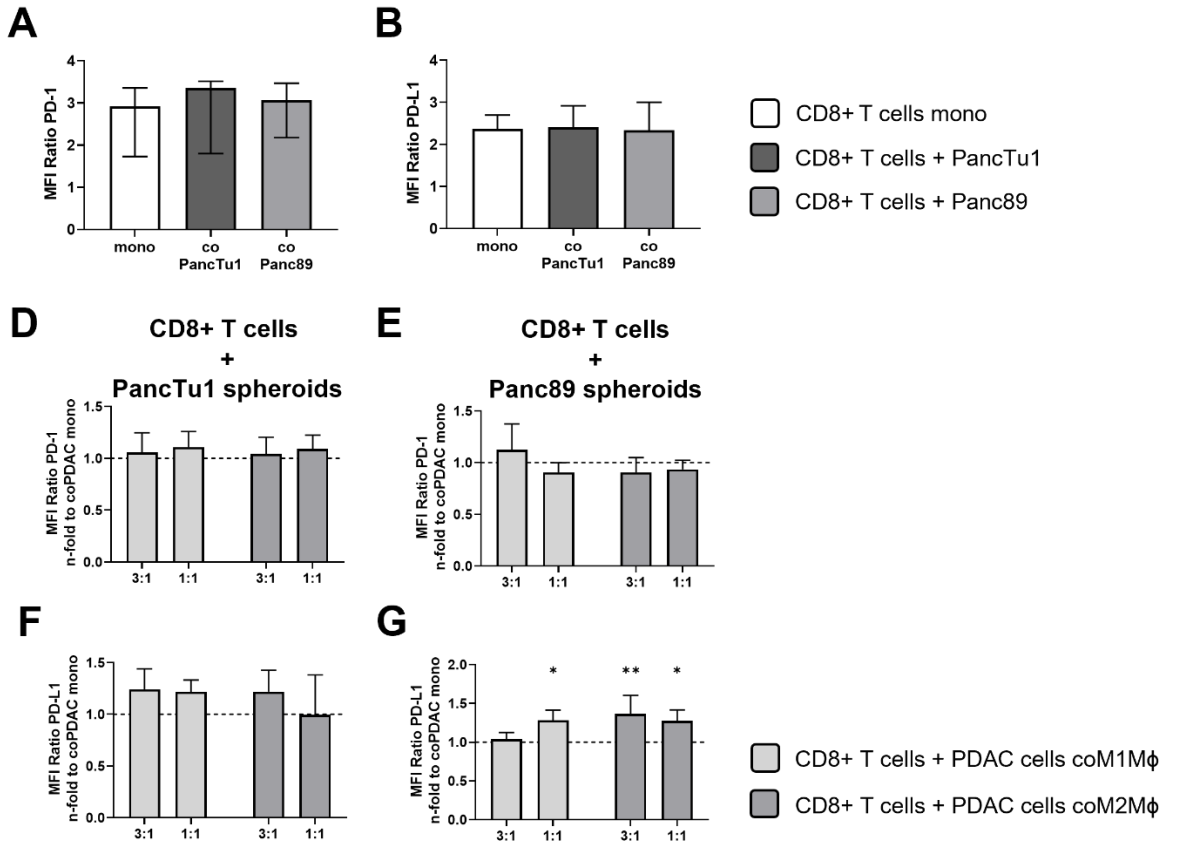

Figure 32: Cell surface levels of PD-1 and PD-L1, on CD8+ T cells are not altered by PDAC cell presence, but PD-L1 expression is increased on CD8+ T cells by macrophage-enriched PDAC spheroids. PancTu1 or Panc89 cells were mono-cultured or co-cultured with either M1- or M2-like macrophages in ultra-low attachment plates to form spheroids. After 48 h, pre-activated CD8+ T cells were added to spheroids for 24 h. **(A)** PD-1 and **(B)** PD-L1 surface expression on mono-cultured (white) or co-cultured CD8+ T cells with PancTu1 (dark grey) or Panc89 (light grey) mono spheroids examined by flow cytometric analysis. Not normally distributed data are depicted as median with interquartile range in both directions. n=4. Effect of M1-like (light grey) or M2-like macrophage (dark grey) co-culture PDAC spheroids on **(D+E)** PD-1 and **(F+G)** PD-L1 expression of CD8+ T cells. Data are normalized to CD8+ T cells cultured with PDAC mono spheroids. Ratio 3:1: $1.5x10^4$ PDAC cells and $0.5x10^4$ macrophages; ratio 1:1: $1x10^4$ PDAC cells and $1x10^4$ macrophages. Data are presented as MFI ratio and denotes median fluorescence intensity ratio of specific staining antibody and its isotype control ($MFI^{specific}/MFI^{isotype}$). Parametric data are depicted as mean with standard deviation in one direction. Two-way ANOVA with Dunnett's multiple comparison test comparing all samples with a control of 1. The dashed lines mark an MFI ratio of "1". * = $p < 0.05$; ** = $p < 0.01$. n=4. (partially published data [209]).

Besides the effects observed on the activation stage and expression levels of immune modulatory molecules, the effector phenotype of CD8+ T cells was investigated after culture with either mono-cultured PDAC spheroids or macrophage-enriched PDAC spheroids. First, CD8+ T cells were cultured with mono-cultured PDAC spheroids to examine the impact of PDAC cell presence on the release of cytotoxic molecules and IFNγ by CD8+ T cells. In general, concentrations of Granzyme A, Granzyme B, Granulysin, Perforin, and IFNγ were markedly increased in supernatants of CD8+ T cells cultured with either PDAC spheroid (Figure 33A-E). In detail, the concentration of Granzyme A, Granzyme B and IFNγ was even higher in supernatants obtained from CD8+ T cells after co-culture with PancTu1 spheroids compared to Panc89 spheroids (PancTu1 vs. Panc89: Granzyme A = 9596 pg/ml vs. 6205 pg/ml; Granzyme B = 21234 pg/ml vs. 15797 pg/ml; IFNγ = 314034 pg/ml vs. 39369 pg/ml) (Figure 33A+B+E).

No differences in Granulysin and Perforin concentrations were observed in supernatants of CD8+ T cells cultured with either PDAC spheroids (Figure 33C+D).

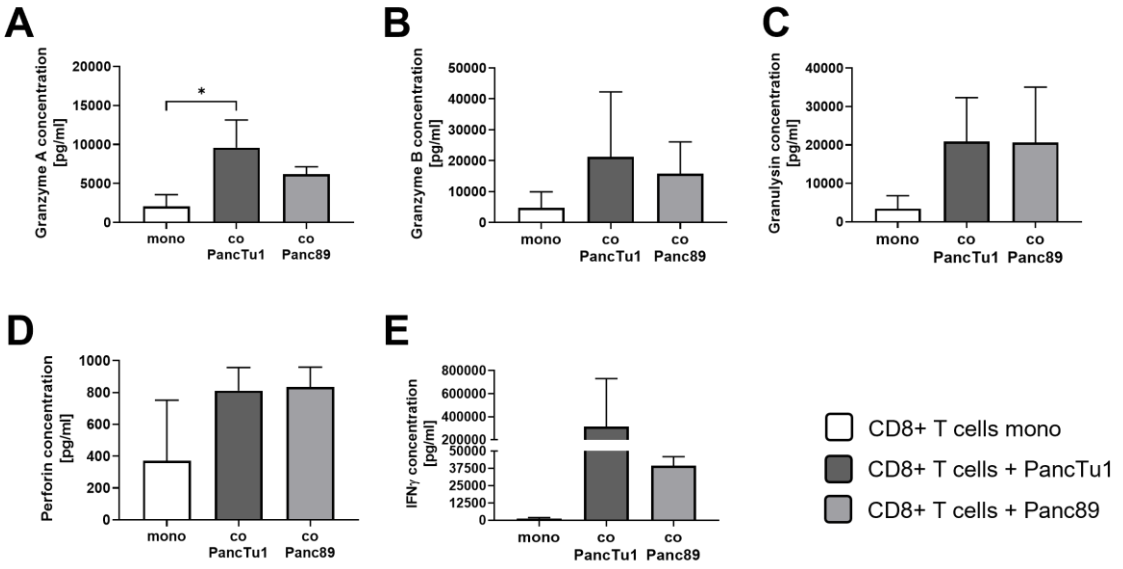

Figure 33: Concentrations of cytotoxic molecules Granzyme A, Granzyme B, Granulysin, Perforin, and the cytokine IFNγ are enhanced in supernatants of CD8+ T cells cultured with PDAC cell mono spheroids. PancTu1 or Panc89 cells were mono-cultured in ultra-low attachment plates to form spheroids. After 48 h, pre-activated CD8+ T cells were added to spheroids for 24 h. **(A)** Granzyme A, **(B)** Granzyme B, **(C)** Granulysin, **(D)** Perforin, and **(E)** IFNγ concentration of CD8+ T cells mono-cultured (white) or co-cultured with PancTu1 (dark grey) or Panc89 (light grey) mono spheroids. Concentrations were measured by multiplex assay. Parametric data are depicted as mean with standard deviation in one direction. One-way ANOVA with Tukey's multiple comparison test. * = $p < 0.05$. n=3.

Next, it was examined whether attendance of either macrophage population or ratio intensified the concentration of cytotoxic molecules and IFNγ released by CD8+ T cells in culture supernatants. The following data were normalized to supernatants of CD8+ T cells cultured with PDAC mono spheroids to specifically visualize the effect of PDAC primed macrophages. Indeed, in supernatants of CD8+ T cells cultured with macrophage-enriched PancTu1 spheroids, release of Granzyme A, Granzyme B, Perforin, and IFNγ was higher compared to co-culture with mono spheroids. This cell ratio-dependent effect was more pronounced in PDAC spheroids with M1-like macrophages (Figure 34A+B+D+E). Only Granulysin concentration was either not altered or decreased (Figure 34C).

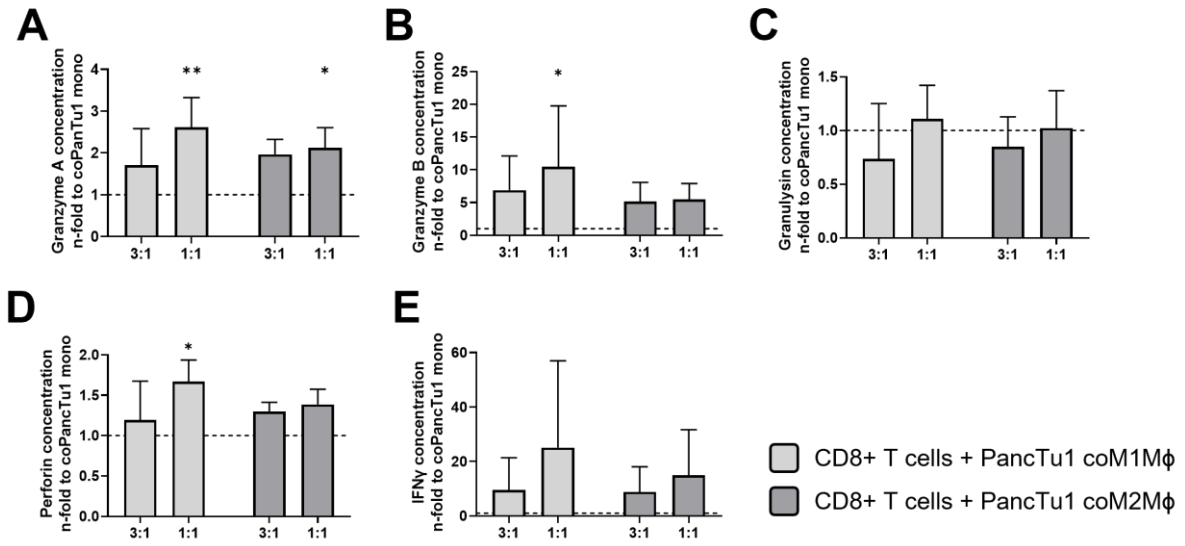

Figure 34: Concentrations of cytotoxic molecules Granzyme A, Granzyme B, Perforin and IFNγ are increased in supernatants of CD8+ T cells cultured with macrophage-enriched PancTu1 spheroids. PancTu1 cells were mono-cultured or co-cultured with either M1- or M2-like macrophages in ultra-low attachment plates to form spheroids. After 48 h, pre-activated CD8+ T cells were added to spheroids for 24 h. **(A)** Granzyme A, **(B)** Granzyme B, **(C)** Granulysin, **(D)** Perforin and **(E)** IFNγ release of CD8+ T cells cultured with PancTu1 spheroids containing M1-like (light grey) or M2-like macrophages (dark grey). Concentrations were measured by multiplex assay and data are normalized to concentration of CD8+ T cells cultured with mono-cultured PancTu1 spheroids. Ratio 3:1: 1.5x10^4 PDAC cells and 0.5x10^4 macrophages; ratio 1:1: 1x10^4 PDAC cells and 1x10^4 macrophages. Parametric data are depicted as mean with standard deviation in one direction. Two-way ANOVA with Dunnett's multiple comparison test comparing all samples with a control of 1. The dashed lines mark a concentration ratio of "1". * = $p < 0.05$; ** = $p < 0.01$. n=3. (partially published data [209]).

Similar to this, the culture of CD8+ T cells with Panc89 co-culture spheroids led to a significant or marked enhancement of Granzyme A, Granzyme B, Perforin, and IFNγ concentrations (Figure 35A+B+D+E). However, in contrast to CD8+ T cells cultured with macrophage-enriched PancTu1 spheroids, no association with the amount of macrophages was observed, despite for IFNγ.

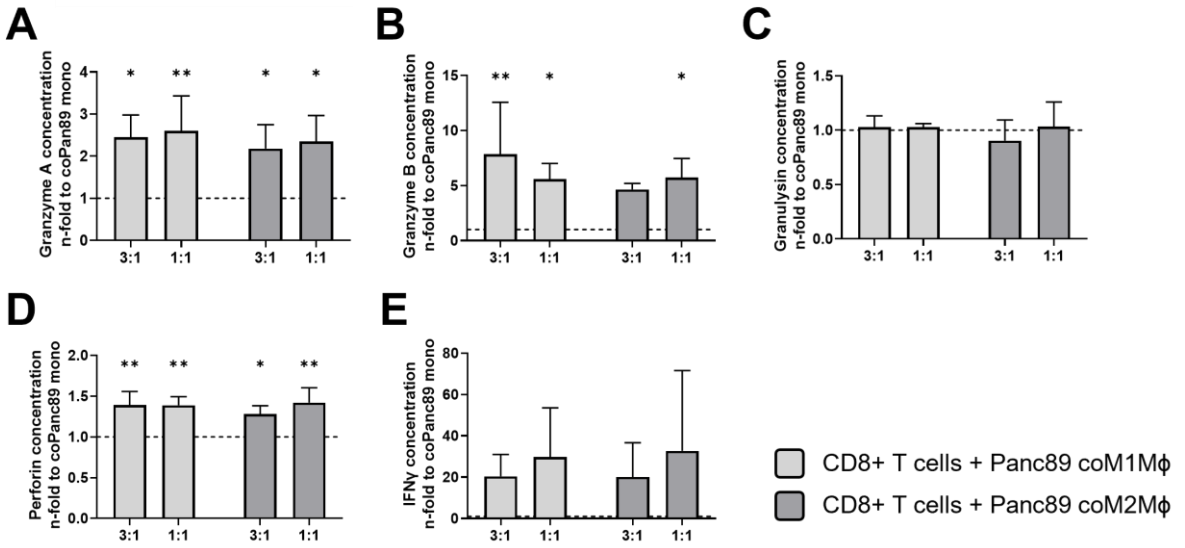

Figure 35: Concentrations of cytotoxic molecules Granzyme A, Granzyme B, Perforin and IFNγ are increased in supernatants of CD8+ T cells cultured with macrophage-enriched Panc89 spheroids. Panc89 cells were mono-cultured or co-cultured with

either M1- or M2-like macrophages in ultra-low attachment plates to form spheroids. After 48 h, pre-activated CD8+ T cells were added to spheroids for 24 h. **(A)** Granzyme A, **(B)** Granzyme B, **(C)** Granulysin, **(D)** Perforin and **(E)** IFNγ release of CD8+ T cells cultured with Panc89 spheroids containing M1-like (light grey) or M2-like macrophages (dark grey). Concentrations were measured by multiplex assay and data are normalized to concentration of CD8+ T cells cultured with mono-cultured Panc89 spheroids. Ratio 3:1: $1.5x10^4$ PDAC cells and $0.5x10^4$ macrophages; ratio 1:1: $1x10^4$ PDAC cells and $1x10^4$ macrophages. Parametric data are depicted as mean with standard deviation in one direction. Two-way ANOVA with Dunnett's multiple comparison test comparing all samples with a control of 1. The dashed lines mark a concentration ratio of "1". * = $p < 0.05$; ** = $p < 0.01$. n=3. (partially published data [209]).

Since the activation stage and effector phenotype of CD8+ T cells were intensified by macrophage-enriched PDAC spheroids, it was next examined whether this correlates with PDAC cell death induction. For this purpose, supernatants of all culture conditions were investigated according to their caspase-cleaved Keratin 18 (ccK18) levels, a specific marker for epithelial (carcinoma) cell death. Supernatants of mono-cultured and macrophage-enriched PDAC spheroids in the presence (+) or absence (-) of CD8+ T cells were analyzed. In the absence of CD8+ T cells, slightly elevated ccK18 levels were only detectable in supernatants of PancTu1 spheroids with M2-like macrophages (1:1). When CD8+ T cells were added to mono-cultured and macrophage-enriched PancTu1 spheroids, ccK18 levels were slightly elevated and at comparable levels in all culture conditions (Figure 36A). Compared to PancTu1 spheroids, ccK18 levels of all Panc89 spheroid cultures were lower in the absence of CD8+ T cells, indicating a better viability in spheroid culture (ccK18 level mono-cultured PancTu1 vs. Panc89: 385 vs. 171) (Figure 36A+B). Moreover, ccK18 levels increased in supernatants of CD8+ T cells cultured with Panc89 spheroids with increasing amounts of either macrophage population (Figure 36B). The attendance of CD8+ T cells also increased ccK18 levels in supernatants of all culture conditions and the trend of increasing ccK18 levels with increased number of macrophage types was also detectable (Figure 36B). The highest ccK18 levels were detected in supernatants of CD8+ T cells and Panc89 co-culture spheroids at a 1:1 ratio.

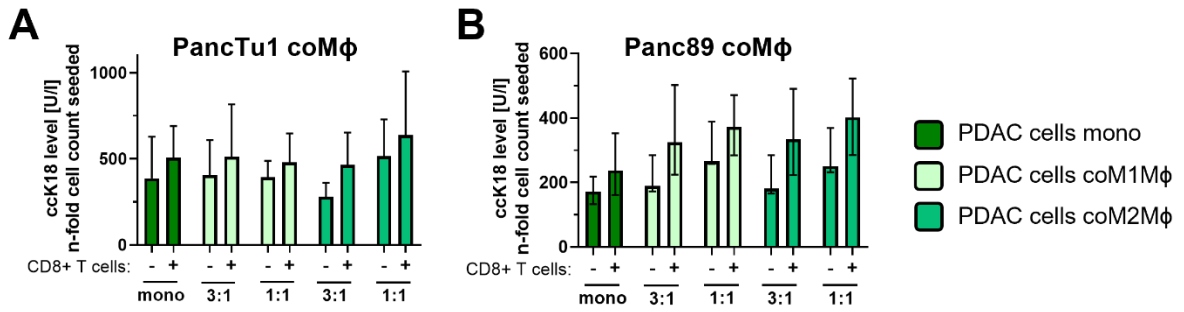

Figure 36: CD8+ T cells induce PDAC cell death in all PDAC spheroid cultures. PancTu1 and Panc89 cells were mono-cultured or co-cultured with either M1- or M2-like macrophages in ultra-low attachment plates to form spheroids. After 48 h, spheroids were cultured in the absence or presence of pre-activated CD8+ T cells for further 24 h. Supernatant levels of caspase-cleaved Keratin 18 (ccK18) in mono-cultured or macrophage-enriched PDAC spheroids. **(A)** PancTu1 spheroids in mono- or co-culture with macrophages without (-) or with CD8+ T cells (+). **(B)** Panc89 spheroids in mono- or co-culture with macrophages without (-) or with CD8+ T cells (+). Mono: $2x10^4$ PDAC cells; ratio 3:1: $1.5x10^4$ PDAC cells and $0.5x10^4$ macrophages; ratio 1:1: $1x10^4$ PDAC cells and $1x10^4$ macrophages. Parametric data are depicted as mean with standard deviation in one direction and non-parametric data are depicted as median with interquartile range in both directions. n=3. (published data [209]).

Overall, these data indicate that the activation status of CD8+ T cells is more enhanced by the macrophage-enriched PDAC spheroids rather than PDAC mono spheroids. Moreover, the cytotoxic phenotype of CD8+ T cells was increased after culture with PDAC mono spheroids and even more in macrophage-enriched PDAC spheroids. This intensification of the effector phenotype seems to be dependent on the amount of macrophages of both macrophage populations. In summary, these data indicate that the effector phenotype of CD8+ T cells exemplified by expression activation markers and release of effector molecules is not impaired in the presence of PD-L1-expressing macrophages, particularly with an M1-like phenotype. In contrast, these findings rather suggest that the effector phenotype of CD8+ T cells is maintained or even promoted in presence of macrophages and PDAC cells independent of their PD-L1 expression, which however is not associated with enhanced cell death of PDAC cells.

4.4.4. Antibody-mediated blockade of PD-1 and PD-L1 only slightly affects the effector phenotype of CD8+ T cells and PDAC cell death

Since both macrophage types, as well as PancTu1 and CD8+ T cells, exhibited considerable PD-L1 expression (Figure 19, Figure 24, and Figure 27) along with PD-1 expression on CD8+ T cells (Figure 19), it was next investigated whether antibody-mediated blocking of PD-L1 (by Durvalumab) or PD-1 (by Pembrolizumab) impacts the effector phenotype of CD8+ T cells and enhances PDAC cell death. To specifically outline the effects of PD-1 and PD-L1 blocking, the following data were normalized to the respective isotype control antibodies. First, the activation status of CD8+ T cells was examined. CD69 surface levels on CD8+ T cells cultured with PancTu1 spheroids revealed that only Durvalumab treatment in co-culture with M2-like macrophages (3:1) and Pembrolizumab application in co-culture with M1-like macrophages (3:1) was elevated. Applying Pembrolizumab in all other co-culture conditions with macrophages even lowered CD69 expression on CD8+ T cells (Figure 37A). No alteration of CD69 levels was observed when CD8+ T cells were cultured with either condition of Panc89 spheroids; it was rather reduced after Pembrolizumab treatment of Panc89 spheroids with M1-like macrophages (Figure 37B). The expression of CD25 on CD8+ T cells was also lowered when macrophage-enriched PancTu1 spheroids were treated with Pembrolizumab (despite co-culture with M1-like macrophages in 3:1 ratio), whereas CD8+ T cells in co-culture with Panc89 and both macrophage types almost remained unaffected (except Pembrolizumab treated co-culture with M1-like macrophages in 1:1 ratio) (Figure 37C+D).

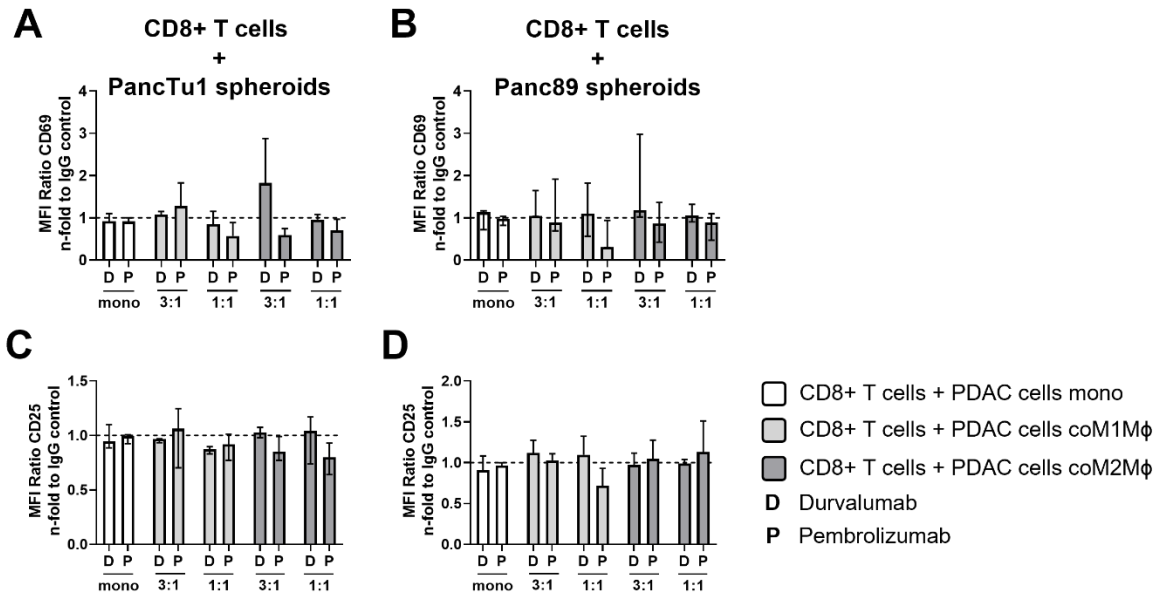

Figure 37: Activation status of CD8+ T cell culture with mono-cultured or macrophage-enriched PDAC spheroids. PancTu1 or Panc89 cells were mono-cultured or co-cultured with either M1- or M2-like macrophages for 24 h in ultra-low attachment plates to form spheroids. After 48 h, mono- or co-cultures were treated with either Durvalumab (D) or Pembrolizumab (P) or their respective isotype controls (10 µg/ml), and CD8+ T cells were added for 24 h. Immunofluorescence staining of activation marker **(A+B)** CD69 and **(C+D)** CD25 were analyzed on CD8+ T cells cultured with mono-cultured PDAC cell spheroids (white), or co-culture PDAC spheroids with M1-like macrophages (light grey) or M2-like macrophages (dark grey). Surface levels were measured by flow cytometer and data are normalized to the respective IgG control samples of indicated co-culture conditions. Mono: $2x10^4$, ratio 3:1: $1.5x10^4$ PDAC cells and $0.5x10^4$ macrophages; ratio 1:1: $1x10^4$ PDAC cells and $1x10^4$ macrophages. Data are presented as MFI ratio and denotes median fluorescence intensity ratio of specific staining antibody and its isotype control ($MFI^{specific}/MFI^{isotype}$). Parametric data are depicted as mean with standard deviation in one direction and non-parametric data are depicted as median with interquartile range in both directions. The dashed lines mark an MFI ratio of "1". n=3. (published data [209]).

It was next analyzed whether and how the expression of PD-1 and PD-L1 is altered after application of blocking antibodies Durvalumab and Pembrolizumab. PD-1 surface levels were not changed after Durvalumab treatment in comparison to respective IgG controls in all co-culture conditions with each PDAC cell line but were significantly decreased on CD8+ T cells derived from all co-culture settings treated with Pembrolizumab (Figure 38A+B). This finding can be explained by the fact that Pembrolizumab bound to PD-1 blocks the PD-1 epitope recognized by the staining antibody. Therefore, these results confirmed successful inhibition of PD-1 in the experimental set-up. Successful inhibition of PD-L1 by Durvalumab was also confirmed as PD-L1 was not detectable in Durvalumab-treated CD8+ T cells after either culture condition (Figure 38C+D).

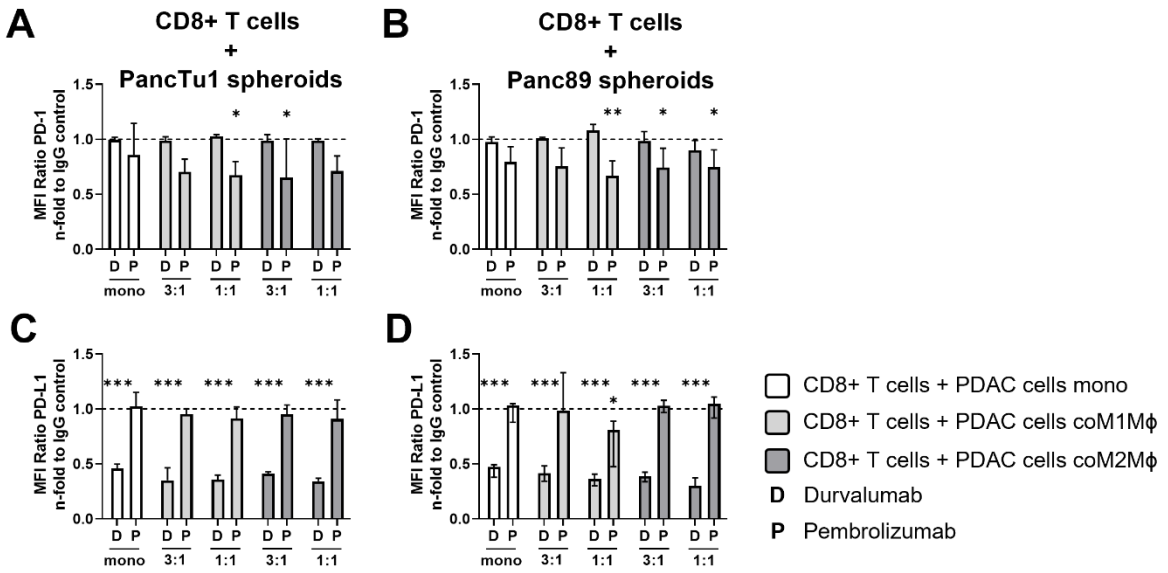

Figure 38: Surface expression levels PD-1 and PD-L1 on CD8+ T cells after culture with mono-cultured or macrophage-enriched PDAC spheroid and Durvalumab or Pembrolizumab treatment. PancTu1 or Panc89 cells were mono-cultured or co-cultured with either M1- or M2-like macrophages for 24 h in ultra-low attachment plates to form spheroids After 48 h, mono- or co-cultures were treated with either Durvalumab (D) or Pembrolizumab (P) or their respective isotype controls (10 µg/ml) and CD8+ T cells were added for 24 h. Immunofluorescence staining of **(A+B)** PD-1 and **(C+D)** PD-L1 was analyzed on CD8+ T cells cultured with mono-cultured PDAC spheroids (white), or co-culture PDAC spheroids with M1-like macrophages (light grey) or M2-like macrophages (dark grey). Surface levels were measured by flow cytometer and data are normalized to the respective IgG control samples of indicated co-culture conditions. Mono: $2x10^{4,}$ ratio 3:1: $1.5x10^4$ PDAC cells and $0.5x10^4$ macrophages; ratio 1:1: $1x10^4$ PDAC cells and $1x10^4$ macrophages. Parametric data are depicted as mean with standard deviation in one direction and non-parametric data are depicted as median with interquartile range in both directions. Two-way ANOVA with Dunnett's multiple comparison test comparing all samples with control of 1. The dashed lines mark an MFI ratio of "1". * = $p < 0.05$; ** = $p < 0.01$; *** = $p < 0.001$. n=3. (partially published data [209]).

Since the blocking of both PD-L1 and PD-1 was confirmed via flow cytometric analysis, it was examined if blocking of PD-1 and PD-L1 affects the effector phenotype of CD8+ T cells. For this purpose, the levels of Granzyme A and B, as well as Granulysin, Perforin, and IFNγ were investigated in supernatants from the different Durvalumab or Pembrolizumab treated spheroids. Overall, neither Granzyme A nor Granzyme B levels in supernatants of CD8+ T cells cultured with either mono- or co-culture spheroids were altered after Durvalumab or Pembrolizumab treatment (Figure 39A+B). Also, Granulysin and Perforin levels remained unaffected after Durvalumab or Pembrolizumab treatment (Figure 39C+D). However, Durvalumab treatment led to a slightly increased IFNγ concentration by trend into supernatants of CD8+ T cells co-cultured with PancTu1 spheroids at a ratio of 3:1 with either macrophage population, while Pembrolizumab slightly diminished IFNγ concentration under almost all co-culture conditions (Figure 39E).

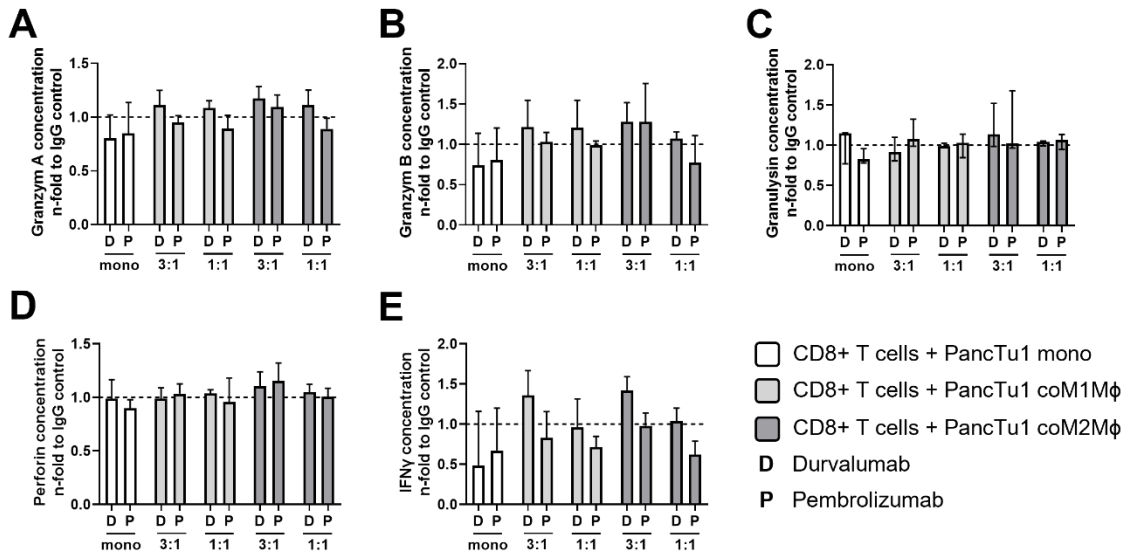

Figure 39: Concentrations of cytotoxic molecules Granzyme A, Granzyme B, Perforin, Granulysin, and IFNγ in supernatants of CD8+ T cells cultured with mono-cultured or macrophage-enriched PancTu1 spheroids and Durvalumab or Pembrolizumab treatment. PancTu1 cells were mono-cultured or co-cultured with either M1- or M2-like macrophages for 24 h in ultra-low attachment plates to form spheroids. After 48 h, mono- or co-cultures were treated with either Durvalumab (D) or Pembrolizumab (P) or their respective isotype controls (10 µg/ml), and CD8+ T cells were added for 24 h. **(A)** Granzyme A, **(B)** Granzyme B, **(C)** Granulysin, **(D)** Perforin and **(E)** IFNγ release of CD8+ T cells cultured with mono-cultured PancTu1 spheroids (white) or co-cultured spheroids with M1-like (light grey) or M2-like macrophages (dark grey). Concentrations were measured by multiplex assay and data are normalized to the respective isotype control samples of indicated co-culture conditions. Mono: $2x10^4$, ratio 3:1: $1.5x10^4$ PDAC cells and $0.5x10^4$ macrophages; ratio 1:1: $1x10^4$ PDAC cells and $1x10^4$ macrophages. Parametric data are depicted as mean with standard deviation in one direction and non-parametric data are depicted as median with interquartile range in both directions. The dashed lines mark a concentration ratio of "1". n=3. (partially published data [209]).

Neither Granzyme A and B nor Granulysin and Perforin levels in supernatants of CD8+ T cells cultured with either mono- or co-cultured Panc89 spheroids were altered after Durvalumab treatment (Figure 40A-D). Only IFNγ levels were increased by trend in supernatants of CD8+ T cells cultured with Panc89 co-culture spheroids with M1 macrophages at a 1:1 ratio (Figure 40E). Pembrolizumab treatment mostly did not alter the supernatant levels of Granzyme A and B, Granulysin, Perforin, and IFNγ despite slightly decreased levels of Ganzyme A and B as well as IFNγ in supernatants of CD8+ T cells cultured with Panc89 co-culture spheroids with M1 macrophages (Figure 40A+B+E). However, in supernatants of CD8+ T cells cultured with mono-cultured Panc89 spheroids enhanced IFNγ levels were detectable (n-fold IFNγ concentration: 1.97) (Figure 40E).

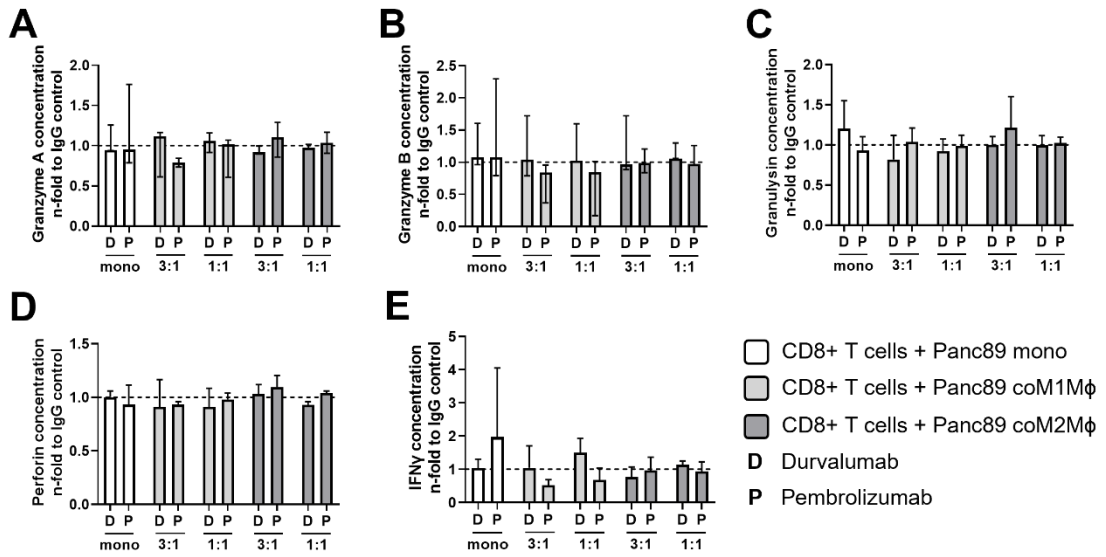

Figure 40: Concentrations of cytotoxic molecules Granzyme A, Granzyme B, Perforin, Granulysin, and IFNγ in supernatants of CD8+ T cells cultured with mono-cultured or macrophage-enriched Panc89 spheroids and Durvalumab or Pembrolizumab treatment. Panc89 cells were mono-cultured or co-cultured with either M1- or M2-like macrophages for 24 h in ultra-low attachment plates to form spheroids. After 48 h, mono- or co-cultures were treated with either Durvalumab (D) or Pembrolizumab (P) or their respective isotype controls (10 µg/ml), and CD8+ T cells were added for 24 h. **(A)** Granzyme A, **(B)** Granzyme B, **(C)** Granulysin, **(D)** Perforin and **(E)** IFNγ release of CD8+ T cells cultured with mono-cultured PancTu1 spheroids (white) or co-cultured spheroids with M1-like (light grey) or M2-like macrophages (dark grey). Concentrations were measured by multiplex assay and data are normalized to the respective isotype control samples of indicated co-culture conditions. Mono: $2x10^4$, ratio 3:1: $1.5x10^4$ PDAC cells and $0.5x10^4$ macrophages; ratio 1:1: $1x10^4$ PDAC cells and $1x10^4$ macrophages. Parametric data are depicted as mean with standard deviation in one direction and non-parametric data are depicted as median with interquartile range in both directions. The dashed lines mark a concentration ratio of "1". n=3. (partially published data [209]).

Finally, ccK18 levels of mono- and macrophage-enriched PDAC cell spheroids after culture with CD8+ T cells and Durvalumab or Pembrolizumab treatment were measured to assess the CD8+ T cell-mediated PDAC cell death. In line with the findings regarding the effector phenotype of CD8+ T cells, no considerable effects were observed on PancTu1 or Panc89 cell death by either antibody treatment in all culture conditions. Only slightly enhanced PDAC cell death was observed in supernatants of M2-like macrophage-enriched PancTu1 spheroids (3:1) when treated with Pembrolizumab (n-fold ccK18 level: 1.19) and Durvalumab at a 1:1 ratio (n-fold ccK18 level: 1.20) (Figure 41A). The highest Panc89 spheroid cell death was detected in supernatants of Pembrolizumab-treated Panc89 spheroids co-cultured with M2-like macrophages (1:1) (n-fold ccK18 level: 1.24) (Figure 41B).

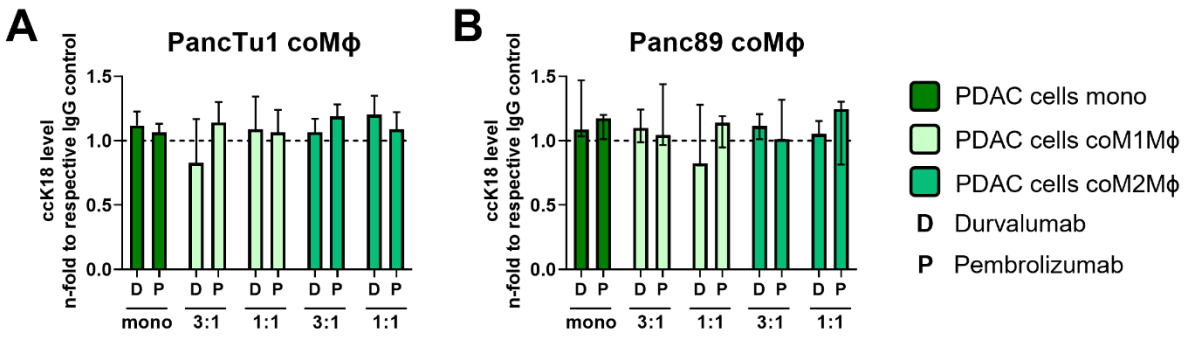

Figure 41: PancTu1 and Panc89 spheroid cell death after co-culture with CD8+ T cells and treatment of either Durvalumab or Pembrolizumab. PancTu1 and Panc89 cells were mono-cultured or co-cultured with either M1- or M2-like macrophages in ultra-low attachment plates to form spheroids. After 48 h, mono- or co-cultures were treated with either Durvalumab (D) or Pembrolizumab (P) or their respective isotype controls (10 µg/ml) and CD8+ T cells were added for 24 h. Levels of caspase-cleaved Keratin 18 (ccK18) in supernatants of CD8+ T cells cultured with mono-cultured or macrophage-enriched PDAC spheroids. **(A)** PancTu1 spheroids in mono-culture or co-culture with macrophages and Durvalumab or Pembrolizumab treatment. **(B)** Panc89 spheroids in mono- or co-culture with macrophages and Durvalumab or Pembrolizumab treatment. Data are normalized to the respective isotype control samples of indicated co-culture conditions. Mono: $2x10^4$ PDAC cells; ratio 3:1: $1.5x10^4$ PDAC cells and $0.5x10^4$ macrophages; ratio 1:1: $1x10^4$ PDAC cells and $1x10^4$ macrophages. Parametric data are depicted as mean with standard deviation in one direction and non-parametric data are depicted as median with interquartile range in both directions. n=3. (published data [209]).

In summary, although PD-L1 and PD-1 were efficiently blocked on CD8+ T cells, no or only a slightly enhanced effector phenotype was observed in co-cultures of PancTu1 spheroids with macrophages and Durvalumab treatment. Blocking either PD-L1 or PD-1 did not benefit the effector phenotype of CD8+ T cells in co-culture with spheroids comprising Panc89 cells and macrophages independently of the amount and subtype of macrophages and treatment. Moreover, no or only minor improvement of CD8+ T cell-mediated tumor cell death in both PDAC cell spheroid models were detected independently of the subtype and amount of macrophages and treatment with either Durvalumab or Pembrolizumab.

4.4.5. Gemcitabine treatment impacts activation status and effector phenotype of CD8+ T cells

Standard chemotherapy agents can modify the expression of tumor-specific membrane antigens which can result in superior antigen presentation by APCs and more effective cytotoxic T lymphocytes response [226]. Therefore, the modulation of tumor-specific membrane proteins by cytostatic drugs may serve as a promising strategy to improve immunotherapy [226]. As Gemcitabine is still the standard-of-care treatment in PDAC [227,228], it was examined whether PD-L1 expression on PancTu1 and Panc89 cells is affected by treatment with Gemcitabine. As a positive control for PD-L1 induction, PDAC cells were stimulated with IFNγ. PancTu1 cells hardly showed a PD-L1 enhancement after Gemcitabine treatment (n-fold MFI ratio PD-L1: 1.34), but it was observable after IFNγ treatment (n-fold MFI ratio PD-L1: 3.72)

(Figure 42A. In contrast to PancTu1 cells, PD-L1 induction was observed after Gemcitabine treatment in Panc89 cells albeit to a lesser extent than after IFNγ treatment (n-fold MFI ratio PD-L1: 2.23) (Figure 42B).

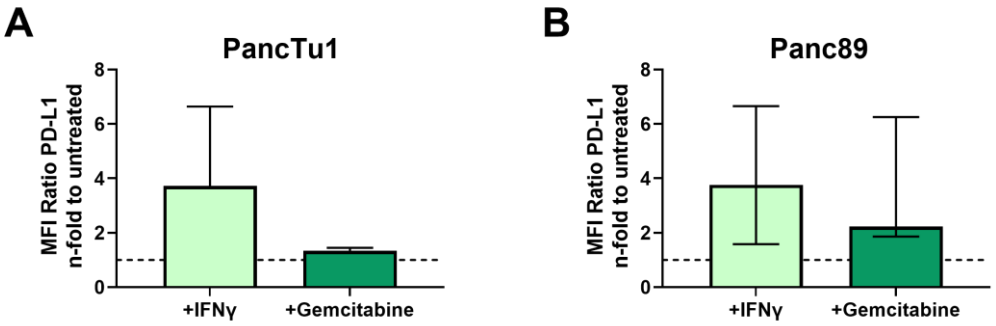

Figure 42: Gemcitabine treatment enhances PD-L1 expression on Panc89 cells, but not on PancTu1 cells. PancTu1 and Panc89 cells were mono-cultured and either remained untreated or were stimulated with IFNγ (10 ng/ml) as a positive PD-L1 inducer or Gemcitabine (10 µg/ml) for 72 h. Immunofluorescence staining of PD-L1 with following flow cytometric analysis. PD-L1 expression on **(A)** PancTu1 cells and **(B)** Panc89 cells normalized to respective untreated cells. Data are presented as MFI ratio and denotes median fluorescence intensity ratio of specific staining antibody and its isotype control ($MFI^{specific}/MFI^{isotype}$). Parametric data are depicted as mean with standard deviation in one direction and non-parametric data are depicted as median with interquartile range in both directions.

Next, it was investigated whether pre-treatment with Gemcitabine of PDAC mono- and co-culture spheroids impacts the effector phenotype of CD8+ T cells. For this purpose, the following data are normalized to the respective untreated samples of each culture condition to highlight the effect of Gemcitabine treatment. Although Gemcitabine was no longer present when CD8+ T cells were added to the spheroids, CD69 expression decreased on CD8+ T cells in the presence of spheroids of both PDAC cell lines (Figure 43A+B). While CD8+ T cells cultured with macrophage-enriched PancTu1 spheroids showed higher CD69 levels compared to T cells in culture with mono-cultured PancTu1 spheroids (except 3:1 ratio of M2-like macrophages), macrophages seemed to decrease CD69 expression on CD8+ T cells in culture with Panc89 spheroids (Figure 43B). The CD25 levels were also lowered when CD8+ T cells were exposed to mono- or co-culture spheroids of both PDAC cell lines independently of macrophage subtype or ratio (Figure 43C+D).

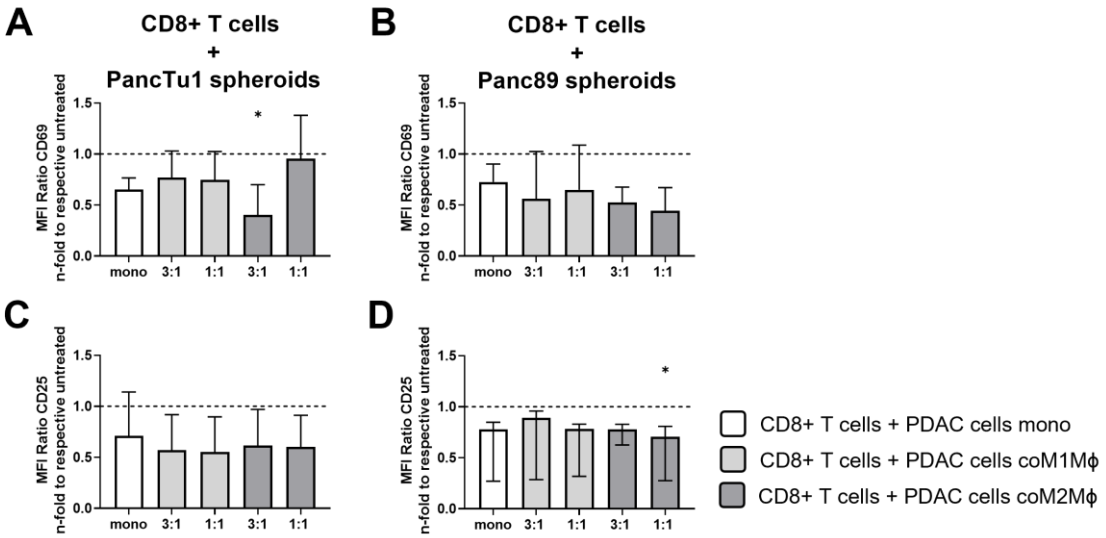

Figure 43: The activation stage of CD8+ T cells is reduced after culture with Gemcitabine treated PDAC spheroids. PancTu1 or Panc89 cells were mono-cultured or co-cultured with either M1- or M2-like macrophages for 24 h in ultra-low attachment plates to form spheroids. After 24 h, mono- or co-cultures were treated with Gemcitabine (10 µg/ml). After 24 h, medium was changed and CD8+ T cells were added for 24 h. Activation markers **(A+B)** CD69 and **(C+D)** CD25 were analyzed on cell surfaces of CD8+ T cells cultured with mono-culture PDAC cell spheroids (white), or co-culture PDAC cell spheroids with M1-like macrophages (light grey) or M2-like macrophages (dark grey). Surface levels were examined by flow cytometric analysis and data are normalized to the respective untreated samples of indicated culture conditions. Mono: $2x10^{4,}$ ratio 3:1: $1.5x10^4$ PDAC cells and $0.5x10^4$ macrophages; ratio 1:1: $1x10^4$ PDAC cells and $1x10^4$ macrophages. Data are presented as MFI ratio and denotes median fluorescence intensity ratio of specific staining antibody and its isotype control ($MFI^{specific}/MFI^{isotype}$). Parametric data are depicted as mean with standard deviation in one direction and non-parametric data are depicted as median with interquartile range in both directions. The dashed lines mark an MFI ratio of "1". Kruskal-Wallis test with Dunn's multiple comparison test or One-way ANOVA with Dunnett's multiple comparison test samples with control of 1. * = $p < 0.05$. n=4.

Next, it was analyzed whether Gemcitabine pre-treatment also affects the expression of immune checkpoint molecules PD-1 and PD-L1 of CD8+ T cells. Similar to the decreased expression of activation markers, a considerable reduction of PD-1 surface levels was observed on CD8+ T cells after culture with all PDAC spheroids independent of the amount and subtype of macrophages (Figure 44A+B). In contrast, PD-L1 expression on CD8+ T cells was almost unaffected after culture with any Gemcitabine treated PDAC culture (Figure 44C+D).

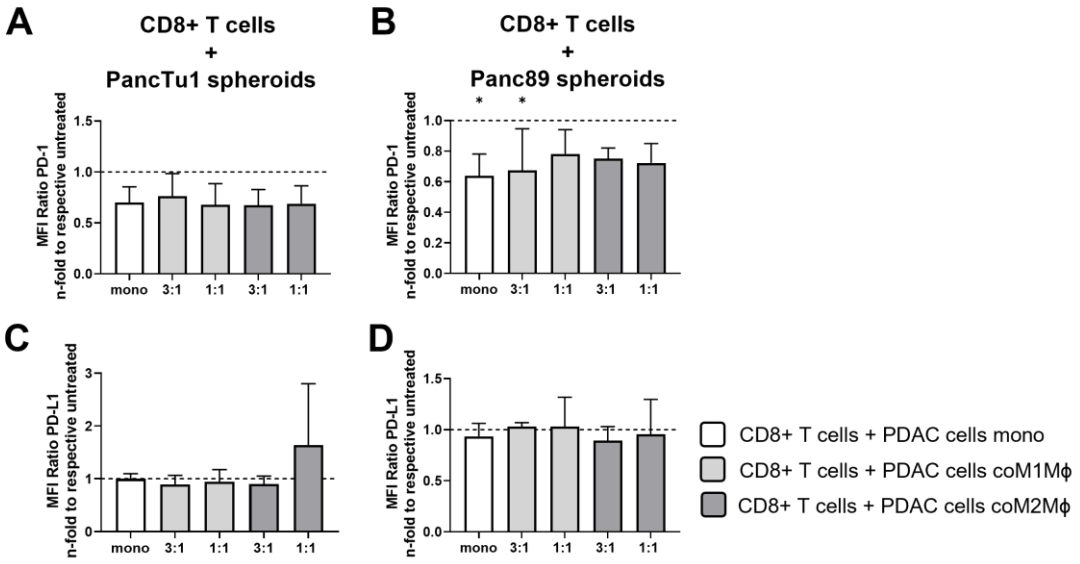

Figure 44: PD-1 surface levels of CD8+ T cells are decreased after culture with Gemcitabine treated PDAC spheroids. PancTu1 or Panc89 cells were mono- or co-cultured with either M1- or M2-like macrophages for 24 h in ultra-low attachment plates to form spheroids. After 24 h, mono- or co-culture spheroids were treated with Gemcitabine (10 µg/ml). After 24 h, medium was changed and CD8+ T cells were added for 24 h. Cell surface levels of **(A+B)** PD-1 and **(C+D)** PD-L1 were examined by flow cytometric analysis and data are normalized to the respective untreated samples of indicated culture conditions. Mono: $2x10^{4,}$ ratio 3:1: $1.5x10^4$ PDAC cells and $0.5x10^4$ macrophages; ratio 1:1: $1x10^4$ PDAC cells and $1x10^4$ macrophages. The dashed lines mark an MFI ratio of "1". Data are presented as MFI ratio and denotes median fluorescence intensity ratio of specific staining antibody and its isotype control ($MFI^{specific}/MFI^{isotype}$). Parametric data are depicted as mean with standard deviation in one direction. One-way ANOVA with Dunnett's multiple comparison test comparing all samples with control of 1. * = $p < 0.05$. n=4.

Since the activation stage and PD-1 expression on CD8+ T cells were affected by Gemcitabine pre-treatment of PDAC spheroids, the next step was to examine the effects on the cytotoxic phenotype of CD8+ T cells. All investigated cytotoxic molecules and IFNγ showed reduced concentrations in supernatants of all culture conditions with PancTu1 spheroids (without or with macrophages) when treated with Gemcitabine. In detail, Granzyme A concentration was 2-fold decreased in supernatants of almost all culture conditions compared to untreated samples. Only in supernatants of CD8+ T cells and PancTu1 co-culture spheroids with M1-like macrophages in 1:1 ratio a more substantial and significant decrease in Granzyme A level was shown (n-fold Granzyme A concentration: 0.32) (Figure **45**A). Granzyme B concentrations similarly decreased in supernatants of CD8+ T cells cultured with mono-culture PancTu1 spheroids or M2-like macrophage-enriched PancTu1 spheroids at 1:1 ratio (n-fold Granzyme B concentration for both: 0.66). All other culture conditions led to a stronger reduction of Granzyme B (n-fold Granzyme B concentration: 0.43 – 0.25) (Figure 45B). Moreover, concentrations of Granulysin, Perforin, and IFNγ were markedly reduced in supernatants of CD8+ T cells cultured with PDAC mono- and co-culture spheroids. No marked difference was noted in the different amounts or subtypes of macrophages (Figure 45C-E).

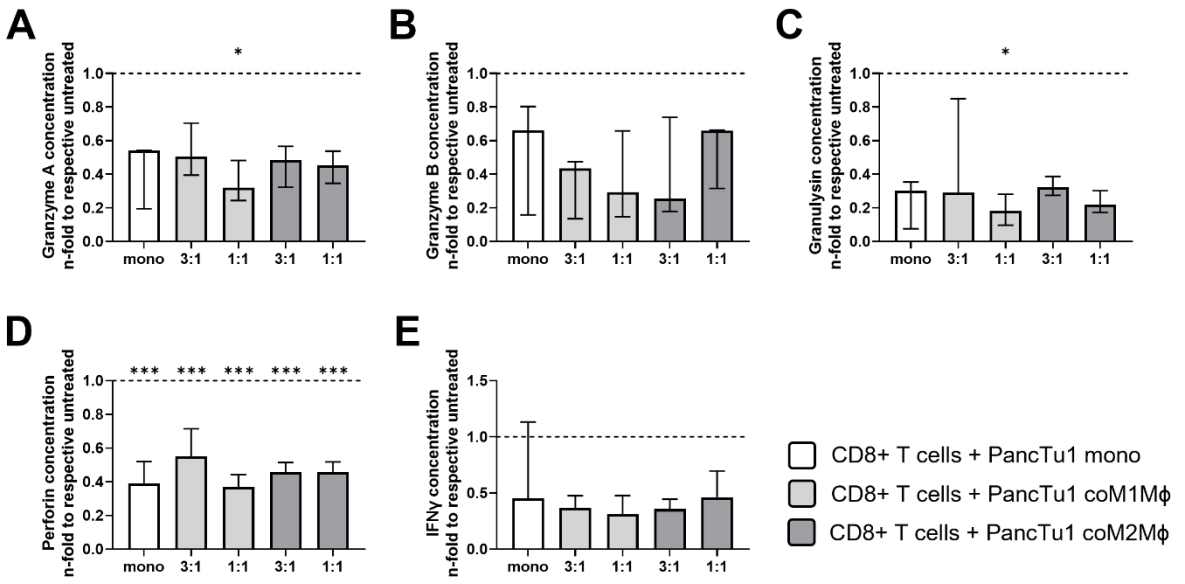

Figure 45: Concentrations of cytotoxic molecules Granzyme A, Granzyme B, Perforin, Granulysin, and IFNγ are decreased in supernatants of CD8+ T cells cultured with Gemcitabine-treated PancTu1 spheroids. PancTu1 cells were mono- or co-cultured with either M1- or M2-like macrophages for 24 h in ultra-low attachment plates to form spheroids. After 24 h, mono- or co-culture spheroids were treated with Gemcitabine (10 µg/ml). After 24 h, medium was changed and CD8+ T cells were added for 24 h. Concentrations of **(A)** Granzyme A, **(B)** Granzyme B, **(C)** Granulysin, **(D)** Perforin and **(E)** IFNγ in supernatants of CD8+ T cells cultured with mono-culture (white) or co-culture PancTu1 spheroids with M1-like (light grey) or M2-like macrophages (dark grey). Concentrations were measured by multiplex assay and data are normalized to the respective untreated samples of indicated co-culture conditions. Mono: $2x10^4$, ratio 3:1: $1.5x10^4$ PDAC cells and $0.5x10^4$ macrophages; ratio 1:1: $1x10^4$ PDAC cells and $1x10^4$ macrophages. Parametric data are depicted as mean with standard deviation in one direction and analyzed by One-way ANOVA with Dunnett's multiple comparison test comparing all samples with control of 1. Non-parametric data are depicted as median with interquartile range in both directions and were analyzed by Kruskal-Wallis test with Dunn's multiple comparison test comparing all samples with control of 1. The dashed lines mark a concentration ratio of "1". * = $p < 0.05$, *** = $p < 0.001$. n=3.

Similar to this, CD8+ T cells in culture with Panc89 mono- or co-culture spheroids with both macrophage types secreted reduced levels of all analyzed cytotoxic molecules into cell culture supernatants (Figure 46A-D). In detail, Granzyme A and B concentrations were mostly reduced in supernatants of CD8+ T cells cultured with Panc89 spheroids containing M1-like macrophages at a 3:1 ratio (n-fold Granzyme vs. Granzyme B concentration: 0.37 vs. 0.41). Supernatants of CD8+ T cells and all other macrophage co-culture conditions showed similarly reduced levels of respective Granzymes compared to mono-cultured Panc89 spheroids (Figure 46A+B). Granulysin concentration was mostly reduced compared to all other investigated molecules and was not altered due to different culture conditions (Figure 46C). Moreover, the Perforin concentration of CD8+ T cells in culture with mono-cultured Panc89 spheroids was the lowest (n-fold Perforin concentration: 0.42). However, compared to supernatants of CD8+ T cells cultured with untreated spheroids, the concentration of Perforin was also clearly reduced in all other PDAC spheroids conditions. Similar observations were made for IFNγ. Only IFNγ concentration in supernatants of CD8+ T cells in culture with mono-cultured Panc89 spheroids revealed an increase compared to untreated samples (Figure 46E).

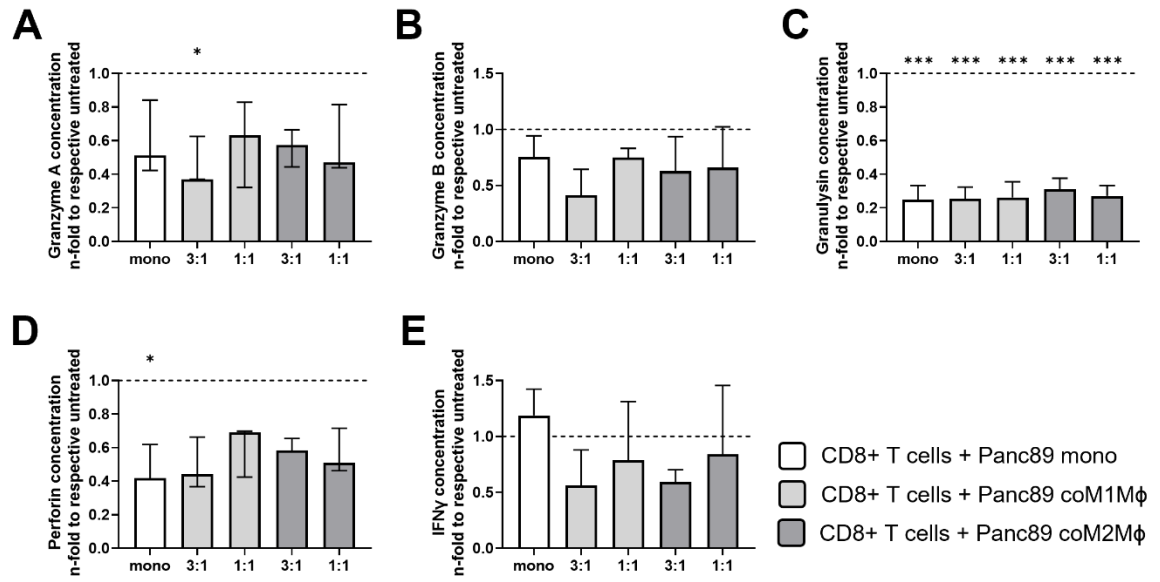

Figure 46: Concentrations of cytotoxic molecules Granzyme A, Granzyme B, Perforin, Granulysin, and IFNγ are decreased in supernatants of CD8+ T cells cultured with Gemcitabine-treated Panc89 spheroids. Panc89 cells were mono- or co-cultured with either M1- or M2-like macrophages for 24 h in ultra-low attachment plates to form spheroids. After 24 h, mono- or co-culture spheroids were treated with Gemcitabine (10 µg/ml). After 24 h, medium was changed and CD8+ T cells were added for 24 h. Concentration of **(A)** Granzyme A, **(B)** Granzyme B, **(C)** Granulysin, **(D)** Perforin and **(E)** IFNγ in supernatants of CD8+ T cells cultured with mono-culture (white) or co-culture Panc89 spheroids with M1-like (light grey) or M2-like macrophages (dark grey). Concentrations were measured by multiplex assay and data are normalized to the respective untreated samples of indicated culture conditions. Mono: $2x10^4$, ratio 3:1: $1.5x10^4$ PDAC cells and $0.5x10^4$ macrophages; ratio 1:1: $1x10^4$ PDAC cells and $1x10^4$ macrophages. Parametric data are depicted as mean with standard deviation in one direction and analyzed by One-way ANOVA with Dunnett's multiple comparison test comparing all samples with control of 1. Non-parametric data are depicted as median with interquartile range in both directions were analyzed by Kruskal-Wallis test with Dunn's multiple comparison test comparing all samples with control of 1. The dashed lines mark a concentration ratio of "1". * = $p < 0.05$, *** = $p < 0.001$. n=3.

Lastly, it was investigated whether Gemcitabine pre-treatment of PDAC mono- and co-culture spheroids impacts PDAC cell death in the absence or presence of CD8+ T cells determined by the release of ccK18. Interestingly, supernatants of PancTu1 spheroids showed diminished ccK18 levels compared to untreated samples under all culture conditions (Figure 47A). The presence of CD8+ T cells only marginally affected the ccK18 levels of spheroids with M1-like macrophages at 3:1 ratio compared with PancTu1 spheroids and macrophages (n-fold ccK18 – vs. + CD8+ T cells: 0.82 vs. 1.04). All other culture settings revealed similar ccK18 levels in the presence or absence of CD8+ T cells. Further, Panc89 cell death was neither increased due to culture with CD8+ T cells nor due to Gemcitabine treatment (Figure 47B). Only a slight enhancement of ccK18 levels was detected in mono-cultured Panc89 spheroids.

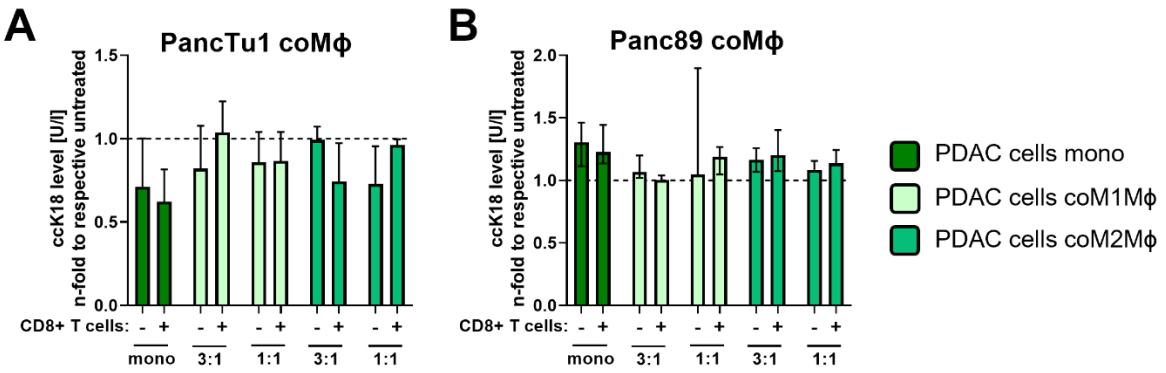

Figure 47: PancTu1 cell death was slightly reduced whereas Panc89 cell death was almost unaffected by Gemcitabine pre-treatment and the presence of CD8+ T cells. PancTu1 and Panc89 cells were mono- or co-cultured with either M1- or M2-like macrophages for 24 h in ultra-low attachment plates to form spheroids. After 24 h, mono- or co-culture spheroids were treated with Gemcitabine (10 µg/ml). After 24 h, medium was changed and CD8+ T cells were added for 24 h. Supernatant levels of caspase-cleaved Keratin 18 (ccK18) of **(A)** PancTu1 spheroids in mono- or co-culture with macrophages , or **(B)** Panc89 spheroids in mono- or co-culture with macrophages in the absence (-) or presence (+) of CD8+ T cells. Data are normalized to the respective untreated samples of indicated co-culture conditions. Mono: $2x10^4$ PDAC cells; ratio 3:1: $1.5x10^4$ PDAC cells and $0.5x10^4$ macrophages; ratio 1:1: $1x10^4$ PDAC cells and $1x10^4$ macrophages. Parametric data are depicted as mean with standard deviation in one direction and non-parametric data are depicted as median with interquartile range in both directions. PancTu1: n=3; Panc89: n=4.

In summary, Gemcitabine pre-treatment of PDAC cell spheroids with macrophage affected the activation status and the effector phenotype of CD8+ T cells and slightly decreased PDAC cell death of PancTu1 spheroids.

4.4.6. Sequential treatment with Gemcitabine and immune checkpoint blockade does not improve CD8+ T cell-mediated PDAC cell death

As immune checkpoint inhibition single treatment with Durvalumab and Pembrolizumab failed in the 3D co-culture model and Gemcitabine has been identified as an inducer of PD-L1 expression [229,230] (Figure 42), it was investigated whether sequential therapy of low dose Gemcitabine followed by immune checkpoint blockade modulates the effector phenotype of CD8+ T cells and leads to elevated induction of PDAC cell death. To specifically outline the effects of combined treatment, data of ICI treatment were normalized to respective isotype control treatment. For this purpose, the different mono- or macrophage-enriched PDAC spheroids were treated with Gemcitabine for 24 h, then cultured with pre-activated CD8+ T cells and simultaneously treated with Durvalumab, Pembrolizumab or respective isotype control. First, the activation status of CD8+ T cells was investigated. Analyzing CD69 surface expression on CD8+ T cells under the different culture conditions revealed that combined treatment with Durvalumab led to decreased CD69 expression on CD8+ T cells cultured with PancTu1 co-culture spheroids with M1-like macrophages (n-fold MFI ratio 3:1 vs. 1:1: 0.83 vs. 0.87) and Panc89 spheroids enriched with M1-like macrophages (3:1) (n-fold MFI ratio: 0.59) (Figure 48A+B). In contrast,

combined treatment with Pembrolizumab increased CD69 levels after co-culture with M1-like macrophage-enriched spheroids of both PDAC cell lines (Figure 48A+B). CD25 surface levels mostly remained unaffected by Durvalumab or Pembrolizumab treatment despite combined treatment with Pembrolizumab which reduced CD69 levels in CD8+ T cells derived from PancTu1 spheroids comprising M2-like macrophages (1:1) (Figure 48C+D).

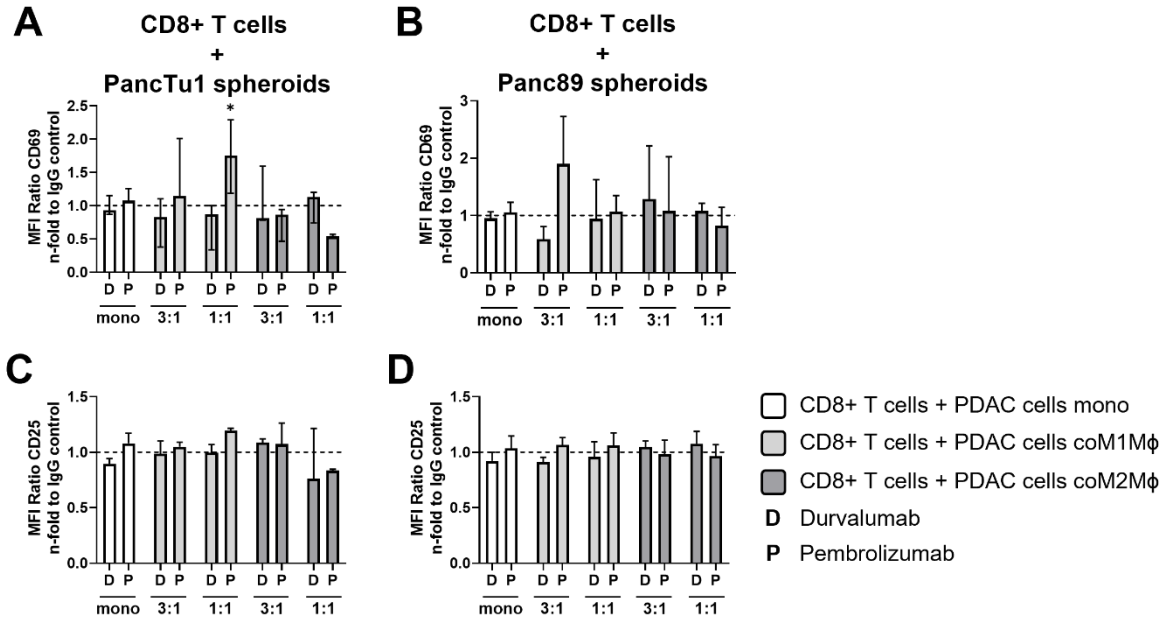

Figure 48: Activation stage of CD8+ T cells in co-culture with PancTu1 or Panc89 co-culture spheroids with macrophages after sequential treatment with Gemcitabine and Durvalumab or Pembrolizumab. PancTu1 or Panc89 cells were mono-cultured or co-cultured with either M1- or M2-like macrophages for 24 h in ultra-low attachment plates to form spheroids. After 24 h, mono- or co-cultures were treated with Gemcitabine (10 µg/ml) for 24 h. Afterwards, medium was changed, and cultures were treated with either Durvalumab (D) or Pembrolizumab (P) or their respective isotype control (10 µg/ml) and simultaneous CD8+ T cell co-culture was started for 24 h. Activation marker **(A+B)** CD69 and **(C+D)** CD25 were analyzed on surfaces of CD8+ T cells cultured with mono-cultured PDAC cell spheroids (white) or co-cultured PDAC cell spheroids with M1-like macrophages (light grey) or M2-like macrophages (dark grey). Surface levels were measured by flow cytometer and data are normalized to the respective IgG control samples of indicated co-culture conditions. Mono: $2x10^{4,}$ ratio 3:1: $1.5x10^4$ PDAC cells and $0.5x10^4$ macrophages; ratio 1:1: $1x10^4$ PDAC cells and $1x10^4$ macrophages. Data are presented as MFI ratio and denotes median fluorescence intensity ratio of specific staining antibody and its isotype control ($MFI^{specific}/MFI^{isotype}$). Parametric data are depicted as mean with standard deviation in one direction and non-parametric data are depicted as median with interquartile range in both directions. Two-way ANOVA with Dunnett's multiple comparison test comparing all samples with control of 1. The dashed lines mark an MFI ratio of "1". * = $p < 0.05$. n=3. (published data [209]).

Next, the surface expression of PD-1 and PD-L1 on CD8+ T cells was analyzed after sequential treatment. PD-1 surface expression on CD8+ T cells was not altered by sequential treatment with Gemcitabine and Durvalumab under all culture conditions, while it was again reduced after treatment with Pembrolizumab due to the competition of immunofluorescence staining and blocking antibodies (Figure 49A+B). The PD-L1 surface levels on CD8+ T cells were also significantly decreased in both PDAC cell spheroids in all culture conditions due to the same binding epitope of staining and blocking antibody (Figure 49C+D). However, applying Pembrolizumab revealed no alteration despite CD8+ T

cells cultured with PancTu1 spheroids containing M1-like macrophages at a 1:1 ratio (n-fold MFI ratio PD-L1: 1.22) (Figure 49C).

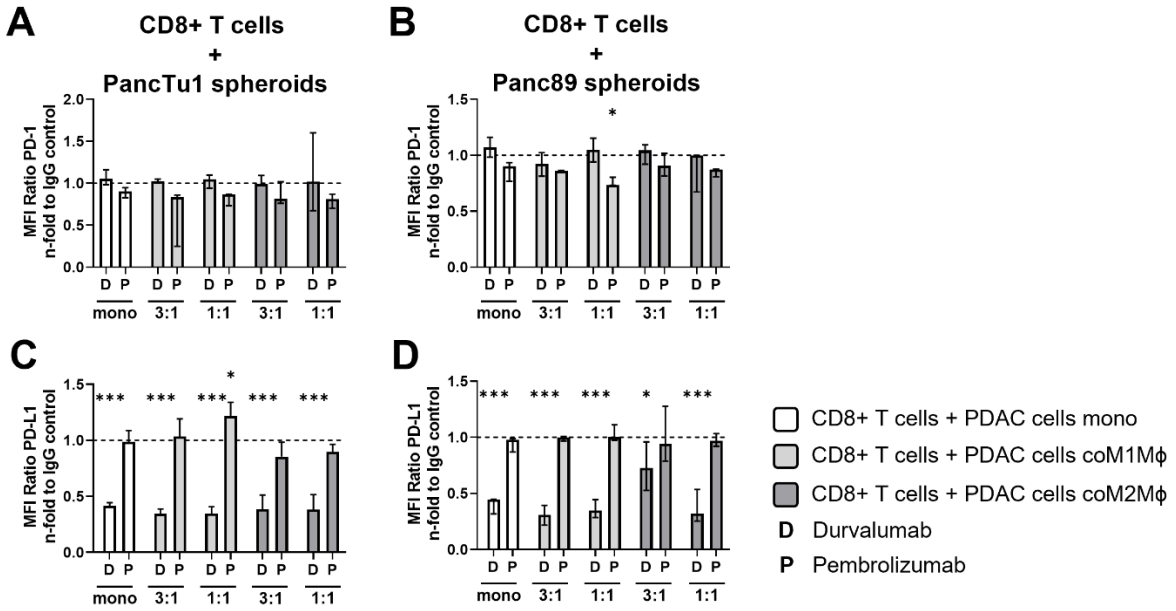

Figure 49: Expression of immune checkpoint molecules PD-1 and PD-L1 on CD8+ T cells after PancTu1 and Panc89 co-culture spheroids and sequential treatment with Gemcitabine and Durvalumab or Pembrolizumab. PancTu1 or Panc89 cells were mono-cultured or co-cultured with either M1- or M2-like macrophages for 24 h in ultra-low attachment plates to form spheroids. After 24 h, mono- or co-cultures were treated with Gemcitabine (10 µg/ml) for 24 h. Afterwards, medium was changed, and cultures were treated with either Durvalumab (D) or Pembrolizumab (P) or their respective isotype control (10 µg/ml) and simultaneous CD8+ T cell co-culture was started for 24 h. Surface expression of **(A+B)** PD-1 and **(C+D)** PD-L1 was analyzed on surfaces of CD8+ T cells cultured with mono-cultured PDAC cell spheroids (white), or co-cultured PDAC cell spheroids with M1-like macrophages (light grey) or M2-like macrophages (dark grey). Surface levels were measured by flow cytometer and data are normalized to the respective isotype control samples of indicated co-culture conditions. Mono: $2x10^{4,}$ ratio 3:1: $1.5x10^4$ PDAC cells and $0.5x10^4$ macrophages; ratio 1:1: $1x10^4$ PDAC cells and $1x10^4$ macrophages. Data are presented as MFI ratio and denotes median fluorescence intensity ratio of specific staining antibody and its isotype control ($MFI^{specific}/MFI^{isotype}$). Parametric data are depicted as mean with standard deviation in one direction and non-parametric data are depicted as median with interquartile range in both directions. Two-way ANOVA with Dunnett's multiple comparison test comparing all samples with control of 1. The dashed lines mark an MFI ratio of "1". * = $p < 0.05$; *** = $p < 0.001$. n=3. (published data [209]).

In line with the marginal effects on the activation markers, concentrations of Granzyme A and B, Granulysin, Perforin, and IFNγ in supernatants of any culture of CD8+ T cells and PancTu1 macrophage spheroids were hardly affected by sequential therapy of Gemcitabine and either immune checkpoint inhibitor (Figure 50A-E).

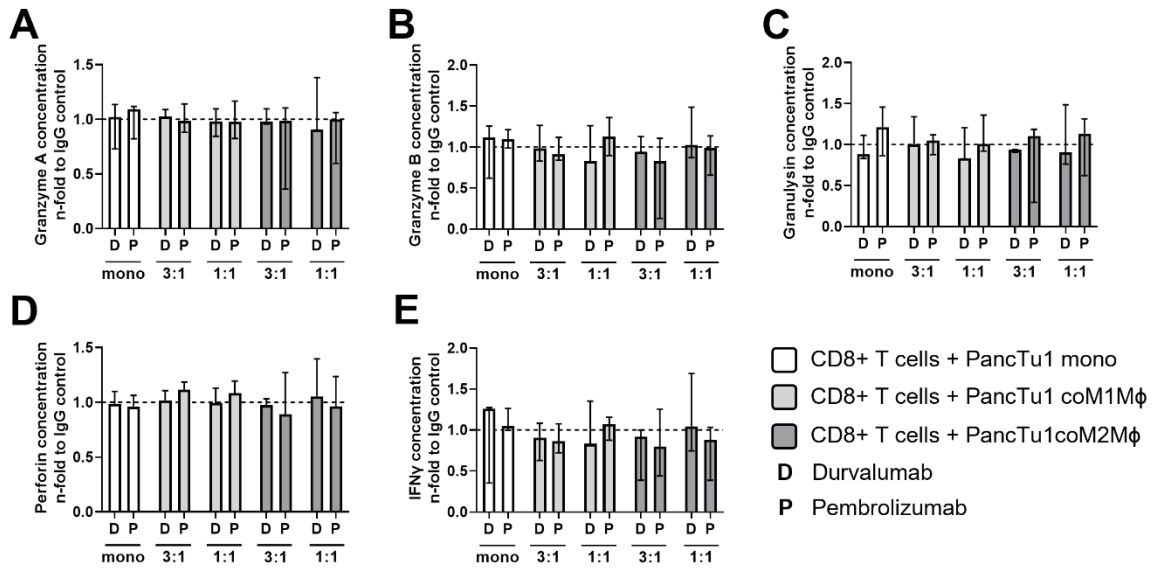

Figure 50: Concentrations of cytotoxic molecules Granzyme A and B, Perforin, Granulysin, and IFNγ by CD8+ T cells after PancTu1 spheroid co-culture and sequential treatment of Gemcitabine and either Durvalumab or Pembrolizumab. PancTu1 cells were mono-cultured or co-cultured with either M1- or M2-like macrophages for 24 h in ultra-low attachment plates to form spheroids. After 24 h, mono- or co-cultures were treated with Gemcitabine (10 µg/ml) for 24 h. Afterwards, medium was changed, and cultures were treated with either Durvalumab (D) or Pembrolizumab (P) or their respective isotype control (10 µg/ml) and simultaneous CD8+ T cell co-culture was started for 24 h. **(A)** Granzyme A, **(B)** Granzyme B, **(C)** Granulysin, **(D)** Perforin and **(E)** IFNγ concentrations in supernatants of CD8+ T cells cultured with mono-cultured PancTu1 spheroids (white) or co-cultured spheroids with M1-like (light grey) or M2-like macrophages (dark grey). Concentrations were measured by multiplex assay and data are normalized to the respective isotype control samples of indicated co-culture conditions. Mono: $2x10^4$, ratio 3:1: $1.5x10^4$ PDAC cells and $0.5x10^4$ macrophages; ratio 1:1: $1x10^4$ PDAC cells and $1x10^4$ macrophages. Parametric data are depicted as mean with standard deviation in one direction and non-parametric data are depicted as median with interquartile range in both directions. The dashed lines mark a concentration ratio of "1". n=3. (partially published data [209]).

Concentrations of cytotoxic molecules by CD8+ T cells in co-culture with Panc89 macrophage spheroids was also hardly affected by sequential treatment of Gemcitabine and ICI. Only culture with co-culture spheroids containing M2-like macrophages in a 1:1 ratio after Durvalumab treatment showed slightly increased concentrations by trend of Granzyme A and B, Perforin, and IFNγ (n-fold concentration Granzyme A vs. B vs. Perforin vs. IFNγ: 1.25 vs. 1.21 vs. 1.14 vs. 2.11) (Figure 51A+B+D+E).

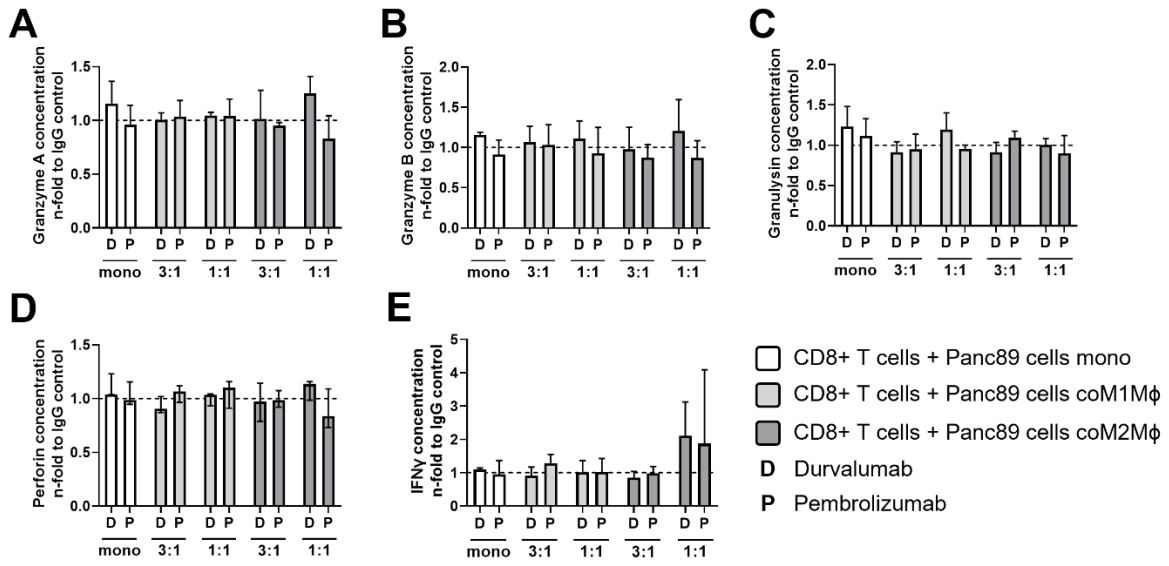

Figure 51: Concentrations of cytotoxic molecules Granzyme A, Granzyme B, Perforin, Granulysin, and IFNγ by CD8+ T cells after Panc89 spheroid co-culture and sequential treatment of Gemcitabine and either Durvalumab or Pembrolizumab. Panc89 cells were mono-cultured or co-cultured with either M1- or M2-like macrophages for 24 h in ULA plates to form spheroids. After 24 h, mono- or co-cultures were stimulated with Gemcitabine (10 µg/ml) for 24 h. Afterwards, medium was changed and Durvalumab (D) or Pembrolizumab (P) treatment and CD8+ T cells were added for 24 h. **(A)** Granzyme A, **(B)** Granzyme B, **(C)** Granulysin, **(D)** Perforin and **(E)** IFNγ concentrations in supernatants of CD8+ T cells cultured with mono-cultured Panc89 spheroids (white) or co-cultured spheroids with M1-like (light grey) or M2-like macrophages (dark grey). Concentrations were measured by multiplex assay and data are normalized to the respective isotype control samples of indicated co-culture conditions. Mono: $2x10^4$, ratio 3:1: $1.5x10^4$ PDAC cells and $0.5x10^4$ macrophages; ratio 1:1: $1x10^4$ PDAC cells and $1x10^4$ macrophages. Parametric data are depicted as mean with standard deviation in one direction and non-parametric data are depicted as median with interquartile range in both directions. The dashed lines mark a concentration ratio of "1". n=3. (partially published data [209]).

Lastly, the PDAC cell death was investigated and measured by determining ccK18 levels in supernatants of CD8+ T cell cultures with mono- and co-culture spheroids. In line with the non-affected activation status and effector phenotype of CD8+ T cells, no considerable increase in the induction of PancTu1 and Panc89 cell death was noted after the different treatments exemplified by the almost unaltered ccK18 levels of the different spheroid cultures (Figure 52A+B).

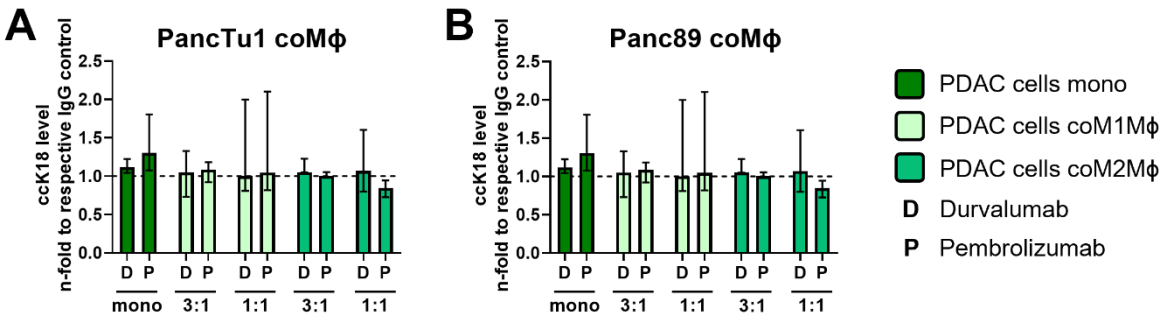

Figure 52: PancTu1 and Panc89 spheroid cell death after co-culture with CD8+ T cells and sequential treatment of Gemcitabine and either Durvalumab or Pembrolizumab.PancTu1 or Panc89 cells were mono-cultured or co-cultured with either M1- or M2-like macrophages for 24 h in ULA plates to form spheroids. After 24 h, mono- or co-cultures were stimulated with Gemcitabine (10 µg/ml) for 24 h. Afterwards, medium was changed and Durvalumab (D) or Pembrolizumab (P) treatment and CD8+ T cells were added for 24 h. Levels of caspase-cleaved Keratin 18 (ccK18) in supernatants of mono-cultured or macrophage-enriched PDAC spheroids. **(A)** PancTu1 spheroids in mono- or co-culture with macrophages after combination treatment of Gemcitabine and Durvalumab or Pembrolizumab. **(B)** Panc89 spheroids in mono or co-culture with macrophages after combination treatment of Gemcitabine and Durvalumab or Pembrolizumab. Data are normalized to the respective isotype control samples of indicated co-culture conditions. Mono: $2x10^4$ PDAC cells; ratio 3:1: $1.5x10^4$ PDAC cells and $0.5x10^4$ macrophages; ratio 1:1: $1x10^4$ PDAC cells and $1x10^4$ macrophages. Non-parametric data are depicted as median with interquartile range in both directions. n=3. (published data [209]).

Overall, these data indicate that sequential treatment of PDAC with Gemcitabine and ICIs does not improve the effector phenotype of CD8+ T cells and PDAC cell death irrespective of the presence and subtype of macrophages.

5. Discussion

The hallmarks of cancer by Hanahan and Weinberg demonstrated that tumor formation is a multistep process. The six original hallmark capabilities, including evading growth suppressors, sustaining proliferative signaling, resisting cell death, inducing angiogenesis, enabling replicative immortality, and activation invasion and metastases, were extended by new hallmarks of cancer during the last years [231–233]. Additionally, deregulating cellular energetics, avoiding immune destruction, genome instability and mutation, and tumor-promoting inflammation were added in 2011, and nonmutational epigenetic reprogramming, polymorphic microbiomes, unlocking phenotypic plasticity, and senescent cells were revealed in 2022 [232,233]. Several of these cancer hallmarks address and are modulated by the TME [234] and are topic of this thesis.

In detail, this study examined *in situ* and *in vitro* the effect of the TME, especially CD8+ T cells and macrophages, on PDAC cells and *vice versa* with a particular focus on the role of PD-L1 as a potential immune evasion strategy of PDAC cells. For this purpose, both immune cell populations were determined *in situ* in primary tumors and their corresponding liver metastases of PDAC patients. Especially the abundance and location of PD-L1 expression were compared with the presence of macrophages and CD8+ T cells which is discussed in section 5.1. In order to investigate the impact of exhausted CD8+ T cells on PDECs and whether blocking of PD-L1 by Durvalumab on CD8+ T cells or on both CD8+ T cells and PDECs impacts the PDEC viability, *in vitro* experiments using 2D cultures were performed and are discussed in section 5.2. Further, it was investigated how CD8+ T cells in pre-co-culture with macrophages alter their activation status and whether this impacts PDEC viability. These results are discussed in section 5.3. As 2D cell culture in a flat bottom cannot fully represent the pathophysiological conditions of PDAC, a 3D model system containing different PD-L1-expressing PDAC cells and macrophage types and ratios was established to better mimic the situation in PDAC. Moreover, the addition of CD8+ T cells to the different 3D co-culture conditions included an important effector cell population to this PDAC immune cell interplay (discussed in section 5.4). Lastly, it was investigated whether the application of Pembrolizumab and Durvalumab to block the PD-1/PD-L1 axis alone or in combination with Gemcitabine increases PDAC cell death under the different stromal conditions (section 5.5).

5.1. *In situ* analysis of PD-L1 expression and abundance of macrophages and CD8+ T cells in metastatic PDAC by immunohistochemistry staining

Most PDAC patients are diagnosed at late stages of the disease due to the lack of specific symptoms and the poor specificity of tumor biomarkers [13]. Moreover, PDAC often metastasizes, especially to distant organs, including the liver (76-80 % of patients), the peritoneum (48-59 %), or the lung (45-48 %) [3,235]. To date, the only curative treatment option is resection of the primary tumor but most of the patients are not eligible due to the late diagnosis or comorbidities. Only 20 % of PDAC patients have a respectable tumor at time of occurrence and even if the primary tumor is successfully resected, the 5-year survival rate of these patients is only 27 % [2]. Therefore, improved therapeutic treatments are urgently needed.

The expression of the immune checkpoint regulator PD-L1 is upregulated in several human cancer entities, such as NSCLC, melanoma, and gastric cancer resulting in T cell inactivation and tumor immune evasion [236]. Several studies also identified enhanced expression of PD-L1 in PDAC patients [55,81,170,171,176] and correlated a high PD-L1 expression with poor survival of patients [81,168,169]. To investigate whether PD-L1-mediated immune evasion might operate during PDAC progression, an analysis of serial PDAC tumor tissues and their corresponding liver metastases was performed regarding the PD-L1 frequency and intensity. Furthermore, the abundance of immune cell populations, including macrophages (especially M2-like macrophages) and T cells (particularly CD8+ T cells) was examined. The study of Rahn *et al.* already revealed that 69.6 % of analyzed primary PDAC tissues (all stages T3N1M0) showed no or low PD-L1 expression [170] and Principe *et al.* reported that 43.7 % of non-metastasized PDAC tissue samples had no PD-L1 expression [171]. In contrast, in the small cohort of this study, considerable PD-L1 expression was observed in all primary tumors as well as their corresponding liver metastases. This might be explained by the fact that these patients mostly exhibited poorly differentiated tumors, as Rahn *et al.* also observed higher PD-L1 levels in poorly differentiated primary PDAC [55]. Furthermore, the fact that PD-L1 was detected in the primary context as well as their liver metastases might indicate that PD-L1-mediated immune evasion operates during metastases formation in PDAC. The PD-L1 expression in primary and metastatic sites is also a topic of investigation in other cancer malignancies. In colorectal cancer (CRC) patients and epithelial ovarian cancer patients PD-L1 expression in the primary tumor as well as metastatic site was observed with the expression being more pronounced in the metastases [237,238]. Especially corresponding peritoneal metastases of ovarian cancer showed often PD-L1 expression (68 % of cases) [238]. Further, the study of Lee *et al.* revealed that 67 % of patients with NSCLC expressed PD-L1 in the primary tumor and within this group of patients, occurrence of synchronous brain metastases was significantly higher compared to PD-L1 negative patients (31.5 % vs. 19.1 %). Unfortunately, the PD-L1 status of brain metastases was not

noted, but the significant association between PD-L1 expression and synchronous brain metastases denotes that PD-L1-positive NSCLC patients should be closer examined for the occurrence of brain metastases [239].

In contrast, more primary tumors of breast cancer patients express PD-L1 in comparison to their metastatic lesions (63.7 % vs. 42.2 %), but the rate of PD-L1 positivity varied by the metastatic location [240]. When differentiated between tumor cell-expressed PD-L1 (primary tumor vs. metastasis: 18.7 % vs. 17.8 %) and immune cell-expressed PD-L1 (51.2 % vs. 37.1 %) in unmatched tumors and metastases, the difference in PD-L1 levels seems to be dependent on the immune cell populations. Studies investigating paired primary breast cancer tumors and metastases outlined a discordance in PD-L1 expression [240,241]. In detail, the pooled discordance rate differed according to the PD-L1-expressing cell populations: discordant primary/metastatic PD-L1 status was observed in 13.6 % of patients when expressed on tumor cells, 39.5 % when assessed on immune cells, and 47.6 % when expressed on both, immune and tumor cells [241]. In a study of penile squamous cell carcinoma, 62.2 % of patients expressed PD-L1 on tumor cells in the primary tumor, and patients with lymph node metastases were significantly more likely to express PD-L1 compared to patients without metastases. Further, in patients with matched primary tumors and lymph node metastases, a strong positive correlation with PD-L1 expression was detected. All primary tumors were PD-L1 positive and 77.8 % of corresponding metastases also exhibited PD-L1 expression. Moreover, the differentiation status of penile squamous cancer might have an impact on the PD-L1 expression, as 80 % of poorly differentiated tumors were PD-L1 positive whereas only 40 % of well-differentiated tumors expressed PD-L1 [242]. These results of differentiation status are in line with the results of PD-L1 expression in poorly differentiated PDAC tumors of this study cohort. Furthermore, the previous study of Rahn *et al*. also demonstrated implications, that poorly differentiated PDAC tumors exhibit elevated PD-L1 expression [55]. Taken together, the results of different studies investigating the PD-L1 status in primary tumors and metastases show a discordance in PD-L1 expression, as no specific PD-L1 expression pattern during all different disease progressions was observed. Nevertheless, most of the study results leave the suggestion that PD-L1 expression in primary tumors is associated with occurrence of metastases indicating a PD-L1-mediated immune evasion during disease progression as well as consideration of closer screening for metastases at secondary sites when the primary tumor is PD-L1 positive.

Furthermore, the immunohistological analyses of PDAC tissues also revealed that the PD-L1 expression is predominantly located in the TME, especially at the invasion fronts along with high proportions of macrophages (CD68+ and CD163+). This suggests that the main source of PD-L1 in the primary and metastatic lesions of PDAC are stromal cells. This was further confirmed by the results of double

immunohistochemical stainings, which revealed that PD-L1 is expressed to a much higher extent by macrophages than by PDAC cells. This finding is in line with the study of Rahn *et al.* demonstrating that in primary PDAC 76.5 % of PD-L1 positive cells are stromal cells [170]. In breast cancer, immune cells in the primary tumor and metastatic lesions also show higher PD-L1 expression compared to tumor cells [240], and in NSCLC, PD-L1 expression co-localizes with macrophages [243]. In contrast, Zhang *et al.* reported that in PDAC more PD-L1 positive cells are tumor cells than immune cells (PD-L1 positivity immune cells vs. tumor cells: 20 % vs. 30 %). Nonetheless, they observed more frequently PD-L1 positive tumor cells when immune cells also expressed PD-L1. Furthermore, PD-L1 positive immune cells were significantly related to high infiltration of CD3, CD4, CD8, FOXP3, and CD68 positive cells [172]. Although PD-L1 expression was also reported to be found on CD8+ T cells [213,244], double immunohistochemical staining of CD8 and PD-L1 in liver metastases demonstrated that CD8+ T cells do not express PD-L1. Li *et al.* detected a positive correlation of PD-L1 expression level with high immune cell infiltration, including macrophages and CD8+ T cells, in pancreatic cancer [173]. Additionally, several studies reported a high infiltration of macrophages, particularly CD163+ macrophages, in primary PDAC [24,55,56,59], indicating an anti-inflammatory phenotype which is associated with poor prognosis and reduced survival of patients [58,59,174,175]. Furthermore, another study analyzing biopsies of liver metastases from PDAC patients revealed that metastatic tumor cells were surrounded by CD68+ macrophages which was the most abundant immune cell population [143]. Taken together, these results underlie the finding of this thesis that macrophages are a main immune cell population in primary PDAC and liver metastases and that PD-L1 is predominantly expressed by stromal cells, especially macrophages, in metastatic PDAC.

Although the presence of CD8+ T cells in PDAC is associated with better survival outcomes, the number of infiltrated CD8+ T cells is very low [71–73]. However, despite the low infiltration of CD8+ T cells, they were also observed in primary and secondary lesions of PDAC in PD-L1-expressing areas in the present study. Similar to this, Blando *et al.* observed in pancreatic tumors minimal to moderate infiltration of CD3, CD4, and CD8 cells [217], which fits with the detection of small amounts of CD8+ T cells in this study (highest score frequency: > 1 %). In liver metastases of CRC patients, a higher density of CD8+ T cells (≥ 10 %) was predominantly observed in PD-L1 positive (94.4 % of cases) compared to PD-L1 negative liver metastases [237] supporting the view that CD8+ T cells are predominantly located in PD-L1-expressing areas. The study of Principe *et al.* supports this finding as they found an association of PD-L1 expression with an increase of tumor-infiltrating lymphocytes in PDAC biopsies. Further, *PD-L1* gene expression was positively correlated with mRNA expression of T cell markers *CD3E* and *CD3G* as well as *IFNγ* gene. The IFNγ protein expression was predominantly localized in CD3+ T cell infiltrating areas suggesting T cells as a main source of IFNγ [171], which is a well-known inducer of PD-L1 [245]. In the small

study cohort of this thesis, CD8+ T cells were predominantly located at the invasion fronts of the primary tumor or metastasis and thus separated from tumor cells by PD-L1-expressing macrophages. This also can be underlined by the findings of Blando *et al.* and Rahn *et al.* as they demonstrated T cell infiltrates in the stromal area of the tumor but excluded from tumoral areas [55,217]. One reason for the low infiltration of CD8+ T cells into the tumor can be seen in the desmoplastic stroma containing ECM which acts as a physical barrier for immune cell populations and in particular CD8+ T cells [246]. The ECM in pancreatic tumors is characterized by markedly enhanced stiffness and density compared to healthy pancreas tissue [247]. More than 90 % of ECM molecules are produced by stromal cells, such as myofibroblasts, and the predominantly existing ECM proteins are collagens. But also hyaluronan and laminins are responsible for the pronounced desmoplastic stroma in PDAC [247]. Further, the low CD8+ infiltration in PDAC tumors may occur due to a stromal compartment-specific infiltrative defect. In detail, CD8+ T cells, as well as B-cells, NK cells, and Tregs, are unable to sufficiently infiltrate the juxtatumoral stroma of PDAC tumors. In KPC mice, the application of all-*trans* retinoic acid (ATRA) resulting in quiescence of pancreatic stellate cells (PSCs) and thereby reduce number of myofibroblasts which promote desmoplastic reaction, and led to an increased proportion of CD8+ T cells within the juxtatumoral stroma [248,249]. CXCL12-rich stroma initiated by activated PSCs favors the migration of CD8+ T cells away from the juxtatumoral stroma [73]. These findings support the importance of desmoplastic stroma as a physical barrier preventing immune surveillance in PDAC. Therefore, stroma-reducing treatment approaches like targeting hyaluronic acid by hyaluronidases to enhance drug delivery may contribute to induced anti-tumor immunity by enhanced T cell-mediated immunotherapies [248,250].

Overall, although the studied cohort in this thesis was small, this first comparative analysis of primary tumors and corresponding metastases from PDAC patients provides a unique insight into the potential role of PD-L1 and macrophages in immune evasion of PDAC. However, to validate these findings the analysis of more matching tissue samples might be reasonable.

5.2. Impact of activation culture on CD8+ T cells and their impairment potential of PDEC viability in the absence or presence of Durvalumab

As macrophages and CD8+ T cells were found in the TME of PDAC and both expressed PD-L1, the next aim of the study was to investigate whether and how both cell populations impact each other. Further, it was examined whether CD8+ T cells pre-cultured with macrophages decrease PDEC viability in 2D cultures. The last aim was to analyze whether blocking of PD-L1 only on CD8+ T cells or during co-culture with PDECs impacts PDEC viability and CD8+ T cell phenotype.

First, the early activation marker CD69 was significantly increased on CD8+ T cells during activation culture. Already after one day of activation culture, CD69 levels were enhanced until day 3, when surface expression dropped again. This is in line with the rapid increase of CD69 after 3 to 12 h after start of activation of PBMCs [251]. As CD69 is associated with T cell exhaustion [252], it can be hypothesized that activated T cells exhibit an exhausted phenotype. The study of Mita *et al.* revealed that CD8+ T cells of $CD69^{-/-}$ Balb/c mice showed enhanced IFNγ production compared to $CD69^{+/+}$ T cells which indicates a correlation between CD69 expression and T cell exhaustion [252]. The late activation marker CD25 as part of the IL-2 receptor was also increased during activation culture, but the increase started on day 2. Reddy *et al.* also reported delayed enhancement of CD25 expression on PBMCs after 24 h stimulation [251].

During activation culture of CD8+ T cells, surface levels of PD-1 were also enhanced until the end of the activation period. It can be speculated that during activation and enhancement of CD69 and CD25 expression, CD8+ T cells upregulate PD-1 to protect themselves against overactivation. It is also reported that higher PD-1 expression on CD8+ T cells is observed during T cell exhaustion [210–212]. T cell exhaustion is characterized by the loss of effector function such as decreased proliferation, diminished release of cytokines, and reduced secretion of cytolytic molecules due to continuous antigen stimulation in a pathological situation, e.g., in cancer [253]. The overexpression of co-inhibitory immune checkpoints can induce T cell exhaustion via direct signaling through the interaction with their ligands [210]. In CRC patients, elevated mRNA levels of co-inhibitory receptors PD-1, TIM-3, CTLA-4, and TIGIT on T cells and T cell exhaustion-related genes were found in tumor tissues indicating an exhausted T cell phenotype [210]. Although secretion of IFNγ is decreased by progressing T cell exhaustion, *in vivo* studies detected some killing activity of virus-specific T cells [254,255]. In this thesis, IFNγ concentrations during activation culture were increased, but the enlargement was reduced again the longer the cells were cultured in the absence of the activation stimuli.

Besides the elevated PD-1 surface levels on activated CD8+ T cells, PD-L1 expression was also observed on activated CD8+ T cells. The expression of PD-L1 on activated T cells is also reported in the literature [213,256–258], but the role of PD-L1-expressing CD8+ T cells is controversially discussed. Liu *et al*. proposed that in mouse renal cell carcinoma tumor-reactive CD8+ T cells expressing PD-L1 are functional effector T cells exemplified by increased IFNγ production after re-stimulation [258]. In contrast, Zheng *et al.* reported that PD-L1+ CD8+ T cells exerted regulatory functions which inhibit T cell proliferation and cytotoxic abilities in lung cancer patients [213]. They identified that PD-L1 high-expressing CD8+ T cells produce diminished IFNγ and TNFα levels compared to PD-L1 low-expressing T cells. According to the two different functions of PD-L1 on CD8+ T cells, the results of this study implicate that PD-L1 expression might have an effector function as IFNγ and all cytotoxic molecules

were enhanced. Although there was evidence that activated CD8+ T cells in this study exhibit an exhausted phenotype, the results of cytotoxic molecules and IFNγ concentrations leave the suggestion that CD8+ T cells still have effector function.

Expression of CD80, which is mostly expressed by APCs, was also increased on CD8+ T cells during activation culture and was also reported in the literature [215]. CD80 has several interaction partners which could result either in induction of co-stimulatory or co-inhibitory signals. In the field of PD-L1 binding partners, it is discussed whether PD-L1 can bind to CD80 in *trans* (interaction of both molecules when expressed on two different cells). PD-L1 and CD80 *trans*-binding was reported to result in suppressed T cell activation and cytokine production. The highest binding affinity of CD80 has CTLA-4, followed by PD-L1, and lastly, CD28 [259,260]. Besides the PD-1/PD-L1 co-inhibitory interaction, PD-L1/CD80 binding is required to induce and maintain peripheral T cell tolerance [261]. In contrast, it was also reported that PD-L1 and CD80 can only interact in *cis* (interaction of both molecules on the same cell surface) [130,262], which was supported by other studies [112,152]. The consequences of PD-L1/CD80 *cis*-binding are dependent on the cell surface expression of involved molecules. Each monomer of homodimeric CTLA-4 binds to one monomer of CD80 from two distinct CD80 dimers and stabilizes homodimer formation of CD80. Contrastingly, CD86 is only present as a monomer in CTLA-4 binding. Further, CD28 binds monomeric CD80. Garrett-Thomson *et al.* reported that the presence of CTLA-4 interrupts *cis*-binding of PD-L1/CD80, resulting in unbound PD-L1 which can be bound by PD-1 [97]. Both reorganization patterns reveal co-inhibitory signals resulting in T cell suppression.

Zhao *et al.* proposed a model of *cis*-bound PD-L1/CD80, which promotes the co-stimulatory CD28 binding while repressing co-inhibitory pathways of PD-1 and CTLA-4 [130]. The *cis*-PD-L1/CD80 binding on APCs results in restriction of PD-1 binding on T cells to PD-L1 when substantial amounts of CD80 are present, indicating a limitation of PD-1 co-inhibitory signal. Simultaneously, CD28-mediated co-stimulatory signaling is promoted due to the ability of *cis*-bound CD80 to interact with CD28. Further, treatment with immune checkpoint inhibitor Atezolizumab (α-PD-L1 antibody) depleted CD80 on APCs in a CTLA-4-dependent manner [130,263]. The treatment with Atezolizumab can disrupt *cis*-bound PD-L1/CD80 heterodimers and free CD80 for high-avidity CTLA-4 interaction, resulting in Treg-mediated CD80 depletion on APCs and suppressing CD28 co-stimulation [130]. Since CTLA-4 was only present in negligible amounts on activated CD8+ T cells in the results of this thesis, this co-inhibitory axis of CTLA-4/CD80 may not be essential in CD8+ T cells. It can be speculated that in addition to the co-inhibitory PD-1/PD-L1 axis which might be not efficient enough, *trans*-binding of PD-L1 and CD80 operates to protect CD8+ T cells against overactivation. Thus, CD80 surface levels strongly increased at day 3 when CD69 and CD25 showed also highest expression. Right after this enhancement, activation markers CD69 and CD25 were reduced, although activation stimuli were still present.

According to the CD69 and PD-1 expression, activated T cells seemed to have an exhausted phenotype as often described in PDAC [73,211]. Nevertheless, the concentrations of cytotoxic molecules and IFNγ after 4-day activation culture were elevated. To examine whether PD-L1 on CD8+ T cells has inhibitory function that impedes PDEC viability, blocking of PD-L1 by Durvalumab treatment was performed. In general, CD8+ T cells were able to decrease viability of H6c7-KRAS cells, but not of PancTu1 cells. Since H6c7-KRAS cells were immortalized by retroviral infection containing E6 and E7 genes of HPV, they express E6/E7 peptides which may be recognized by CD8+ T cells, as MHC class I CTLs are known to be responsible to recognize and kill virus-infected cells [264], even when the cells express foreign MHCs [265,266]. Durvalumab was a potent blocking antibody which was confirmed by flow cytometric analyses, as after application of Durvalumab, the antibody used for flow cytometry against PD-L1 (clone MIH3) was no longer able to bind to PD-L1 so that fluorescence intensities were markedly diminished. Although PD-L1 was efficiently blocked by Durvalumab, neither the activation status nor the PDEC viability was affected indicating that blocking PD-L1 on CD8+ T cells is not able to improve the effector phenotype of CD8+ T cells. As H6c7-KRAS cells have strong PD-L1 surface expression and PancTu1 cells moderate PD-L1 surface levels, their unblocked PD-L1 molecules might interact with PD-1 on CD8+ T cells which underlie the unimpacted PDEC viability. It was further investigated whether blocking of PD-L1 in direct co-culture of CD8+ T cells and PDEC affect the PDEC viability. Indeed, when PD-L1 molecules on both, PDEC and CD8+ T cells were blocked by Durvalumab, the PDEC viability, especially in H6c7-KRAS cells was decreased pointing to an inhibiting role of PDEC-expressed PD-L1.

5.3. PD-L1 characterization in the CD8+ T cell/macrophages interplay with PDECs

The *in situ* results revealed that CD8+ T cells are in close proximity to PD-L1-expressing macrophages. Furthermore, most of the macrophages seemed to have an anti-inflammatory CD163+ phenotype which was also reported in different studies investigating PDAC tissues [24,55,56,59]. Therefore, the next aim was to investigate CD8+ T cells after direct co-culture with pro- and anti-inflammatory macrophages and whether these macrophage-primed T cells affect the PDEC viability. For this purpose, CD8+ T cells and macrophages were isolated from leucocyte retaining systems of one blood donor to accomplish a syngeneic system.

First, the polarization of pro- and anti-inflammatory macrophages was tested in mono-culture to check whether polarization with GM-CSF and M-CSF results in different subtypes of macrophages. The cell morphology of M1- and M2-like macrophages was mostly spindle-shaped, but M1-like macrophages formed more round cells and clustered compared to M2-like macrophages which were also observed by Jaguin *et al.* [43]. The cell surface levels of mono-cultured M1- and M2-like macrophages clearly

differed regarding CD206, CD163, and CD14. CD206 was considerably higher on M1-like macrophages which can be explained by the fact that GM-CSF used for polarization of M1-macrophages induced the expression of mannose receptor CD206 [47]. In contrast, when monocytes are polarized with LPS and IFNγ into M1-like macrophages, CD206 surface levels are not increased [43]. Surface levels of CD163 and CD14 were clearly higher on M2-like macrophages which is well in line with the study of Ambarus *et al.* [47] and characteristic of an M2-like phenotype [267]. The expression of the co-stimulatory molecule CD80 did not differ between M1- and M2-like macrophages, while CD86 was slightly higher on M1-like macrophages. Actually, both CD80 and CD86 should be stronger expressed in M1-like macrophages compared to M2-like macrophages [44,47]. Although CD80 expression was similar in M1- and M2-like macrophages, surface levels of CD206, CD163, CD14, and CD86 fit with the different phenotypes in the literature and indicate that the *in vitro* polarization of M1- and M2-like macrophages resulted in two different macrophage subtypes.

Next, the phenotype of macrophages was investigated after co-culture with CD8+ T cells. As it is known that macrophages have a high plasticity and are able to switch their phenotypes due to surrounding microenvironment [24,37,225], their phenotype was examined in the presence of CD8+ T cells. To maintain the pro-inflammatory M1-like phenotype, GM-CSF was added to macrophage-CD8+ T cell co-culture and M-CSF to preserve an anti-inflammatory M2-like phenotype. Since CD8+ T cells produce among others IFNγ which is known to promote macrophage polarization into pro-inflammatory M1-like macrophages [47,268,269], the additional application of respective polarization stimuli was needed to examine the impact of clearly defined macrophage subtypes on CD8+ T cells. Despite adding GM-CSF and M-CSF respectively to co-cultures with CD8+ T cells, diminished differences between M1- and M2-like macrophages for CD206, CD163, and CD14 surface levels were observed, albeit the trends were still similar compared to mono-cultures. Since IFNγ is an inducer of CD80 and CD86 [47], it was not surprising that surface levels of both molecules were markedly enhanced after co-culture with CD8+ T cells on both macrophage subtypes. In contrast, it was unexpected that M2-like macrophages exhibited slightly higher surface expression of CD80 and CD86 than M1-like macrophages after CD8+ T cell co-culture. This indicated that M2-like macrophages lose some anti-inflammatory abilities as CD80 expression is associated with an M1-like phenotype [43]. Although the different phenotypes of macrophages were not that pronounced in co-culture with CD8+ T cells compared to macrophage mono-cultures, the difference between both subtypes was still observable.

Next, the surface levels of PD-L1 on macrophages were examined. Immunofluorescence stainings and flow cytometric analyses revealed that mono-cultured M1-like macrophages exhibited higher PD-L1 levels compared to mono-cultured M2-like macrophages. One explanation for this might be that GM-CSF used for M1-like polarization is able to induce PD-L1 expression [270]. When both macrophage types

were co-cultured with CD8+ T cells, the PD-L1 expression was clearly enhanced compared to the respective mono-culture, presumably due to IFNγ production of CD8+ T cells, which induced PD-L1 expression [271].

As the two different phenotypes were stable in co-culture with CD8+ T cells, the impact of pro- or anti-inflammatory macrophages was investigated on CD8+ T cells. CD8+ T cells in co-culture with either M1-like or M2-like macrophages showed increased surface levels of CD69 and CD25 compared to mono-cultured T cells. Of note, the activation status of CD8+ T cells co-cultured with M1-like macrophages was higher than in co-culture with M2-like macrophages. This is well in line with the pro-inflammatory properties of M1-like macrophages [43]. Nevertheless, co-culture with M2-like macrophages led also to an increase of activation status supporting the view that M2-like macrophages gained pro-inflammatory properties in the presence of CD8+ T cells. As elevated CD69 expression is also associated with an exhausted phenotype of T cells [252], it can also be a sign of T cell dysfunction. Interestingly, although M1- and M2-like macrophages obtained high PD-L1 expression after co-culture with CD8+ T cells, the inhibiting role of PD-1/PD-L1 axis on CD8+ T cells was not observed on the activation status of CD8+ T cells. Singhal *et al.* reported that PD-L1 expressed by TAMs in early-stage lung cancer did not inhibit a T cell response, and rather protected macrophages from destruction by T cells [272]. The cell surface levels of PD-1 and PD-L1 were also clearly enhanced after co-culture with both macrophage subtypes compared to mono-cultured CD8+ T cells indicating that T cells try to regulate their activation by themselves (similar to CD8+ T cells during activation culture). However, attendance of M2-like macrophages led to a diminished increase compared to co-culture with M1-like macrophages. This can be explained by the fact that the activation status of CD8+ T cells in co-culture with macrophages was not that enhanced like after co-culture with M1-like macrophages. Therefore, the inhibiting axis of PD-1/PD-L1 expressed by CD8+ T cells was not as needed as in the presence of M1-like macrophages. These results also fit together with the results of the CD8+ T cell activation culture, but enhanced PD-1 expression is associated with T cell exhaustion [210–212]. CD80 surface levels were only slightly increased in CD8+ T cells co-cultured with both types of macrophages, probably due to the relatively low activation status of CD8+ T cells under these conditions. It can be suggested that the inhibiting properties of PD-L1/CD80 *trans*-interaction of CD8+ T cells are not necessary to protect T cells from overactivation wherefore high CD80 levels were not needed.

Lastly, it was tested whether this enhanced activation of CD8+ T cells after co-culture with macrophages is able to decrease PDEC viability. However, the confluence of both PDEC lines H6c7-KRAS and PancTu1 were not impacted by the CD8+ T cell attendance. It can be speculated that the enhanced CD69 and PD-1 expression on CD8+ T cells exemplifies an exhausted phenotype [210–212,252] and therefore no decreased PDEC viability was observed. Further, the PDEC viability assay has some

limitations. The PDEC viability was only assessed by measuring the fluorescence confluence. Here, it is difficult to discriminate between senescent and apoptotic PDECs, as senescent cells enlarge their sizes [273], whereas apoptotic cells become smaller [273]. Thus, the confluence might be bigger the more senescent cells are in culture and the smaller confluence is abolished when apoptotic cells are in culture. Further, it cannot be excluded that some macrophages from previous CD8+ T cell/macrophage co-culture were added with the CD8+ T cells to the PDEC culture, internalize Celltracker green, and adhere to the plate surface. Therefore, another assay specifically investigating PDEC death like the M30 cyto death assay which examines caspase-cleaved Keratin 18 in supernatants would be a better option and exclude the mentioned limitations.

Overall, although M2-like macrophages lose some of their anti-inflammatory phenotypes after co-culture with CD8+ T cells, the two different subtypes of macrophages were still distinct. The attendance of M1- and M2-like macrophages had an enhancing effect on activation status of CD8+ T cells, albeit both macrophage subtypes exhibited high PD-L1 expression. This indicates that either PD-L1 expressed by macrophages is not able to inhibit CD8+ T cell activation or macrophages enhance exhaustion of CD8+ T cells, wherefore no alterations on PDEC viability were observed.

5.4. 3D co-culture model of PDAC cells and macrophages

The progress on 3D model systems to better mimic *in vivo* tumor conditions increased over the past years. To this end, 3D cell culture systems provide a more physiologically relevant architecture with respect to cell-cell communication, ECM proteins, nutrient gradients, and hypoxic tumor regions [274,275]. In order to simulate the TME conditions in primary PDAC and liver metastases identified *in situ*, a 3D co-culture spheroid model containing PDAC cells and different ratios and types of macrophages was established.

First, it was evaluated which PDEC lines have spheroid formation abilities. H6c7-KRAS, PancTu1, Panc89, and A818-6 cells formed dense spheroids in ULA plates during 72 h. Panc89 and PancTu1 cells were also investigated regarding their spheroid formation ability as previous studies showed that they are able to form dense spheroids, which was also observed in this study [276,277]. A818-6 cells were also reported to form dense spheroids in medium [277], and medium in a 3.1 % agarose pre-coated plate [278]. BxPc3 cells also appeared as spheroids, but several cells were not included in the spheroids which is in line with the literature [267]. Colo357 and PT-45 cells formed loose spheroids, whereas Panc1 cells could not form any spheroids at all. In contrast, Panc1 cells were reported in the literature to form spheroids after 5 days [279]. In the study of Minami *et al.,* Panc1 cells formed larger and denser spheroids compared to the results of this study. Taking note of the larger incubation time for spheroid formation in both

studies (5 days and 7 days), this may be an explanation for the different spheroid formation features of Panc1 cells [276,279]. According to Sempere *et al.,* Colo357 cells can form dense spheroids in a 3 % Matrigel/soft agar mixture [280] or in medium [277]. Adding ECM molecules to the PDAC cells could switch their spheroid formation abilities, as Panc1 and BxPc3 cells formed spheroids in a collagen matrix. Interestingly, BxPc3 cells also showed more single cells which were not included in the spheroids when a collagen matrix was present [281]. This implicates the strong effect of ECM on the cell morphology. In the present study, the 3D model excluded components of ECM to focus only on cell-cell interactions of the involved cell populations.

As PDAC is characterized by a high heterogeneity regarding its PD-L1 expression [55], the established 3D model should simulate different PD-L1-expressing tumor conditions. Thus, the next step was to screen for PD-L1 expression on all PDEC lines tested for spheroid formation ability. H6c7-KRAS cells exhibited the highest PD-L1 surface levels, followed by PT-45, PancTu1, A818-6, and BxPc3 cells which all expressed moderate levels of PD-L1. On Colo357 and Panc89 cells only low PD-L1 surface expression was detected and Panc1 cells showed no PD-L1 levels. The PD-L1 expression patterns of these 8 PDEC lines corresponds to the findings of Heckl *et al.* and Rahn [218,282]. For further investigation, high PD-L1-expressing H6c7-KRAS, moderate-expressing PancTu1, and low-expressing Panc89 cells were used. Furthermore, the viability of PDECs in spheroids was determined by PI staining. H6c7-KRAS cells showed a high PI staining indicative for high cell death and an unstable cell viability. This can be explained by the fact that H6c7-KRAS cells have a mesenchymal phenotype (data not shown). Minami *et al.* already reported about an association of PDAC cells with an epithelial phenotype and spheroid formation. They also observed high Vimentin and low E-cadherin expression on Panc1 cells, which are characterized by a mesenchymal phenotype and did not form dense spheroids in this study. In contrast, low Vimentin mRNA expression, but high E-cadherin expression was observed in Panc89 cells [276], indicative for an epithelial phenotype, which formed dense spheroids. The results of spheroid formation, PD-L1 expression, and induction as well as spheroid viability revealed that only PancTu1 and Panc89 cells are suitable to establish a stroma-enriched 3D co-culture model.

To simulate the TME conditions in primary PDAC and liver metastases identified *in situ*, a 3D co-culture model containing two different PDAC cell lines with different ratios and types of macrophages was established in order to investigate whether the presence and amount of different types of macrophages impact PD-L1 expression in PDAC cells as well as CD8+ T cell activity. The 3D co-culture model well simulated the TME conditions detected *in situ*, as macrophages were mostly located at high frequencies at the margin of tumor spheroids. Additionally, the M2-like phenotype of macrophages, indicated by expression of CD163 and CD14, was further promoted by both PDAC cell spheroid co-cultures. This observation is supported by several studies reporting a high abundance of M2

macrophages in the TME of human and murine PDAC [55,63,283]. Moreover, either macrophage population exhibited considerable PD-L1 expression being in line with the *in situ* analysis which revealed PD-L1 expression more on stromal cells/macrophages rather than tumor cells. In order to reflect tumor heterogeneity regarding PD-L1 expression in PDAC, PancTu1 cells exhibiting moderate PD-L1 expression and Panc89 cells exhibiting low PD-L1 expression, which was inducible, were chosen as PDAC cell models for the *in vitro* studies. While PD-L1 expression was not altered in both PDAC cell lines due to the attendance of either macrophage subtype, it was clearly enhanced in both macrophage populations after co-culture with either PDAC cell line. In contrast to the results of this study, Xia *et al.* showed a PD-L1 increase on PDAC cells due to the attendance of M2-like macrophages [81]. One explanation for this discrepancy might be that in this study a higher macrophage to PDAC cell ratio was used. Moreover, they identified TGFβ1 as a main inducer of PD-L1 expression [81], which seemed not to be the inducer of PD-L1 expression in the 3D model system of this study, as TGFβ1 was not detectable or only in small amounts in the culture supernatants (data not shown). Thus, these findings support the view that macrophages are a superior source of PD-L1 expression in PDAC, however, the identification of the inducing factors in this PDAC 3D model system is subject of future investigation.

Next, it was investigated whether the attendance of PD-L1-expressing macrophages impacts the effector phenotype of CD8+ T cells. Interestingly, the effector phenotype of CD8+ T cells was rather promoted by either co-culture with macrophages reflected by an increase of the early activation marker CD69. In contrast, mono-cultured PDAC spheroids in culture with CD8+ T cells did not result in any change of CD69 or CD25 surface levels. Furthermore, PD-1 surface expression was neither altered by presence of mono-cultured nor by macrophage-enriched PDAC spheroids. However, PD-L1 surface levels were either enhanced by trend (PancTu1/macrophage spheroids) or significantly enhanced (Panc89/macrophage spheroids) on CD8+ T cells due to the attendance of macrophages. This might be explained by the fact that also the production of cytotoxic molecules and IFNγ was increased by the presence of macrophages. It is still not fully understood, why PD-1 expression on T cells was not altered which is a matter of future investigation.

The release of Granzyme A/B, Granulysin, Perforin, and IFNγ by CD8+ T cells was enhanced after the culture with mono-cultured PDAC spheroids but even more increased in the presence of both types of macrophages. Of note, the release of IFNγ and effector molecules Granzyme A and B was more increased in the presence of a higher number of (M1) macrophages indicating a relationship between the T cell effector phenotype and the abundance of (pro-inflammatory) macrophages. In PDAC patients, a high density of CD8+ T cells in tumor areas is associated with better survival outcomes [71,72]. Further, several therapy approaches aiming at a phenotype switch from M2 to M1 macrophages thereby inducing CD8+ T cell responses, T cell recruitment, and IFN responses [29,284,285] underlie the

results of an enhanced CD8+ T cell effector phenotype in the presence of M1 macrophages. Although macrophages showed higher PD-L1 expression in co-culture with PDAC cells, the effector phenotype of CD8+ T cells was rather intensified, but which was not associated with elevated PDAC cell death. Here, it can be speculated whether infiltration of CD8+ T cells into the spheroids is impaired not allowing a further increase in PDAC cell death induction. To this end, there are not any reliable conclusions on this issue because the available imaging modalities do not properly decipher whether CD8+ T cells are infiltrated into the spheroids or whether they are attached at the margin. However, the latter would be in line with the *in situ* findings demonstrating that CD8+ T cells are separated from the tumor cells.

5.5. Different treatment options in 3D model of PDAC/macrophages spheroids and CD8+ T cells

As high tumoral PD-L1 expression is correlated with poor survival of PDAC patients [81,286], the concept of inhibiting the PD-1/PD-L1 axis to enhance T cell cytotoxicity is promising. However, single-agent immunotherapy with Durvalumab or Pembrolizumab has still failed in clinical trials for PDAC [24]. In order to elucidate whether different ratios and phenotypes of macrophages may impact treatment efficacy of Durvalumab or Pembrolizumab, treatment of mono- and co-culture spheroids with either antibody was performed. Despite considerable expression of PD-L1 and PD-1 on macrophages and CD8+ T cells, respectively, ICI treatment did not lead to enhanced activation status, production of cytotoxic molecules, and IFNγ as well as PDAC cell death in either mono- or co-culture model. These findings are in line with the above-mentioned clinical situation. Another determinant for ICI responses is the TMB. In other malignancies including melanoma, non-small-cell lung cancer, and urothelial cell carcinoma, patients with high TMB clearly more benefit from ICI therapy compared to patients with low TMB [287]. One explanation for this is that tumors with high TMB exhibit more immunogenic neoantigens, which can be recognized by T cells thereby fostering ICI therapy [287]. In PDAC, only 1.1 % of patients show a high TMB, supporting the low response rate towards ICI treatment. However, preliminary results of anti-PD-1 treatment in the subgroup of PDAC patients with high TMB revealed promising effects [288].

Gemcitabine which is widely used as an anti-cancer chemotherapeutic agent in several solid cancer malignancies is still the standard-of-care treatment in PDAC [227,228,289]. Gemcitabine is a deoxycytidine nucleoside analog that exhibits anti-proliferative properties such as blocking cell cycle progression at the G1/S-phase [290]. In PDAC, Gemcitabine treatment does not result into long-term survival benefits in most of the patients. This might be the fact because of the poor penetration of the drug into the hypo-vascularized and dense tumor-stroma. Further, initially sensitive tumors develop Gemcitabine

chemoresistance within weeks of treatment [289]. Moreover, PDAC is characterized by a dense tumor-stroma and this might be responsible to create a physical barrier for the drug to penetrate the tumor [289]. In this thesis, the 3D PDAC/macrophage model in combination with CD8+ T cells was used to investigate the effect of Gemcitabine treatment as mono-therapy to investigate the effects on CD8+ T cell effector phenotype and PDAC cell death. First, the activation status and surface levels of immune checkpoint molecules on CD8+ T cells were examined. Although CD8+ T cells were not cultured with Gemcitabine directly, as the medium had been changed before CD8+ T cell culture was started, the surface levels of CD69, CD25, and PD-1 decreased on CD8+ T cells in all culture conditions compared to their untreated spheroids. One explanation for this might be that remaining Gemcitabine was still able to impact CD8+ T cells, as for the medium change 15 µl of Gemcitabine-containing medium remained into each well to ensure that mostly all macrophages remain in the culture. Thus, a final concentration of 0.15 µg Gemcitabine was still in the culture setting with CD8+ T cells. Single-agent treatment with Gemcitabine is known to decrease CD8+ T cell infiltration in mouse tumor allografts and human pancreatic cancer tissues [291]. The study of Smith *et al*. reported that CD8+ T cells directly treated with Gemcitabine led to no enhancement of CD69 expression. The PD-1 expression on activated CD8+ T cells was also not altered by Gemcitabine treatment compared to untreated cells [290] underlying that Gemcitabine has no promoting immunogenic role. Another explanation for the reduced surface levels of CD69, CD25, and PD-1 might be that Gemcitabine treatment affects PDAC spheroids and macrophages, which indirectly, impact CD8+ T cells. The release of cytotoxic molecules and IFNγ was also diminished in all culture conditions with both PDAC spheroids indicating again an immune-inhibiting effect of Gemcitabine on CD8+ T cells. Smith *et al.* also reported a decreasing effect on IFNγ expression by CD8+ T cells with increasing Gemcitabine concentrations and PD-L1 expression increase on PDAC cells [290] underlying the results of this study and promote the view that Gemcitabine has a poor immune modulatory effect in PDAC.

In a pancreatic cancer mouse model, Gemcitabine treatment led to prolonged survival and increase of CD8+ T cells [292]. In contrast, the attendance of CD8+ T cells after Gemcitabine treatment did not enhance PDAC cell death in both PDAC cell spheroids under all culture conditions compared to the respective untreated samples. Of note, Gemcitabine pre-treatment of mono-cultured PancTu1 spheroids resulted in decreased PDAC cell death. PancTu1 cells are described to exhibit Gemcitabine resistance [293], e.g., Gemcitabine treatment leads to up-regulation of CD95 and CD95L which enhances the production of IL-6 and IL-8 as well as cancer stem cell markers resulting in chemoresistance. Accordingly, enhanced CD95L expression can be inhibited with CD95L inhibitors which restores the sensitivity of PDAC cells towards Gemcitabine [294]. This might be an explanation, why Gemcitabine treatment resulted in lower PDAC cell death of PancTu1 spheroids than Panc89 spheroids, although

the induced ccK18 levels of Panc89 spheroids were only small. Additionally, macrophages, highly abundant in PDAC, contribute to chemotherapeutic resistance. Buchholz *et al.* showed that murine and human macrophages can rapidly metabolize and inactivate the chemotherapeutic drug Gemcitabine resulting in profound therapy resistance [66]. Another study could show that murine bone marrow-derived macrophages when exposed to PDAC cells release pyrimidine species, among others deoxycytidine, which inhibits Gemcitabine through molecular competition, representing another mechanism of macrophage-mediated chemoresistance in PDAC [295]. However, a potential resistance to Gemcitabine mediated by macrophages was not observed in this study as PDAC spheroids in co-culture with macrophages showed no decreased PDAC cell death compared to mono-cultured PDAC spheroids after Gemcitabine treatment.

As mono-treatment with Durvalumab and Pembrolizumab failed in this 3D co-culture model and Gemcitabine has been identified as an inducer of PD-L1 expression [229,230], investigations of whether sequential treatment with Gemcitabine and ICI showed superior effects on the effector phenotype of CD8+ T cells and induction of PDAC cell death were performed. This concept was further supported by data from a murine model of pancreatic cancer liver metastasis, demonstrating that the combination of Gemcitabine treatment and anti-PD-1 antibody is associated with infiltration of CD8+ T cells and M1 macrophages along with prolonged survival of the mice [69]. However, Gemcitabine treatment only led to a slight increase of PD-L1 expression in Panc89 cells, and the combination of Gemcitabine pre-treatment and ICI did neither impact the CD8+ T cell activation status nor increased PDAC cell death. Nevertheless, several clinical studies evaluating different combinational treatments are ongoing, e.g., an open label, single arm, multicenter clinical trial investigates the combination of AZD0171 (humanized monoclonal antibody binding to leukemia inhibitory factor, promoting anti-tumor inflammation through TAM modulation and cancer stem cell inhibition) and Durvalumab as well as standard-of-care chemotherapy in metastatic PDAC patients (NCT04999969). Another randomized multicenter phase Ib/II clinical trial study investigates efficacy of a combination of neoadjuvant chemoradiation therapy with Pembrolizumab treatment in PDAC patients (NCT02305186).

Besides the PD-L1/PD-1 axis, several other mechanisms might operate in PDAC impairing CD8+ T cell-mediated tumor reactivity and limiting the effects of PD-1/PD-L1 blockade. Although the PD-1/PD-L1 axis is a major player in regulating T cell functions and was efficiently blocked in the *in vitro* experiments of this study, several other co-inhibitory interactions can restrain the anti-tumor function of CD8+ T cells in the TME [216]. These co-inhibitory molecules include ICOS, TIGIT, PD-1, and LAG-3 were identified at elevated levels on CD8+ T cells in PDAC tissues [103], suggesting that the TIGIT-CD155 or LAG-3-MHC interaction are more potent immunosuppressive mechanisms in PDAC. Especially TIGIT, which is expressed on tumor-infiltrating cytotoxic T cells in multiple malignancies, and its ligand CD155,

often expressed by tumor-infiltrating myeloid cells and upregulated on cancer cells, provide a promising target to overcome the local suppression of immune surveillance [216]. As CD155-TIGIT interaction is associated with cancer resistance to PD-1 blockade, targeting this interaction might be a promising strategy to increase the efficacy of PD-1 inhibition [216]. Accordingly, Pearce *et al.* could recently show that CD8+ tissue-resident memory T cells in PDAC patients co-express PD-1 and TIGIT on their cell surfaces and blocking of both molecules enhanced IFNγ secretion and T cell proliferation, suggesting a promising route to improve ICI efficacy [296]. In line with this hypothesis, Freed-Pastor *et al.* showed that targeting the TIGIT-CD155 axis in combination with CD40 agonists and anti-PD-1 treatment elicits profound anti-tumor responses in pancreatic cancer mouse models *in vivo* [297]. Furthermore, Gulhati *et al.* demonstrated an enhanced expression of LAG-3, Tnfrsf9 (41BB), and Havcr2 (TIM-3) in genetically engineered PDAC mouse model under anti-PD-1 monotherapy [283], supporting the view that combined targeting of different immune regulatory mechanisms might be an efficient strategy to induce a potent tumor-directed immunity in PDAC. Preclinical and clinical studies underscore this hypothesis as co-blockade of PD-1 and a second co-inhibitory molecule such as CTLA-4 augments the anti-tumor immunity compared to single PD-1 blockade in different solid malignancies [216]. Taken together, these findings support the view that the interplay of several co-inhibitory mechanisms rather than the PD-L1/PD-1 axis alone leads to PDAC immune evasion. Accordingly, targeting only one co-inhibitory axis by antibody blocking is not effective in improving tumor elimination and thereby the clinical situation of PDAC patients. Rather the combinational targeting approaches of different co-inhibitory receptors or ligands might improve the therapy of PDAC.

The stroma-enriched 3D co-culture systems well reflect several conditions in PDAC and its liver metastases regarding PD-L1 expression in PDAC and stromal cells as well as TME composition regarding macrophages and the effector phenotype of CD8+ T cells. However, it cannot fully mimic the complete spatial composition and dynamic changes in PDAC TME, e.g., several other determinants of immune evasion were not considered, like the presence of ECM or additional immunosuppressive stromal cells such as myofibroblasts. 3D models which include ECM better mimic the hypoxic conditions and tumor structure in PDAC [298]. Furthermore, it has to be critically mentioned that no reliable information on whether and to which extent CD8+ T cells and macrophages infiltrated into PDAC spheroids and whether ICI treatment penetration can be provided. For obtaining clear information regarding the spatial distribution of immune and PDAC cells in the spheroid model of this thesis, studies are planned to generate FFPE sections from spheroids for immunohistochemical stainings as performed with patient-derived tissues. Additionally, T cells and macrophages were isolated and generated from PBMCs of healthy donors, thus being from another donor as the used PDAC cell lines. Accordingly, well-

defined time periods of co-cultures of CD8+ T cells and mono- and co-culture spheroids had to be used in order to avoid allogeneic T cell reactions. Furthermore, PBMCs of healthy donors might exhibit a different composition and activation status compared to PBMCs of PDAC patients [103]. To overcome these limitations and to validate the findings obtained by this model system, future studies are planned to use PDAC cells and tumor-associated macrophages from PDAC tissues as well as PBMCs/CD8+ T cells from the same PDAC patient. Finally, the results of the IHC stainings of matching primary tumors and liver metastases provided already valuable and unique insight into PD-L1 expression and the tumor-stroma interplay during malignant progression of PDAC. However, to validate these findings the analysis of more matching tissue samples might be reasonable. Despite these limitations, this study clearly revealed novel insights into the interplay of PDAC cells and macrophages and its impact on PD-L1 and immune evasion of PDAC thereby providing an explanation for the poor therapeutic effects of ICI treatment in PDAC.

6. Conclusion

The results of this thesis revealed that PD-L1 expression in primary PDAC correlates with PD-L1 expression in liver metastases with macrophages being a main source of PD-L1 expression. These cells can be predominantly found at the invasion fronts in primary tumors as well as in liver metastases presenting a barrier for CD8+ T cells which were also mainly detectable at the invasive fronts. This *in situ* condition was well mimicked by a 3D co-culture spheroid model using two PDAC cell lines with different PD-L1 expression statuses as well as different ratios and types of macrophages. In line with the *in situ* findings, macrophages were the main source of PD-L1 expression, however, the effector phenotype of CD8+ T cells was not impaired in the presence of PD-L1 expressing macrophages which was not associated with PDAC cell death induction. Despite the considerable PD-L1 and PD-1 expression in the different spheroid models, treatment with PD-1 and PD-L1 inhibitors Pembrolizumab and Durvalumab, respectively, as well as pre-treatment with Gemcitabine did neither boost the CD8+ T cell effector phenotype nor increased PDAC cell death. Considering the recent literature, the results of this thesis underscore the view that the PD-1/PD-L1 axis is not the main immunosuppressive mechanism of T cell-mediated tumor immunity in PDAC.

7. References

1. Siegel RL, Miller KD, Fuchs HE, Jemal A. Cancer Statistics, 2021. *CA Cancer J Clin*. **2021**;71(1):7–33. DOI:10.3322/CAAC.21654

2. Mcguigan A, Kelly P, Turkington RC, Jones C, Coleman HG, Mccain S. Pancreatic cancer: A review of clinical diagnosis, epidemiology, treatment and outcomes. *World J Gastroenterol*. **2018**;24(43):4846–61. DOI:10.3748/wjg.v24.i43.4846

3. Yachida S, White CM, Naito Y, Zhong Y, Brosnan JA, Macgregor-Das AM, Morgan RA, Saunders T, Laheru DA, Herman JM, Hruban RH, Klein AP, Jones S, Velculescu V, Wolfgang CL, Iacobuzio-Donahue CA. Clinical significance of the genetic landscape of pancreatic cancer and implications for identification of potential long-term survivors. *Clin Cancer Res*. **2012**;18(22):6339–47. DOI:10.1158/1078-0432.CCR-12-1215/273485/AM/CLINICAL-SIGNIFICANCE-OF-THE-GENETIC-LANDSCAPE-OF

4. Gesellschaft der epidemiologischen Krebsregister in Deutschland. Pankreaskarzinom in Deutschland für 2017/2018. *Robert Koch Inst*. **2017**;(Abgerufen am 29.11.2022):60–3.

5. Midha S, Chawla S, Garg PK. Modifiable and non-modifiable risk factors for pancreatic cancer: A review. *Cancer Lett*. **2016**;381(1):269–77. DOI:10.1016/j.canlet.2016.07.022

6. Wood HE, Gupta S, Kang JY, Quinn MJ, Maxwell JD, Mudan S, Majeed A. Pancreatic cancer in England and Wales 1975–2000: patterns and trends in incidence, survival and mortality. *Aliment Pharmacol Ther*. **2006**;23(8):1205–14. DOI:10.1111/J.1365-2036.2006.02860.X

7. Yu J, Blackford AL, Dal Molin M, Wolfgang CL, Goggins M. Time to progression of pancreatic ductal adenocarcinoma from low-to-high tumour stages. *Gut*. **2015**;64(11):1783–9. DOI:10.1136/GUTJNL-2014-308653

8. Wolpin BM, Chan AT, Hartge P, Chanock SJ, Kraft P, Hunter DJ, Giovannucci EL, Fuchs CS. ABO blood group and the risk of pancreatic cancer. *J Natl Cancer Inst*. **2009**;101(6):424–31. DOI:10.1093/JNCI/DJP020

9. Shinoda S, Nakamura N, Roach B, Bernlohr DA, Ikramuddin S, Yamamoto M. Obesity and Pancreatic Cancer: Recent Progress in Epidemiology, Mechanisms and Bariatric Surgery. *Biomedicines*. **2022**;10(6). DOI:10.3390/BIOMEDICINES10061284

10. Mizrahi JD, Surana R, Valle JW, Shroff RT. Pancreatic cancer. *Lancet*. **2020**;395(10242):2008–20. DOI:10.1016/S0140-6736(20)30974-0

11. Bailey JM, DelGiorno KE, Crawford HC. The secret origins and surprising fates of pancreas tumors. *Carcinogenesis*. **2014**;35(7):1436. DOI:10.1093/CARCIN/BGU056

12. Hezel AF, Kimmelman AC, Stanger BZ, Bardeesy N, DePinho RA. Genetics and biology of

pancreatic ductal adenocarcinoma. *Genes Dev*. **2006**;20(10):1218–49. DOI:10.1101/GAD.1415606

13. Taherian M, Wang H, Wang H. Pancreatic Ductal Adenocarcinoma: Molecular Pathology and Predictive Biomarkers. *Cells*. **2022**;11(19):3068. DOI:10.3390/CELLS11193068

14. Mohammed S, Van Buren G, Fisher WE. Pancreatic cancer: Advances in treatment. *World J Gastroenterol*. **2014**;20(28):9354. DOI:10.3748/WJG.V20.I28.9354

15. Lüttges J, Klöppel G. Das duktale pankreaskarzinom und seine vorläufer. *Pathologe*. **2005**;26(1):12–7. DOI:10.1007/s00292-004-0735-0

16. Opitz F V., Haeberle L, Daum A, Esposito I. Tumor Microenvironment in Pancreatic Intraepithelial Neoplasia. *Cancers (Basel)*. **2021**;13(24). DOI:10.3390/CANCERS13246188

17. Gu M, Gao Y, Chang P. KRAS Mutation Dictates the Cancer Immune Environment in Pancreatic Ductal Adenocarcinoma and Other Adenocarcinomas. *Cancers (Basel)*. **2021**;13(10):2429. DOI:10.3390/CANCERS13102429

18. Moffitt RA, Marayati R, Flate EL, Volmar KE, Loeza SGH, Hoadley KA, Rashid NU, Williams LA, Eaton SC, Chung AH, Smyla JK, Anderson JM, Kim HJ, Bentrem DJ, Talamonti MS, Iacobuzio-Donahue CA, Hollingsworth MA, Yeh JJ. Virtual microdissection identifies distinct tumor- and stroma-specific subtypes of pancreatic ductal adenocarcinoma. *Nat Genet*. **2015**;47(10):1168. DOI:10.1038/NG.3398

19. Valkenburg KC, de Groot AE, Pienta KJ. Targeting the tumour stroma to improve cancer therapy. *Nat Rev Clin Oncol*. **2018**;15(6):366–81. DOI:10.1038/s41571-018-0007-1

20. Cunha GR, Bigsby RM, Cooke PS, Sugimura Y. Stromal-epithelial interactions in adult organs. *Cell Differ*. **1985**;17(3):137–48. DOI:10.1016/0045-6039(85)90481-6

21. Cunha GR, Donjacour AA, Sugimura Y. Stromal–epithelial interactions and heterogeneity of proliferative activity within the prostate. *Biochem Cell Biol*. **1986**;64(6):608–14. DOI:10.1139/o86-084

22. Kalluri R. The biology and function of fibroblasts in cancer. *Nat Rev Cancer*. **2016**;16(9):582–98. DOI:10.1038/nrc.2016.73

23. McCubrey JA, Yang L V., Abrams SL, Steelman LS, Follo MY, Cocco L, Ratti S, Martelli AM, Augello G, Cervello M. Effects of TP53 Mutations and miRs on Immune Responses in the Tumor Microenvironment Important in Pancreatic Cancer Progression. *Cells*. **2022**;11(14). DOI:10.3390/CELLS11142155

24. Wandmacher AM, Mehdorn AS, Sebens S. The Heterogeneity of the Tumor Microenvironment as Essential Determinant of Development, Progression and Therapy Response of Pancreatic

Cancer. *Cancers (Basel)*. **2021**;13(19):4932. DOI:10.3390/cancers13194932

25. Bulle A, Lim KH. Beyond just a tight fortress: contribution of stroma to epithelial-mesenchymal transition in pancreatic cancer. *Signal Transduction and Targeted Therapy. Springer Nature*; **2020**. DOI:10.1038/s41392-020-00341-1

26. Hessmann E, Buchholz SM, Demir IE, Singh SK, Gress TM, Ellenrieder V, Neesse A, Hessmann E, Buchholz SM, Demir IE, Singh SK, Gress TM, Ellenrieder V, Neesse A. Microenvironmental determinants of pancreatic cancer. *Physiol Rev*. **2020**;100(4):1707–51. DOI:10.1152/PHYSREV.00042.2019

27. Huber M, Brehm CU, Gress TM, Buchholz M, Alhamwe BA, von Strandmann EP, Slater EP, Bartsch JW, Bauer C, Lauth M. The Immune Microenvironment in Pancreatic Cancer. *Int J Mol Sci*. **2020**;21(19):7307. DOI:10.3390/IJMS21197307

28. Pathria P, Louis TL, Varner JA. Targeting Tumor-Associated Macrophages in Cancer. *Trends Immunol*. **2019**;40(4):310–27. DOI:10.1016/j.it.2019.02.003

29. Yang S, Liu Q, Liao Q. Tumor-Associated Macrophages in Pancreatic Ductal Adenocarcinoma: Origin, Polarization, Function, and Reprogramming. *Front Cell Dev Biol*. **2020**;8. DOI:10.3389/FCELL.2020.607209

30. DeNardo DG, Ruffell B. Macrophages as regulators of tumour immunity and immunotherapy. *Nat Rev Immunol*. **2019**;19(6):369–82. DOI:10.1038/s41577-019-0127-6

31. Yona S, Kim KW, Wolf Y, Mildner A, Varol D, Breker M, Strauss-Ayali D, Viukov S, Guilliams M, Misharin A, Hume DA, Perlman H, Malissen B, Zelzer E, Jung S. Fate mapping reveals origins and dynamics of monocytes and tissue macrophages under homeostasis. *Immunity*. **2013**;38(1):79. DOI:10.1016/J.IMMUNI.2012.12.001

32. Schulz C, Perdiguero EG, Chorro L, Szabo-Rogers H, Cagnard N, Kierdorf K, Prinz M, Wu B, Jacobsen SEW, Pollard JW, Frampton J, Liu KJ, Geissmann F. A lineage of myeloid cells independent of Myb and hematopoietic stem cells. *Science*. **2012**;336(6077):86–90. DOI:10.1126/SCIENCE.1219179

33. Hashimoto D, Chow A, Noizat C, Teo P, Beasley MB, Leboeuf M, Becker CD, See P, Price J, Lucas D, Greter M, Mortha A, Boyer SW, Forsberg EC, Tanaka M, van Rooijen N, García-Sastre A, Stanley ER, Ginhoux F, Frenette PS, Merad M. Tissue resident macrophages self-maintain locally throughout adult life with minimal contribution from circulating monocytes. *Immunity*. **2013**;38(4):792–804. DOI:10.1016/J.IMMUNI.2013.04.004

34. Mass E, Ballesteros I, Farlik M, Halbritter F, Günther P, Crozet L, Jacome-Galarza CE, Händler K, Klughammer J, Kobayashi Y, Gomez-Perdiguero E, Schultze JL, Beyer M, Bock C, Geissmann F. Specification of tissue-resident macrophages during organogenesis. *Science*. **2016**;353(6304).

DOI:10.1126/SCIENCE.AAF4238

35. Shi C, Pamer EG. Monocyte recruitment during infection and inflammation. *Nat Rev Immunol*. **2011**;11(11):762–74. DOI:10.1038/nri3070

36. Murphy K, Weaver C. Janeway Immunologie. Janeway Immunologie. **2018**. DOI:10.1007/978-3-662-56004-4

37. Horwood NJ. Macrophage Polarization and Bone Formation: A review. *Clin Rev Allergy Immunol*. **2016**;51(1):79–86. DOI:10.1007/s12016-015-8519-2

38. Lankadasari MB, Mukhopadhyay P, Mohammed S, Harikumar KB. TAMing pancreatic cancer: Combat with a double edged sword. *Molecular Cancer*. **2019**;18(1):1-13. DOI:10.1186/s12943-019-0966-6

39. Mills C. M1 and M2 Macrophages: Oracles of Health and Disease. *Crit Rev Immunol*. **2012**;32(6):463–88. DOI:10.1615/CritRevImmunol.v32.i6.10

40. Mills CD, Kincaid K, Alt JM, Heilman MJ, Hill AM. M-1/M-2 Macrophages and the Th1/Th2 Paradigm. *J Immunol*. **2000**;164(12):6166–73. DOI:10.4049/jimmunol.164.12.6166

41. Murray PJ, Allen JE, Biswas SK, Fisher EA, Gilroy DW, Goerdt S, Gordon S, Hamilton JA, Ivashkiv LB, Lawrence T, Locati M, Mantovani A, Martinez FO, Mege JL, Mosser DM, Natoli G, Saeij JP, Schultze JL, Shirey KA, Sica A, Suttles J, Udalova I, vanGinderachter JA, Vogel SN, Wynn TA. Macrophage activation and polarization: nomenclature and experimental guidelines. *Immunity*. **2014**;41(1):14. DOI:10.1016/J.IMMUNI.2014.06.008

42. Martinez FO, Gordon S. The M1 and M2 paradigm of macrophage activation: time for reassessment. *F1000Prime Rep*. **2014**;6. DOI:10.12703/P6-13

43. Jaguin M, Houlbert N, Fardel O, Lecureur V. Polarization profiles of human M-CSF-generated macrophages and comparison of M1-markers in classically activated macrophages from GM-CSF and M-CSF origin. *Cell Immunol*. **2013**;281(1):51–61. DOI:10.1016/J.CELLIMM.2013.01.010

44. Oneissi Martinez F, Sica A, Mantovani A, Locati M. Macrophage activation and polarization., *Frontiers in Bioscience.* **2008**;13:453–461

45. Mantovani A, Sica A, Sozzani S, Allavena P, Vecchi A, Locati M. The chemokine system in diverse forms of macrophage activation and polarization. *Trends Immunol*. **2004**;25(12):677–86. DOI:10.1016/j.it.2004.09.015

46. Gordon S, Taylor PR. Monocyte and macrophage heterogeneity. *Nat Rev Immunol 2005 512*. **2005**;5(12):953–64. DOI:10.1038/nri1733

47. Ambarus CA, Krausz S, van Eijk M, Hamann J, Radstake TRDJ, Reedquist KA, Tak PP, Baeten DLP.

Systematic validation of specific phenotypic markers for in vitro polarized human macrophages. *J Immunol Methods*. **2012**;375(1–2):196–206. DOI:10.1016/j.jim.2011.10.013

48. Pratt HG, Steinberger KJ, Mihalik NE, Ott S, Whalley T, Szomolay B, Boone BA, Eubank TD. Macrophage and Neutrophil Interactions in the Pancreatic Tumor Microenvironment Drive the Pathogenesis of Pancreatic Cancer. *Cancers (Basel)*. **2022**;14(1). DOI:10.3390/cancers14010194

49. Verreck FAW, de Boer T, Langenberg DML, Hoeve MA, Kramer M, Vaisberg E, Kastelein R, Kolk A, de Waal-Malefyt R, Ottenhoff THM. Human IL-23-producing type 1 macrophages promote but IL-10-producing type 2 macrophages subvert immunity to (myco)bacteria. *Proc Natl Acad Sci*. **2004**;101(13):4560–5. DOI:10.1073/pnas.0400983101

50. Zhu Y, Herndon JM, Sojka DK, Kim KW, Knolhoff BL, Zuo C, Cullinan DR, Luo J, Bearden AR, Lavine KJ, Yokoyama WM, Hawkins WG, Fields RC, Randolph GJ, DeNardo DG. Tissue-Resident Macrophages in Pancreatic Ductal Adenocarcinoma Originate from Embryonic Hematopoiesis and Promote Tumor Progression. *Immunity*. **2017**;47(2):323-338.e6. DOI:10.1016/j.immuni.2017.07.014

51. Sanford DE, Belt BA, Panni RZ, Mayer A, Deshpande AD, Carpenter D, Mitchem JB, Plambeck-Suess SM, Worley LA, Goetz BD, Wang-Gillam A, Eberlein TJ, Denardo DG, Goedegebuure SP, Linehan DC. Inflammatory monocyte mobilization decreases patient survival in pancreatic cancer: a role for targeting the CCL2/CCR2 axis. *Clin Cancer Res*. **2013**;19(13):3404. DOI:10.1158/1078-0432.CCR-13-0525

52. Zuo C, Baer JM, Knolhoff BL, Belle JI, Liu X, Hogg GD, Fu C, Kingston NL, Brenden MA, De AA, Lastra L, Dodhiawala PB, Zhou C, James CA, Ding L, Lim KH, Fields RC, Hawkins WG, Zhao G, Weber JD, Denardo DG. Macrophage proliferation machinery leads to PDAC progression, but susceptibility to innate immunotherapy. *bioRxiv*. **2021**;2021.11.08.467770. DOI:10.1101/2021.11.08.467770

53. Liu Q, Li Y, Niu Z, Zong Y, Wang M, Yao L, Lu Z, Liao Q, Zhao Y. Atorvastatin (Lipitor) attenuates the effects of aspirin on pancreatic cancerogenesis and the chemotherapeutic efficacy of gemcitabine on pancreatic cancer by promoting M2 polarized tumor associated macrophages. *J Exp Clin Cancer Res*. **2016**;35(1):1–16. DOI:10.1186/s13046-016-0304-4

54. Yang S, Liu Q, Liao Q. Tumor-Associated Macrophages in Pancreatic Ductal Adenocarcinoma: Origin, Polarization, Function, and Reprogramming. *Front Cell Dev Biol*. **2021**;8(January):1–24. DOI:10.3389/fcell.2020.607209

55. Rahn S, Krüger S, Mennrich R, Goebel L, Wesch D, Oberg HH, Vogel I, Ebsen M, Röcken C, Helm O, Sebens S. POLE Score: A comprehensive profiling of programmed death 1 ligand 1 expression in pancreatic ductal adenocarcinoma. *Oncotarget*. **2019**;10(16):1572–88. DOI:10.18632/oncotarget.26705

56. Helm O, Mennrich R, Petrick D, Goebel L, Freitag-wolf S, Ro C, Sipos B, Kabelitz D, Scha H, Oberg H, Wesch D, Sebens S. Comparative Characterization of Stroma Cells and Ductal Epithelium in Chronic Pancreatitis and Pancreatic Ductal Adenocarcinoma. **2014**;9(5). DOI:10.1371/journal.pone.0094357

57. Helm O, Held-Feindt J, Grage-Griebenow E, Reiling N, Ungefroren H, Vogel I, Krüger U, Becker T, Ebsen M, Röcken C, Kabelitz D, Schäfer H, Sebens S. Tumor-associated macrophages exhibit pro- and anti-inflammatory properties by which they impact on pancreatic tumorigenesis. *Int J Cancer*. **2014**;135(4):843–61. DOI:10.1002/IJC.28736

58. Hu H, Hang JJ, Han T, Zhuo M, Jiao F, Wang LW. The M2 phenotype of tumor-associated macrophages in the stroma confers a poor prognosis in pancreatic cancer. *Tumor Biol*. **2016**;37(7):8657–64. DOI:10.1007/s13277-015-4741-z

59. Knudsen ES, Vail P, Balaji U, Ngo H, Botros IW, Makarov V, Riaz N, Balachandran V, Leach S, Thompson DM, Chan TA, Witkiewicz AK. Stratification of Pancreatic Ductal Adenocarcinoma: Combinatorial Genetic, Stromal, and Immunologic Markers. *Clin Cancer Res*. **2017**;23(15):4429–40. DOI:10.1158/1078-0432.CCR-17-0162

60. Hao NB, Lü MH, Fan YH, Cao YL, Zhang ZR, Yang SM. Macrophages in tumor microenvironments and the progression of tumors. *Clin Dev Immunol*. **2012**;2012. DOI:10.1155/2012/948098

61. Ruffell B, Coussens LM. Macrophages and therapeutic resistance in cancer. *Cancer Cell*. **2015**;27(4):462–72. DOI:10.1016/J.CCELL.2015.02.015

62. Cassetta L, Pollard JW. Targeting macrophages: therapeutic approaches in cancer. *Nat Rev Drug Discov 2018*. **2018**;17(12):887–904. DOI:10.1038/nrd.2018.169

63. Kurahara H, Shinchi H, Mataki Y, Maemura K, Noma H, Kubo F, Sakoda M, Ueno S, Natsugoe S, Takao S. Significance of M2-Polarized Tumor-Associated Macrophage in Pancreatic Cancer. *J Surg Res*. **2011**;167(2):e211–9. DOI:10.1016/J.JSS.2009.05.026

64. Bishehsari F, Zhang L, Barlass U, Preite NZ, Turturro S, Najor MS, Shetuni BB, Zayas JP, Mahdavinia M, Abukhdeir AM, Keshavarzian A. KRAS Mutation and Epithelial-Macrophage Interplay in Pancreatic Neoplastic Transformation. *Int J cancer*. **2018**;143(8):1994. DOI:10.1002/IJC.31592

65. Mantovani A, Marchesi F, Malesci A, Laghi L, Allavena P. Tumor-Associated Macrophages as Treatment Targets in Oncology. *Nat Rev Clin Oncol*. **2017**;14(7):399-416 DOI:10.1038/nrclinonc.2016.217

66. Buchholz SM, Goetze RG, Singh SK, Ammer-Herrmenau C, Richards FM, Jodrell DI, Buchholz M, Michl P, Ellenrieder V, Hessmann E, Neesse A. Depletion of Macrophages Improves Therapeutic Response to Gemcitabine in Murine Pancreas Cancer. *Cancers*. **2020**;12(7):1978

DOI:10.3390/cancers12071978

67. Weizman N, Krelin Y, Shabtay-Orbach A, Amit M, Binenbaum Y, Wong RJ, Gil Z. Macrophages mediate gemcitabine resistance of pancreatic adenocarcinoma by upregulating cytidine deaminase. *Oncogene*. **2014**;33(29):3812–9. DOI:10.1038/onc.2013.357

68. Binenbaum Y, Fridman E, Yaari Z, Milman N, Schroeder A, David G Ben, Shlomi T, Gil Z. Transfer of miRNA in macrophage-derived exosomes induces drug resistance in pancreatic adenocarcinoma. *Cancer Res*. **2018**;78(18):5287–99. DOI:10.1158/0008-5472.CAN-18-0124

69. Ho TTB, Nasti A, Seki A, Komura T, Inui H, Kozaka T, Kitamura Y, Shiba K, Yamashita T, Yamashita T, Mizukoshi E, Kawaguchi K, Wada T, Honda M, Kaneko S, Sakai Y. Combination of gemcitabine and anti-PD-1 antibody enhances the anticancer effect of M1 macrophages and the Th1 response in a murine model of pancreatic cancer liver metastasis. *J Immunother Cancer*. **2020**;8(2):1–12. DOI:10.1136/jitc-2020-001367

70. Panni RZ, Herndon JM, Zuo C, Hegde S, Hogg GD, Knolhoff BL, Breden MA, Li X, Krisnawan VE, Khan SQ, Schwarz JK, Rogers BE, Fields RC, Hawkins WG, Gupta V, DeNardo DG. Agonism of CD11b reprograms innate immunity to sensitize pancreatic cancer to immunotherapies. *Sci Transl Med*. **2019**;11(499). DOI:10.1126/SCITRANSLMED.AAU9240

71. Masugi Y, Abe T, Ueno A, Fujii-Nishimura Y, Ojima H, Endo Y, Fujita Y, Kitago M, Shinoda M, Kitagawa Y, Sakamoto M. Characterization of spatial distribution of tumor-infiltrating CD8+ T cells refines their prognostic utility for pancreatic cancer survival. *Mod Pathol*. **2019**;32(10):1495–507. DOI:10.1038/s41379-019-0291-z

72. Kiryu S, Ito Z, Suka M, Bito T, Kan S, Uchiyama K, Saruta M, Hata T, Takano Y, Fujioka S, Misawa T, Yamauchi T, Yanagisawa H, Sato N, Ohkusa T, Sugiyama H, Koido S. Prognostic value of immune factors in the tumor microenvironment of patients with pancreatic ductal adenocarcinoma. *BMC Cancer*. **2021**;21(1):1–13. DOI:10.1186/S12885-021-08911-4/FIGURES/5

73. Goulart MR, Stasinos K, Fincham REA, Delvecchio FR, Kocher HM. T cells in pancreatic cancer stroma. *World J Gastroenterol*. **2021**;27(46):7956. DOI:10.3748/WJG.V27.I46.7956

74. Jang JE, Hajdu CH, Liot C, Miller G, Dustin ML, Bar-Sagi D. Crosstalk between Regulatory T Cells and Tumor-Associated Dendritic Cells Negates Anti-tumor Immunity in Pancreatic Cancer. *Cell Rep*. **2017**;20(3):558–71. DOI:10.1016/j.celrep.2017.06.062

75. Ullman NA, Burchard PR, Dunne RF, Linehan DC. Immunologic Strategies in Pancreatic Cancer: Making Cold Tumors Hot. *J Clin Oncol*. **2022**;40(24):2789. DOI:10.1200/JCO.21.02616

76. Russ BE, Prier JE, Rao S, Turner SJ. T cell immunity as a tool for studying epigenetic regulation of cellular differentiation. *Front Genet*. **2013**;4(11):218. DOI:10.3389/FGENE.2013.00218

77. Liao W, Lin JX, Leonard WJ. Interleukin-2 at the Crossroads of Effector Responses, Tolerance, and Immunotherapy. *Immunity*. **2013**;38(1)**:**13–25. DOI:10.1016/j.immuni.2013.01.004

78. Wörmann SM, Diakopoulos KN, Lesina M, Algül H. The immune network in pancreatic cancer development and progression. *Oncogene.* **2014**;33(23):2956–67. DOI:10.1038/onc.2013.257

79. Padoan A, Plebani M, Basso D. Inflammation and Pancreatic Cancer: Focus on Metabolism, Cytokines, and Immunity. *Int J Mol Sci*. **2019**;20(3):676. DOI:10.3390/IJMS20030676

80. Grandér D, Sangfelt O, Erickson S. How does interferon exert its cell growth inhibitory effect? *Eur J Haematol*. **1997**;59(3):129–35. DOI:10.1111/J.1600-0609.1997.TB00965.X

81. Xia Q, Jia J, Hu C, Lu J, Li J, Xu H, Fang J, Feng D, Wang L, Chen Y. Tumor-associated macrophages promote PD-L1 expression in tumor cells by regulating PKM2 nuclear translocation in pancreatic ductal adenocarcinoma. *Oncogene*. **2022**;41(6):865. DOI:10.1038/S41388-021-02133-5

82. Torphy RJ, Zhu Y, Schulick RD. Immunotherapy for pancreatic cancer: Barriers and breakthroughs. *Ann Gastroenterol Surg*. **2018**;2(4):274. DOI:10.1002/AGS3.12176

83. Moro-García MA, Mayo JC, Sainz RM, Alonso-Arias R. Influence of Inflammation in the Process of T Lymphocyte Differentiation: Proliferative, Metabolic, and Oxidative Changes. *Front Immunol*. **2018**;9(MAR):1. DOI:10.3389/FIMMU.2018.00339

84. Dutta A, Zhao B, Love PE. New insights into TCR β-selection. *Trends Immunol*. **2021**;42(8):735–50. DOI:10.1016/J.IT.2021.06.005

85. Lodygin D, Flügel A. Intravital real-time analysis of T-cell activation in health and disease. *Cell Calcium*. **2017**;64:118-129. DOI:10.1016/j.ceca.2016.12.007

86. Cobb RM, Oestreich KJ, Osipovich OA, Oltz EM. Accessibility Control of V(D)J Recombination. *Adv Immunol*. **2006**;91:45–109. DOI:10.1016/S0065-2776(06)91002-5

87. Garbe AI, Krueger A, Gounari F, Zúñiga-Pflücker JC, Von Boehmer H. Differential synergy of Notch and T cell receptor signaling determines αβ versus γδ lineage fate. *J Exp Med*. **2006**;203(6):1579–90. DOI:10.1084/JEM.20060474

88. Dutta A, Venkataganesh H, Love PE. New Insights into Epigenetic Regulation of T Cell Differentiation. *Cells*. **2021**;10(12). DOI:10.3390/CELLS10123459

89. Kondo K, Ohigashi I, Takahama Y. Thymus machinery for T-cell selection. *Int Immunol*. **2019**;31(3):119. DOI:10.1093/INTIMM/DXY081

90. Cyster JG. Leukocyte migration: Scent of the T zone. *Curr Biol*. **2000**;10(1). DOI:10.1016/S0960-9822(99)00253-5

91. Saxena V, Li L, Paluskievicz C, Kasinath V, Bean A, Abdi R, Jewell CM, Bromberg JS. Role of Lymph

Node Stroma and Microenvironment in T Cell Tolerance. *Immunol Rev*. **2019**;292(1):9. DOI:10.1111/IMR.12799

92. Wieczorek M, Abualrous ET, Sticht J, Álvaro-Benito M, Stolzenberg S, Noé F, Freund C. Major histocompatibility complex (MHC) class I and MHC class II proteins: Conformational plasticity in antigen presentation. *Front Immunol*. **2017**;8(MAR):292. DOI:10.3389/FIMMU.2017.00292/BIBTEX

93. Burgdorf S, Schölz C, Kautz A, Tampé R, Kurts C. Spatial and mechanistic separation of cross-presentation and endogenous antigen presentation. *Nat Immunol*. **2008**;9(5):558–66. DOI:10.1038/ni.1601

94. Neefjes J, Jongsma MLM, Paul P, Bakke O. Towards a systems understanding of MHC class i and MHC class II antigen presentation. *Nat Rev Immunol*. **2011**;11(12):823–36. DOI:10.1038/NRI3084

95. Guerder S, Flavell RA. T-Cell Activation: Two for T. *Curr Biol*. **1995**;5(8):866–8. DOI:10.1016/S0960-9822(95)00175-8

96. Esensten JH, Helou YA, Chopra G, Weiss A, Bluestone JA. CD28 Costimulation: From Mechanism to Therapy. *Immunity.* **2016**;44(5):973-988. DOI:10.1016/j.immuni.2016.04.020

97. Garrett-Thomsonid SC, Massimi A, Fedorov E V, Bonanno JB, Scandiuzzi L, Hillerich B, Seidel RD, Love JD, Garforth SJ, Guha C, Almo SC. Mechanistic dissection of the PD-L1:B7-1 co-inhibitory immune complex. *Plos One.* **2020**;15(6):e0233578 DOI:10.1371/journal.pone.0233578

98. Wang C, Sun W, Ye Y, Bomba HN, Gu Z. Bioengineering of Artificial Antigen Presenting Cells and Lymphoid Organs. *Theranostics*. **2017**;7(14):3504. DOI:10.7150/THNO.19017

99. Chen L, Flies DB. Molecular mechanisms of T cell co-stimulation and co-inhibition. *Nat Rev | Immunol*. **2013**;13(4):227-242. DOI:10.1038/nri3405

100. Seifert AM, Eymer A, Heiduk M, Wehner R, Tunger A, von Renesse J, Decker R, Aust DE, Welsch T, Reissfelder C, Weitz J, Schmitz M, Seifert L. Pd-1 expression by lymph node and intratumoral regulatory t cells is associated with lymph node metastasis in pancreatic cancer. *Cancers (Basel)*. **2020**;12(10):1–13. DOI:10.3390/cancers12102756

101. Deronic A, Nilsson A, Thagesson M, Werchau D, Enell Smith K, Ellmark P. The human anti-CD40 agonist antibody mitazalimab (ADC-1013; JNJ-64457107) activates antigen-presenting cells, improves expansion of antigen-specific T cells, and enhances anti-tumor efficacy of a model cancer vaccine in vivo. *Cancer Immunol Immunother*. **2021**;70(12):3629-3642. DOI:10.1007/s00262-021-02932-5

102. Postow MA, Callahan MK, Wolchok JD. Immune Checkpoint Blockade in Cancer Therapy. *J Clin*

Oncol. **2015**;33(17):1974–82. DOI:10.1200/JCO.2014.59.4358

103. Steele NG, Carpenter ES, Kemp SB, Sirihorachai VR, The S, Delrosario L, Lazarus J, Amir E ad D, Gunchick V, Espinoza C, Bell S, Harris L, Lima F, Irizarry-Negron V, Paglia D, Macchia J, Chu AKY, Schofield H, Wamsteker EJ, Kwon R, Schulman A, Prabhu A, Law R, Sondhi A, Yu J, Patel A, Donahue K, Nathan H, Cho C, Anderson MA, Sahai V, Lyssiotis CA, Zou W, Allen BL, Rao A, Crawford HC, Bednar F, Frankel TL, Pasca di Magliano M. Multimodal Mapping of the Tumor and Peripheral Blood Immune Landscape in Human Pancreatic Cancer. *Nat cancer*. **2020**;1(11):1097. DOI:10.1038/S43018-020-00121-4

104. Hargadon KM. Tumor microenvironmental influences on dendritic cell and T cell function: A focus on clinically relevant immunologic and metabolic checkpoints. *Clin Transl Med*. **2020**;10(1):374. DOI:10.1002/CTM2.37

105. Messal N, Serriari NE, Pastor S, Nunès JA, Olive D. PD-L2 is expressed on activated human T cells and regulates their function. *Mol Immunol*. **2011**;48(15–16):2214–9. DOI:10.1016/J.MOLIMM.2011.06.436

106. Kabacaoglu D, Ciecielski KJ, Ruess DA, Algül H. Immune checkpoint inhibition for pancreatic ductal adenocarcinoma: Current limitations and future options. *Front Immunol*. **2018**;9(AUG). DOI:10.3389/fimmu.2018.01878

107. Watts TH. Staying alive: T cell costimulation, CD28, and Bcl-xL. *J Immunol*. **2010**;185(7):3785–7. DOI:10.4049/JIMMUNOL.1090085

108. Curtsinger JM, Mescher MF. Inflammatory Cytokines as a Third Signal for T Cell Activation. *Curr Opin Immunol*. **2010**;22(3):333-340. DOI:10.1016/j.coi.2010.02.013

109. Fisher RI, Rosenberg SA FG. Long-term survival update for high-dose recombinant interleukin-2 in patients with renal cell carcinoma. *Cancer J Sci Am*. **2000**;6 Suppl 1:S55-7

110. Epardaud M, Elpek KG, Rubinstein MP, Yonekura AR, Bellemare-Pelletier A, Bronson R, Hamerman JA, Goldrath AW, Turley SJ. Interleukin-15/interleukin-15R alpha complexes promote destruction of established tumors by reviving tumor-resident CD8+ T cells. *Cancer Res*. **2008**;68(8):2972–83. DOI:10.1158/0008-5472.CAN-08-0045

111. Petrella TM, Tozer R, Belanger K, Savage KJ, Wong R, Smylie M, Kamel-Reid S, Tron V, Chen BE, Hunder NN, Hagerman L, Walsh W, Eisenhauer EA. Interleukin-21 has activity in patients with metastatic melanoma: a phase II study. *J Clin Oncol*. **2012**;30(27):3396–401. DOI:10.1200/JCO.2011.40.0655

112. Obst R. The timing of T cell priming and cycling. *Front Immunol*. **2015**;6(NOV):563. DOI:10.3389/FIMMU.2015.00563/BIBTEX

113. Macián F, Im SH, García-Cózar FJ, Rao A. T-cell anergy. *Curr Opin Immunol*. **2004**;16(2):209–16. DOI:10.1016/j.coi.2004.01.013

114. Mueller DL. Mechanisms maintaining peripheral tolerance. *Nat Immunol 2010 111*. **2009**;11(1):21–7. DOI:10.1038/ni.1817

115. Kumar P, Bhattacharya P, Prabhakar BS. A comprehensive review on the role of co-signaling receptors and Treg homeostasis in autoimmunity and tumor immunity. *J Autoimmun*. **2018**;95:77–99. DOI:10.1016/J.JAUT.2018.08.007

116. Boussiotis VA. Molecular and Biochemical Aspects of the PD-1 Checkpoint Pathway IMMUNE CHECKPOINT BLOCKADE AS CANCER THERAPY. *N Engl J Med.* **2016**;375(18):1767-1778. DOI:10.1056/NEJMra1514296

117. Šmahel M. PD-1/PD-L1 Blockade Therapy for Tumors with Downregulated MHC Class I Expression. *Int J Mol Sci*. **2017**;18(6). DOI:10.3390/IJMS18061331

118. Butte MJ, Keir ME, Phamduy TB, Sharpe AH, Freeman GJ. Programmed Death-1 Ligand 1 Interacts Specifically with the B7-1 Costimulatory Molecule to Inhibit T Cell Responses. *Immunity*. **2007**;27(1):111–22. DOI:10.1016/J.IMMUNI.2007.05.016

119. Schildberg FA, Klein SR, Freeman GJ, Sharpe AH. Coinhibitory Pathways in the B7-CD28 Ligand-Receptor Family. *Immunity*. **2016**;44(5):955–72. DOI:10.1016/J.IMMUNI.2016.05.002

120. Stamper CC, Zhang Y, Tobin JF, Erbe D V., Ikemizu S, Davis SJ, Stahl ML, Seehra J, Somers WS, Mosyak L. Crystal structure of the B7-1/CTLA-4 complex that inhibits human immune responses. *Nature*. **2001**;410(6828):608–11. DOI:10.1038/35069118

121. Schwartz JCD, Zhang X, Fedorov AA, Nathenson SG, Almo SC. Structural basis for co-stimulation by the human CTLA-4/B7-2 complex. *Nature*. **2001**;410(6828):604–8. DOI:10.1038/35069112

122. Valk E, Rudd CE, Schneider H. CTLA-4 trafficking and surface expression. *Trends Immunol*. **2008**;29(6):272. DOI:10.1016/J.IT.2008.02.011

123. Chuang E, Lee KM, Robbins MD, Duerr JM, Alegre ML, Hambor JE, Neveu MJ, Bluestone JA, Thompson CB. Regulation of Cytotoxic T Lymphocyte-Associated Molecule-4 by Src Kinases. *J Immunol*. **1999**;162(3):1270–7. DOI:10.4049/JIMMUNOL.162.3.1270

124. Chuang E, Fisher TS, Morgan RW, Robbins MD, Duerr JM, Vander Heiden MG, Gardner JP, Hambor JE, Neveu MJ, Thompson CB. The CD28 and CTLA-4 receptors associate with the serine/threonine phosphatase PP2A. *Immunity*. **2000**;13(3):313–22. DOI:10.1016/S1074-7613(00)00031-5

125. Pentcheva-Hoang T, Egen JG, Wojnoonski K, Allison JP. B7-1 and B7-2 selectively recruit CTLA-4 and CD28 to the immunological synapse. *Immunity*. **2004**;21(3):401–13.

DOI:10.1016/J.IMMUNI.2004.06.017

126. Martin M, Schneider H, Azouz A, Rudd CE. Cytotoxic T lymphocyte antigen 4 and CD28 modulate cell surface raft expression in their regulation of T cell function. *J Exp Med*. **2001**;194(11):1675–81. DOI:10.1084/JEM.194.11.1675

127. Darlington PJ, Baroja ML, Chau TA, Siu E, Ling V, Carreno BM, Madrenas J. Surface cytotoxic T lymphocyte-associated antigen 4 partitions within lipid rafts and relocates to the immunological synapse under conditions of inhibition of T cell activation. *J Exp Med*. **2002**;195(10):1337–47. DOI:10.1084/JEM.20011868

128. Chikuma S, Imboden JB, Bluestone JA. Negative regulation of T cell receptor-lipid raft interaction by cytotoxic T lymphocyte-associated antigen 4. *J Exp Med*. **2003**;197(1):129–35. DOI:10.1084/JEM.20021646

129. Mir MA. Introduction to Costimulation and Costimulatory Molecules. *Dev Costimulatory Mol Immunother Dis*. **2015**;1–43. DOI:10.1016/B978-0-12-802585-7.00001-7

130. Zhao Y, Lee CK, Lin CH, Gassen RB, Xu X, Huang Z, Xiao C, Bonorino C, Lu LF, Bui JD, Hui E. PD-L1:CD80 Cis-Heterodimer Triggers the Co-stimulatory Receptor CD28 While Repressing the Inhibitory PD-1 and CTLA-4 Pathways. *Immunity*. **2019**;51(6):1059-1073.e9. DOI:10.1016/j.immuni.2019.11.003

131. Kalluri R, Weinberg RA. The basics of epithelial-mesenchymal transition. *J Clin Invest*. **2009**;119(6):1420–8. DOI:10.1172/JCI39104

132. Thiery JP, Acloque H, Huang RYJ, Nieto MA. Epithelial-Mesenchymal Transitions in Development and Disease. *Cell*. **2009**;139(5):871–90. DOI:10.1016/J.CELL.2009.11.007/ATTACHMENT/7E0CAE36-4693-4EE3-AF81-C2E478E595A2/MMC1.PDF

133. Du B, Shim JS. Targeting Epithelial–Mesenchymal Transition (EMT) to Overcome Drug Resistance in Cancer. *Molecules*. **2016**;21(7). DOI:10.3390/MOLECULES21070965

134. Yang J, Antin P, Berx G, Blanpain C, Brabletz T, Bronner M, Campbell K, Cano A, Casanova J, Christofori G, Dedhar S, Derynck R, Ford HL, Fuxe J, García de Herreros A, Goodall GJ, Hadjantonakis AK, Huang RJY, Kalcheim C, Kalluri R, Kang Y, Khew-Goodall Y, Levine H, Liu J, Longmore GD, Mani SA, Massagué J, Mayor R, McClay D, Mostov KE, Newgreen DF, Nieto MA, Puisieux A, Runyan R, Savagner P, Stanger B, Stemmler MP, Takahashi Y, Takeichi M, Theveneau E, Thiery JP, Thompson EW, Weinberg RA, Williams ED, Xing J, Zhou BP, Sheng G. Guidelines and definitions for research on epithelial–mesenchymal transition. *Nat Rev Mol Cell Biol 2020 216*. **2020**;21(6):341–52. DOI:10.1038/s41580-020-0237-9

135. Kaimori A, Potter J, Kaimori JY, Wang C, Mezey E, Koteish A. Transforming growth factor-beta1

induces an epithelial-to-mesenchymal transition state in mouse hepatocytes in vitro. *J Biol Chem*. **2007**;282(30):22089–101. DOI:10.1074/JBC.M700998200

136. Kiefel H, Bondong S, Hazin J, Ridinger J, Schirmer U, Riedle S, Altevogt P. L1CAM: A major driver for tumor cell invasion and motility. *Cell Adh Migr*. **2012**;6(4):374. DOI:10.4161/CAM.20832

137. Miquel M, Zhang S, Pilarsky C. Pre-clinical Models of Metastasis in Pancreatic Cancer. *Front Cell Dev Biol*. **2021**;9:748631. DOI:10.3389/FCELL.2021.748631

138. Lamouille S, Xu J, Derynck R. Molecular mechanisms of epithelial–mesenchymal transition. *Nat Publ Gr*. **2014**;15(3):178-196. DOI:10.1038/nrm3758

139. Rodriguez-Aznar E, Wiesmüller L, Sainz B, Hermann PC. EMT and Stemness—Key Players in Pancreatic Cancer Stem Cells. *Cancers 2019, Vol 11, Page 1136*. **2019**;11(8):1136. DOI:10.3390/CANCERS11081136

140. Cates JMM, Byrd RH, Fohn LE, Tatsas AD, Washington MK, Black CC. Epithelial-Mesenchymal Transition Markers in Pancreatic Ductal Adenocarcinoma. *Pancreas*. **2009**;38(1):e1. DOI:10.1097/MPA.0B013E3181878B7F

141. Ahmed S, Bradshaw AD, Gera S, Zahidunnabi Dewan M, Xu R. The TGF-β/Smad4 Signaling Pathway in Pancreatic Carcinogenesis and Its Clinical Significance. *J Clin Med*. **2017**;6(1). DOI:10.3390/JCM6010005

142. Yu M, Ting DT, Stott SL, Wittner BS, Ozsolak F, Paul S, Ciciliano JC, Smas ME, Winokur D, Gilman AJ, Ulman MJ, Xega K, Contino G, Alagesan B, Brannigan BW, Milos PM, Ryan DP, Sequist L V., Bardeesy N, Ramaswamy S, Toner M, Maheswaran S, Haber DA. RNA sequencing of pancreatic circulating tumour cells implicates WNT signalling in metastasis. *Nature*. **2012**;487(7408):510–3. DOI:10.1038/NATURE11217

143. Nielsen SR, Quaranta V, Linford A, Emeagi P, Rainer C, Santos A, Ireland L, Sakai T, Sakai K, Kim YS, Engle D, Campbell F, Palmer D, Ko JH, Tuveson DA, Hirsch E, Mielgo A, Schmid MC. Macrophage-secreted granulin supports pancreatic cancer metastasis by inducing liver fibrosis. *Nat Cell Biol*. **2016**;18(5):549–60. DOI:10.1038/ncb3340

144. Wilson WR, Hay MP. Targeting hypoxia in cancer therapy. *Nat Rev Cancer*. **2011**:11(6):393-410. DOI:10.1038/nrc3064

145. Thienpont B, Steinbacher J, Zhao H, D'Anna F, Kuchnio A, Ploumakis A, Ghesquière B, Van Dyck L, Boeckx B, Schoonjans L, Hermans E, Amant F, Kristensen VN, Koh KP, Mazzone M, Coleman ML, Carell T, Carmeliet P, Lambrechts Di. Tumour hypoxia causes DNA hypermethylation by reducing TET activity. *Nature*. **2016**;537(7618):63–8. DOI:10.1038/nature19081

146. Kim SK, Cho SW. The Evasion Mechanisms of Cancer Immunity and Drug Intervention in the

Tumor Microenvironment. *Front Pharmacol*. **2022**;13:1494. DOI:10.3389/FPHAR.2022.868695/BIBTEX

147. Vesely MD, Schreiber RD. Cancer Immunoediting: antigens, mechanisms and implications to cancer immunotherapy. *Ann N Y Acad Sci*. **2013**;1284(1):1. DOI:10.1111/NYAS.12105

148. Labani-Motlagh A, Ashja-Mahdavi M, Loskog A. The Tumor Microenvironment: A Milieu Hindering and Obstructing Antitumor Immune Responses. *Front Immunol*. **2020**;11:940. DOI:10.3389/FIMMU.2020.00940

149. Starzer AM, Preusser M, Berghoff AS. Immune escape mechanisms and therapeutic approaches in cancer: the cancer-immunity cycle. *https://doi.org/101177/17588359221096219*. **2022**;14:17588359221096219. DOI:10.1177/17588359221096219

150. Kim JM, Chen DS. Immune escape to PD-L1/PD-1 blockade: seven steps to success (or failure). *Ann Oncol Off J Eur Soc Med Oncol*. **2016**;27(8):1492–504. DOI:10.1093/ANNONC/MDW217

151. Chen DS, Mellman I. Elements of cancer immunity and the cancer–immune set point. *Nat* **2017**;541(7637):321–30. DOI:10.1038/nature21349

152. Chen DS, Mellman I. Oncology Meets Immunology: The Cancer-Immunity Cycle. *Immunity*. **2013**;39(1):1–10. DOI:10.1016/J.IMMUNI.2013.07.012

153. Preusser M, Berghoff AS, Thallinger C, Zielinski CC. Cancer immune cycle: a video introduction to the interaction between cancer and the immune system. *ESMO Open*. **2016**;1(3):e000056. DOI:10.1136/ESMOOPEN-2016-000056

154. Tang S, Ning Q, Yang L, Mo Z, Tang S. Mechanisms of immune escape in the cancer immune cycle. *Int Immunopharmacol*. **2020**;86(June):106700. DOI:10.1016/j.intimp.2020.106700

155. Voron T, Colussi O, Marcheteau E, Pernot S, Nizard M, Pointet AL, Latreche S, Bergaya S, Benhamouda N, Tanchot C, Stockmann C, Combe P, Berger A, Zinzindohoue F, Yagita H, Tartour E, Taieb J, Terme M. VEGF-A modulates expression of inhibitory checkpoints on CD8+ T cells in tumors. *J Exp Med*. **2015**;212(2):139–48. DOI:10.1084/JEM.20140559

156. Apte RS, Chen DS, Ferrara N. VEGF in Signaling and Disease: Beyond Discovery and Development. *Cell*. **2019**;176(6):1248. DOI:10.1016/J.CELL.2019.01.021

157. Fukumura D, Kloepper J, Amoozgar Z, Duda DG, Jain RK. Enhancing cancer immunotherapy using antiangiogenics: opportunities and challenges. *Nat Rev Clin Oncol*. **2018**;15(5):325–40. DOI:10.1038/NRCLINONC.2018.29

158. Khan KA, Kerbel RS. Improving immunotherapy outcomes with anti-angiogenic treatments and vice versa. *Nat Rev Clin Oncol 2018 155*. **2018**;15(5):310–24. DOI:10.1038/nrclinonc.2018.9

159. Sharpe AH, Pauken KE. The diverse functions of the PD1 inhibitory pathway. *Nat Rev Immunol 2017 183*. **2017**;18(3):153–67. DOI:10.1038/nri.2017.108

160. Xu W, Atkins MB, McDermott DF. Checkpoint inhibitor immunotherapy in kidney cancer. *Nat Rev Urol*. **2020**;17(3):137–50. DOI:10.1038/S41585-020-0282-3

161. Wang X, Teng F, Kong L, Yu J. PD-L1 expression in human cancers and its association with clinical outcomes. *Onco Targets Ther*. **2016**;9:5023. DOI:10.2147/OTT.S105862

162. Qian J, Wang C, Wang B, Yang J, Wang Y, Luo F, Xu J, Zhao C, Liu R, Chu Y. The IFN-γ/PD-L1 axis between T cells and tumor microenvironment: hints for glioma anti-PD-1/PD-L1 therapy. *J Neuroinflammation*. **2018**;15(1):290. DOI:10.1186/s12974-018-1330-2

163. Abiko K, Matsumura N, Hamanishi J, Horikawa N, Murakami R, Yamaguchi K, Yoshioka Y, Baba T, Konishi I, Mandai M. IFN-γ from lymphocytes induces PD-L1 expression and promotes progression of ovarian cancer. *Br J Cancer*. **2015**;112(9):1501–9. DOI:10.1038/bjc.2015.101

164. Imai Y, Chiba T, Kondo T, Kanzaki H, Kanayama K, Ao J, Kojima R, Kusakabe Y, Nakamura M, Saito T, Nakagawa R, Suzuki E, Nakamoto S, Muroyama R, Tawada A, Matsumura T, Nakagawa T, Kato J, Kotani A, Matsubara H, Kato N. Interferon-γ induced PD-L1 expression and soluble PD-L1 production in gastric cancer. *Oncol Lett*. **2020**;20(3):2161. DOI:10.3892/OL.2020.11757

165. Spranger S, Spaapen RM, Zha Y, Williams J, Meng Y, Ha TT, Gajewski TF. Up-regulation of PD-L1, IDO, and T(regs) in the melanoma tumor microenvironment is driven by CD8(+) T cells. *Sci Transl Med*. **2013**;5(200):200ra116. DOI:10.1126/scitranslmed.3006504

166. Azuma T, Yao S, Zhu G, Flies AS, Flies SJ, Chen L. B7-H1 is a ubiquitous antiapoptotic receptor on cancer cells. *Blood*. **2008**;111(7):3635. DOI:10.1182/BLOOD-2007-11-123141

167. Gato-Cañas M, Zuazo M, Arasanz H, Ibañez-Vea M, Lorenzo L, Fernandez-Hinojal G, Vera R, Smerdou C, Martisova E, Arozarena I, Wellbrock C, Llopiz D, Ruiz M, Sarobe P, Breckpot K, Kochan G, Escors D. PDL1 Signals through Conserved Sequence Motifs to Overcome Interferon-Mediated Cytotoxicity. *Cell Rep*. **2017**;20(8):1818–29. DOI:10.1016/J.CELREP.2017.07.075

168. Knudsen ES, Vail P, Balaji U, Ngo H, Botros IW, Makarov V, Riaz N, Balachandran V, Leach S, Thompson DM, Chan TA, Witkiewicz AK. Stratification of pancreatic ductal adenocarcinoma: Combinatorial genetic, stromal, and immunologic markers. *Clin Cancer Res*. **2017**;23(15):4429–40. DOI:10.1158/1078-0432.CCR-17-0162

169. Nomi T, Sho M, Akahori T, Hamada K, Kubo A, Kanehiro H, Nakamura S, Enomoto K, Yagita H, Azuma M, Nakajima Y. Clinical Significance and Therapeutic Potential of the Programmed Death-1 Ligand/Programmed Death-1 Pathway in Human Pancreatic Cancer. *Clin Cancer Res*. **2007**:13(7):2151-7. DOI:10.1158/1078-0432.CCR-06-2746

170. Rahn S, Krüger S, Röcken C, Helm O, Sebens S. Response to: “Patterns of PD-L1 expression and CD8 T cell infiltration in gastric adenocarcinomas and associated immune stroma.” *Gut*. **2019**;68(1):179–80. DOI:10.1136/GUTJNL-2017-315843

171. Principe DR, Underwood PW, Kumar S, Timbers KE, Koch RM, Trevino JG, Munshi HG, Rana A. Loss of SMAD4 Is Associated With Poor Tumor Immunogenicity and Reduced PD-L1 Expression in Pancreatic Cancer. *Front Oncol*. **2022**;12. DOI:10.3389/FONC.2022.806963/FULL

172. Zhang Y, Chen X, Mo S, Ma H, Lu Z, Yu S, Chen J. PD-L1 and PD-L2 expression in pancreatic ductal adenocarcinoma and their correlation with immune infiltrates and DNA damage response molecules. *J Pathol Clin Res*. **2022**;8(3):257. DOI:10.1002/CJP2.259

173. Li J, Yin L, Chen Y, An S, Xiong Y, Huang G, Liu J. PD-L1 correlated gene expression profiles and tumor infiltrating lymphocytes in pancreatic cancer. *Int J Med Sci*. **2021**;18(14):3150. DOI:10.7150/IJMS.61771

174. Kurahara H, Takao S, Maemura K, Mataki Y, Kuwahata T, Maeda K, Sakoda M, Iino S, Ishigami S, Ueno S, Shinchi H, Natsugoe S. M2-Polarized tumor-associated macrophage infiltration of regional lymph nodes is associated with nodal lymphangiogenesis and occult nodal involvement in pn0 pancreatic cancer. *Pancreas*. **2013**;42(1):155–9. DOI:10.1097/MPA.0b013e318254f2d1

175. Kurahara H, Shinchi H, Mataki Y, Maemura K, Noma H, Kubo F, Sakoda M, Ueno S, Natsugoe S, Takao S. Significance of M2-polarized tumor-associated macrophage in pancreatic cancer. *J Surg Res*. **2011**;167(2):e211–9. DOI:10.1016/j.jss.2009.05.026

176. Wang X, Li X, Wei X, Jiang H, Lan C, Yang S, Wang H, Yang Y, Tian C, Xu Z, Zhang J, Hao J, Ren H. PD-L1 is a direct target of cancer-FOXP3 in pancreatic ductal adenocarcinoma (PDAC), and combined immunotherapy with antibodies against PD-L1 and CCL5 is effective in the treatment of PDAC. *Signal Transduct Target Ther*. **2020**;5(1). DOI:10.1038/S41392-020-0144-8

177. Hu Z, Ott PA, Wu CJ. Towards personalized, tumour-specific, therapeutic vaccines for cancer. *Nat Rev Immunol*. **2018**;18(3):168–82. DOI:10.1038/NRI.2017.131

178. June CH, Sadelain M. Chimeric Antigen Receptor Therapy. *N Engl J* Med. **2018**;379(1):64–73. DOI:10.1056/NEJMRA1706169

179. Liu J, Chen Z, Li Y, Zhao W, Wu JB, Zhang Z. PD-1/PD-L1 Checkpoint Inhibitors in Tumor Immunotherapy. *Front Pharmacol*. **2021**;12. DOI:10.3389/FPHAR.2021.731798

180. Havel JJ, Chowell D, Chan TA. The evolving landscape of biomarkers for checkpoint inhibitor immunotherapy. *Nat Rev Cancer 2019 193*. **2019**;19(3):133–50. DOI:10.1038/s41568-019-0116-x

181. FDA approves cemiplimab-rwlc for non-small cell lung cancer with high PD-L1 expression | FDA.

https://www.fda.gov/drugs/resources-information-approved-drugs/fda-approves-cemiplimab-rwlc-non-small-cell-lung-cancer-high-pd-l1-expression

182. FDA grants approval to atezolizumab for alveolar soft part sarcoma | FDA. https://www.fda.gov/drugs/resources-information-approved-drugs/fda-grants-approval-atezolizumab-alveolar-soft-part-sarcoma

183. FDA approves avelumab for urothelial carcinoma maintenance treatment | FDA. https://www.fda.gov/drugs/drug-approvals-and-databases/fda-approves-avelumab-urothelial-carcinoma-maintenance-treatment

184. Alvarez-Argote J, Dasanu CA. Durvalumab in cancer medicine: a comprehensive review. *Expert Opin Biol Ther*. **2019**;19(9):927–35. DOI:10.1080/14712598.2019.1635115

185. Arru C, De Miglio MR, Cossu A, Muroni MR, Carru C, Zinellu A, Paliogiannis P. Durvalumab Plus Tremelimumab in Solid Tumors: A Systematic Review. *Adv Ther*. **2021**;38(7):3674. DOI:10.1007/S12325-021-01796-6

186. FDA approves durvalumab for locally advanced or metastatic biliary tract cancer | FDA. https://www.fda.gov/drugs/resources-information-approved-drugs/fda-approves-durvalumab-locally-advanced-or-metastatic-biliary-tract-cancer

187. FDA approves cemiplimab-rwlc in combination with platinum-based chemotherapy for non-small cell lung cancer | FDA. https://www.fda.gov/drugs/resources-information-approved-drugs/fda-approves-cemiplimab-rwlc-combination-platinum-based-chemotherapy-non-small-cell-lung-cancer

188. FDA approves atezolizumab with chemotherapy and bevacizumab for first-line treatment of metastatic non-squamous NSCLC | FDA. https://www.fda.gov/drugs/fda-approves-atezolizumab-chemotherapy-and-bevacizumab-first-line-treatment-metastatic-non-squamous

189. Nguyen CM, Jacob SE. Pembrolizumab. *J Dermatol Nurses Assoc*. **2022**;9(2):95–7. DOI:10.1097/JDN.0000000000000264

190. Alvarez-Argote J, Dasanu CA. Durvalumab in cancer medicine: a comprehensive review. *Expert Opin Biol Ther*. **2019**;19(9):927–35. DOI:10.1080/14712598.2019.1635115

191. Twomey JD, Zhang B. Cancer Immunotherapy Update: FDA-Approved Checkpoint Inhibitors and Companion Diagnostics. *AAPS J*. **2021**;23(2):1–11. DOI:10.1208/S12248-021-00574-0/FIGURES/2

192. O'Reilly EM, Oh DY, Dhani N, Renouf DJ, Lee MA, Sun W, Fisher G, Hezel A, Chang SC, Vlahovic G, Takahashi O, Yang Y, Fitts D, Philip PA. Durvalumab With or Without Tremelimumab for Patients With Metastatic Pancreatic Ductal Adenocarcinoma. *JAMA Oncol*. **2019**;5(10):1431.

DOI:10.1001/jamaoncol.2019.1588

193. Brahmer JR, Tykodi SS, Chow LQM, Hwu WJ, Topalian SL, Hwu P, Drake CG, Camacho LH, Kauh J, Odunsi K, Pitot HC, Hamid O, Bhatia S, Martins R, Eaton K, Chen S, Salay TM, Alaparthy S, Grosso JF, Korman AJ, Parker SM, Agrawal S, Goldberg SM, Pardoll DM, Gupta A, Wigginton JM. Safety and Activity of Anti–PD-L1 Antibody in Patients with Advanced Cancer. *N Engl J Med*. **2012**;366(26):2455–65. DOI:10.1056/nejmoa1200694

194. Naimi A, Mohammed RN, Raji A, Chupradit S, Yumashev AV, Suksatan W, Shalaby MN, Thangavelu L, Kamrava S, Shomali N, Sohrabi AD, Adili A, Noroozi-Aghideh A, Razeghian E. Tumor immunotherapies by immune checkpoint inhibitors (ICIs); the pros and cons. *Cell Commun Signal*. **2022**;20(1):44. DOI:10.1186/S12964-022-00854-Y

195. Iwai Y, Hamanishi J, Chamoto K, Honjo T. Cancer immunotherapies targeting the PD-1 signaling pathway. *J Biomed Sci*. **2017**;24(1):26. DOI:10.1186/s12929-017-0329-9

196. Poh AR, Ernst M. Tumor-Associated Macrophages in Pancreatic Ductal Adenocarcinoma: Therapeutic Opportunities and Clinical Challenges. *Cancers (Basel)*. **2021**;13(12). DOI:10.3390/CANCERS13122860

197. Lehnert L, Lerch MM, Hirai Y, Kruse ML, Schmiegel W, Kalthoff H. Autocrine stimulation of human pancreatic duct-like development by soluble isoforms of epimorphin in vitro. *J Cell Biol*. **2001**;152(5):911–21. DOI:10.1083/jcb.152.5.911

198. Sipos B, Möser S, Kalthoff H, Török V, Löhr M, Klöppel G. A comprehensive characterization of pancreatic ductal carcinoma cell lines: Towards the establishment of an in vitro research platform. *Virchows Arch*. **2003**;442(5):444–52. DOI:10.1007/S00428-003-0784-4/METRICS

199. Tan MH, Nowak NJ, Loor R, Ochi H, Sandberg AA, Lopez C, Pickren JW, Berjian R, Douglass HO, Chu TM. Characterization of a new primary human pancreatic tumor line. *Cancer Invest*. **1986**;4(1):15–23. DOI:10.3109/07357908609039823

200. Kalthoff H, Schmiegel W, Roeder C, Kasche D, Schmidt A, Lauer G, Thiele HG, Honold G, Pantel K, Riethmüller G, Scherer E, Maurer J, Maacke H, Deppert W. p53 and K-RAS alterations in pancreatic epithelial cell lesions. *Oncogene*. **1993**;8(2):289–98.

201. Qian J, Niu J, Li M, Chiao PJ, Tsao MS. In vitro Modeling of Human Pancreatic Duct Epithelial Cell Transformation Defines Gene Expression Changes Induced by K-ras Oncogenic Activation in Pancreatic Carcinogenesis. *Cancer Res*. **2005**;65(12):5045–53. DOI:10.1158/0008-5472.CAN-04-3208

202. Furukawa T, Duguid WP, Rosenberg L, Viallet J, Galloway DA, Tsao MS. Long-term culture and immortalization of epithelial cells from normal adult human pancreatic ducts transfected by the E6E7 gene of human papilloma virus 16. *Am J Pathol*. **1996**;148(6):1763.

203. Lieber M, Mazzetta J, Nelson-Rees W, Kaplan M, Todaro G. Establishment of a continuous tumor-cell line (panc-1) from a human carcinoma of the exocrine pancreas. *Int J cancer*. **1975**;15(5):741–7. DOI:10.1002/IJC.2910150505

204. Moore PS, Sipos B, Orlandini S, Sorio C, Real FX, Lemoine NR, Gress T, Bassi C, Klöppel G, Kalthoff H, Ungefroren H, Löhr M, Scarpa A. Genetic profile of 22 pancreatic carcinoma cell lines: Analysis of K-ras, p53, p16 and DPC4/Smad4. *Virchows Arch*. **2001**;439(6):798–802. DOI:10.1007/s004280100474

205. Sipos B, Möser S, Kalthoff H, Török V, Löhr M, Klöppel G. A comprehensive characterization of pancreatic ductal carcinoma cell lines: Towards the establishment of an in vitro research platform. *Virchows Arch*. **2003**;442(5):444–52. DOI:10.1007/S00428-003-0784-4/TABLES/5

206. Benz C, Dondelinger F, McKean PG, Urbaniak MD. Cell cycle synchronisation of Trypanosoma brucei by centrifugal counter-flow elutriation reveals the timing of nuclear and kinetoplast DNA replication. *Sci Rep*. **2017**;7(1):1–10. DOI:10.1038/s41598-017-17779-z

207. Trickett A, Kwan YL. T cell stimulation and expansion using anti-CD3/CD28 beads. *J Immunol Methods*. **2003**;275(1–2):251–5. DOI:10.1016/S0022-1759(03)00010-3

208. Rieger AM, Nelson KL, Konowalchuk JD, Barreda DR. Modified Annexin V/Propidium Iodide Apoptosis Assay For Accurate Assessment of Cell Death. *J Vis Exp*. **2011**;(50):2597. DOI:10.3791/2597

209. Daunke T, Beckinger S, Rahn S, Krüger S, Heckl S, Wesch D, Pilarsky C, Eckstein M, Hartmann A, Wandmacher AM, Susanne S. Analysis of the immune checkpoint regulator PD-L1 in the tumor-stroma interplay in pancreatic ductal adenocarcinoma. Under Revision in *Front Immunol*. **2023**

210. Saleh R, Taha RZ, Toor SM, Sasidharan Nair V, Murshed K, Khawar M, Al-Dhaheri M, Petkar MA, Abu Nada M, Elkord E. Expression of immune checkpoints and T cell exhaustion markers in early and advanced stages of colorectal cancer. *Cancer Immunol Immunother*. **2020**;69(10):1989–99. DOI:10.1007/S00262-020-02593-W/FIGURES/4

211. Wherry EJ. T cell exhaustion. *Nat Immunol*. **2011**;12(6):492–9. DOI:10.1038/ni.2035

212. Yi JS, Cox MA, Zajac AJ. T-cell exhaustion: characteristics, causes and conversion. *Immunology*. **2010**;129(4):474. DOI:10.1111/J.1365-2567.2010.03255.X

213. Zheng Y, Han L, Chen Z, Li Y, Zhou B, Hu R, Chen S, Xiao H, Ma Y, Xie G, Yang J, Ding X, Shen L. PD-L1+CD8+ T cells enrichment in lung cancer exerted regulatory function and tumor-promoting tolerance. *iScience*. **2022**;25(2):103785. DOI:10.1016/J.ISCI.2022.103785

214. Li L, Lu G, Liu Y, Gong L, Zheng X, Zheng H, Gu W, Yang L. Low Infiltration of CD8+ PD-L1+ T Cells and M2 Macrophages Predicts Improved Clinical Outcomes After Immune Checkpoint Inhibitor

Therapy in Non-Small Cell Lung Carcinoma. *Front Oncol*. **2021**;11. DOI:10.3389/FONC.2021.658690

215. Rollins MR, Gibbons Johnson RM. CD80 Expressed by CD8+ T Cells Contributes to PD-L1-Induced Apoptosis of Activated CD8+ T Cells. *J Immunol Res*. **2017**;2017:7659462. DOI:10.1155/2017/7659462

216. Ge Z, Peppelenbosch MP, Sprengers D, Kwekkeboom J. TIGIT, the Next Step Towards Successful Combination Immune Checkpoint Therapy in Cancer. *Front Immunol*. **2021**;12:699895. DOI:10.3389/FIMMU.2021.699895

217. Blando J, Sharma A, Higa MG, Zhao H, Vence L, Yadav SS, Kim J, Sepulveda AM, Sharp M, Maitra A, Wargo J, Tetzlaff M, Broaddus R, Katz MHG, Varadhachary GR, Overman M, Wang H, Yee C, Bernatchez C, Iacobuzio-Donahue C, Basu S, Allison JP, Sharma P. Comparison of immune infiltrates in melanoma and pancreatic cancer highlights VISTA as a potential target in pancreatic cancer. *Proc Natl Acad Sci U S A*. **2019**;116(5):1692–7. DOI:10.1073/PNAS.1811067116/-/DCSUPPLEMENTAL

218. Rahn S. Characterization of programmed death ligand 1 expression and analyses of its immune-regulatory role in pancreatic ductal adenocarcinoma. Dissertation zur Erlangung des akademischen Grades Dr. rer. nat.. **2019**.

219. Bhat P, Leggatt G, Waterhouse N, Frazer IH. Interferon-γ derived from cytotoxic lymphocytes directly enhances their motility and cytotoxicity. *Cell Death Dis*. **2017**;8. DOI:10.1038/cddis.2017.67

220. Lu S, Li D, Xi L, Calderone R. Interplay of interferon-gamma and macrophage polarization during Talaromyces marneffei infection. *Microb Pathog*. **2019**;134:103594. DOI:10.1016/J.MICPATH.2019.103594

221. Daunke T. Die Analyse des Immuncheckpoint Regulators PD-L1 in der Interaktion von Stroma- und Tumorzellen im Pankreasadenokarzinom. Masterarbeit. **2020**.

222. Thiem A, Hesbacher S, Kneitz H, Di Primio T, Heppt M V., Hermanns HM, Goebeler M, Meierjohann S, Houben R, Schrama D. IFN-gamma-induced PD-L1 expression in melanoma depends on p53 expression. *J Exp Clin Cancer Res*. **2019**;38(1):1–15. DOI:10.1186/S13046-019-1403-9/FIGURES/5

223. Guan J, Lim KS, Mekhail T, Chang CC. Programmed Death Ligand-1 (PD-L1) Expression in the Programmed Death Receptor-1 (PD-1)/PD-L1 Blockade: A Key Player Against Various Cancers. *Arch Pathol Lab Med*. **2017**;141(6):851–61. DOI:10.5858/ARPA.2016-0361-RA

224. Atanasov G, Pötner C, Aust G, Schierle K, Dietel C, Benzing C, Krenzien F, Bartels M, Eichfeld U, Schmelzle M, Bahra M, Pascher A, Wiltberger G. TIE2-expressing monocytes and M2-polarized

macrophages impact survival and correlate with angiogenesis in adenocarcinoma of the pancreas. *Oncotarget*. **2018**;9(51):29715–26. DOI:10.18632/ONCOTARGET.25690

225. Locati M, Curtale G, Mantovani A. Diversity, Mechanisms and Significance of Macrophage Plasticity. *Annu Rev Pathol*. **2020**;15:123. DOI:10.1146/ANNUREV-PATHMECHDIS-012418-012718

226. Szlasa W, Janicka N, Sauer N, Michel O, Nowak B, Saczko J, Kulbacka J. Chemotherapy and Physical Therapeutics Modulate Antigens on Cancer Cells. *Front Immunol*. **2022**;13:889950. DOI:10.3389/FIMMU.2022.889950

227. Conroy T, Bachet JB, Ayav A, Huguet F, Lambert A, Caramella C, Maréchal R, Van Laethem JL, Ducreux M. Current standards and new innovative approaches for treatment of pancreatic cancer. *Eur J Cancer*. **2016**;57:10–22. DOI:10.1016/J.EJCA.2015.12.026

228. Manji GA, Olive KP, Saenger YM, Oberstein P. Current and Emerging Therapies in Metastatic Pancreatic Cancer. *Clin Cancer Res*. **2017**;23(7):1670–8. DOI:10.1158/1078-0432.CCR-16-2319

229. Del Re M, Vivaldi C, Rofi E, Salani F, Crucitta S, Catanese S, Fontanelli L, Massa V, Cucchiara F, Fornaro L, Capuano A, Fogli S, Vasile E, Danesi R. Gemcitabine Plus Nab-Paclitaxel Induces PD-L1 mRNA Expression in Plasma-Derived Microvesicles in Pancreatic Cancer. *Cancers (Basel)*. **2021**;13(15):3738. DOI:10.3390/CANCERS13153738

230. Du B, Wen X, Wang Y, Lin M, Lai J. Gemcitabine and checkpoint blockade exhibit synergistic anti-tumor effects in a model of murine lung carcinoma. *Int Immunopharmacol*. **2020**;86(April):106694. DOI:10.1016/j.intimp.2020.106694

231. Hanahan D, Weinberg RA. The hallmarks of cancer. *Cell*. **2000**:100(1):57-70. DOI:10.1016/S0092-8674(00)81683-9

232. Hanahan D, Weinberg RA. Hallmarks of Cancer: The Next Generation. *Cell*. **2011**;57(1):E41–6. DOI:10.1016/j.cell.2011.02.013

233. Hanahan D. Hallmarks of Cancer: New Dimensions. *Cancer Discov*. **2022**;12(1):31–46. DOI:10.1158/2159-8290.CD-21-1059

234. Hanahan D, Coussens LM. Accessories to the Crime: Functions of Cells Recruited to the Tumor Microenvironment. *Cancer Cell*. **2012**;21(3):309–22. DOI:10.1016/j.ccr.2012.02.022

235. Lacobuzio-Donahue CA, Fu B, Yachida S, Luo M, Abe H, Henderson CM, Vilardell F, Wang Z, Keller JW, Banerjee P, Herman JM, Cameron JL, Yeo CJ, Halushka MK, Eshleman JR, Raben M, Klein AP, Hruban RH, Hidalgo M, Laheru D. DPC4 Gene Status of the Primary Carcinoma Correlates With Patterns of Failure in Patients With Pancreatic Cancer. *J Clin Oncol*. **2009**;27(11):1806. DOI:10.1200/JCO.2008.17.7188

236. Han Y, Liu D, Li L. PD-1/PD-L1 pathway: current researches in cancer. *Am J Cancer Res*. **2020**;10(3):727.

237. Wei XL, Luo X, Sheng H, Wang Y, Chen DL, Li JN, Wang FH, Xu RH. PD-L1 expression in liver metastasis: its clinical significance and discordance with primary tumor in colorectal cancer. *J Transl Med*. **2020**;18(1):1–10. DOI:10.1186/S12967-020-02636-X/TABLES/3

238. Parvathareddy SK, Siraj AK, Al-Badawi IA, Tulbah A, Al-Dayel F, Al-Kuraya KS. Differential expression of PD-L1 between primary and metastatic epithelial ovarian cancer and its clinico-pathological correlation. *Sci Reports 2021 111*. **2021**;11(1):1–9. DOI:10.1038/s41598-021-83276-z

239. Lee K, Choi YJ, Kim JS, Kim DS, Lee SY, Shin BK, Kang EJ. Association between PD-L1 expression and initial brain metastasis in patients with non-small cell lung cancer and its clinical implications. *Thorac Cancer*. **2021**;12(15):2143–50. DOI:10.1111/1759-7714.14006

240. Rozenblit M, Huang R, Danziger N, Hegde P, Alexander B, Ramkissoon S, Blenman K, Ross JS, Rimm DL, Pusztai L. Comparison of PD-L1 protein expression between primary tumors and metastatic lesions in triple negative breast cancers. *J Immunother Cancer*. **2020**;8:1558. DOI:10.1136/jitc-2020-001558

241. Boman C, Zerdes I, Mårtensson K, Bergh J, Foukakis T, Valachis A, Matikas A. Discordance of PD-L1 status between primary and metastatic breast cancer: A systematic review and meta-analysis. *Cancer Treat Rev*. **2021**;99:102257. DOI:10.1016/J.CTRV.2021.102257

242. Udager AM, Liu TY, Skala SL, Magers MJ, Mcdaniel AS, Spratt DE, Feng FY, Siddiqui J, Cao X, Fields KL, Morgan TM, Palapattu GS, Weizer AZ, Chinnaiyan AM, Alva A, Montgomery JS, Tomlins SA, Jiang H, Mehra & R. Frequent PD-L1 expression in primary and metastatic penile squamous cell carcinoma: potential opportunities for immunotherapeutic approaches. *Ann Oncol*. **2016**;27:1706–12. DOI:10.1093/annonc/mdw216

243. Liu Y, Zugazagoitia J, Ahmed FS, Henick BS, Gettinger S, Herbst RS, Schalper KA, Rimm DL. Immune cell PD-L1 co-localizes with macrophages and is associated with outcome in PD-1 pathway blockade therapy. *Clin Cancer Res*. **2019**; DOI:10.1158/1078-0432.CCR-19-1040

244. Brochez L, Meireson A, Chevolet I, Sundahl N, Ost P, Kruse V. Challenging PD-L1 expressing cytotoxic T cells as a predictor for response to immunotherapy in melanoma. *Nat Commun*. **2018**;9(1):2921. DOI:10.1038/s41467-018-05047-1

245. Garcia-Diaz A, Shin DS, Moreno BH, Saco J, Escuin-Ordinas H, Rodriguez GA, Zaretsky JM, Sun L, Hugo W, Wang X, Parisi G, Saus CP, Torrejon DY, Graeber TG, Comin-Anduix B, Hu-Lieskovan S, Damoiseaux R, Lo RS, Ribas A. Interferon Receptor Signaling Pathways Regulating PD-L1 and PD-L2 Expression. *Cell Rep*. **2017**;19(6):1189. DOI:10.1016/J.CELREP.2017.04.031

246. Öhlund D, Handly-Santana A, Biffi G, Elyada E, Almeida AS, Ponz-Sarvise M, Corbo V, Oni TE, Hearn SA, Lee EJ, Chio IIC, Hwang C Il, Tiriac H, Baker LA, Engle DD, Feig C, Kultti A, Egeblad M, Fearon DT, Crawford JM, Clevers H, Park Y, Tuveson DA. Distinct populations of inflammatory fibroblasts and myofibroblasts in pancreatic cancer. *J Exp Med*. **2017**;214(3):579–96. DOI:10.1084/jem.20162024

247. Malik R, Luong T, Cao X, Han B, Shah N, Franco-Barraza J, Han L, Shenoy VB, Lelkes PI, Cukierman E. Rigidity controls human desmoplastic matrix anisotropy to enable pancreatic cancer cell spread via extracellular signal-regulated kinase 2. *Matrix Biol*. **2019**;81:50–69. DOI:10.1016/J.MATBIO.2018.11.001

248. Alzhrani R, Alsaab HO, Vanamala K, Bhise K, Tatiparti K, Barari A, Sau S, Iyer AK. Overcoming the Tumor Microenvironmental Barriers of Pancreatic Ductal Adenocarcinomas for Achieving Better Treatment Outcomes. *Adv Ther*. **2021**;4(6):2000262. DOI:10.1002/ADTP.202000262

249. Watt J, Kocher HM. The desmoplastic stroma of pancreatic cancer is a barrier to immune cell infiltration. *Oncoimmunology*. **2013**;2(12). DOI:10.4161/ONCI.26788

250. Masugi Y. The Desmoplastic Stroma of Pancreatic Cancer: Multilayered Levels of Heterogeneity, Clinical Significance, and Therapeutic Opportunities. *Cancers (Basel)*. **2022**;14(13):1–19. DOI:10.3390/cancers14133293

251. Reddy M, Eirikis E, Davis C, Davis HM, Prabhakar U. Comparative analysis of lymphocyte activation marker expression and cytokine secretion profile in stimulated human peripheral blood mononuclear cell cultures: An in vitro model to monitor cellular immune function. *J Immunol Methods*. **2004**;293(1–2):127–42. DOI:10.1016/j.jim.2004.07.006

252. Mita Y, Kimura MY, Hayashizaki K, Koyama-Nasu R, Ito T, Motohashi S, Okamoto Y, Nakayama T. Crucial role of CD69 in anti-tumor immunity through regulating the exhaustion of tumor-infiltrating T cells. *Int Immunol*. **2018**;30(12):559–67. DOI:10.1093/INTIMM/DXY050

253. Wherry EJ, Kurachi M. Molecular and cellular insights into T cell exhaustion. *Nat Rev Immunol.* **2015;**15(8):486–99. DOI:10.1038/nri3862

254. Agnellini P, Wolint P, Rehr M, Cahenzli J, Karrer U, Oxenius A. Impaired NFAT nuclear translocation results in split exhaustion of virus-specific CD8+ T cell functions during chronic viral infection. *Proc Natl Acad Sci U S A*. **2007**;104(11):4565–70. DOI:10.1073/PNAS.0610335104/SUPPL_FILE/10335TABLE1.PDF

255. Fuller MJ, Khanolkar A, Tebo AE, Zajac AJ. Maintenance, Loss, and Resurgence of T Cell Responses During Acute, Protracted, and Chronic Viral Infections. *J Immunol*. **2004**;172(7):4204–14. DOI:10.4049/JIMMUNOL.172.7.4204

256. Fanelli G, Romano M, Nova-Lamperti E, Sunderland MW, Nerviani A, Scottà C, Bombardieri M,

Quezada SA, Sacks SH, Noelle RJ, Pitzalis C, Lechler RI, Lombardi G, Becker PD. PD-L1 signaling on human memory CD4+ T cells induces a regulatory phenotype. *PLOS Biol*. **2021**;19(4):e3001199. DOI:10.1371/JOURNAL.PBIO.3001199

257. Pulko V, Harris KJ, Liu X, Gibbons RM, Harrington SM, Krco CJ, Kwon ED, Dong H. B7-H1 expressed by activated CD8 T cells is essential for their survival. *J Immunol*. **2011**;187(11):5606. DOI:10.4049/JIMMUNOL.1003976

258. Liu X, Wu X, Cao S, Harrington SM, Yin P, Mansfield AS, Dong H. B7-H1 antibodies lose antitumor activity due to activation of p38 MAPK that leads to apoptosis of tumor-reactive CD8+ T cells. *Sci Rep*. **2016**;6:36722. DOI:10.1038/SREP36722

259. Butte MJ, Keir ME, Phamduy TB, Sharpe AH, Freeman GJ. Programmed death-1 ligand 1 interacts specifically with the B7-1 costimulatory molecule to inhibit T cell responses. *Immunity*. **2007**;27(1):111–22. DOI:10.1016/J.IMMUNI.2007.05.016

260. Butte MJ, Peña-Cruz V, Kim MJ, Freeman GJ, Sharpe AH. Interaction of Human PD-L1 and B7-1. *Mol Immunol*. **2008**;45(13):3567. DOI:10.1016/J.MOLIMM.2008.05.014

261. Park JJ, Omiya R, Matsumura Y, Sakoda Y, Kuramasu A, Augustine MM, Yao S, Tsushima F, Narazaki H, Anand S, Liu Y, Strome SE, Chen L, Tamada K. B7-H1/CD80 interaction is required for the induction and maintenance of peripheral T-cell tolerance. *Blood*. **2010**;116(8):1291–8. DOI:10.1182/blood-2010-01-265975

262. Chaudhri A, Xiao Y, Klee AN, Wang X, Zhu B, Freeman GJ. PD-L1 Binds to B7-1 Only In Cis on the Same Cell Surface. *Cancer Immunol Res*. **2018**;6(8):921–9. DOI:10.1158/2326-6066.CIR-17-0316

263. Sugiura D, Maruhashi T, Okazaki IM, Shimizu K, Maeda TK, Takemoto T, Okazaki T. Restriction of PD-1 function by cis-PD-L1/CD80 interactions is required for optimal T cell responses. *Science (80-)*. **2019**;364(6440):558–66. DOI:10.1126/science.aav7062

264. Scott M, Nakagawa M, Moscicki AB. Cell-mediated immune response to human papillomavirus infection. *Clin Diagn Lab Immunol*. **2001**;8(2):209–20. DOI:10.1128/CDLI.8.2.209-220.2001

265. Colf LA, Bankovich AJ, Hanick NA, Bowerman NA, Jones LL, Kranz DMM, Garcia KC. How a Single T Cell Receptor Recognizes Both Self and Foreign MHC. *Cell*. **2007**;129(1):135–46. DOI:10.1016/J.CELL.2007.01.048

266. Marino J, Paster J, Benichou G. Allorecognition by T lymphocytes and allograft rejection. *Front Immunol*. **2016**;7(DEC):582. DOI:10.3389/FIMMU.2016.00582/BIBTEX

267. Kuen J, Darowski D, Kluge T, Majety M. Pancreatic cancer cell/fibroblast co-culture induces M2 like macrophages that influence therapeutic response in a 3D model. *PLoS One*. **2017**;12(7):e0182039. DOI:10.1371/journal.pone.0182039

268. Orecchioni M, Ghosheh Y, Pramod AB, Ley K. Macrophage polarization: Different gene signatures in M1(Lps+) vs. Classically and M2(LPS-) vs. Alternatively activated macrophages. *Front Immunol*. **2019**;10(MAY):1084. DOI:10.3389/FIMMU.2019.01084/BIBTEX

269. Mantovani A, Sica A, Locati M. Macrophage polarization comes of age. *Immunity*. **2005**;23(4):344-6. DOI:10.1016/j.immuni.2005.10.001

270. Shinchi Y, Ishizuka S, Komohara Y, Matsubara E, Mito R, Pan C, Yoshii D, Yonemitsu K, Fujiwara Y, Ikeda K, Tamada K, Sakagami T, Suzuki M. The expression of PD-1 ligand 1 on macrophages and its clinical impacts and mechanisms in lung adenocarcinoma. *Cancer Immunol Immunother*. **2022**;71:2645-2661. DOI:10.1007/S00262-022-03187-4/FIGURES/7

271. Sun C, Mezzadra R, Schumacher TN. Regulation and Function of the PD-L1 Checkpoint. *Immunity*. **2018**;48(3):434–52. DOI:10.1016/J.IMMUNI.2018.03.014

272. Singhal S, Stadanlick J, Annunziata MJ, Rao AS, Bhojnagarwala PS, O'brien S, Moon EK, Cantu E, Danet-Desnoyers G, Ra HJ, Litzky L, Akimova T, Beier UH, Hancock WW, Albelda SM, Eruslanov EB. Human tumor-associated monocytes/macrophages and their regulation of T cell responses in early-stage lung cancer HHS Public Access. *Sci Transl Med*. **2019**;11(479). DOI:10.1126/scitranslmed.aat1500

273. Gabuardi TL, Lee HG, Lee KJ. Role of senescent cells in the motile behavior of active, non-senescent cells in confluent populations. *Sci Reports 2022 121*. **2022**;12(1):1–11. DOI:10.1038/s41598-022-07865-2

274. Yeon SE, No DY, Lee SH, Nam SW, Oh IH, Lee J, Kuh HJ. Application of concave microwells to pancreatic tumor spheroids enabling anticancer drug evaluation in a clinically relevant drug resistance model. *PLoS One*. **2013**;8(9). DOI:10.1371/JOURNAL.PONE.0073345

275. Linde N, Gutschalk CM, Hoffmann C, Yilmaz D, Mueller MM. Integrating macrophages into organotypic co-cultures: a 3D in vitro model to study tumor-associated macrophages. *PLoS One*. **2012**;7(7). DOI:10.1371/JOURNAL.PONE.0040058

276. Minami F, Sasaki N, Shichi Y, Gomi F, Michishita M, Ohkusu-Tsukada K, Toyoda M, Takahashi K, Ishiwata T. Morphofunctional analysis of human pancreatic cancer cell lines in 2-and 3-dimensional cultures. *Sci Reports*. **2021**;11:6775. DOI:10.1038/s41598-021-86028-1

277. Sipos B, Möser S, Kalthoff H, Török V, Löhr M, Klöppel G. A comprehensive characterization of pancreatic ductal carcinoma cell lines: Towards the establishment of an in vitro research platform. *Virchows Arch*. **2003**;442(5):444–52. DOI:10.1007/s00428-003-0784-4

278. Tawfik D, Zaccagnino A, Bernt A, Szczepanowski M, Klapper W, Schwab A, Kalthoff H, Trauzold A. The A818-6 system as an in-vitro model for studying the role of the transportome in pancreatic cancer. *BMC Cancer*. **2020**;20(1):1–17. DOI:10.1186/S12885-020-06773-

W/TABLES/3

279. Borchardt H, Schulz A, Datta K, Muders MH, Aigner A. Silencing of Neuropilins and GIPC1 in pancreatic ductal adenocarcinoma exerts multiple cellular and molecular antitumor effects. *Sci Rep*. **2019**;9(1). DOI:10.1038/S41598-019-51881-8

280. Sempere LF, Gunn JR, Korc M. A novel 3-dimensional culture system uncovers growth stimulatory actions by TGFβ in pancreatic cancer cells. *Cancer Biol Ther*. **2011**;12(3):198. DOI:10.4161/CBT.12.3.15979

281. Kim SK, Jang SD, Kim H, Chung S, Park JK, Kuh HJ. Phenotypic heterogeneity and plasticity of cancer cell migration in a pancreatic tumor three-dimensional culture model. *Cancers (Basel)*. **2020**;12(5):1–17. DOI:10.3390/cancers12051305

282. Heckl SM, Mau F, Senftleben A, Daunke T, Beckinger S, Abdullazade S, Schreiber S, Röcken C, Sebens S, Schäfer H. medical sciences Programmed Death-Ligand 1 (PD-L1) Expression Is Induced by Insulin in Pancreatic Ductal Adenocarcinoma Cells Pointing to Its Role in Immune Checkpoint Control. *Med Sci*. **2021**;9(3):48. DOI:10.3390/medsci9030048

283. Gulhati P, Schalck A, Jiang S, Shang X, Wu CJ, Hou P, Ruiz SH, Soto LS, Parra E, Ying H, Han J, Dey P, Li J, Deng P, Sei E, Maeda DY, Zebala JA, Spring DJ, Kim M, Wang H, Maitra A, Moore D, Clise-Dwyer K, Wang YA, Navin NE, DePinho RA. Targeting T cell checkpoints 41BB and LAG3 and myeloid cell CXCR1/CXCR2 results in antitumor immunity and durable response in pancreatic cancer. *Nat Cancer*. **2023**;4(1):62-80. DOI:10.1038/s43018-022-00500-z

284. Zhu Y, Knolhoff BL, Meyer MA, Nywening TM, West BL, Luo J, Wang-Gillam A, Goedegebuure SP, Linehan DC, De Nardo DG. CSF1/CSF1R Blockade Reprograms Tumor-Infiltrating Macrophages and Improves Response to T Cell Checkpoint Immunotherapy in Pancreatic Cancer Models. *Cancer Res*. **2014**;74(18):5057. DOI:10.1158/0008-5472.CAN-13-3723

285. Jones KI, Tiersma J, Yuzhalin AE, Gordon-Weeks AN, Buzzelli J, Im JH, Muschel RJ. Radiation combined with macrophage depletion promotes adaptive immunity and potentiates checkpoint blockade. *EMBO Mol Med*. **2018**;10(12):1–16. DOI:10.15252/emmm.201809342

286. Hussain SM, Kansal RG, Alvarez MA, Hollingsworth TJ, Elahi A, Miranda-Carboni G, Hendrick LE, Pingili AK, Albritton LM, Dickson P V., Deneve JL, Yakoub D, Hayes DN, Kurosu M, Shibata D, Makowski L, Glazer ES. Role of TGF-β in pancreatic ductal adenocarcinoma progression and PD-L1 expression. *Cell Oncol*. **2021**;44(3):673–87. DOI:10.1007/S13402-021-00594-0/FIGURES/7

287. Ning B, Liu Y, Wang M, Li Y, Xu T, Wei Y. The Predictive Value of Tumor Mutation Burden on Clinical Efficacy of Immune Checkpoint Inhibitors in Melanoma: A Systematic Review and Meta-Analysis. *Front Pharmacol*. **2022**;13:748674. DOI:10.3389/FPHAR.2022.748674/FULL

288. Lawlor RT, Mattiolo P, Mafficini A, Hong SM, Piredda ML, Taormina S V., Malleo G, Marchegiani

G, Pea A, Salvia R, Kryklyva V, Shin J Il, Brosens LA, Milella M, Scarpa A, Luchini C. Tumor mutational burden as a potential biomarker for immunotherapy in pancreatic cancer: Systematic review and still-open questions. *Cancers (Basel)*. **2021**;13(13):3119. DOI:10.3390/CANCERS13133119/S1

289. Amrutkar M, Gladhaug IP. Pancreatic Cancer Chemoresistance to Gemcitabine. *Cancers (Basel)*. **2017**;9(11). DOI:10.3390/CANCERS9110157

290. Smith PL, Yogaratnam Y, Samad M, Kasow S, Dalgleish AG. Effect of Gemcitabine based chemotherapy on the immunogenicity of pancreatic tumour cells and T-cells. *Clin Transl Oncol*. **2021**;23(1):110. DOI:10.1007/S12094-020-02429-0

291. Glorieux C, Xia X, You X, Wang Z, Han Y, Yang J, Noppe G, Meester C de, Ling J, Robert A, Zhang H, Li SP, Wang H, Chiao PJ, Zhang L, Li X, Huang P. Cisplatin and gemcitabine exert opposite effects on immunotherapy with PD-1 antibody in K-ras-driven cancer. *J Adv Res*. **2022**;40:109. DOI:10.1016/J.JARE.2021.12.005

292. Li D, Schaub N, Guerin TM, Bapiro TE, Richards FM, Chen V, Talsania K, Kumar P, Gilbert DJ, Schlomer JJ, Kim SJ, Sorber R, Teper Y, Bautista W, Palena C, Ock CY, Jodrell DI, Pate N, Mehta M, Zhao Y, Kozlov S, Rudloff U. T Cell–Mediated Antitumor Immunity Cooperatively Induced by TGFbR1 Antagonism and Gemcitabine Counteracts Reformation of the Stromal Barrier in Pancreatic Cancer. *Mol Cancer Ther*. **2021**;20(10):1926–40. DOI:10.1158/1535-7163.MCT-20-0620/673357/AM/T-CELL-MEDIATED-ANTI-TUMOR-IMMUNITY-COOPERATIVELY

293. Schniewind B, Christgen M, Kurdow R, Haye S, Kremer B, Kalthoff H, Ungefroren H. Resistance of pancreatic cancer to gemcitabine treatment is dependent on mitochondria-mediated apoptosis. *Int J cancer*. **2004**;109(2):182–8. DOI:10.1002/IJC.11679

294. Rashid K, Röder C, Goumas F, Egberts JH, Kalthoff H. CD95L inhibition impacts gemcitabine-mediated effects and non-apoptotic signaling of tnf-α and trail in pancreatic tumor cells. *Cancers (Basel)*. **2021**;13(21):5458. DOI:10.3390/CANCERS13215458/S1

295. Halbrook CJ, Pontious C, Kovalenko I, Lapienyte L, Dreyer S, Lee HJ, Thurston G, Zhang Y, Lazarus J, Sajjakulnukit P, Hong HS, Kremer DM, Nelson BS, Kemp S, Zhang L, Chang D, Biankin A, Shi J, Frankel TL, Crawford HC, Morton JP, Pasca di Magliano M, Lyssiotis CA. Macrophage-Released Pyrimidines Inhibit Gemcitabine Therapy in Pancreatic Cancer. *Cell Metab*. **2019**;29(6):1390-1399.e6. DOI:10.1016/J.CMET.2019.02.001

296. Pearce H, Croft W, Nicol SM, Margielewska-Davies S, Powell R, Cornall R, Davis SJ, Marcon F, Pugh MR, Fennell E, Powell-Brett S, Mahon BS, Brown RM, Middleton G, Roberts K, Moss P. Tissue-resident memory T cells in pancreatic ductal adenocarcinoma co-express PD-1 and TIGIT and functional inhibition is reversible by dual antibody blockade. *Cancer Immunol Res*. **2023**; DOI:10.1158/2326-6066.CIR-22-0121

297. Falcomatà C, Bärthel S, Schneider G, Rad R, Schmidt-Supprian M, Saur D. Context-Specific Determinants of the Immunosuppressive Tumor Microenvironment in Pancreatic Cancer. *Cancer Discov*. **2023**;13(2):278-297. DOI:10.1158/2159-8290.CD-22-0876

298. Zeeberg K, Cardone RA, Greco MR, Saccomano M, Nøhr-Nielsen A, Alves F, Pedersen SF, Reshkin SJ. Assessment of different 3D culture systems to study tumor phenotype and chemosensitivity in pancreatic ductal adenocarcinoma. *Int J Oncol*. **2016**;49(1):243–52. DOI:10.3892/IJO.2016.3513/HTML

List of figures

Supplementary data

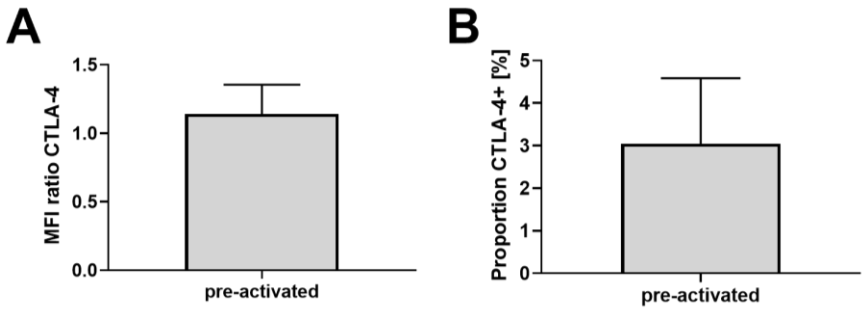

Supplementary figure 1: Low CTLA-4 expression on pre-activated CD8+ T cells. Isolation of primary human lymphocytes from leucocyte retaining systems was performed by density gradient centrifugation followed by counter flow centrifugation. To isolate CD8+ T cells from human lymphocytes, a magnetic-activated cell sorting (MACS) system was used. Afterwards, untouched CD8+ T cells were stimulated with immobilized CD3 and soluble CD28-targeting antibodies as well as IL-2 for 4 days. At day 3, CD8+ T cell were again stimulated with IL-2. After 4 days, **(A)** MFI ratio of CTLA-4 and **(B)** proportion of CTLA-4+ cells were investigated by flow cytometric analysis. n=4.

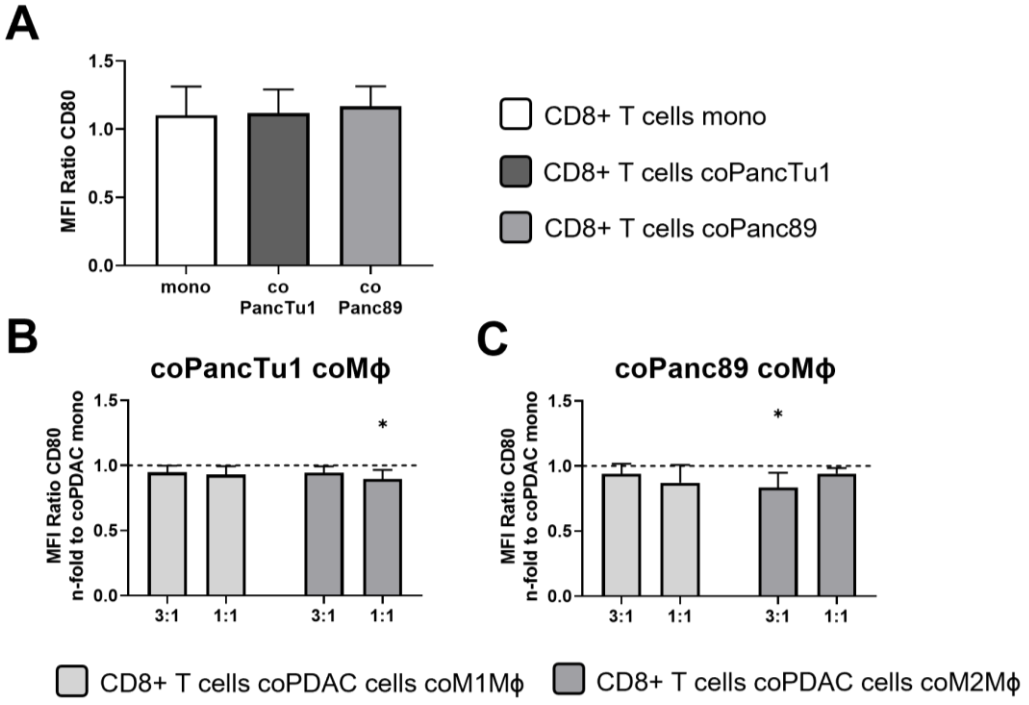

Supplementary figure 2: Cell surface levels of CD80 on CD8+ T cells were not altered by the presence of PDAC spheroids and rathe decreased due to macrophage attendance. PancTu1 or Panc89 cells were mono-cultured or co-cultured with either M1- or M2-like macrophages in ultra-low attachment plates to form spheroids. After 48 h, pre-activated CD8+ T cells were added to spheroids for 24 h. **(A)** CD80 surface expression on mono-cultured (white) or co-cultured CD8+ T cells with PancTu1 (dark grey) or Panc89 (light grey) mono spheroids examined by flow cytometric analysis. n=4. Effect of M1-like (light grey) or M2-like macrophage (dark grey) on CD80 expression of CD8+ T cells after culture with **(B)** PancTu1 co-culture spheroids or **(C)** Panc89 co-culture spheroids. Data are normalized to CD8+ T cells cultured with PDAC mono spheroids. Ratio 3:1: $1.5x10^4$ PDAC cells and $0.5x10^4$ macrophages; ratio 1:1: $1x10^4$ PDAC cells and $1x10^4$ macrophages. Data are presented as MFI ratio and denotes median fluorescence intensity ratio of specific staining antibody and its isotype control ($MFI^{specific}/MFI^{isotype}$). Parametric data are depicted as mean with standard deviation in one direction. Two-way ANOVA with Dunnett's multiple comparison test comparing all samples with control of 1. The dashed lines mark an MFI ratio of "1". * = $p < 0.05$; ** = $p < 0.01$. n=4.

Declaration on oath

Hiermit versichere ich, Tina Daunke (geboren am 06.10.1992 in Räckelwitz), an Eides statt, dass ich die vorliegende wissenschaftliche Abhandlung mit dem Titel:

„The expression and role of the immune checkpoint regulator Programmed Cell Death Protein 1-Ligand 1 in the tumor-stroma interplay of pancreatic ductal adenocarcinoma"

nach den Regeln guter wissenschaftlicher Praxis der Deutschen Forschungsgemeinschaft eigenständig verfasst und keine anderen als die angegebenen Hilfsmittel und Quellen benutzt habe. Dabei habe ich keine Hilfe, außer der wissenschaftlichen Beratung durch meine Doktormutter Prof. Dr. rer. nat. Susanne Sebens und durch die namentlich erwähnten Kooperationspartner in Anspruch genommen.
Weder wurde diese Arbeit bisher im Rahmen eines Prüfungsverfahrens vorgelegt, noch wurde ein akademischer Grad entzogen. Teile dieser Arbeit sind bereits veröffentlicht und dementsprechend in dieser Arbeit als solche gekennzeichnet.

Kiel, Mai 2023

_____

Tina Daunke

Acknowledgments

Mein besonderer Dank gilt meiner Doktormutter Prof. Dr. Susanne Sebens für die Möglichkeit, diese Arbeit in ihrer Arbeitsgruppe anfertigen zu können, die Bereitstellung des interessanten Themas, die umfangreiche persönliche Betreuung sowie die täglich ansteckende Begeisterung im Bereich der Tumorbiologie.

Des Weiteren möchte ich Prof. Dr. Regina Scherließ und Prof. Dr. Thomas Roeder herzlich dafür danken, dass sie die Aufgabe als Zweitgutachter*in übernommen haben.

Zudem möchte ich mich bei den vielen Kollegen der AG Sebens und des Instituts für experimentelle Tumorforschung bedanken, die ich in den Jahren kennen lernen durfte. Ich werde mich immer gern an die Freaky Fridays, Sportstunden und Sommer- und Weihnachtsfeste zurückerinnern. Besonderer Dank geht dabei an Sandra Ussat, Sascha Rahn, Charlotte Kayser, Leon Aldag, Lisa Philipp, Anna Willms und Silje Beckinger. Vor allem bei Letzterer möchte ich von ganzem Herzen bedanken. Nicht nur die fachlichen Diskussionen und thematischen Ideenfindungen in holprigen Phasen waren während der anspruchsvollen Doktorarbeitszeit eine große Hilfe, sondern du bist mir mittlerweile so sehr ans Herz gewachsen, dass ich dich zu meiner Familie zähle.

Weiterhin möchte ich besonders Prof. Dr. Daniela Wesch und Dr. Hans Heinrich Oberg vom Institut für Immunologie für die Organisation der Blutspendeproben und Einarbeitung in die Durchflusszytometrie bedanken. Zudem danke ich der TriBanK und Prof. Dr. Christian Pilarsky, Dr. Markus Eckstein und Prof. Dr. Arndt Hartmann für die Bereitstellung klinischer Daten und des Patientenmaterials. Zusätzlich möchte ich Christoph Röcken für die Unterstützung hinsichtlich der histologischen Analysen danken sowie Sandra Krüger und Steffen Heckl für die Anfertigung der histologischen Schnitte und Färbungen.

Mein größter Dank geht an meinen Mann Normen. Danke, dass du an mich geglaubt hast und mir immer gezeigt hast, wie stolz du auf mich bist. Ich danke dir auch für deine Geduld, dein offenes Ohr (obwohl das nicht dein Fachgebiet ist) und deine unbändige Unterstützung, mich in anstrengenden Phasen wieder aufzubauen. Du bist mein Fels in der Brandung!

Original Publications

Flynn CM, Kespohl B, **Daunke T**, Garbers Y, Düsterhöft S, Rose-John S, Haybaeck J, Lokau J, Aparicio-Siegmund S, Garbers C. Interleukin-6 controls recycling and degradation, but not internalization of its receptors. *J Biol Chem*. **2021**;296:100434. DOI:10.1016/j.jbc.2021.100434.

Otto L, Rahn S, **Daunke T**, Walter F, Winter E, Möller JL, Rose-John S, Wesch D, Schäfer H, Sebens S. Initiation of Pancreatic Cancer: The Interplay of Hyperglycemia and Macrophages Promotes the Acquisition of Malignancy-Associated Properties in Pancreatic Ductal Epithelial Cells. *Int J Mol Sci*. **2021**;22(10). DOI:10.3390/IJMS22105086

Heckl SM, Mau F, Senftleben A, **Daunke T**, Beckinger S, Abdullazade S, Schreiber S, Röcken C, Sebens S, Schäfer H. Programmed Death-Ligand 1 (PD-L1) Expression Is Induced by Insulin in Pancreatic Ductal Adenocarcinoma Cells Pointing to Its Role in Immune Checkpoint Control. *Med Sci* **2021**;9(3). DOI.org/10.3390/medsci9030048.

Group Young Researchers in Inflammatory Carcinogenesis*, Wandmacher AM, Mehdorn A-S, Sebens S. The Heterogeneity of the Tumor Microenvironment as Essential Determinant of Development, Progression and Therapy Response of Pancreatic Cancer. *Cancers (Basel).* **2021**;13(19):4932. DOI:10.3390/cancers13194932

* Group members (in alphabetical order): Aldag L, Beckinger S, **Daunke T**, Philipp LM, Surrow A, Yesilyurt UU. These authors share first authorship and contributed equally to this work.

Mehdorn AS, Gemoll T, Busch H, Kern K, Beckinger S, **Daunke T**, Kahlert C, Uzunoglu FG, Hendricks A, Buertin F, Wittel UA, Sunami Y, Röcken C, Becker T, Sebens S. Biomarkers in Liquid Biopsies for Prediction of Early Liver Metastases in Pancreatic Cancer. *Cancers.* **2022**;14(19):1-18. DOI:10.3390/cancers14194605

Beckinger S, **Daunke T**, Aldag L, Krüger S, Heckl S, Wesch D, Schäfer H, Röcken C, Rahn S, Sebens S. Hepatic myofibroblasts exert immunosuppressive effects independent of the immune checkpoint regulator PD-L1 in liver metastasis of pancreatic ductal adenocarcinoma. *Front Oncol*. **2023**;13:1805. DOI:10.3389/FONC.2023.1160824

Daunke T† , Beckinger S†, Rahn S, Krüger S, Heckl S, Schäfer H, Wesch D, Pilarsky C, Eckstein M, Hartmann A, Röcken C, Wandmacher AM, Sebens S. Expression and role of the immune checkpoint regulator PD-L1 in the tumor-stroma interplay of pancreatic ductal adenocarcinoma. *Front Immunol*. 2023; 14(6):1-19. DOI:10.3389/fimmu.2023.1157397

† These authors have contributed equally to this work and share first authorship.

Hellmold D, Kubelt C, **Daunke T**, Beckinger S, Janssen O, Hauck M, Schütt F, Adelung R, Lucius R, Haag J, Sebens S, Synowitz M, Held-Feindt J. Sequential treatment with Temozolomide plus naturally-derived AT101 as an alternative therapeutic strategy: Insights into chemoresistance mechanisms of surviving glioblastoma cells. *Int J Mol Sci*. **2023**;24(10);9075. DOI:org/10.3390/ijms24109075

Conference Papers

Daunke T, Rahn S, Krüger S, Wesch D, Röcken C, Sebens S (2022) Analysis of immune checkpoint regulator PD-L1 on tumor and stroma cells in pancreatic cancer. German Pancreas Club, Lübeck (online)

Daunke T, Beckinger S, Rahn S, Krüger S, Wesch D, Röcken C, Sebens S (2022) *In situ* and *in vitro* analysis of immune checkpoint regulator PD-L1 in the tumor-stroma interplay of pancreatic ductal adenocarcinoma. Signal Transduction Society, Weimar

Daunke T, Beckinger S, Rahn S, Krüger S, Wesch D, Pilarsky C, Eckstein M, Röcken C, Sebens S (2022) Analysis of immune checkpoint regulator PD-L1 in the tumor-stroma interplay in pancreatic ductal adenocarcinoma. New Developments in Immunology, Inflammation and Infection, Borstel

Beckinger S, Aldag L., **Daunke T**, Krüger S, Rahn S, Heckl S, Wesch D, Röcken C, Sebens S (2022) The impact of the liver microenvironment on the immune checkpoint regulator PD-L1 in liver metastasis of pancreatic cancer. Signal Transduction Society, Weimar

Beckinger S, Aldag L., **Daunke T**, Krüger S, Rahn S, Heckl S, Wesch D, Röcken C, Sebens S (2022) The impact of immune checkpoint inhibitors on $CD8^+$ T cells in liver metastasis of pancreatic cancer. New Developments in Immunology, Inflammation and Infection, Borstel

Seemann C, Quaester S, Beckinger S, **Daunke T**, Philipp L-M, Sebens S (2022) Characterization of Premalignant and Malignant Pancreatic Cancer Cells in a Physiological and Inflamed Hepatic Microenvironment. Deutscher Krebskongress, Berlin

Quaester S, Beckinger S, **Daunke T**, Philipp L-M, Seemann C, Rahn S, Sebens S (2022) Inflammation and Migration: Influence of the hepatic microenvironment on the migration behavior of premalignant and malignant pancreatic ductal epithelial cells. Deutscher Krebskongress, Berlin

Hellmold D, Kubelt C, **Daunke T**, Beckinger S, Janssen O, Hauck M, Schütt F, Adelung R, Sebens S, Synowitz M, Held-Feindt J (2022) Influence of the tumor microenvironment on the therapeutic response of residual tumor cells after GBM resection. Deutsche Gesellschaft für Neurochirurgie, Köln

Hellmold D, Kubelt C, **Daunke T**, Beckinger S, Janssen O, Hauck M, Schütt F, Adelung R, Sebens S, Synowitz M, Held-Feindt J (2022) Insights into the influence of the tumor microenvironment on the response of residual tumor cells to chemotherapy after GBM resection. Brain Tumor Meeting, Berlin

Aldag L, Beckinger S, Heckl S, Krüger S, **Daunke T**, Röcken C, Wesch D, Sebens S (2022) Influence of the liver microenvironment on tumor cell growth and immune evasion in liver metastasis of pancreatic cancer. European Pancreatic Club, Kyiv (online)

Meschke E, Veil C, Beckinger S, **Daunke T**, Ussat S, Sebens S, Longardt AC, Schrappe M, Ankermann T, Knecht C, Bergholz R (2023) Leucine-rich α-2-glycoprotein 1 im Urin zur Diagnostik der Nekrotisierenden Enterokolitis – vorläufige Ergebnisse. Deutscher Chirurgie Kongress, München

Veil C, Meschke E, Beckinger S, **Daunke T**, Ussat S, Sebens S, Schrappe M, Klein M, Ankermann T, Knecht C, Bergholz R (2023) Leucine-rich a-2-glycoprotein 1 im Urin zur Differentialdiagnostik der Appendizitis - vorläufige Ergebnisse. Deutscher Chirurgie Kongress, München

Baumann L, Kayser C, Hauser C, Gundlach J-P, Beckinger S, **Daunke T**, Rahn S, Röcken C, Behrens H-M, Mehdorn A-S, Sebens S (2023) Do surgical tumor resection and chemotherapy lead to liver inflammation and outgrowth of liver metastases? Insights from a clinically adapted pancreatic cancer mouse model. European Pancreatic Club, Tyrol

Appendix

cancers

MDPI

Review

The Heterogeneity of the Tumor Microenvironment as Essential Determinant of Development, Progression and Therapy Response of Pancreatic Cancer

Group Young Researchers in Inflammatory Carcinogenesis [1,†], Anna Maxi Wandmacher [2], Anne-Sophie Mehdorn [3,‡] and Susanne Sebens [1,*,‡]

[1] Institute for Experimental Cancer Research, Kiel University and University Hospital Schleswig-Holstein Campus Kiel, Arnold-Heller-Str. 3, Building U30 Entrance 1, 24105 Kiel, Germany; stu208555@mail.uni-kiel.de (L.A.); silje.beckinger@email.uni-kiel.de (S.B.); tina.daunke@email.uni-kiel.de (T.D.); lisa.philipp@email.uni-kiel.de (L.-M.P.); stu207555@mail.uni-kiel.de (A.S.); stu212154@mail.uni-kiel.de (U.-U.Y.)

[2] Department of Internal Medicine II, University Hospital Schleswig-Holstein Campus Kiel, Arnold-Heller-Str. 3, 24105 Kiel, Germany; annamaxi.wandmacher@uksh.de

[3] Department of General, Visceral, Thoracic, Transplantation and Pediatric Surgery, University Hospital Schleswig-Holstein Campus Kiel, Arnold-Heller-Str. 3, Building C, 24105 Kiel, Germany; Anne-Sophie.Mehdorn@uksh.de

* Correspondence: susanne.sebens@email.uni-kiel.de

† Group members (in alphabetical order): Leon Aldag, Silje Beckinger, Tina Daunke, Lisa-Marie Philipp, Arne Surrow, Umut-Ulas Yesilyurt.

‡ These authors share last authorship and contributed equally to this work.

Simple Summary: Pancreatic ductal adenocarcinoma (PDAC) is still one of the deadliest cancers in western countries. It is commonly diagnosed at advanced stages and most anti-cancer therapies have failed to substantially improve prognosis of PDAC patients. PDAC is characterized by a profound inflammatory tumor microenvironment (TME) comprising various non-neoplastic cells e.g., myofibroblasts, macrophages, T cells and endothelial cells which can exhibit different functional phenotypes. Furthermore, the microbiome is altered in the tumor and other body compartments of PDAC patients adding to the great TME heterogeneity and its impact on PDAC development, progression and therapy responses. This review summarizes the recent knowledge on the diverse phenotypes of these different stromal components. A better understanding of tumor cells as well as TME heterogeneity and considering tumor-suppressing and tumor-promoting phenotypes might provide an important step towards a more effective treatment for this highly malignant tumor.

Abstract: Pancreatic ductal adenocarcinoma (PDAC) is commonly diagnosed at advanced stages and most anti-cancer therapies have failed to substantially improve prognosis of PDAC patients. As a result, PDAC is still one of the deadliest tumors. Tumor heterogeneity, manifesting at multiple levels, provides a conclusive explanation for divergent survival times and therapy responses of PDAC patients. Besides tumor cell heterogeneity, PDAC is characterized by a pronounced inflammatory stroma comprising various non-neoplastic cells such as myofibroblasts, endothelial cells and different leukocyte populations which enrich in the tumor microenvironment (TME) during pancreatic tumorigenesis. Thus, the stromal compartment also displays a high temporal and spatial heterogeneity accounting for diverse effects on the development, progression and therapy responses of PDAC. Adding to this heterogeneity and the impact of the TME, the microbiome of PDAC patients is considerably altered. Understanding this multi-level heterogeneity and considering it for the development of novel therapeutic concepts might finally improve the dismal situation of PDAC patients. Here, we outline the current knowledge on PDAC cell heterogeneity focusing on different stromal cell populations and outline their impact on PDAC progression and therapy resistance. Based on this information, we propose some novel concepts for treatment of PDAC patients.

check for updates

Citation: Group Young Researchers in Inflammatory Carcinogenesis; Wandmacher, A.M.; Mehdorn, A.-S.; Sebens, S. The Heterogeneity of the Tumor Microenvironment as Essential Determinant of Development, Progression and Therapy Response of Pancreatic Cancer. *Cancers* **2021**, *13*, 4932. https://doi.org/10.3390/cancers13194932

Academic Editor: Eva Diamantis Karamitopoulou

Received: 26 August 2021
Accepted: 14 September 2021
Published: 30 September 2021

Publisher's Note: MDPI stays neutral with regard to jurisdictional claims in published maps and institutional affiliations.

Keywords: PDAC; tumor stroma; immune cells; endothelial cells; CAFs; myofibroblasts; microbiome; macrophages; personalized medicine

1. Clinical Situation and Challenges

Pancreatic ductal adenocarcinoma (PDAC) is the 4th most frequent cause of cancer related deaths in western countries [1]. Since 80% of PDAC are diagnosed at advanced tumor stages, curative treatment options are limited. Accordingly, the overall 5-year survival rate is still less than 10% [1]. Besides late diagnosis, an early metastatic dissemination as well as a profound therapy resistance contribute to the clinical challenges in the treatment of PDAC and thereby to the patient's dismal situation [2,3].

Originating from pancreatic ductal epithelial cells (PDEC) or pancreatic acinar cells, PDAC can develop via different precursor lesions, such as pancreatic intraepithelial neoplasia (PanIN), intraductal papillary mucinous neoplasm (IPMN), mucinous cystic neoplasm, or other lesions [4], to an invasive carcinoma with the liver being the main site of metastasis [5,6]. During this multi-step progression various epi-/genetic alterations are acquired e.g., mutations in the oncogene *KRAS* which is one of the earliest genetic alterations and found in 99% of even early low-grade PanIN [7,8]. Besides genetic and epigenetic changes in PDEC and later on PDAC cells, the adjacent microenvironment also undergoes considerable alterations. These involve enrichment of different leukocyte cell populations (e.g., monocytes, lymphocytes), activation and modification of tissue resident cells (e.g., fibroblasts/stellate cells, endothelial cells), remodeling of the extracellular matrix (ECM) and changes of the microbiome [9–11]. Accordingly, composition and proportion of the microenvironment in close vicinity to precursor/PDAC cells are highly variable as they evolve concomitantly with PDAC progression. Furthermore, the TME is mutually dependent on both environmental factors (e.g., aging, exposure to lifestyle factors) and the (epi-)genetic make-up of PDEC and PDAC cells, respectively [12]. This indicates a dynamic co-evolution of neoplastic and non-neoplastic cells during pancreatic tumorigenesis being characterized and driven by a high heterogeneity of both different tumor cell clones and stromal cell populations. PDAC is characterized by a pronounced inflammatory tumor microenvironment (TME), which often accounts for the major tumor mass. Therefore, it is not surprising that therapies targeting genetically related alterations (e.g., altered signaling by mutant *KRAS* or sustained Epidermal Growth Factor Receptor (EGFR)-signaling caused by *EGFR* overexpression) have failed to improve treatment of PDAC patients as the blocked signaling pathways are bypassed by the stroma-mediated signaling which further sustains the cellular processes in the transformed cells [13,14]. Similarly, chemotherapeutic regimens have largely failed to improve the prognosis of PDAC patients because PDAC cells exhibit multiple strategies by which they evade the effect of cytostatic drugs. Importantly, these strategies are promoted by the stromal cells and additionally, the TME itself impairs the drug efficacy of PDAC (e.g., by metabolization of cytostatic drugs) [15–18]. In this context, the microbiome seems to play an important role, too. Several studies have already shown that the gut and tumor microbiome are altered in PDAC patients, promoting tumor progression and reducing treatment responses of PDAC cells, thereby substantially impairing survival of PDAC patients [11,19,20].

Finally, immune checkpoint inhibitors have revolutionized the treatment of various solid tumors even at advanced stages such as non-small cell lung carcinoma but have failed in the treatment of PDAC patients [21–23]. Besides a heterogeneous expression pattern of the immune checkpoint regulator programmed cell death 1 ligand 1 (PD-L1) on PDAC cells [24], another reason might be the high heterogeneity of the stromal compartment not only with respect to PD-L1 expression, but also regarding the cellular composition (inflamed versus non-inflamed tumors) [25,26].

Thus, experimental and clinical data strongly support the view that the failure of current therapeutic strategies is due to an insufficient consideration of the heterogeneity of

PDAC cells but also stromal cells. In order to improve our understanding of this heterogeneity, we herein outline the recent knowledge on TME diversity and its impact on PDAC development, progression and therapy resistance. Being aware of the numerous publications in this field in recent years, we apologize for only citing a selection. Furthermore, considering this knowledge we propose some concepts for novel therapeutic strategies to improve prognosis of PDAC patients.

2. Heterogeneity of the Tumor Cell Compartment in PDAC

Comprehensive (single cell) omics analyses revealed a high diversity of tumors at multiple levels, namely interpatient, intertumor and intratumor heterogeneity altogether providing an explanation for the noticeable differences in therapy responses and survival of cancer patients [27]. In stroma-rich PDAC, those analyses were combined with microdissection allowing a distinct investigation of tumor and stromal cells. In recent years, mainly three studies revealed substantial insights into interpatient heterogeneity. Collisson et al. classified PDAC into "classical", "quasi-mesenchymal" and "exocrine-like" subtypes. Besides differences in the expression profile, the classical phenotype was an independent prognostic factor for longer overall survival of resected PDAC patients and classical PDAC lines were more resistant towards Gemcitabine treatment than cell lines with a quasi-mesenchymal phenotype [28].

Moffitt et al. identified two tumor cell subtypes ("basal-like" and "classical", the latter one overlapping with those identified by Collisson et al.) but additionally two stromal subtypes ("normal" and "activated"). Here, patients with a tumor of the "basal-like" subtype or exhibiting an activated stroma had a worse prognosis compared to either corresponding subgroup. However, basal-like tumors seemed to show better responses towards adjuvant therapy. Importantly, the normal stroma signature was associated with high expression of genes typical for pancreatic stellate cells (PSC), while an activated stroma signature was characterized by high expression of genes related to macrophages and myofibroblasts, both being abundant in the PDAC stroma [29].

Finally, Bailey et al. identified four subtypes, namely "squamous", "pancreatic progenitor", "immunogenic" and "aberrantly differentiated endocrine exocrine (ADEX)". These subtypes clearly differed with respect to genetic and epigenetic alterations as well as transcription profiles. Additionally, the "immunogenic" subtype was characterized by an enrichment of different immune cell subsets and enhanced immune evasion pathways e.g., mediated by the immune checkpoint regulators Cytotoxic T-Lymphocyte-Associated Protein 4 (CTLA-4) and Programmed cell death protein 1 (PD-1) [30].

Extending these findings, Birnbaum et al. compared the tumor subtypes identified by Collisson, Moffitt and Bailey and confirmed the independent prognostic value of the classification from the latter two studies [31]. Additionally, Rashid et al. provided evidence that a tumor classification into two subtypes (basal-like and classical) according to Moffitt et al. exhibits the highest robustness and clinical relevance by demonstrating that basal-like tumors showed a strong resistance to FOLFIRINOX compared to classical tumors [32]. Although all studies revealed important insights into interpatient tumor heterogeneity, prospective trails are still needed to validate the clinical utility of this tumoral subtyping in particular with respect to optimized treatment.

With respect to intratumor heterogeneity, it is assumed that phenotypic and genotypic diversity of tumor cell clones within (primary and secondary) tumors originate from clonal expansions and differentiation hierarchies according to the current model of cancer stem cells (CSC) [33,34]. Thus, intratumor heterogeneity can occur and manifest on multiple levels based on the expansion of tumor cell clones with different genetic (driver as well as passenger mutations) and epigenetic alterations (hypermethylated DNA regions, histone modifications) as well as divergent differentiation stages (CSC versus non-CSC stage). These alterations in turn essentially contribute to different metabolic requirements (dependence on glucose, lactate or glutamine) as well as phenotypic diversity within the tumor mass resulting in e.g., proliferating versus resting, sessile versus motile/invasive

or therapy responsive or resistant tumor cell clones [35,36]. Important to note, expansion and evolution of certain tumor cell clones are highly dependent on the adjacent stroma which co-evolves with the different tumor cell clones during pancreatic tumorigenesis, applying to the primary as well as to the secondary context [37,38]. Although it can be speculated whether the metastatic tumor stroma induces the above-mentioned epigenetic, metabolic and thereby phenotypic alterations or selects for those clones that have acquired these alterations before leaving the primary tumor, a fundamental role of the stromal compartment in this heterogeneity determining process is meanwhile indisputable.

Thus, it is necessary to unravel all levels of tumor diversity and in particular stromal cell heterogeneity (Figure 1) to gain a complete picture of PDAC complexity which has to be considered for optimized treatment strategies.

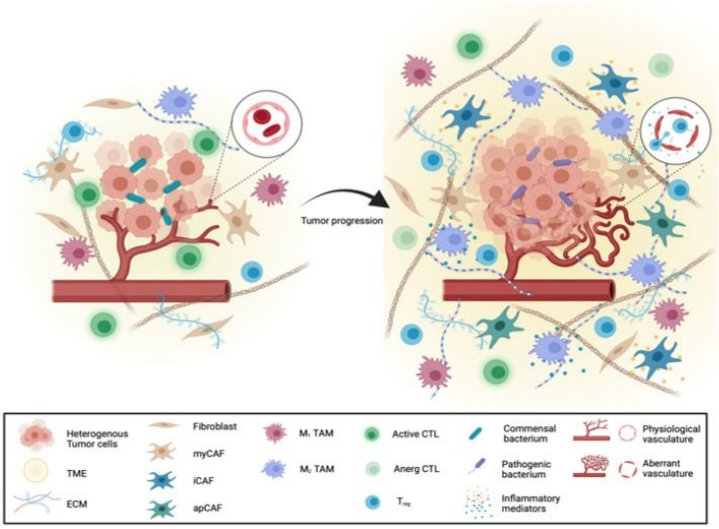

Figure 1. Pancreatic cancer is characterized by a high tumor and stroma heterogeneity. During pancreatic tumorigenesis, tumor cells acquire multiple alterations resulting in a heterogeneous pool of tumor cell clones. Along with the evolution of these divergent tumor cell clones, the tumor microenvironment (TME) also undergoes fundamental alterations involving, (i) activation of fibroblasts and transdifferentiation into carcinoma associated fibroblasts (CAFs) with different phenotypes (myCAF, iCAF, apCAF), (ii) alteration of the extent and composition of the extracellular matrix (ECM), (iii) enrichment of immunosuppressive and tumor-promoting immune cells e.g., tumor-associated macrophages with different phenotypes (M1 TAM versus M2 TAM), anergy cytotoxic T cells (CTL) and regulatory T cells (Treg), (iv) enrichment of pathological bacteria and extrusion of commensal bacteria, (v) elevation of inflammatory mediators and (vi) formation of new and modified blood vessels. Overall, this TME heterogeneity is an essential driver of PDAC development and progression. Figure created with BioRender.com.

3. Heterogeneity of the Stromal Compartment in PDAC

3.1. Heterogeneity of Carcinoma Associated Fibroblasts

The most abundant inflammatory stroma cells in PDAC are myofibroblasts, also termed carcinoma associated fibroblasts (CAF). CAF are abundant in primary PDAC as well as in metastases e.g., in the liver. During cancer development, several cell types can transdifferentiate into CAF. Besides PSC, adipocytes, monocytes, bone marrow-derived mesenchymal stem cells and endothelial cells (EC) can give rise to CAF in the pancreas [39–43]. In the liver, the main

source of CAF is hepatic stellate cells (HSC), with CAF also originating from hepatic sinusoidal endothelial cells or portal mesenchymal cells [44–50].

Under physiological conditions, most pancreatic fibroblasts are a heterogeneous group of desmin+ PSC which produce and maintain physiological levels of ECM proteins such as collagen IV, laminin, fibronectin and glycosaminoglycans. Thereby, these cells essentially contribute to the physiological pancreas homeostasis [51–56]. PSC are located at the base of the acini and contain high amounts of vitamin A vesicles [51]. Upon activation PSC lose these lipid vesicles and transdifferentiate into myofibroblasts, thereby increasing their proliferative and migratory potential, suppressing pro-apoptotic gene expression and secreting cell cycle promoting proteins [57–59]. Furthermore, myofibroblasts produce elevated amounts of ECM proteins at an altered composition, resulting in fibrosis. This fibrotic ECM is composed of less elastin and more fibronectin as well as crosslinked collagen type I and III [60]. Baron et al. distinguished two groups of pancreatic myofibroblasts: The first phenotype is characterized by production of ECM, and the second phenotype, called immune-activated PSC, exhibits and releases high expression levels of immunomodulating cytokines, interleukins and chemokines (e.g., chemokine (C-X-C motif) ligand 3 (CXCL3), Interleukin-33 (IL-33), IL-2) [61]. Exposure to stressful conditions including exogenous toxins, surgical intervention, inflammatory injury or mediators released by immune cells [56,62,63] promotes proliferation and activation of PSC into myofibroblasts leading to increased alpha-smooth muscle actin (α-SMA) expression. Stimuli leading to the transdifferentiation and activation of myofibroblasts/CAF are Transforming Growth Factor-beta (TGF-β), Platelet-derived Growth Factor (PDGF) and IL-6 [64–67]. Meanwhile, it is well known that CAF can exhibit different phenotypes and different CAF populations have been discovered in recent years. In the pancreas, major subgroups are myofibroblastic CAF (myCAF), inflammatory CAF (iCAF) and major histocompatibility complex II (MHCII) antigen presenting CAF (apCAF) [68]. MyCAF, which are tumor-adjacent and express high levels of α-SMA, are activated in a TGF-β dependent manner [69,70]. In contrast, iCAF are localized distant from the tumor, express low α-SMA levels and exhibit rather tumor-promoting and immunosuppressive properties by secreting inflammatory cytokines, like IL-6, CXCL12 and Granulocyte-Colony stimulating Factor (G-CSF). In contrast to myCAF, iCAF differentiation is stimulated by cancer-secreted IL-1 via the Januskinase-Signal Transducer and Activator of Transcription (JAK-STAT) pathway and antagonized by TGF-β. In vitro, PSC can differentiate into either myCAF or iCAF and even after this differentiation, iCAF can transdifferentiate into tumor-suppressive myCAF [68,69]. These findings strongly support the existence of different (functional) CAF phenotypes which seem to be interchangeable and highly context dependent. In both murine and human tissues, Hutton et al. recently identified two further functionally distinct pancreatic fibroblast populations by cluster of differentiation 105 (CD105) expression. While CD105+ fibroblasts did hardly impact tumor growth in vivo, CD105- fibroblasts promoted anti-tumor immunity and suppressed tumor growth. Characteristics of the established myCAF and iCAF populations were found in either lineage, whereas all apCAF were CD105-. In contrast to myCAF and iCAF populations, CD105+ and CD105- pancreatic fibroblasts seemed not to be interconvertible [71].

As outlined above, CAF are the major source of ECM in the TME. Cross-linked and oriented collagens cause a stiffened matrix, which stimulates accelerated cell cycle progression in adjacent tumor cells and thus fuels tumor growth [72]. Besides, the dense stroma acts as a physical barrier for drugs and immune cells [69]. Neumann et al. showed that the response to chemotherapeutic treatment (e.g., Gemcitabine, Nab-paclitaxel) is reduced when tumor cells are directly cocultured with human CAF compared to monocultured tumor cells [73]. Furthermore, T cells are unable to infiltrate into the dense matrix, which might be one reason for the limited clinical success of immunotherapy in PDAC patients [74]. By compressing blood and lymphatic vessels, perfusion is impaired and the interstitial fluid pressure increased, which induces hypoxia mediated progression and promotes cancer invasiveness, respectively [75–78]. Hypoxia in turn selects the most malignant

cancer cells and through hypoxia-inducible factor 1 (HIF-1) suppresses tumor suppressor genes while promoting the metastatic cascade [79–82]. By promoting M2-like polarization in macrophages and increasing PD-L1 expression in cancer cells, tumor-associated macrophages (TAM) and dendritic cells (DC), HIF-1 supports immunosuppression in the TME [83–87].

Besides the ECM-mediated effects, CAF exert several direct effects on the tumor. Thus, CAF promote an immunosuppressive TME by selecting tumor-promoting immune cells and inhibiting tumor-suppressive ones. Hence, in a KPC mouse model, increased PD-L1 and PD-L2 expression was demonstrated on CAF compared to fibroblasts [88]. Multiple murine and human studies showed their capability of excluding cytotoxic T cells (CTL) from tumor islands and inhibiting T cell activity in multifaceted ways [88–91]. In a mouse model, Feig et al. found CAF-derived CXCL12 to coat PDAC cells and protect them from CD8+ T cell invasion [90]. Lakins et al. showed murine CAF to cross-present tumor-derived antigens on MHC I and upon contact with CTL, induce cell death via PD-1/PD-L2 and Fas/FasL interaction [91]. While preventing CTL functions, CAF recruit immunosuppressive immune cells, such as myeloid derived suppressor cells (MDSCs) and monocytes, and promote monocyte differentiation into M2-like macrophages via Macrophage-Colony Stimulating Factor (M-CSF) [92–96]. MDSC-promoting factors secreted by CAF include IL-6, Vascular Endothelial Growth Factor (VEGF) and M-CSF [97]. In PDAC, iCAF have been identified to be the major source of these immunomodulating ligands, which might explain their above-mentioned localization at the edge of the tumor [24,70,98–100]. Another CAF subpopulation found in murine and human PDAC and breast cancer are apCAF [101], which are characterized by expression of MHC II molecules and their capability to present antigens to CD4+ T cells. However, apCAF lack costimulatory molecules required to promote T cell proliferation. Thus, MHC II molecules on apCAF were hypothesized to act as decoy receptors and exert immunosuppression via induction of anergy in T cells or transdifferentiation into regulatory T cells (Tregs) [100]. Furthermore, CAF can enhance cell growth [102], induce Epithelial-Mesenchymal-Transition (EMT) thereby facilitating PDAC cell dissemination and metastasis and promote an apoptosis and drug resistant phenotype in PDAC as well as precursor cells in a paracrine manner [17,18,103,104].

The mechanisms of myofibroblasts/CAF generation and their functional impact on tumorigenesis apply also to HSC and the derived hepatic myofibroblasts (HMF) [105–107]. HSC make up 5% of all liver cells and share many properties with PSC [108,109]. In the physiological liver, HSC perform a variety of tasks to maintain organ homeostasis by paracrine secretion of hepatocyte mitogens such as Hepatocyte Growth Factor (HGF) and Epidermal Growth Factor (EGF), and they store 50–80% of all retinoids in the body [110–115]. In contrast in the inflamed liver, HMF essentially impact immune responses inducing infiltration of neutrophils and lymphocytes or by acting as professional antigen presenting cells (APC), while also inhibiting T cells via the expression of PD-L1 [116–120]. In a KPC mouse model, Costa-Silva et al. [105] demonstrated that PDAC-derived circulating exosomes are taken up by Kupffer cells inducing TGF-β expression in these liver resident macrophages. TGF-β in turn activates HSC to HMF leading to an increased production of fibronectin and collagen I and III. This pre-metastatic niche was shown to be crucial for the onset of PDAC metastases [105,121–124]. Recently, Bhattacharjee et al. also identified different CAF populations in murine and human liver tissues based on subpopulations previously characterized in pancreatic and breast cancer. Thus, most liver CAF exhibit a myCAF-like expression profile with high collagen and α-SMA levels, while a smaller subpopulation expresses less α-SMA, but more growth factors and cytokines, and is therefore defined as iCAF [125]. Besides the role in immunomodulation and ECM remodeling, HSC and HMF differentially impact cell growth of PDAC cells, thereby controlling outgrowth of liver metastases. Accordingly, Lenk et al. showed that both murine and human HSC inhibit PDEC and promote a dormant phenotype in an IL-8 dependent manner, while HMF promote reawakening of the dormant stage and enhance proliferation in a VEGF dependent fashion [106].

3.2. Approaches for Targeted Therapy of Carcinoma Associated Fibroblasts

In light of the broad impact of CAF on PDAC progression, immune modulation and drug response, targeting CAF, CAF-derived factors or factors leading to their generation have emerged as attractive targets for PDAC therapy (Table 1).

TGF-β, produced by CAF and being their main activator, enhances tumor progression and dampens the immune and therapy responses [126,127]. Thus, it represents a promising target to interfere with CAF function [128]. However, an early phase clinical trial testing the therapeutic efficacy of pharmacological TGF-blockade with the small molecule inhibitor Galunisertib in combination with chemotherapy for the treatment of unresectable PDAC did not reveal convincing results [129]. Additionally, data from a phase Ib clinical trial investigating Galunisertib in combination with the anti-PD-L1 antibody Durvalumab did not yield clinical improvements for patients with metastatic PDAC [130]. Of note, Özdemir et al. showed in a PDAC mouse model that complete depletion of α-SMA+ myofibroblasts led to enhanced tumor growth, decreased immune cell infiltration and increased number of Treg in the TME. These findings indicate that complete depletion of CAF is not a reasonable treatment strategy, as tumor-restraining CAF populations are eliminated, too. However, concomitant depletion of CAF and blocking of CTLA-4 decreased tumor growth and prolonged survival of PDAC bearing mice [131].

Furthermore, it has been shown that tumor derived ligands of the Sonic Hedgehog (Shh) signaling system leads to activation of stellate cells into CAF [132]. Based on this finding, Shh inhibitors were tested in preclinical and clinical trials to improve PDAC treatment. However, depletion or pharmacological inhibition of Shh reduced stroma formation but accelerated tumor growth of tumor bearing KPC mice [133]. In line with this finding, combined treatment of metastatic PDAC patients with Gemcitabine and Shh inhibitors, targeting the signal transducing component Smoothened (SMO), showed no superior effect compared to Gemcitabine monotherapy [134]. Another clinical trial investigated the efficacy of the SMO inhibitor Saridegib (IPI-926) in combination with FOLFIRINOX for treatment of patients with advanced PDAC demonstrating an antitumor activity along with acceptable safety [135]. However, since a study demonstrated that patients being treated with IPI-926 in combination with Gemcitabine showed even shorter survival times than patients treated with Gemcitabine alone, this study was terminated prematurely (see Infinity Pharmaceuticals company website) and other trials investigating the therapeutic efficacy of Hh inhibitors were withdrawn or stopped.

Due to the tumor boosting effect, achieved by depleting the entire CAF population, recent research has rather focused on stromal reprogramming than on stroma depletion by e.g., reversal of CAF activation or shifting the CAF populations. Since activated myofibroblasts can be reversed into a quiescent phenotype by retinoic acid [136], all-trans retinoic acid (ATRA) has been used for myofibroblast reversal. Thus, ATRA treatment of tumor bearing KPC mice resulted in an enhanced CTL infiltration in the tumor tissue, which was explained by reduced secretion of the chemokine CXCL12 by reverted stellate cells [88]. Another strategy aiming at a stromal (CAF) reprogramming is the treatment with Calcipotriol, which is a derivative of vitamin D. The vitamin D receptor itself is a transcriptional factor suppressing the activation of PSC. Treatment with Calcipotriol led to stroma remodeling and combined treatment with Gemcitabine reduced tumor growth and increased overall survival of PDAC bearing mice [137]. Recently, Biffi et al. demonstrated a phenotypic shift from tumor-promoting iCAF to tumor suppressive myCAF by JAK inhibition, which was associated with reduced tumor growth and increased collagen deposition in tumor bearing KPC mice, further impairing drug penetration into the tumor stroma [70]. This was also seen in clinical trials where the combination of a JAK inhibitor and chemotherapy did not prolong the overall survival [138].

Taken together, CAF represent a heterogeneous cell population in the TME of PDAC at the primary site as well as in metastases exerting diverse functions on other stromal cells (immune cells, EC) and PDAC cells. Importantly, CAF and their quiescent/non-activated counterpart, the stellate cells may exert tumor-restraining functions, which have been

taken into consideration for the development of stroma-targeted therapeutic strategies to improve PDAC treatment.

Table 1. Overview of the cited therapeutic approaches targeting carcinoma associated fibroblasts (CAF).

Study System	Targeting Strategy	Reference
Preclinical studies		
PKT mouse model	Myofibroblast depletion by Ganciclovir	[131]
PKT mouse model	Myofibroblast depletion by Ganciclovir + anti-CTLA-4 antibody	[131]
KPC mouse model	Depletion or pharmacological inhibition of Shh	[133]
KPC mouse model	Myofibroblast reversal by ATRA	[88]
KPC mouse model	Vitamin D derivative Calcipotriol + Gemcitabine	[137]
KPC mouse model	Phenotype shift by JAK inhibitor (AZD1480)	[70]
Clinical trials		
Phase 1b/2 clinical trial	TGF-β blockade by Galusertinib + Gemcitabine	[129]
Phase 1b clinical trial	TGF-β blockade by Galusertinib + PD-L1 antibody Durvalumab	[130]
Phase 1b/2 clinical trial	Shh blockade by Vismodegib + Gemcitabine	[134]
Phase 1 clinical trial	SMO inhibition by Saridegib (IPI-926) + FOLFIRINOX	[135]
Phase 3 clinical trial	JAK1/JAK2 inhibition by Ruxolitinib + Capecitabine	[138]

3.3. Heterogeneity of Macrophages

Besides CAF, macrophages are also found in high numbers in many tumor entities representing the most abundant leucocyte population in the TME [139], also applying to PDAC [140]. Other, but less abundant, myeloid cell populations in PDAC are DC and MDSC. Tjomsland et al. showed that increased numbers of DC in the peripheral blood are associated with a better survival in PDAC patients [141]. However, most human PDAC specimens are characterized by low numbers of DC [142] and even if DC are present, they are mostly located at the tumor margins [142], a finding which could be similarly found in a modified KPC mouse model [143]. DC comprise a variety of subtypes including conventional and plasmacytoid DC exhibiting distinct phenotypes [144]. Of note, DC are key APC for the activation of T cells. Accordingly, these cells essentially determine the efficacy of anti-tumor immunosurveillance and immunotherapeutic treatment strategies, such as immune checkpoint inhibition and vaccinations. As described for other stromal cell populations, also MDSC can exhibit different phenotypes. In humans, three major MDSC subsets were identified: polymorphonuclear (PMN)-MDSCs, monocytic (M)-MDSCs and "early-stage MDSCs" (e-MDSC) [145]. Trovato et al. demonstrated that the MDSC frequency in PDAC was significantly correlated with overall survival and metastatic disease in PDAC patients, but only in some patients the immunosuppressive activity of purified MSDC was detectable. However, this finding was ascribed only to the monocytic subset [146]. One reason for the activity and expansion of MDSC in PDAC seems to be CD200, a regulator of myeloid cell activity, which is expressed in the PDAC TME. Choueiry et al. showed that MDSC isolated from human PDAC tissues express elevated levels of the CD200 receptor, by which CD200 can activate MDSC. Additionally, they found in a mouse model that the CD200 blockade impaired tumor progression and enhanced the efficacy of PD-1 immune checkpoint inhibition [147] supporting the immunosuppressive nature of these cells. Besides, it was shown that MDSC decrease T cell proliferation and lead to an enhanced apoptosis of activated T cells [148]. However, the exact mechanisms by which

MDSC exert their immunosuppressive functions are still not fully elucidated and we refer to other excellent reviews on this cell type [149].

Owing to their prominent abundance in PDAC, we will focus in the following text mainly on the recent knowledge on TAM. TAM mainly originate from tissue resident macrophages or from blood derived monocytes which infiltrate into the injured tissue (e.g., due to cell infection or otherwise induced cell damage). Ontogeny studies in a murine PDAC model revealed that monocyte-derived TAM acquire functions such as antigen presentation, whereas embryonically-derived TAM show a more pro-fibrotic transcriptional profile indicating their role in ECM production and relating the origin of TAM to distinct functional phenotypes [150]. Importantly, in dependence on the environmental factors, monocytes/macrophages acquire different phenotypes exerting distinct functional effects. According to a simplified model, macrophages can differentiate into M1- and M2-macrophages. While interferon-gamma (IFN-γ) and bacterial lipopolysaccharide (LPS) promote polarization of pro-inflammatory M1-macrophages, IL-4, IL-13, IL-10 and TGF-β foster an anti-inflammatory M2-phenotype in humans [151–153]. Thus, the composition of the TME (e.g., oxygen level, amount and type of other stromal or tumor cells) impacts phenotype and effector function of macrophages and promotes the switch from one type to another, a process which also occurs under physiological conditions [154]. As outlined above, CAF promote an immunosuppressive environment e.g., via CXCL12 and M-CSF secretion thereby recruiting monocytes and promoting the accumulation of M2-polarized macrophages [90,155,156]. Moreover, a hypoxic TME provokes an M2-polarization, while an oxygen enriched microenvironment drives M1-polarization [83]. In a murine PDAC model, PDAC cell derived small extracellular vesicles (sEV) covered with Ezrin were shown to foster a polarization towards an M2-phenotype and supporting metastasis formation in the liver [157]. Studies in another PDAC mouse model showed that uptake of PDAC-derived exosomes by Kupffer cells contributes to formation of a pre-metastatic niche in the liver involving the recruitment of bone marrow-derived macrophages [105]. Granulin, expressed by circulating monocytes and hepatic metastasis-associated macrophages, leads to activation of HSC into HMF thereby promoting liver metastasis formation [158]. Thus, CAF and TAM maintain a vicious stimulatory cycle that sustains and further fuels itself, contributing to a tumor-promoting TME.

M1-macrophages secrete different pro-inflammatory cytokines such as IL-12, IL-23 and express elevated levels of B7 family members (B7-1, B7-2) and MHC II for appropriate activation of a TH1 response by which these cells foster anti-tumor effects [159]. In contrast, M2-macrophages secrete anti-inflammatory cytokines such as IL-10, TGF-β and others to prevent T cells from effectively exerting their anti-tumor functions [160].

Although the frequency and phenotype of macrophages are subject to high dynamic variation of the pancreatic microenvironment during tumorigenesis [140], TAM in PDAC predominantly exhibit M2-characteristics. These are associated with diverse pro-tumoral effects including promotion of tumorigenesis, immunosuppression, metastasis acceleration and chemotherapeutic resistance [159]. In primary PDAC, a high infiltration of macrophages, particularly CD163+ macrophages, is observed [24,140,161–163], indicating an M2-type which has been associated with a poor prognosis and decreased survival [162–165]. Additionally, the number of TAM is inversely associated with the maturity of the tumor stroma, as an immature (highly cellular and collagen poor) stroma correlates with an increased the number of TAM [163]. As M2-macrophages secrete a plethora of growth factors, cytokines and chemokines (e.g., IL-10, IL-6, Tumor Necrosis Factor-alpha (TNF-α), TGF-β, chemokine (C-C motif) ligand 20 (CCL20)), they are potent inducers of the EMT [161,166]. Furthermore, PDAC tumor growth and metastasis formation are dependent on phosphatidylinositol 3-kinases (PI3Kγ) expression in macrophages [167]. Of note, TAM can co-exist as M1- or M2-macrophages or also intermediate forms in the TME which are associated with anti- or pro-tumoral functions [168]. Accordingly, Helm et al. could demonstrate that human PDAC-derived TAM can exhibit both M1- and M2-properties and that also M1-macrophages are able to increase migratory and invasive abilities of PDAC cells [161,168]. In line with these findings, Chen et al. showed that M2-

polarized macrophages cause inflammation via IL-1β release. This increased IL-1β release in turn promotes EMT induction and thereby formation of metastases in an orthotropic PDAC mouse model [169].

Macrophages also contribute to apoptosis and therapy resistance of PDAC. Buchholz et al. showed that murine and human macrophages can rapidly metabolize and inactivate the chemotherapeutic drug Gemcitabine resulting in profound therapy resistance [15]. Another study could show that murine bone marrow derived macrophages when exposed to PDAC cells release pyrimidine species, among others deoxycytidine, which inhibits gemcitabine through molecular competition representing another mechanism of macrophage mediated chemoresistance [170]. Liu et al. suggest that macrophages contribute to immunosuppression and failure of immunotherapies by demonstrating an accumulation of MDSC and M2-polarized TAM in tumoral lesions of different PDAC mouse models which is accompanied by a reduction of CTL and T helper cells. Besides, the number of M2-macrophages increased after application of Gemcitabine in this model system, which could be another mechanism for drug resistance [171]. Weizman et al. identified in humans another TAM-mediated mechanism of chemoresistance via upregulation of cytidine deaminase (CDA) which leads to reduction of Gemcitabine-induced apoptosis. CDA is the enzyme which transports chemotherapeutics into cells and is responsible for their metabolization [172]. Using a genetic mouse model, Binenbaum et al. revealed that TAM communicate with cancer cells via so called macrophage-derived exosomes which are internalized by cancer cells leading to reduced Gemcitabine concentrations by upregulation of CDA in the PDAC cells [173]. Moreover, tumor-derived exosomes can be taken up by human and murine macrophages, thereby increasing expression of the immune checkpoint molecule PD-L1 on these cells and promoting macrophage-mediated immune suppression. Uptake of tumor-derived exosomes also alters the cytokine secretion (IL-6, IL-1β, IL-10 and TNFα) of macrophages thereby facilitating several pro-tumoral functions [174].

3.4. Approaches for Targeted Therapy of Macrophages

As macrophages exert diverse pro-tumoral effects e.g., promoting an immunosuppressive TME and drug resistance, these stromal cells have been qualified as a reasonable target for cancer therapy (Table 2). Accordingly, several preclinical and clinical trials targeting macrophages have been conducted. One approach to simultaneously harness multiple immune cell types including macrophages against cancer cells is the treatment with CD40 agonists [175]. CD40 is a cell surface receptor primarily expressed by B cells, DC and myeloid cells including macrophages. Through interaction with its ligand CD40L (expressed on CD4+ T cells), CD40 is activated. This activation results in various physiological effects including increased expression of MHC II and T cell costimulatory receptors on its target cells [175,176]. Consequently, antigen presentation and CTL activation are promoted. Moreover, in the KPC mouse model, CD40 agonist treatment resulted in macrophage activation with increased expression of matrix metalloproteinases. Via this mechanism, macrophages reduced the pronounced PDAC-associated desmoplasia [177]. Recently, macrophage-mediated stroma depletion and reprogramming towards an M2-phenotype were confirmed for human PDAC by translational data obtained from a clinical trial that assessed the CD40 agonist Selicrelumab [178]. Moreover, in a PDAC mouse model, CD40 agonists synergized with checkpoint inhibitors [179]. Whilst early clinical trials suggested a positive clinical effect of CD40 agonist monotherapy or combination with Nivolumab [177,180], this could not be confirmed in phase II clinical trials [181]. However, multiple clinical trials evaluating CD40 agonists for the treatment of PDAC in combination with chemotherapeutic or targeted agents are ongoing (NCT03214250; NCT04536077; NCT04807972; NCT04888312) and may yield more promising results. Furthermore, the combination of an anti-PD-1 antibody with Gemcitabine showed a beneficial effect in a murine PDAC liver metastasis model, which was explained by an increase of M1-macrophages and a TH1 response [182].

Table 2. Overview of the cited therapeutic approaches targeting macrophages.

Study System	Targeting Strategy	Reference
Preclinical studies		
KPC mice	CD40 agonist treatment by CP-870,893	[177]
KPC mice	CD11b agonist treatment by ADH-503	[183]
C57BL/6 mice including Batf3 KO, CD40 KO, MyD88 KO, STING KO and IFNAR KO	CD40 agonist treatment by FGK45 combined with anti-PD-1 by RMP1-14 and/or anti-CTLA-4 by 9H10	[179]
Clinical studies		
Phase1 clinical trial	CD40 agonist treatment by Selicrelumab	[178]
Phase 1b clinical trial	CD40 agonist treatment by Sotigalimab in monotherapy or in combination with PD-1 blockade by Nivolumab	[180]
Phase 2 clinical trial	CD40 agonist treatment by Sotigalimab in monotherapy or in combination with PD-1 blockade by Nivolumab	[181]
Phase 1b/2 clinical trial	CD40 agonist treatment by Sotigalimab in combination with PD-1 blockade (Nivolumab) + Gemcitabine + Nab-Paclitaxel, or Sotigalimab + Gemcitabine + Nab-Paclitaxel.	NCT03214250
Phase 2 clinical trial	Addition of recombinant fms-like tyrosine kinase 3 (Flt-3) ligand (CDX-301) to the CD40 agonistic antibody (CDX-1140)	NCT04536077
Phase 2 clinical trial	modified FOLFIRINOX (mFFX) combined with ABBV-927 with or without Budigalimab	NCT04807972
Phase 1b/2 clinical trial	CD40 agonist Mitazalimab in combination with modified FOLFIRINOX	NCT04888312

Since specific targeting of macrophages spares other immunosuppressive monocytic cell populations which may impair the therapeutic efficacy, targeting of the integrin CD11b/CD18 which highly expressed on several myeloid cell subsets has been suggested as a promising strategy for PDAC treatment. Using the CD11b small-molecule agonist (ADH-503) in KPC mice, a partial activation of CD11b along with TAM repolarization was observed. In addition, increased numbers of immunosuppressive myeloid cells in tumor tissues were observed as well as enhanced dendritic cell activity. Thus, this strategy targeting multiple immunosuppressive myeloid cells led to an improved antitumor T cell response which might be even more effective in combination with immune checkpoint inhibitors [183].

However, to date no convincing strategies targeting macrophages have been elaborated and implemented in treatment of PDAC patients. One explanation might be that as demonstrated for CAF, macrophages represent a heterogeneous cell population exerting highly context-dependent pro- and anti-tumoral effects. Thus, this dynamic phenotype

switching, which also seemed to be influenced by the different therapeutic strategies, have to be considered in an effective and sustainable anti-tumor therapy of PDAC patients.

3.5. Heterogeneity of T Cells

Although we focus on T lymphocytes in this article, we want to briefly mention the other group of lymphocytes, namely the B cells. The role of B cells in PDAC is still controversially discussed but in general, B cells are described to be rather tumor promoting. Thus, Pylayeva-Gupta et al. showed that B cells secrete IL-35, which promotes the proliferation of tumor cells [184]. Furthermore, coculture of B cells isolated from PDAC patients enhanced the production of collagen by fibroblasts, resulting in ECM remodeling [185]. In a mouse model, it was shown that B cells are recruited by the B cell chemoattractant CXCL13 already during PanIN formation. Similarly, accumulation of B cells was also observed in PanIN lesions in PDAC patients [184,185]. Overall, there are not a lot of studies focusing on B cells in PDAC but it might be useful to investigate further on B cells in order to understand the complex microenvironment better.

Besides diverse CAF and macrophage phenotypes, different T cell populations can be found in the TME of the primary tumor and metastases in PDAC patients. Owing to their different effector phenotypes, T cells essentially impact the process of tumor and metastases formation in several ways. In general, an increase of immunosuppressive (T) cells can be observed during PDAC development, while tumor directed immune functions are impaired and/or even lost [140,186,187]. Key players of the immune response against tumor cells are CD8+ CTL. Accordingly, several studies showed that a high tumor infiltration of CD8+ CTL is associated with a longer overall survival of PDAC patients [188–191].

Rahn et al. showed in human PDAC tissues that CTL are predominantly present in the TME and less in close proximity to PDAC cells [24]. One reason for this can be seen in the desmoplastic stroma containing the ECM which acts as a physical barrier for immune cells and in particular CTL [69,192]. Similar findings were reported on liver metastases. Accordingly, in a KPC mouse model small metastatic lesions in the liver show a high CD8+ T cell infiltration compared to large metastatic lesions. Furthermore, in small lesions CD8+ T cells express CD69 and no PD-1, indicating that these CTL still exhibit their effector phenotype, while in large metastatic lesions CTL express PD-1 but no CD69, indicating T cell exhaustion [193]. Importantly, this exhausted state is characterized by elevated expression of inhibitory receptors (PD-1, CTLA-4 and T cell immunoglobulin domain and mucin domain-3 (TIM-3)), decreased production of cytotoxic molecules (perforin, granzyme A/B and granulysin), decreased production of chemokines (TNF-α and IFN-γ) and higher CTL apoptosis [194,195]. For optimal CTL survival and effector function, CD4+ T helper cells are pivotal. In line with this finding, a high tumor infiltration of CD8+ CTL together with CD4+ T cells correlate with a better prognosis for PDAC patients [188,189]. CD4+ T cells are another very heterogeneous T cell population, as they can differentiate into divergent subsets (TH1, TH2, TH17 and Treg). The differentiation of TH0 helper cells into different subsets is dependent on cytokines (IL-12, IL-4, TGFβ, IL-6 and IL-2) in the microenvironment [196]. The different subsets are characterized by expression of distinct cytokines and therefore show divergent impacts on all cells in the TME. Similar to CAF and macrophages, the effects can be either tumor-promoting or tumor-suppressing.

TH1 cells are regarded as tumor-suppressing as they exert various immune response activating functions e.g., they release IFNγ, which promotes recruitment of CTL, M1-macrophages and Natural Killer (NK) cells, and IL-2 which activates CTL [197,198]. On the other hand, IFNγ also induces PD-L1 expression on tumor cells, T cells, myofibroblasts and macrophages, thereby supporting CTL inhibition and immune escape in PDAC [199].

However, PDAC cells and the TME rather promote differentiation of TH2 cells which are regarded as immune-suppressing and thereby tumor-promoting [200], mainly because of the release of cytokines like IL-4, IL-5, IL-6, IL-10 and IL-13 [187]. IL-4 and IL-10 foster the differentiation of monocytes into M2-macrophages [201], IL-4 and IL-13 trigger the collagen synthesis in myofibroblasts thereby contributing to ECM remodeling [202] and

IL-13 has been shown to enhance growth of PDAC cells [203]. Accordingly, elevated levels of TH2 cytokines can be detected in plasma samples [187] and the TME of PDAC patients comprises higher numbers of TH2 cells compared to TH1 cells [204]. Moreover, high plasma levels of TH2 cytokines in patients with resectable PDAC are associated with a shorter survival [205].

Furthermore, human PDAC tissues contain higher numbers of TH17 cells compared to normal pancreatic tissue, which is associated with a shorter median survival of PDAC patients [206]. TH17 cells are regarded mainly as tumor-promoting because this T cell subset is characterized by elevated release of IL-17, IL-21 and IL-22 [197]. Importantly, IL-17 has been shown to enhance initiation and progression of PanIN in a murine PanIN model, thus being a trigger in early pancreatic tumorigenesis [207].

Another important immunosuppressive cell population in PDAC tissues are Treg. Especially in human PDAC, Tregs are mostly located in the stroma and only rarely in the epithelial layer of pancreatic ducts. Furthermore, Hiraoka et al. demonstrated a significant increase in the number of Treg during progression from low grade PanIN to an invasive PDAC. Additionally, a high prevalence of Treg in PDAC is significantly correlated with distant metastases, advanced tumor stage and high tumor grade as well as poorer prognosis [208,209]. The mechanisms by which Treg enrich in human and murine PDAC can be diverse e.g., tumor associated Treg can derive from peripheral Treg recruitment, expansion of tissue resident Treg, differentiation from local naïve T cells or conversion of conventional T cells [210]. Here, tumor- or CAF derived TGF-β can induce conversion of CD4+ CD25- T cells into Treg [211,212]. It was also shown that Forkhead box protein 3 (FoxP3) expressing tumor cells recruit Treg by directly trans-activating CCL5 [213]. Yang et al. observed a correlation of highly expressed secreted frizzled-related protein 4 (SFRP4) and Treg infiltration in tumors of KPC mice and PDAC patients [214]. Shen et al. speculated that PDAC cell-derived sEVs induce an enrichment of human FoxP3+ Treg and further an overexpression of immune checkpoint molecules PD-1, PD-L1, CTLA-4 and TIM-3 as well as an enrichment of FoxP3+ Treg [215]. Finally, L1 cell adhesion molecule (L1CAM) expression in the pancreatic ductal epithelium was shown to promote enrichment of human Treg in PDAC by e.g., enhancing migration of Treg, decreasing proliferation of CD4+ effector T cells and promoting conversion into a CD4+CD25-CD69+ regulatory T cell phenotype [216]. Moreover, these CD4+CD25-CD69+ Treg are detectable at high numbers in human PDAC tissues and correlate with nodal invasion and higher grading in PDAC patients [216]. One mechanism by which Treg suppress the anti-tumor response is by interaction of CTLA-4 with CD80/CD86 on DC leading to a reduced expression of MHC class II, CD40 and CD86 molecules, all being important for Treg maturation and activation. Besides, tumor-associated DC express Indolamine-pyrrole 2,3-dioxygenase (IDO), which suppress T cell responses and promote immune tolerance [217]. Moreover, Treg crosstalk with and are dependent on MDSCs as in a PDAC mouse model, depletion of MDSC led to a reduced recruitment and/or induction of Treg in pancreatic tumors and development/expansion of Treg seems to require a direct cell–cell interaction with MDSC [148]. Furthermore, TGF-β is not only a trigger for Treg development but also production of reactive oxygen species (ROS) by these cells contributing to oxidative stress in the TME [218].

Finally, γδ T cells represent a promising tumor-suppressive T cell population because of their ability to recognize antigens in an MHC-independent manner, to present antigens to CD3+ αβ T cells as well as their phagocytic properties. γδ T cells have a prevalence of 1–10% in the blood [219]. In human PDAC tissues, γδ T cells are mainly found in the tumor stroma or adjacent to or within ductal epithelium [220]. γδ T cell infiltration can be promoted by CAF derived CXCL12 [221,222]. However, the presence of γδ T cells is not sufficient to exert potent anti-tumor responses, because it has been shown that Galectin-3 which is expressed on PDAC cells but also αβ- and γδ T cells, inhibits T cell proliferation and is thus regarded as an intrinsic tumor escape mechanism [223,224]. Furthermore, kynurenine, a downstream metabolite of IDO, was identified as an inhibitor of γδ T cell

cytotoxicity and proliferation in PDAC [225]. However, Daley et al. showed that γδ T cells can inhibit αβ T cell activation via checkpoint receptor ligation leading to suppression of CD4+ and CD8+ T cells and acquisition of an activated CD44+CD62L- phenotype. Additionally, γδ T cells were shown to decrease TNF-α expression of αβ T cells in vitro. Importantly, these processes can be reversed by PD-L1 blockade suggesting that γδ T cells are important modulators of a checkpoint receptor-dependent immunosuppression and pinpoint also to a tumor-suppressing role of these cells in PDAC [226].

First attempts have been undertaken to consider this T cell heterogeneity to provide a rationale for patient stratification and optimized treatment choice. Depending on the number of infiltrating lymphocytes, tumors have been categorized into immunological subtypes: T cell inflamed ("hot tumors") or non-T cell inflamed ("cold tumors"). Owing to the low T cell infiltration especially of CD8+ CTL, PDAC is mostly characterized as a cold tumor [227]. Importantly, immunotherapies are often not effective in "cold" tumors explaining their common failure in PDAC [25,228].

3.6. Approaches for Targeted Therapy of T Cells

Since single agent immunotherapy with cancer vaccines or immune checkpoint inhibitors has failed so far in clinical trials [21,22,229,230], multi-agent combinations and combinations with radiotherapy have been evaluated as treatment option for PDAC. In order to boost T cell responses against cancer cells, combinations of two checkpoint inhibitors (Durvalumab and Tremelimumab) targeting the CTLA-4 and PD-1/PDL-1 axes have been evaluated [231,232]. Moreover, clinical trials were designed to assess combinations of cancer vaccines (e.g., GVAX and CRS-207) and checkpoint inhibitors or checkpoint inhibitors with oncolytic viruses (Pelareorep) or chemokine receptor inhibitors (BL-8040) based on promising preclinical data [233–236]. To date these approaches have not yielded relevant clinical improvements for PDAC patients. However, a high number of clinical trials investigating innovative immune checkpoint inhibitor-based combinations (e.g., with IL-6 antagonists (NCT04258150), agonists of stimulator of interferon genes (NCT03010176) and kinase inhibitors (NCT04820179) are underway.

As outlined above, γδ T cells represent an attractive effector T cell population for cancer therapy as they recognize antigens and kill target cells MHC independently. Thus, bispecific Abs binding CD3 or Vγ9 on γδ T cells and HER2/neu on PDAC cells enhanced the cytotoxicity of γδ T cells via granzyme B and perforin release and led to a reduced tumor growth in a subcutaneous PDAC Xenograft model [219]. Furthermore, the tribody [(HER2)2xCD16] activated human γδ T cells and NK cells to lyse HER2 expressing PDAC cells via granzyme B release [237]. Additionally, monitoring of γδ T cells subpopulations in PDAC patient's blood and determination of their cytotoxicity can also help to optimize γδ T cell-based immunotherapy [238].

Depleting Treg could also be an option to improve PDAC therapy. As Treg express CCR5, a current phase1/2 clinical trial investigates the therapeutic efficacy of CCR2 and CCR5 inhibitors in advanced PDAC with the aim to reduce Treg, MDSC and M2-polarized TAM and to increase anti-tumor immunity [209]. The bispecific antibody ATOR-1015 [CTLA-4xOX40] induced CD8+ T cell activation and Treg depletion in several syngeneic tumor models including a PDAC model, thereby resulting in a tumor-specific and long-term immunological memory. Furthermore, ATOR-1015 enhanced the response to PD-1 blockade, thus providing a reasonable combination with PD-L1 inhibitors [239]. However, depletion of the entire Treg population might bear the risk for the development of autoimmunity. Additionally, preclinical studies in a PDAC mouse model demonstrated that Treg depletion does not lead to diminished immunosuppressive activity and accelerates tumor growth. Since Tregs release high amounts TGF-β, Treg depletion resulted in a reduced TGF-β levels by which in turn tumor-restraining α-SMA+ CAF were reprogramed into iCAFs. Furthermore, increased numbers of myeloid cells were observed in the tumors indicating that specific targeting of this particular T cell population essentially alters the

stroma cell dynamics in the TME by which unexpected tumor promoting effects might be induced [240].

In summary, PDAC-associated T cells are characterized by a great diversity exemplified by their abundance (high versus low numbers), spatial localization (in close proximity to tumor cells versus located in the TME) and effector phenotype (activated versus anergy/exhausted). Adding to this huge complexity, distinct T cell populations exert both tumor-promoting and tumor-suppressing functions. Importantly, the immunological TME composition and overall immunity in a tumor and patient, respectively, seem to be highly dependent on a variety of host intrinsic (e.g., genetics) and extrinsic factors (e.g., exposure to pathogens or environmental factors) [241] defining the above-mentioned parameters which have to be considered for an effective anti-PDAC therapy.

3.7. Heterogeneity of Endothelial Cells

In general, human PDAC tissues exhibit a high microvascular density and poorly perfused blood vessels, the latter showing a heterogeneous distribution pattern in PDAC subtypes [242,243]. Moreover, a high microvascular density along with a diminished integrity of these microvessels is associated with disease progression and poorer survival in PDAC patients [244]. This immature vasculature and the high intratumoral pressure in PDAC due to the pronounced desmoplastic stroma results in an irregular as well as disorganized tubular architecture. Murine and human studies revealed that this in turn impairs drug delivery, suppresses lymphocyte infiltration and increases hypoxia within the tumor mass [133,245–247]. In general, blood vessels support tumor growth by enabling influx of nutrients and oxygen. In addition, EC also affect tumor cells, stromal cells in the TME and therapy responses [248–250].

Tumor angiogenesis is induced by proangiogenic factors such as VEGF released by tumor and stromal cells [251]. Upon this "endothelial cell activation", changes in the gene expression profile and phenotypes of EC occur by which these cells exert their pleiotropic effects in the tumor [252,253]. Thus, increased expression levels of Vascular Endothelial Growth Factor Receptor (VEGF-R), EGF-R and diverse cell adhesion molecules (e.g., Intercellular Adhesion Molecule (ICAM), Vascular Cell Adhesion Molecule (VCAM), E-selectin) as well as an increased secretion of cytokines (e.g., IL-8) are observed in activated EC or tumor associated endothelial cells (TEC). These alterations essentially contribute to tumor inflammation and immune evasion in human as well as in murine tumors [254–260]. Thus, human derived material as well as murine xenografts revealed that TEC are not only morphologically distinct from their physiological counterparts, but also exhibit diverse genetic and phenotypic alterations by which these cells impact tumor development and progression as well as therapy responses. Furthermore, TEC can undergo Endothelial-Mesenchymal-Transition thereby giving rise to CAF and contributing to CAF enrichment in PDAC. In humans, this process seems to be mediated by inflammatory factors such as TNF-α [261–263].

Furthermore, Issa et al. demonstrated that upregulation of L1CAM expression on human PDAC-derived TEC increase adhesion and transmigration of PDAC cells to and through the PDAC-derived endothelium, thereby facilitating PDAC metastasis [264]. Sano et al. described that elevated expression of VCAM-1 on TEC promotes progression of PDAC as well as PanIN in a genetically engineered mouse model, but also increases the incidence of cancer-associated thrombosis in mice and patients, which is known as a poor prognostic factor in PDAC. Moreover, this is accompanied by an increased infiltration of immunosuppressive leucocytes into the tumor tissues. Blocking VCAM-1 reduces the number of thrombotic/thromboembolic events as well as infiltration of TAM and tumor-associated neutrophils and prolonged overall survival of treated mice [265]. In line with these findings, PDAC-derived TEC exhibit an enhanced expression of distinct adhesion molecules (e.g., E-selectin, ICAM-1, VCAM-1, Mucosal vascular address in cell adhesion molecule 1 (MAdCAM-1)) compared to EC from healthy pancreas. These PDAC-derived EC promote transendothelial migration of Treg thereby contributing to the immunosuppressive

TME in human as well as murine PDAC [266]. In contrast, downregulation of these adhesion molecules (e.g., ICAM-1/2, VCAM-1, MAdCAM-1, E-selectin) on TEC leads to a decreased infiltration of putative tumor-directed lymphocytes into the TME [209,267].

3.8. Approaches for Targeted Therapy of Endothelial Cells/Angiogenesis

Overall, these data indicate that TEC can exhibit different phenotypes and functions compared to their physiological counterpart, which is dependent on the tumor entity and TME composition e.g., the amount of macrophages which are a main source of VEGF. Importantly, the aberrant morphology of TEC and their altered expression profile of adhesion molecules are essential determinants for various malignancy-associated processes, such as immune evasion and drug resistance in PDAC patients [268]. Accordingly, TEC and angiogenesis, the latter being a hallmark of cancer, have been identified as promising targets for cancer therapy and many anti-angiogenic strategies have meanwhile been approved for the treatment of a variety of cancer entities. Demonstrated in preclinical and clinical studies, those strategies primarily aim at the inhibition of angiogenesis, thereby reducing nutrient supply and deactivating EC on the one hand [269–272] and normalizing the vasculature to improve drug delivery and immune cell access into the TME on the other hand [273–276]. Two commonly used anti-angiogenic drugs are Bevacizumab and Aflibercept, both binding to VEGF, and Aflibercept additionally binding to Placenta-derived Growth Factor (PGF). In addition, tyrosine kinase inhibitors (such as Sunitinib, Sorafenib, Pazopanib) that target VEGF-R2 e.g., expressed by TEC [277] are also FDA approved for anti-angiogenic cancer therapy. However, the above-mentioned strategies still fail to significantly improve overall or progression free survival of PDAC patients [278,279].

Accordingly, intensive research efforts are ongoing to identify predictive markers that allow for rational patient stratification in order to select the optimal therapeutic strategy to specifically target the aberrant vasculature in PDAC [280]. Considering the pleiotropic effects of TEC in PDAC, TEC targeting may be more effective in combination with e.g., immune checkpoint inhibitors or modified drugs (e.g., encapsulated forms) to optimize treatment strategies. Furthermore, more studies are required investigating the optimal timing for anti-angiogenetic therapies (particularly in combination with other therapies) in order to exert the maximum effect.

3.9. Heterogeneity of the Microbiome

In recent years compelling evidence has emerged that not only the TME but also the microbiome is altered in PDAC patients—in the tumor as well as in other body compartments. Experimental data support the view that the altered microbiome is not just a surrogate of the disease but rather essentially impacts development, progression and therapy responses of PDAC [11,19,20]. Miller et al. also identified an influence of the microbiome on the TME, thereby promoting PDAC development and explaining reduced therapeutic efficacy of several agents. Hence, ablation of the microbiome was shown to prevent PDAC in preclinical studies [281].

It is still not fully understood how bacteria, detectable in PDAC tissues, enter the pancreas. Potential mechanisms include the oral route or translocation from the lower gastrointestinal tract through the portal circulation or mesenteric lymph nodes [282]. Thus, it has been shown that human cystic pancreatic precursor lesions contain Fusobacterium nucleatum and Granulicatella adiacens, both bacterial populations commonly found in the oral cavity [283,284]. In line with this finding, increased amounts of Fusobacterium species were detected in PDAC tissues and correlated with a worse prognosis of PDAC patients [285]. Another study demonstrated that Gammaproteobacteria are the predominant bacterial species in human PDAC tissues, most of them being members of Enterobacteriaceae and Pseudomonadacea families [19].

It has been shown in patient suffering from malignant melanoma and lung cancer that the gut microbiome impacts the response to immunotherapy and chemotherapy. This finding suggests that the composition of the gut microbiome impacts activation of

the immune system [286–288] and thereby promotes cancer-associated inflammation, a mechanism which might also be relevant in PDAC. Of note, chronic pancreatitis (CP), being a risk factor for PDAC development, can be caused by microbial infections [289].

As outlined above, an inflammatory and desmoplastic environment supports various malignancy-associated processes, such as immune evasion and metastasis and impacts therapy responses [290–292], all processes related to EMT [293]. Importantly, a tumor-associated microbiome was shown to promote EMT, thereby leading to epithelial barrier alterations and tumor-promoting inflammation. In detail, it could be shown that infections by Fusebacterium nucleatum lead to the loss of membranous E-cadherin [294], a key step in EMT [11,295–297]. Owing to the fact that high levels of Fusebacterium are found in human pancreatic precursor lesions and PDAC tissues, it is reasonable that this might be one mechanism by which early EMT is induced in pancreatic tissues. Of note, EMT-associated alterations are already found in PDEC in human CP tissues [296] and lead to early PDEC dissemination prior to tumor formation in the pancreas in a murine mouse model [297]. Zhang et al. postulated that each microbial pathogen conquering the pancreatic tissue has the potential to induce EMT-related pathological changes [11]. Since EMT induction has been also linked to the acquisition of CSC properties and drug resistance [2,6,10], EMT/CSC induction might represent another mechanism by which the altered microbiome contributes to the pronounced therapy resistance in PDAC.

In this context, Geller et al. reported not only the presence of Gammaproteobacteria in human PDAC tissues but also that these bacteria, expressing the long form of the enzyme CDA, are able to metabolize the cytostatic drug Gemcitabine into its inactive form. These findings suggest that the presence of Gammaproteobacteria in PDAC tissues may contribute to Gemcitabine resistance in these patients [19].

Moreover, Riquelme et al. discriminated long-term survivor (LTS) PDAC patients showing a high bacterial alpha diversity from short-time survivor (STS) PDAC patients with a lower alpha diversity. They also demonstrated that the microbiome composition in PDAC tissues differs from that in normal tissues and that the gut microbiome accounts for 25% of the tumor microbiome, supporting translocation of bacteria from the gut into pancreatic tissues as one mechanism for bacterial PDAC tissue colonization [20]. Additionally, they determined greater numbers of CD3+ T cells, CD8+ T cells and granzyme B+ cells in LTS compared to STS PDAC patients, thus correlating a higher CTL infiltration with a higher microbiome diversity. These data indicate that the tumor microbiome composition influences both the extent of immune infiltration and the degree of CD8+ T cell activation in PDAC tissues [20]. It also suggests that alterations of the microbiome directly in the tumor but also in other body compartments (e.g., the gut) essentially contribute to shaping the patient's immune response. In line with these findings, it was shown in different tumor mouse models that the efficacy of the CTLA-4 inhibitor Ipilimumab depends on the presence of distinct commensal gut *Bacteroides* species (spp.) which apparently trigger TH1 immune responses, being important for the anti-tumor effects. Hence, administration of antibiotics decreased the therapeutic effect of Ipilimumab [298]. Moreover, this study also demonstrated that fecal microbiota transplantation (FMT) of human *Bacteroides* spp.-rich feces significantly increases the overall outcome of tumor bearing animals by markedly increasing the response to CTLA-4 blockade. Supporting these data, Tanoue et al. detected an 11-strain consortium of bacteria isolated from gut microbiota of human healthy control donors (HC) which can induce IFN-g+ CD8+ T cells to enhance the efficacy of immune checkpoint inhibitors in tumor-bearing mice [299]. Underscoring the therapeutic potential of FMT, a significant reduction in tumor growth was observed in PDAC bearing mice after FMT from PDAC LTS donors with no evidence of disease (LTS-NED) compared to mice obtaining FMT from STS patients or HC [20]. Moreover, tumors from mice treated with FMT of STS PDAC patients were larger than those from mice who received FMT of HC. Finally, short-term antibiotic treatment of tumor bearing mice which had received FMT from LTS-NED donors led to even larger tumors than those of untreated mice. These data suggest that certain PDAC-associated bacteria exert a tumor-promoting effect on the one

hand and that bacterial ablation by antibiotic treatment decreases the anti-tumoral efficacy of distinct bacterial species e.g., found LTS PDAC patients on the other hand.

3.10. Approaches for Microbiome Modulating Therapies

As already mentioned above, studies provide evidence that the response of cancer patients to blockade of the immune checkpoints PD-1/PD-L1 or CTLA-4 is influenced by the gut microbiome [298,299]. Tumor mouse models revealed that different microbiome compositions cause significant differences in response to treatment with PD-1/PD-L1 inhibitors [298] so that probiotics have been suggested as part of the anti-cancer therapy. Accordingly, Sivan et al. demonstrated reduced tumor growth and a beneficial response to anti-PD-1 therapy in melanoma bearing mice after oral administration of Bifidobacterium spp. containing probiotics. Furthermore, the superior anti-tumor effect from mice with a favorable microbiome composition could be transferred to other mice by FMT or co-housing [298,300]. In summary, these findings strongly support the therapeutic potential of FMT or certain diets/probiotics with the aim to restore the commensal (tumor-suppressing) microbiome and to displace the tumor-promoting microbiome. Combining such strategies with chemo- or immunotherapy might help to overcome therapy resistances and to improve PDAC patient prognosis.

4. Therapeutic Implications and Challenges of TME Targeting

The study by Rashid et al. revealed that consideration of different molecular subtypes e.g., those identified by [28–30], might be reasonable for stratifying PDAC patients for chemotherapy, as they provided evidence for efficacy prediction towards FOLFIRINOX treatment according to molecular tumor subtypes [32]. Adding to the multiple levels of tumor heterogeneity, stromal cell populations as well as the microbiome have been characterized by a high heterogeneity, too, implying both tumor-promoting and tumor-restraining functions. As outlined in the sections above, multiple therapeutic approaches have been developed and tested to target distinct TME components in order to improve treatment outcome of PDAC patients. However, many of these studies revealed unexpected results (e.g., by depleting the entire CAF population leading to even more aggressive tumors [131] or promising preclinical findings could not be confirmed in clinical trials [134]. Thus, until today, less than 5% PDAC patients receive a targeted therapy and significant improvements of survival are still missing [301]. Current clinical trials such as the "Precision-Panc" (NCT04161417) and the "Precision Promise" studies (NCT04229004) are ongoing with the aim to validate the therapeutic efficacy of novel individualized therapies in PDAC patients [302,303]. However, results from these trials are still pending.

The clinical failure of these strategies might also be explained by the use of inadequate preclinical models and/or an insufficient consideration of the stromal cell heterogeneity, to clearly discriminate which stromal phenotype is "friend or foe" [192,304,305]. For any kind of targeted and personalized therapy in cancer patients, pre-therapeutic samples and biopsies, respectively, are of pivotal importance and a critical determinant to assess inter- and intratumoral characteristics as well as changes during treatment courses. These allow identification of the most effective therapy and to eventually select therapies according to the profile identified [32]. In this context, surgically resected specimens provide the largest number of cells, reflect best tumor heterogeneity and enable pathologists to perform comprehensive analyses [306]. In cases of patients with an advanced disease, not being suitable for surgical resection or with recurrent tumors, fine needle aspirated (FNA) samples have been proven to be useful for identification of targets for targeted therapies. However, FNA samples only reflect a small portion of the tumor bearing the risk of not fully representing tumor and stroma heterogeneity [32,301,303]. Nonetheless, FNA-obtained samples are in certain cases the only option to obtain information on tumor and TME characteristics and help to provide individualized therapy to patients with metastatic disease whose tumor is not resectable. Liquid biopsies and analysis of cell free nucleic acids, circulating tumor cells or extracellular vesicles are additional methods to obtain information on tumor cell

characteristics. Repeated blood draws (or collection of other body fluids) are more feasible than repeated biopsy sampling and may therefore complement tissue-based analysis for longitudinal monitoring of PDAC dynamics and therapy response [307]. However, important players of PDAC biology, i.e., the TME and the microbiome are not considered in these approaches.

Of note, Birnbaum et al. already suggested to consider not only the PDAC tumor subtypes but also the stromal subtypes classified by Collisson et al., Moffitt et al. and Bailey et al. for targeted therapy in PDAC patients [28–31]. Even though targeting the TME based on stromal subtypes might be a more efficient therapeutic approach, a challenge will be to fully consider differences in distribution and extent of the TME at different sites (primary tumor versus metastases) which might be associated with divergent functional effects on PDAC development. Furthermore, the TME might be further differentially modified by chemotherapy [303,308]. Additionally, Torphy et al. identified a high stroma content as a factor for a favorable outcome in patients suffering from metastatic PDAC [309], further underscoring that the TME heterogeneity is a critical determinant for targeted stromal therapy.

The current knowledge gained from comprehensive preclinical and clinical trials demonstrating a rather limited efficacy of tumor and TME targeted therapies in PDAC patients, leads us to the following assumptions: (i) due to its extraordinary complexity and peculiarity, the TME in PDAC easily compensates pathways, interactions and effects that are modulated by mono-targeted therapies resulting in limited therapeutic efficiency, (ii) targeted therapies applied so far have impaired both tumor-promoting and tumor-restraining TME populations, thereby counteracting the beneficial therapeutic effects albeit it was intended to solely target the tumor-promoting cell populations, (iii) the functional impact of certain host-derived factors on PDAC development and on shaping therapy responses are still insufficiently understood and considered (e.g., the host microbiome) and (iv) the usage of reliable biomarker (not only in tumor tissue but also other compartments) for therapy decision making has still to be improved for treatment of this tumor entity.

Accordingly, concepts aiming at restoration and normalization of a physiological, tumor-restraining microenvironment, respectively, rather than at precisely targeting distinct TME components might be more effective strategies [180,310]. For example, Kocher et al. focused on the stroma in patients with locally advanced or metastatic PDAC and replenished the Gemcitabine-Nab-Paclitaxel chemotherapy with ATRA in a phase I clinical trial. Clinical safe and tolerable efficiency and successful reprogramming of the TME was detectable [311] which was also observed in other preclinical studies [137]. Another "normalization" or "reprogramming" strategy might be the modulation of the patient's microbiome. As outlined above, the microbiome substantially influences the efficacy of chemotherapeutic drugs in PDAC-patients [11,19,20] as well as the response to immune checkpoint inhibition [298]. Additionally, restoration of a tumor-restraining microbiome by application of distinct microbiome species, e.g., such as FMT, may not only overcome drug resistances, but also help to boost the patient's immune system to induce a long-term control of the tumor burden [11,20].

Overall, the above-mentioned studies and continuously elaborated novel concepts have essentially broadened our understanding of this challenging disease. However, additional studies are needed to further dissect the dynamics and heterogeneity of the TME regarding the tumor-promoting and tumor-restraining functions in order to translate this knowledge into personalized therapeutic concepts to improve the prognosis of PDAC patients. Consideration of this heterogeneity and its impact on PDAC development and therapy responses is enabled by collecting and comprehensively analyzing tumor, stroma and the patient's microbiome to generate an integrated tumor subtype. This identified subtype allows stratification of each patient for the individualized and most effective therapy (Figure 2).

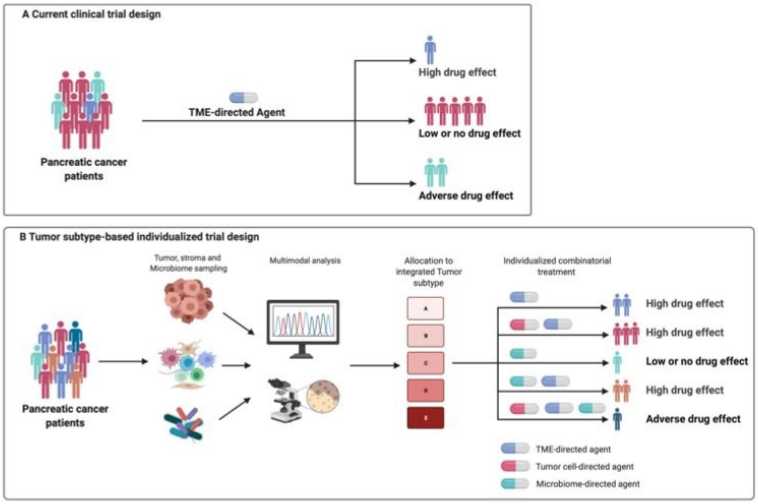

Figure 2. Current and future therapeutic concepts for the treatment of pancreatic cancer patients. (**A**) In current clinical trials, pancreatic cancer patients are not stratified according to distinct tumor and stroma characteristics. Accordingly, the given therapy exerts an anti-tumor effect only in few patients. However, in the majority of patients this strategy fails or has even adverse effects. (**B**) A tumor subtype-based individualized trial design implies sampling of the patient's tumor, stroma and microbiome prior to treatment and multimodal analysis of these samples will generate an integrated tumor subtype for each patient. Considering these tumor, stroma and microbiome characteristics, the identified subtype allows stratification of pancreatic cancer patients for the treatment strategy with the best predicted outcome. Figure created with BioRender.com.

5. Conclusions

Extensive preclinical and clinical evaluation of PDAC has resulted in detailed characterization of its complexity on multiple levels. In this article, we summarized how PDAC biology is determined by a plethora of cell types and microbiota shaping the TME and their context-dependent pro- or anti-tumorigenic characteristics. This challenging level of complexity is further increased by countless interactions between the involved cell types. In the future, increased efforts will be needed to translate these insights into TME heterogeneity into clinically meaningful benefits for PDAC patients. To this end, we propose comprehensive analysis of patient material (tumor, tumor stroma and microbiome) and the development of integrated tumor subtypes based on this data base. Respective integrated tumor subtypes may then serve for informed patient stratification in clinical trials and truly individualized therapeutic decisions.

Author Contributions: Conceptualization, S.S.; Supervision, A.-S.M. and S.S.; Visualization, A.M.W.; Writing—original draft, L.A., S.B., T.D., L.-M.P., A.S., U.-U.Y., A.-S.M. and S.S.; Writing—review and editing, all authors. All authors have read and agreed to the published version of the manuscript.

Funding: Funding by the Research and Training Group 2501 on Translational Evolutionary Research (RTG 2501 TransEvo, DFG for S.S.), by Deutsche Forschungsgemeinschaft (DFG, German Research Foundation)—Projektnummer 413490537 (for A.M.W.) and the Deutsche Krebshilfe (AZ 70112935 for S.S.) is acknowledged. The authors also acknowledge financial support by DFG within the funding program Open Access Publizieren.

Conflicts of Interest: All authors declare no conflict of interest. The funders had no role in the writing of the manuscript.

Abbreviations

ADEX: aberrantly differentiated endocrine exocrine; α-SMA: Alpha-smooth muscle actin; APC: Antigen presenting cells; apCAF: antigen presenting carcinoma associated fibroblasts; ATRA: All-trans retinoic acid; CCL: Chemokine (C-C motif) ligand; CAF: Carcinoma associated fibroblasts; CD: Cluster of differentiation; CDA: Cytidine deaminase; CP: Chronic pancreatitis; CSC: Cancer stem cells; CTLA-4: Cytotoxic T-Lymphocyte-Associated Protein 4; CXCL: chemokine (C-X-C motif) ligand; CTL: Cytotoxic T cells; DC: Dendritic cells; EC: endothelial cells; ECM: Extracellular matrix; EGF: Epidermal Growth Factor; EGFR: Epidermal Growth Factor-Receptor EMT: Epithelial-Mesenchymal-Transition; FNA: Fine needle aspirated; FMT: Fecal microbiota transplantation; FoxP3: Forkhead box protein 3; G-CSF: Granulocyte-Colony Stimulating Factor; HC: Healthy control donor; HGF: Hepatocyte Growth Factor, HIF-1: Hypoxia-inducible factor-1; HSC: Hepatic stellate cells; HMF: Hepatic myofibroblasts; iCAF: inflammatory CAF; ICAM: Intracellular Cell Adhesion Protein; IDO: Indoleamine-pyrrole 2,3-dioxygenase; IL: Interleukin; IFN-γ: Interferon-gamma; IPMN: Intraductal papillary mucinous neoplasm; JAK: Januskinase; L1CAM: L1 cell adhesion molecule; LPS: Lipopolysaccharide; LTS: Long-term survivor; PanIN: Pancreatic Intraepithelial Neoplasia; MAdCAM-1: Mucosal vascular addressin cell adhesion molecule 1; M-CSF: Macrophage-Colony Stimulating Factor MDSC: Myeloid-derived suppressor cell; MHC: Major histocompatibility complex; myCAF: myofibroblastic CAF; NED: No evidence of disease; NK: Natural killer; PDAC: Pancreatic ductal adenocarcinoma; PDEC: Pancreatic ductal epithelial cells; PD-1: Programmed cell death protein 1; PDGF: Platelet-Derived Growth Factor; PD-L1: Programmed cell death 1 ligand 1; PI3K: Phosphatidylinositol 3-kinase; PGF: Placenta-derived Growth Factor; PMN: polymorphonuclear; PSC: Pancreatic stellate cells; ROS: Reactive oxygen species; sEV: small extracellular vesicle; SFRP4: secreted frizzled-related protein 4; Shh: Sonic hedgehog; SMO: Single transducing component smoothened; STAT: Signal transducer and activator of transcription protein; STS: Short-term survivor; TGF-β: Transforming Growth Factor-beta; TAM: Tumor-associated macrophages; TEC: Tumor associated Endothelial Cells, TIM-3: T cell immunoglobulin domain and mucin domain-3; TME: Tumor microenvironment; TNF-α: Tumor Necrosis Factor-alpha; Treg: Regulatory T cells; VCAM: Vascular Cell Adhesion Molecule; VEGF: Vascular Endothelial Growth Factor, VEGF-R: Vascular Endothelial Growth Factor-Receptor.

References

1. Siegel, R.L.; Miller, K.D.; Fuchs, H.E.; Jemal, A. Cancer Statistics, 2021. *CA Cancer J. Clin.* **2021**, *71*, 7–33. [CrossRef]
2. Neesse, A.; Bauer, C.A.; Öhlund, D.; Lauth, M.; Buchholz, M.; Michl, P.; Tuveson, D.A.; Gress, T. Stromal biology and therapy in pancreatic cancer: Ready for clinical translation? *Gut* **2019**, *68*, 159–171. [CrossRef] [PubMed]
3. Michl, P.; Gress, T. Current concepts and novel targets in advanced pancreatic cancer. *Gut* **2013**, *62*, 317–326. [CrossRef] [PubMed]
4. Basturk, O.; Hong, S.-M.; Wood, L.D.; Adsay, V.; Albores-Saavedra, J.; Biankin, A.; Brosens, L.A.; Fukushima, N.; Goggins, M.; Hruban, R.H.; et al. A Revised Classification System and Recommendations From the Baltimore Consensus Meeting for Neoplastic Precursor Lesions in the Pancreas. *Am. J. Surg. Pathol.* **2015**, *39*, 1730–1741. [CrossRef]
5. Tuveson, D.A.; Neoptolemos, J.P. Understanding Metastasis in Pancreatic Cancer: A Call for New Clinical Approaches. *Cell* **2012**, *148*, 21–23. [CrossRef]
6. Neuzillet, C.; Tijeras-Raballand, A.; Bourget, P.; Cros, J.; Couvelard, A.; Sauvanet, A.; Vullierme, M.-P.; Tournigand, C.; Hammel, P. State of the art and future directions of pancreatic ductal adenocarcinoma therapy. *Pharmacol. Ther.* **2015**, *155*, 80–104. [CrossRef]
7. Kanda, M.; Matthaei, H.; Vogelstein, B.; Goggins, M.; Wu, J.; Hong, S.M.; Yu, J.; Borges, M.; Hruban, R.H.; Maitra, A.; et al. Presence of Somatic Mutations in Most Early-Stage Pancreatic Intraepithelial Neoplasia. *Gastroenterology* **2012**, *142*, 730–733.e9. [CrossRef] [PubMed]
8. Hruban, R.H.; Goggins, M.; Parsons, J.; Kern, S.E. Progression model for pancreatic cancer. *Clin. Cancer Res.* **2000**, *6*, 2969–2972.
9. Hessmann, E.; Buchholz, S.M.; Demir, I.E.; Singh, S.K.; Gress, T.M.; Ellenrieder, V.; Neesse, A. Microenvironmental Determinants of Pancreatic Cancer. *Physiol. Rev.* **2020**, *100*, 1707–1751. [CrossRef] [PubMed]
10. Neesse, A.; Algül, H.; Tuveson, D.A.; Gress, T. Stromal biology and therapy in pancreatic cancer: A changing paradigm. *Gut* **2015**, *64*, 1476–1484. [CrossRef]
11. Zhang, W.; Zhang, K.; Zhang, P.; Zheng, J.; Min, C.; Li, X. Research Progress of Pancreas-Related Microorganisms and Pancreatic Cancer. *Front. Oncol.* **2021**, *10*, 1–12. [CrossRef]
12. Murphy, K.; Chambers, C.; Herrmann, D.; Timpson, P.; Pereira, B. Dynamic Stromal Alterations Influence Tumor-Stroma Crosstalk to Promote Pancreatic Cancer and Treatment Resistance. *Cancers* **2021**, *13*, 3481. [CrossRef] [PubMed]

13. Indini, A.; Rijavec, E.; Ghidini, M.; Cortellini, A.; Grossi, F. Targeting KRAS in Solid Tumors: Current Challenges and Future Opportunities of Novel KRAS Inhibitors. *Pharmaceutics* **2021**, *13*, 653. [CrossRef]
14. Verma, H.K.; Kampalli, P.K.; Lakkakula, S.; Chalikonda, G.; Bhaskar, L.V.; Pattnaik, S. A Retrospective Look at Anti-EGFR Agents in Pancreatic Cancer Therapy. *Curr. Drug Metab.* **2020**, *20*, 958–966. [CrossRef]
15. Buchholz, S.M.; Goetze, R.G.; Singh, S.K.; Ammer-Herrmenau, C.; Richards, F.M.; Jodrell, D.I.; Buchholz, M.; Michl, P.; Ellenrieder, V.; Hessmann, E.; et al. Depletion of Macrophages Improves Therapeutic Response to Gemcitabine in Murine Pancreas Cancer. *Cancers* **2020**, *12*, 1978. [CrossRef]
16. Patzak, M.S.; Kari, V.; Patil, S.; Hamdan, F.; Goetze, R.G.; Brunner, M.; Gaedcke, J.; Kitz, J.; Jodrell, D.I.; Richards, F.M.; et al. Cytosolic 5′-nucleotidase 1A is overexpressed in pancreatic cancer and mediates gemcitabine resistance by reducing intracellular gemcitabine metabolites. *EBioMedicine* **2019**, *40*, 394–405. [CrossRef]
17. Müerköster, S.S.; Werbing, V.; Koch, D.; Sipos, B.; Ammerpohl, O.; Kalthoff, H.; Tsao, M.-S.; Fölsch, U.R.; Schäfer, H. Role of myofibroblasts in innate chemoresistance of pancreatic carcinoma-Epigenetic downregulation of caspases. *Int. J. Cancer* **2008**, *123*, 1751–1760. [CrossRef] [PubMed]
18. Müerköster, S.; Wegehenkel, K.; Arlt, A.; Witt, M.; Sipos, B.; Kruse, M.-L.; Sebens, T.; Klöppel, G.; Kalthoff, H.; Fölsch, U.R.; et al. Tumor Stroma Interactions Induce Chemoresistance in Pancreatic Ductal Carcinoma Cells Involving Increased Secretion and Paracrine Effects of Nitric Oxide and Interleukin-1β. *Cancer Res.* **2004**, *64*, 1331–1337. [CrossRef] [PubMed]
19. Geller, L.T.; Barzily-Rokni, M.; Danino, T.; Jonas, O.H.; Shental, N.; Nejman, D.; Gavert, N.; Zwang, Y.; Cooper, Z.A.; Shee, K.; et al. Potential role of intratumor bacteria in mediating tumor resistance to the chemotherapeutic drug gemcitabine. *Science* **2017**, *357*, 1156–1160. [CrossRef] [PubMed]
20. Riquelme, E.; Zhang, Y.; Zhang, L.; Montiel, M.; Zoltan, M.; Dong, W.; Quesada, P.; Sahin, I.; Chandra, V.; Lucas, A.S.; et al. Tumor Microbiome Diversity and Composition Influence Pancreatic Cancer Outcomes. *Cell* **2019**, *178*, 795–806.e12. [CrossRef]
21. Brahmer, J.R.; Tykodi, S.S.; Chow, L.Q.M.; Hwu, W.-J.; Topalian, S.L.; Hwu, P.; Drake, C.G.; Camacho, L.H.; Kauh, J.; Odunsi, K.; et al. Safety and Activity of Anti–PD-L1 Antibody in Patients with Advanced Cancer. *New Engl. J. Med.* **2012**, *366*, 2455–2465. [CrossRef]
22. Royal, R.E.; Levy, C.; Turner, K.; Mathur, A.; Hughes, M.; Kammula, U.S.; Sherry, R.M.; Topalian, S.L.; Yang, J.C.; Lowy, I.; et al. Phase 2 Trial of Single Agent Ipilimumab (Anti-CTLA-4) for Locally Advanced or Metastatic Pancreatic Adenocarcinoma. *J. Immunother.* **2010**, *33*, 828–833. [CrossRef]
23. Patnaik, A.; Kang, S.P.; Rasco, D.; Papadopoulos, K.P.; Elassaiss-Schaap, J.; Beeram, M.; Drengler, R.; Chen, C.; Smith, L.; Espino, G.; et al. Phase I Study of Pembrolizumab (MK-3475; Anti–PD-1 Monoclonal Antibody) in Patients with Advanced Solid Tumors. *Clin. Cancer Res.* **2015**, *21*, 4286–4293. [CrossRef]
24. Rahn, S.; Krüger, S.; Mennrich, R.; Goebel, L.; Wesch, D.; Oberg, H.-H.; Vogel, I.; Ebsen, M.; Röcken, C.; Helm, O.; et al. POLE Score: A comprehensive profiling of programmed death 1 ligand 1 expression in pancreatic ductal adenocarcinoma. *Oncotarget* **2019**, *10*, 1572–1588. [CrossRef]
25. Bonaventura, P.; Shekarian, T.; Alcazer, V.; Valladeau-Guilemond, J.; Valsesia-Wittmann, S.; Amigorena, S.; Caux, C.; Depil, S. Cold Tumors: A Therapeutic Challenge for Immunotherapy. *Front. Immunol.* **2019**, *10*, 168. [CrossRef] [PubMed]
26. De Guillebon, E.; Dardenne, A.; Saldmann, A.; Séguier, S.; Tran, T.; Paolini, L.; Lebbe, C.; Tartour, E. Beyond the concept of cold and hot tumors for the development of novel predictive biomarkers and the rational design of immunotherapy combination. *Int. J. Cancer* **2020**, *147*, 1509–1518. [CrossRef] [PubMed]
27. Grzywa, T.M.; Paskal, W.; Włodarski, P.K. Intratumor and Intertumor Heterogeneity in Melanoma. *Transl. Oncol.* **2017**, *10*, 956–975. [CrossRef]
28. Collisson, E.A.; Sadanandam, A.; Olson, P.; Gibb, W.J.; Truitt, M.; Gu, S.; Cooc, J.; Weinkle, J.; Kim, G.E.; Jakkula, L.; et al. Subtypes of pancreatic ductal adenocarcinoma and their differing responses to therapy. *Nat. Med.* **2011**, *17*, 500–503. [CrossRef] [PubMed]
29. Moffitt, R.A.; Marayati, R.; Flate, E.L.; Volmar, K.E.; Loeza, S.G.H.; Hoadley, K.A.; Rashid, N.U.; Williams, L.A.; Eaton, S.C.; Chung, A.H.; et al. Virtual microdissection identifies distinct tumor- and stroma-specific subtypes of pancreatic ductal adenocarcinoma. *Nat. Genet.* **2015**, *47*, 1168–1178. [CrossRef]
30. Bailey, P.; Chang, D.K.; Nones, K.; Johns, A.L.; Patch, A.-M.; Gingras, M.-C.; Miller, D.K.; Christ, A.N.; Bruxner, T.J.C.; Quinn, M.C.; et al. Genomic analyses identify molecular subtypes of pancreatic cancer. *Nature* **2016**, *531*, 47–52. [CrossRef]
31. Birnbaum, D.J.; Finetti, P.; Birnbaum, D.; Mamessier, E.; Bertucci, F. Validation and comparison of the molecular classifications of pancreatic carcinomas. *Mol. Cancer* **2017**, *16*, 168. [CrossRef] [PubMed]
32. Rashid, N.U.; Peng, X.L.; Jin, C.; Moffitt, R.A.; Volmar, K.E.; Belt, B.A.; Panni, R.Z.; Nywening, T.M.; Herrera, S.G.; Moore, K.J.; et al. Purity Independent Subtyping of Tumors (PurIST), A Clinically Robust, Single-sample Classifier for Tumor Subtyping in Pancreatic Cancer. *Clin. Cancer Res.* **2019**, *26*, 82–92. [CrossRef]
33. Fulawka, L.; Donizy, P.; Halon, A. Cancer stem cells—The current status of an old concept: Literature review and clinical approaches. *Biol. Res.* **2014**, *47*, 66. [CrossRef]
34. Oskarsson, T.; Batlle, E.; Massagué, J. Metastatic Stem Cells: Sources, Niches, and Vital Pathways. *Cell Stem Cell* **2014**, *14*, 306–321. [CrossRef]
35. Hass, R.; Von Der Ohe, J.; Ungefroren, H. Impact of the Tumor Microenvironment on Tumor Heterogeneity and Consequences for Cancer Cell Plasticity and Stemness. *Cancers* **2020**, *12*, 3716. [CrossRef] [PubMed]

36. Hernández-Camarero, P.; López-Ruiz, E.; Marchal, J.A.; Perán, M. Cancer: A mirrored room between tumor bulk and tumor microenvironment. *J. Exp. Clin. Cancer Res.* **2021**, *40*, 217. [CrossRef]
37. Zhan, H.-X.; Xu, J.-W.; Wu, D.; Zhang, T.-P.; Hu, S.-Y. Pancreatic cancer stem cells: New insight into a stubborn disease. *Cancer Lett.* **2015**, *357*, 429–437. [CrossRef] [PubMed]
38. Hermann, P.C.; Sainz, B. Pancreatic cancer stem cells: A state or an entity? *Semin. Cancer Biol.* **2018**, *53*, 223–231. [CrossRef]
39. Arina, A.; Idel, C.; Hyjek, E.M.; Alegre, M.-L.; Wang, Y.; Bindokas, V.P.; Weichselbaum, R.R.; Schreiber, H. Tumor-associated fibroblasts predominantly come from local and not circulating precursors. *Proc. Natl. Acad. Sci. USA* **2016**, *113*, 7551. [CrossRef]
40. Apte, M.V.; Haber, P.S.; Darby, S.J.; Rodgers, S.C.; Mccaughan, G.W.; Korsten, M.A.; Pirola, R.C.; Wilson, J.S. Pancreatic stellate cells are activated by proinflammatory cytokines: Implications for pancreatic fibrogenesis. *Gut* **1999**, *44*, 534–541. [CrossRef]
41. Bochet, L.; Lehuédé, C.; Dauvillier, S.; Wang, Y.Y.; Dirat, B.; Laurent, V.; Dray, C.; Guiet, R.; Maridonneau-Parini, I.; Le Gonidec, S.; et al. Adipocyte-derived fibroblasts promote tumor progression and contribute to the desmoplastic reaction in breast cancer. *Cancer Res.* **2013**, *73*, 5657–5668. [CrossRef] [PubMed]
42. Kidd, S.; Spaeth, E.; Watson, K.; Burks, J.; Lu, H.; Klopp, A.; Andreeff, M.; Marini, F.C. Origins of the Tumor Microenvironment: Quantitative Assessment of Adipose-Derived and Bone Marrow–Derived Stroma. *PLoS ONE* **2012**, *7*, e30563. [CrossRef]
43. Zeisberg, E.M.; Potenta, S.; Xie, L.; Zeisberg, M.; Kalluri, R. Discovery of Endothelial to Mesenchymal Transition as a Source for Carcinoma-Associated Fibroblasts. *Cancer Res.* **2007**, *67*, 10123–10128. [CrossRef] [PubMed]
44. Mederacke, I.; Hsu, C.C.; Troeger, J.S.; Huebener, P.; Mu, X.; Dapito, D.H.; Pradère, J.-P.; Schwabe, R.F. Fate tracing reveals hepatic stellate cells as dominant contributors to liver fibrosis independent of its aetiology. *Nat. Commun.* **2013**, *4*, 2823. [CrossRef]
45. Puche, J.E.; Lee, Y.A.; Jiao, J.; Aloman, C.; Fiel, M.I.; Muñoz, U.; Kraus, T.; Lee, T.; Yee, H.F.; Friedman, S.L. A novel murine model to deplete hepatic stellate cells uncovers their role in amplifying liver damage in mice. *Hepatology* **2013**, *57*, 339–350. [CrossRef]
46. Bhattacharya, S.D.; Mi, Z.; Talbot, L.J.; Guo, H.; Kuo, P.C. Human mesenchymal stem cell and epithelial hepatic carcinoma cell lines in admixture: Concurrent stimulation of cancer-associated fibroblasts and epithelial-to-mesenchymal transition markers. *Surgery* **2012**, *152*, 449–454. [CrossRef]
47. Dufton, N.; Peghaire, C.R.; Osuna-Almagro, L.; Raimondi, C.; Kalna, V.; Chauhan, A.; Webb, G.; Yang, Y.; Birdsey, G.M.; Lalor, P.; et al. Dynamic regulation of canonical TGFβ signalling by endothelial transcription factor ERG protects from liver fibrogenesis. *Nat. Commun.* **2017**, *8*, 1–14. [CrossRef] [PubMed]
48. Ribera, J.; Pauta, M.; Melgar-Lesmes, P.; Córdoba, B.; Bosch, A.; Calvo, M.; Rodrigo-Torres, D.; Sancho-Bru, P.; Mira, A.; Jiménez, W.; et al. A small population of liver endothelial cells undergoes endothelial-to-mesenchymal transition in response to chronic liver injury. *Am. J. Physiol. Liver Physiol.* **2017**, *313*, G492–G504. [CrossRef]
49. Koyama, Y.; Wang, P.; Brenner, D.A.; Kisseleva, T. Stellate Cells, Por-tal Myofibroblasts, and Epithelial-to-Mesenchymal Transition. In *Stellate Cells in Health and Disease*; Chapter 6; Elsevier: Amsterdam, The Netherlands, 2015; pp. 87–106. ISBN 9780128005446.
50. Cassiman, D.; Libbrecht, L.; Desmet, V.; Denef, C.; Roskams, T. Hepatic stellate cell/myofibroblast subpopulations in fibrotic human and rat livers. *J. Hepatol.* **2002**, *36*, 200–209. [CrossRef]
51. Apte, M.; Haber, P.S.; Applegate, T.; Norton, I.D.; Mccaughan, G.; Korsten, M.A.; Pirola, R.C.; Wilson, J. Periacinar stellate shaped cells in rat pancreas: Identification, isolation, and culture. *Gut* **1998**, *43*, 128–133. [CrossRef]
52. Omary, M.B.; Lugea, A.; Lowe, A.W.; Pandol, S.J. The pancreatic stellate cell: A star on the rise in pancreatic diseases. *J. Clin. Investig.* **2007**, *117*, 50–59. [CrossRef] [PubMed]
53. Apte, M.V.; Wilson, J. Dangerous liaisons: Pancreatic stellate cells and pancreatic cancer cells. *J. Gastroenterol. Hepatol.* **2012**, *27*, 69–74. [CrossRef]
54. Frantz, C.; Stewart, K.M.; Weaver, V.M. The extracellular matrix at a glance. *J. Cell Sci.* **2010**, *123 Pt 24*, 4195–4200. [CrossRef] [PubMed]
55. Apte, M.V.; Yang, L.; Phillips, P.; Xu, Z.; Kaplan, W.; Cowley, M.; Pirola, R.C.; Wilson, J.S. Extracellular matrix composition significantly influences pancreatic stellate cell gene expression pattern: Role of transgelin in PSC function. *Am. J. Physiol. Liver Physiol.* **2013**, *305*, G408–G417. [CrossRef] [PubMed]
56. Garcia, P.E.; Scales, M.K.; Allen, B.L.; Di Magliano, M.P. Pancreatic Fibroblast Heterogeneity: From Development to Cancer. *Cells* **2020**, *9*, 2464. [CrossRef]
57. Buchholz, M.; Krebshilfe, F.T.G.P.C.N.O.T.D.; Braun, M.; Heidenblut, A.; Kestler, H.; Klöppel, G.; Schmiegel, W.; Hahn, S.; Lüttges, J.; Gress, T. Transcriptome analysis of microdissected pancreatic intraepithelial neoplastic lesions. *Oncogene* **2005**, *24*, 6626–6636. [CrossRef]
58. Apte, M.V.; Wilson, J.S. Stellate Cell Activation in Alcoholic Pancreatitis. *Pancreas* **2003**, *27*, 316–320. [CrossRef]
59. Marzoq, A.J.; Mustafa, S.A.; Heidrich, L.; Hoheisel, J.D.; Alhamdani, M.S.S. Impact of the secretome of activated pancreatic stellate cells on growth and differentiation of pancreatic tumour cells. *Sci. Rep.* **2019**, *9*, 1–16. [CrossRef]
60. Ryschich, E.; Khamidjanov, A.; Kerkadze, V.; Büchler, M.W.; Zöller, M.; Schmidt, J. Promotion of Tumor Cell Migration by Extracellular Matrix Proteins in Human Pancreatic Cancer. *Pancreas* **2009**, *38*, 804–810. [CrossRef]
61. Baron, M.; Veres, A.; Wolock, S.; Faust, A.L.; Gaujoux, R.; Vetere, A.; Ryu, J.H.; Wagner, B.K.; Shen-Orr, S.S.; Klein, A.M.; et al. A Single-Cell Transcriptomic Map of the Human and Mouse Pancreas Reveals Inter- and Intra-cell Population Structure. *Cell Syst.* **2016**, *3*, 346–360.e4. [CrossRef]
62. Whittle, M.C.; Hingorani, S.R. Fibroblasts in Pancreatic Ductal Adenocarcinoma: Biological Mechanisms and Therapeutic Targets. *Gastroenterology* **2019**, *156*, 2085–2096. [CrossRef]

63. Bolm, L.; Cigolla, S.; Wittel, U.A.; Hopt, U.T.; Keck, T.; Rades, D.; Bronsert, P.; Wellner, U.F. The Role of Fibroblasts in Pancreatic Cancer: Extracellular Matrix Versus Paracrine Factors. *Transl. Oncol.* **2017**, *10*, 578–588. [CrossRef]
64. Shao, Z.-M.; Nguyen, M.; Barsky, S.H. Human breast carcinoma desmoplasia is PDGF initiated. *Oncogene* **2000**, *19*, 4337–4345. [CrossRef]
65. Giannoni, E.; Bianchini, F.; Masieri, L.; Serni, S.; Torre, E.; Calorini, L.; Chiarugi, P. Reciprocal Activation of Prostate Cancer Cells and Cancer-Associated Fibroblasts Stimulates Epithelial-Mesenchymal Transition and Cancer Stemness. *Cancer Res.* **2010**, *70*, 6945–6956. [CrossRef] [PubMed]
66. Ronnov-Jessen, L.; Petersen, O.W. Induction of α-Smooth Muscle Actin by Trans-forming Growth Factor-B1 in Quiescent Human Breast Gland Fibroblasts. *Lab. Investig.* **1993**, *68*, 696–707. [PubMed]
67. Bachem, M.G.; Schünemann, M.; Ramadani, M.; Siech, M.; Beger, H.; Buck, A.; Zhou, S.; Schmid-Kotsas, A.; Adler, G. Pancreatic carcinoma cells induce fibrosis by stimulating proliferation and matrix synthesis of stellate cells. *Gastroenterology* **2005**, *128*, 907–921. [CrossRef]
68. Biffi, G.; Tuveson, D.A. Diversity and Biology of Cancer-Associated Fibroblasts. *Physiol. Rev.* **2021**, *101*, 147–176. [CrossRef]
69. Öhlund, D.; Handly-Santana, A.; Biffi, G.; Elyada, E.; Almeida, A.S.; Ponz-Sarvise, M.; Corbo, V.; Oni, T.E.; Hearn, S.A.; Lee, E.J.; et al. Distinct populations of inflammatory fibroblasts and myofibroblasts in pancreatic cancer. *J. Exp. Med.* **2017**, *214*, 579–596. [CrossRef] [PubMed]
70. Biffi, G.; Oni, T.E.; Spielman, B.; Hao, Y.; Elyada, E.; Park, Y.; Preall, J.; Tuveson, D.A. IL1-Induced JAK/STAT Signaling Is Antagonized by TGFβ to Shape CAF Heterogeneity in Pancreatic Ductal Adenocarcinoma. *Cancer Discov.* **2019**, *9*, 282–301. [CrossRef] [PubMed]
71. Hutton, C.; Heider, F.; Blanco-Gomez, A.; Banyard, A.; Kononov, A.; Zhang, X.; Karim, S.; Paulus-Hock, V.; Watt, D.; Steele, N.; et al. Single-cell analysis defines a pancreatic fibroblast lineage that supports anti-tumor immunity. *Cancer Cell* **2021**, *14*, 1535. [CrossRef]
72. Pickup, M.W.; Mouw, J.K.; Weaver, V.M. The extracellular matrix modulates the hallmarks of cancer. *EMBO Rep.* **2014**, *15*, 1243–1253. [CrossRef]
73. Neumann, C.C.; Von Hörschelmann, E.; Reutzel-Selke, A.; Seidel, E.; Sauer, I.; Pratschke, J.; Bahra, M.; Schmuck, R.B. Tumor–stromal cross-talk modulating the therapeutic response in pancreatic cancer. *Hepatobiliary Pancreat. Dis. Int.* **2018**, *17*, 461–472. [CrossRef]
74. Hartmann, N.; Giese, N.A.; Giese, T.; Poschke, I.; Offringa, R.; Werner, J.; Ryschich, E. Prevailing Role of Contact Guidance in Intrastromal T-cell Trapping in Human Pancreatic Cancer. *Clin. Cancer Res.* **2014**, *20*, 3422–3433. [CrossRef]
75. Tse, J.M.; Cheng, G.; Tyrrell, J.A.; Wilcox-Adelman, S.A.; Boucher, Y.; Jain, R.K.; Munn, L.L. Mechanical compression drives cancer cells toward invasive phenotype. *Proc. Natl. Acad. Sci.* **2012**, *109*, 911–916. [CrossRef]
76. Sanchez, M.E.F.; Barbier, S.; Whitehead, J.; Béalle, G.; Michel, A.; Latorre-Ossa, H.; Rey, C.; Fouassier, L.; Claperon, A.; Brullé, L.; et al. Mechanical induction of the tumorigenic β-catenin pathway by tumour growth pressure. *Nat. Cell Biol.* **2015**, *523*, 92–95. [CrossRef]
77. Martin, J.; Seano, G.; Jain, R.K. Normalizing Function of Tumor Vessels: Progress, Opportunities, and Challenges. *Annu. Rev. Physiol.* **2019**, *81*, 505–534. [CrossRef]
78. Jain, R.K. Normalizing Tumor Microenvironment to Treat Cancer: Bench to Bedside to Biomarkers. *J. Clin. Oncol.* **2013**, *31*, 2205–2218. [CrossRef] [PubMed]
79. Wilson, W.R.; Hay, M. Targeting hypoxia in cancer therapy. *Nat. Rev. Cancer* **2011**, *11*, 393–410. [CrossRef] [PubMed]
80. Carmeliet, P.; Dor, Y.; Herbert, J.-M.; Fukumura, D.; Brusselmans, K.; Dewerchin, M.; Neeman, M.; Bono, F.; Abramovitch, R.; Maxwell, P.; et al. Role of HIF-1α in hypoxia-mediated apoptosis, cell proliferation and tumour angiogenesis. *Nat. Cell Biol.* **1998**, *394*, 485–490. [CrossRef]
81. Thienpont, B.; Steinbacher, J.; Zhao, H.; D'Anna, F.; Kuchnio, A.; Ploumakis, A.; Ghesquière, B.; Van Dyck, L.; Boeckx, B.; Schoonjans, L.; et al. Tumour hypoxia causes DNA hypermethylation by reducing TET activity. *Nat. Cell Biol.* **2016**, *537*, 63–68. [CrossRef]
82. Schito, L.; Semenza, G.L. Hypoxia-Inducible Factors: Master Regulators of Cancer Progression. *Trends Cancer* **2016**, *2*, 758–770. [CrossRef]
83. Ke, X.; Chen, C.; Song, Y.; Cai, Q.; Li, J.; Tang, Y.; Han, X.; Qu, W.; Chen, A.; Wang, H.; et al. Hypoxia modifies the polarization of macrophages and their inflammatory microenvironment, and inhibits malignant behavior in cancer cells. *Oncol. Lett.* **2019**, *18*, 5871–5878. [CrossRef] [PubMed]
84. Noman, M.Z.; Desantis, G.; Janji, B.; Hasmim, M.; Karray, S.; Dessen, P.; Bronte, V.; Chouaib, S. PD-L1 is a novel direct target of HIF-1α, and its blockade under hypoxia enhanced MDSC-mediated T cell activation. *J. Exp. Med.* **2014**, *211*, 781–790. [CrossRef]
85. Jiang, X.; Wang, J.; Deng, X.; Xiong, F.; Ge, J.; Xiang, B.; Wu, X.; Ma, J.; Zhou, M.; Li, X.; et al. Role of the tumor microenvironment in PD-L1/PD-1-mediated tumor immune escape. *Mol. Cancer* **2019**, *18*, 1–17. [CrossRef]
86. Barsoum, I.B.; Smallwood, C.A.; Siemens, D.R.; Graham, C.H. A Mechanism of Hypoxia-Mediated Escape from Adaptive Immunity in Cancer Cells. *Cancer Res.* **2014**, *74*, 665–674. [CrossRef] [PubMed]
87. Engblom, C.; Pfirschke, C.; Pittet, C.E.C.P.M.J. The role of myeloid cells in cancer therapies. *Nat. Rev. Cancer* **2016**, *16*, 447–462. [CrossRef] [PubMed]

88. Ene–Obong, A.; Clear, A.J.; Watt, J.; Wang, J.; Fatah, R.; Riches, J.C.; Marshall, J.F.; Chin–Aleong, J.; Chelala, C.; Gribben, J.G.; et al. Activated Pancreatic Stellate Cells Sequester CD8+ T Cells to Reduce Their Infiltration of the Juxtatumoral Compartment of Pancreatic Ductal Adenocarcinoma. *Gastroenterology* **2013**, *145*, 1121–1132. [CrossRef]
89. Gorchs, L.; Moro, C.F.; Bankhead, P.; Kern, K.P.; Sadeak, I.; Meng, Q.; Rangelova, E.; Kaipe, H. Human Pancreatic Carcinoma-Associated Fibroblasts Promote Expression of Co-inhibitory Markers on CD4+ and CD8+ T-Cells. *Front. Immunol.* **2019**, *10*, 847. [CrossRef]
90. Feig, C.; Jones, J.O.; Kraman, M.; Wells, R.J.; Deonarine, A.; Chan, D.S.; Connell, C.M.; Roberts, E.W.; Zhao, Q.; Caballero, O.L.; et al. Targeting CXCL12 from FAP-expressing carcinoma-associated fibroblasts synergizes with anti-PD-L1 immunotherapy in pancreatic cancer. *Proc. Natl. Acad. Sci. USA* **2013**, *110*, 20212–20217. [CrossRef]
91. Lakins, M.A.; Ghorani, E.; Munir, H.; Martins, C.P.; Shields, J.D. Cancer-associated fibroblasts induce antigen-specific deletion of CD8 + T Cells to protect tumour cells. *Nat. Commun.* **2018**, *9*, 948. [CrossRef]
92. Yavuz, B.G.; Gunaydin, G.; Gedik, M.E.; Kosemehmetoglu, K.; Karakoc, D.; Ozgür, F.F.; Guc, D. Cancer associated fibroblasts sculpt tumour microenvironment by recruiting monocytes and inducing immunosuppressive PD-1+ TAMs. *Sci. Rep.* **2019**, *9*, 1–15. [CrossRef]
93. Yang, X.; Lin, Y.; Shi, Y.; Li, B.; Liu, W.; Ying-Hong, S.; Dang, Y.; Chu, Y.; Fan, J.; He, R. FAP Promotes Immunosuppression by Cancer-Associated Fibroblasts in the Tumor Microenvironment via STAT3–CCL2 Signaling. *Cancer Res.* **2016**, *76*, 4124–4135. [CrossRef] [PubMed]
94. Comito, G.; Giannoni, E.; Segura, C.P.; Barcellos-De-Souza, P.; Raspollini, M.R.; Baroni, G.; Lanciotti, M.; Serni, S.; Chiarugi, P. Cancer-associated fibroblasts and M2-polarized macrophages synergize during prostate carcinoma progression. *Oncogene* **2013**, *33*, 2423–2431. [CrossRef] [PubMed]
95. Mathew, E.; Brannon, A.L.; Del Vecchio, A.; Garcia, P.E.; Penny, M.K.; Kane, K.T.; Vinta, A.; Buckanovich, R.J.; di Magliano, M.P. Mesenchymal Stem Cells Promote Pancreatic Tumor Growth by Inducing Alternative Polarization of Macrophages. *Neoplasia* **2016**, *18*, 142–151. [CrossRef]
96. Zhang, A.; Qian, Y.; Ye, Z.; Chen, H.; Xie, H.; Zhou, L.; Shen, Y.; Zheng, S. Cancer-associated fibroblasts promote M2 polarization of macrophages in pancreatic ductal adenocarcinoma. *Cancer Med.* **2017**, *6*, 463–470. [CrossRef]
97. Mace, T.A.; Ameen, Z.; Collins, A.; Wojcik, S.; Mair, M.; Young, G.S.; Fuchs, J.R.; Eubank, T.D.; Frankel, W.L.; Bekaii-Saab, T.; et al. Pancreatic Cancer-Associated Stellate Cells Promote Differentiation of Myeloid-Derived Suppressor Cells in a STAT3-Dependent Manner. *Cancer Res.* **2013**, *73*, 3007–3018. [CrossRef]
98. Li, J.; Byrne, K.T.; Yan, F.; Yamazoe, T.; Chen, Z.; Baslan, T.; Richman, L.P.; Lin, J.H.; Sun, Y.H.; Rech, A.J.; et al. Tumor Cell-Intrinsic Factors Underlie Heterogeneity of Immune Cell Infiltration and Response to Immunotherapy. *Immunity* **2018**, *49*, 178–193.e7. [CrossRef]
99. Flint, T.R.; Janowitz, T.; Connell, C.M.; Roberts, E.; Denton, A.; Coll, A.P.; Jodrell, D.I.; Fearon, D.T. Tumor-Induced IL-6 Reprograms Host Metabolism to Suppress Anti-tumor Immunity. *Cell Metab.* **2016**, *24*, 672–684. [CrossRef]
100. Elyada, E.; Bolisetty, M.; Laise, P.; Flynn, W.F.; Courtois, E.T.; Burkhart, R.A.; Teinor, J.A.; Belleau, P.; Biffi, G.; Lucito, M.S.; et al. Cross-Species Single-Cell Analysis of Pancreatic Ductal Adenocarcinoma Reveals Antigen-Presenting Cancer-Associated Fibroblasts. *Cancer Discov.* **2019**, *9*, 1102–1123. [CrossRef] [PubMed]
101. Friedman, G.; Levi-Galibov, O.; David, E.; Bornstein, C.; Giladi, A.; Dadiani, M.; Mayo, A.; Halperin, C.; Pevsner-Fischer, M.; Lavon, H.; et al. Cancer-Associated Fibro-blast Compositions Change with Breast-Cancer Progression Linking S100A4 and PDPN Ratios with Clinical Outcome. *bioRxiv* **2020**. [CrossRef]
102. Orimo, A.; Weinberg, R.A. Stromal Fibroblasts in Cancer: A Novel Tumor-Promoting Cell Type. *Cell Cycle* **2006**, *5*, 1597–1601. [CrossRef]
103. Schäfer, H.; Geismann, C.; Heneweer, C.; Egberts, J.-H.; Korniienko, O.; Kiefel, H.; Moldenhauer, G.; Bachem, M.G.; Kalthoff, H.; Altevogt, P.; et al. Myofibroblast-induced tumorigenicity of pancreatic ductal epithelial cells is L1CAM dependent. *Carcinogenesis* **2011**, *33*, 84–93. [CrossRef] [PubMed]
104. Geismann, C.; Morscheck, M.; Koch, D.; Bergmann, F.; Ungefroren, H.; Arlt, A.; Tsao, M.; Bachem, M.G.; Altevogt, P.; Sipos, B.; et al. Up-regulation of L1CAM in Pancreatic Duct Cells Is Transforming Growth Factor β1– and Slug-Dependent: Role in Malignant Transformation of Pancreatic Cancer. *Cancer Res.* **2009**, *69*, 4517–4526. [CrossRef] [PubMed]
105. Costa-Silva, B.; Aiello, N.M.; Ocean, A.J.; Singh, S.; Zhang, H.; Thakur, B.K.; Becker, A.; Hoshino, A.; Mark, M.T.; Molina, H.; et al. Pancreatic cancer exosomes initiate pre-metastatic niche formation in the liver. *Nat. Cell Biol.* **2015**, *17*, 816–826. [CrossRef]
106. Lenk, L.; Pein, M.; Will, O.; Gomez, B.; Viol, F.; Hauser, C.; Egberts, J.-H.; Gundlach, J.-P.; Helm, O.; Tiwari, S.; et al. The hepatic microenvironment essentially determines tumor cell dormancy and metastatic outgrowth of pancreatic ductal adenocarcinoma. *OncoImmunology* **2017**, *7*, e1368603. [CrossRef] [PubMed]
107. Miarka, L.; Hauser, C.; Helm, O.; Holdhof, D.; Beckinger, S.; Egberts, J.-H.; Gundlach, J.-P.; Lenk, L.; Rahn, S.; Mikulits, W.; et al. The Hepatic Microenvironment and TRAIL-R2 Impact Outgrowth of Liver Metastases in Pancreatic Cancer after Surgical Resection. *Cancers* **2019**, *11*, 745. [CrossRef] [PubMed]
108. Häberle, L.; Steiger, K.; Schlitter, A.M.; Safi, S.A.; Knoefel, W.T.; Erkan, M.; Esposito, I. Stromal heterogeneity in pancreatic cancer and chronic pancreatitis. *Pancreatology* **2018**, *18*, 536–549. [CrossRef]
109. Ding, C.; Li, Y.; Guo, F.; Jiang, Y.; Ying, W.; Li, D.; Yang, D.; Xia, X.; Liu, W.; Zhao, Y.; et al. A Cell-type-resolved Liver Proteome. *Mol. Cell. Proteom.* **2016**, *15*, 3190–3202. [CrossRef]

110. Libbrecht, L.; Cassiman, D.; Desmet, V.; Roskams, T. The correlation between portal myofibroblasts and development of intrahepatic bile ducts and arterial branches in human liver. *Liver Int.* **2002**, *22*, 252–258. [CrossRef] [PubMed]
111. Passino, M.A.; Adams, R.A.; Sikorski, S.L.; Akassoglou, K. Regulation of Hepatic Stellate Cell Differentiation by the Neurotrophin Receptor p75NTR. *Science* **2007**, *315*, 1853–1856. [CrossRef]
112. Schirmacher, P.; Geerts, A.; Pietrangelo, A.; Dienes, H.P.; Rogler, C.E. Hepatocyte growth factor/hepatopoietin A is expressed in fat-storing cells from rat liver but not myofibroblast-like cells derived from fat-storing cells. *Hepatology* **1992**, *15*, 5–11. [CrossRef]
113. Kitto, L.J.; Henderson, N.C. Hepatic Stellate Cell Regulation of Liver Regeneration and Repair. *Hepatol. Commun.* **2021**, *5*, 358–370. [CrossRef] [PubMed]
114. Hendriks, H.F.J.; Blaner, W.S.; Wennekers, H.M.; Piantedosi, R.; Brouwer, A.; Leeuw, A.M.; Goodman, D.S.; Knook, D.L. Distributions of retinoids, retinoid-binding proteins and related parameters in different types of liver cells isolated from young and old rats. *JBIC J. Biol. Inorg. Chem.* **1988**, *171*, 237–244. [CrossRef]
115. Haaker, M.W.; Vaandrager, A.B.; Helms, J.B. Retinoids in health and disease: A role for hepatic stellate cells in affecting retinoid levels. *Biochim. Biophys. Acta BBA Mol. Cell Biol. Lipids* **2020**, *1865*, 158674. [CrossRef]
116. Bigorgne, A.E.; John, B.; Ebrahimkhani, M.R.; Shimizu-Albergine, M.; Campbell, J.S.; Crispe, I.N. TLR4-Dependent Secretion by Hepatic Stellate Cells of the Neutrophil-Chemoattractant CXCL1 Mediates Liver Response to Gut Microbiota. *PLoS ONE* **2016**, *11*, e0151063. [CrossRef]
117. Viñas, O. Human hepatic stellate cells show features of antigen-presenting cells and stimulate lymphocyte proliferation. *Hepatology* **2003**, *38*, 919–929. [CrossRef]
118. Mehrfeld, C.; Zenner, S.; Kornek, M.; Lukacs-Kornek, V. The Contribution of Non-Professional Antigen-Presenting Cells to Immunity and Tolerance in the Liver. *Front. Immunol.* **2018**, *9*, 635. [CrossRef]
119. Kobayashi, S.; Seki, S.; Kawada, N.; Morikawa, H.; Nakatani, K.; Uyama, N.; Ikeda, K.; Nakajima, Y.; Arakawa, T.; Kaneda, K. Apoptosis of T cells in the hepatic fibrotic tissue of the rat: A possible inducing role of hepatic myofibroblast-like cells. *Cell Tissue Res.* **2003**, *311*, 353–364. [CrossRef] [PubMed]
120. Yu, M.-C.; Chen, C.-H.; Liang, X.; Wang, L.; Gandhi, C.R.; Fung, J.J.; Lu, L.; Qian, S. Inhibition of T-cell responses by hepatic stellate cells via B7-H1-mediated T-cell apoptosis in mice. *Hepatology* **2004**, *40*, 1312–1321. [CrossRef] [PubMed]
121. Seubert, B.; Grünwald, B.; Kobuch, J.; Cui, H.; Schelter, F.; Schaten, S.; Siveke, J.T.; Lim, N.H.; Nagase, H.; Simonavicius, N.; et al. Tissue inhibitor of metalloproteinases (TIMP)-1 creates a premetastatic niche in the liver through SDF-1/CXCR4-dependent neutrophil recruitment in mice. *Hepatology* **2015**, *61*, 238–248. [CrossRef]
122. Grünwald, B.; Harant, V.; Schaten, S.; Frühschütz, M.; Spallek, R.; Höchst, B.; Stutzer, K.; Berchtold, S.; Erkan, M.; Prokopchuk, O.; et al. Pancreatic Premalignant Lesions Secrete Tissue Inhibitor of Metalloproteinases-1, Which Activates Hepatic Stellate Cells Via CD63 Signaling to Create a Premetastatic Niche in the Liver. *Gastroenterology* **2016**, *151*, 1011–1024.e7. [CrossRef] [PubMed]
123. Lee, J.; Stone, M.L.; Porrett, P.M.; Thomas, S.; Komar, C.A.; Li, J.; Delman, D.; Graham, K.; Gladney, W.L.; Hua, X.; et al. Hepatocytes direct the formation of a pro-metastatic niche in the liver. *Nat. Cell Biol.* **2019**, *567*, 249–252. [CrossRef] [PubMed]
124. Houg, D.S.; Bijlsma, M.F. The hepatic pre-metastatic niche in pancreatic ductal adenocarcinoma. *Mol. Cancer* **2018**, *17*, 95. [CrossRef] [PubMed]
125. Bhattacharjee, S.; Hamberger, F.; Ravichandra, A.; Miller, M.; Nair, A.; Affo, S.; Filliol, A.; Chin, L.; Savage, T.M.; Yin, D.; et al. Tumor restriction by type I collagen opposes tumor-promoting effects of cancer-associated fibroblasts. *J. Clin. Investig.* **2021**, *131*. [CrossRef]
126. Gorelik, L.; Flavell, R.A. Transforming growth factor-β in T-cell biology. *Nat. Rev. Immunol.* **2002**, *2*, 46–53. [CrossRef]
127. Sperb, N.; Tsesmelis, M.; Wirth, T. Crosstalk between Tumor and Stromal Cells in Pancreatic Ductal Adenocarcinoma. *Int. J. Mol. Sci.* **2020**, *21*, 5486. [CrossRef]
128. Liu, S.; Ren, J.; Dijke, P.T. Targeting TGFβ signal transduction for cancer therapy. *Signal Transduct. Target. Ther.* **2021**, *6*, 1–20. [CrossRef] [PubMed]
129. Melisi, D.; Garcia-Carbonero, R.; Macarulla, T.; Pezet, D.; Deplanque, G.; Fuchs, M.; Trojan, J.; Oettle, H.; Kozloff, M.; Cleverly, A.; et al. Galunisertib plus gemcitabine vs. gemcitabine for first-line treatment of patients with unresectable pancreatic cancer. *Br. J. Cancer* **2018**, *119*, 1208–1214. [CrossRef]
130. Melisi, D.; Oh, D.-Y.; Hollebecque, A.; Calvo, E.; Varghese, A.; Borazanci, E.; Macarulla, T.; Merz, V.; Zecchetto, C.; Zhao, Y.; et al. Safety and activity of the TGFβ receptor I kinase inhibitor galunisertib plus the anti-PD-L1 antibody durvalumab in metastatic pancreatic cancer. *J. Immunother. Cancer* **2021**, *9*, e002068. [CrossRef] [PubMed]
131. Özdemir, B.C.; Pentcheva-Hoang, T.; Carstens, J.L.; Zheng, X.; Wu, C.-C.; Simpson, T.R.; Laklai, H.; Sugimoto, H.; Kahlert, C.; Novitskiy, S.V.; et al. Depletion of Carcinoma-Associated Fibroblasts and Fibrosis Induces Immunosuppression and Accelerates Pancreas Cancer with Reduced Survival. *Cancer Cell* **2014**, *25*, 719–734. [CrossRef]
132. Bailey, J.M.; Swanson, B.J.; Hamada, T.; Eggers, J.P.; Singh, P.K.; Caffery, T.; Ouellette, M.M.; Hollingsworth, M.A. Sonic Hedgehog Promotes Desmoplasia in Pancreatic Cancer. *Clin. Cancer Res.* **2008**, *14*, 5995–6004. [CrossRef] [PubMed]
133. Rhim, A.D.; Oberstein, P.E.; Thomas, D.H.; Mirek, E.T.; Palermo, C.F.; Sastra, S.A.; Dekleva, E.N.; Saunders, T.; Becerra, C.P.; Tattersall, I.; et al. Stromal Elements Act to Restrain, Rather Than Support, Pancreatic Ductal Adenocarcinoma. *Cancer Cell* **2014**, *25*, 735–747. [CrossRef]

134. Catenacci, D.V.T.; Junttila, M.R.; Karrison, T.; Bahary, N.; Horiba, M.N.; Nattam, S.R.; Marsh, R.; Wallace, J.; Kozloff, M.; Rajdev, L.; et al. Randomized Phase Ib/II Study of Gemcitabine Plus Placebo or Vismodegib, a Hedgehog Pathway Inhibitor, in Patients With Metastatic Pancreatic Cancer. *J. Clin. Oncol.* **2015**, *33*, 4284–4292. [CrossRef] [PubMed]
135. Ko, A.H.; LoConte, N.; Tempero, M.A.; Walker, E.J.; Kelley, R.K.; Lewis, S.; Chang, W.-C.; Kantoff, E.; Vannier, M.W.; Catenacci, D.V.; et al. A Phase I Study of FOLFIRINOX Plus IPI-926, a Hedgehog Pathway Inhibitor, for Advanced Pancreatic Adenocarcinoma. *Pancreas* **2016**, *45*, 370–375. [CrossRef]
136. Froeling, F.E.; Feig, C.; Chelala, C.; Dobson, R.; Mein, C.E.; Tuveson, D.; Clevers, H.; Hart, I.R.; Kocher, H.M. Retinoic Acid–Induced Pancreatic Stellate Cell Quiescence Reduces Paracrine Wnt–β-Catenin Signaling to Slow Tumor Progression. *Gastroenterology* **2011**, *141*, 1486–1497.e14. [CrossRef]
137. Sherman, M.H.; Yu, R.T.; Engle, D.D.; Ding, N.; Atkins, A.R.; Tiriac, H.; Collisson, E.A.; Connor, F.; Van Dyke, T.; Kozlov, S.; et al. Vitamin D Receptor-Mediated Stromal Reprogramming Suppresses Pancreatitis and Enhances Pancreatic Cancer Therapy. *Cell* **2014**, *159*, 80–93. [CrossRef]
138. Hurwitz, H.; Van Cutsem, E.; Bendell, J.; Hidalgo, M.; Li, C.-P.; Salvo, M.G.; Macarulla, T.; Sahai, V.; Sama, A.; Greeno, E.; et al. Ruxolitinib + capecitabine in advanced/metastatic pancreatic cancer after disease progression/intolerance to first-line therapy: JANUS 1 and 2 randomized phase III studies. *Investig. New Drugs* **2018**, *36*, 683–695. [CrossRef]
139. Belgiovine, C.; Digifico, E.; Anfray, C.; Ummarino, A.; Andón, F.T. Targeting Tumor-Associated Macrophages in Anti-Cancer Therapies: Convincing the Traitors to Do the Right Thing. *J. Clin. Med.* **2020**, *9*, 3226. [CrossRef]
140. Helm, O.; Mennrich, R.; Petrick, D.; Goebel, L.; Freitag-Wolf, S.; Röder, C.; Kalthoff, H.; Röcken, C.; Sipos, B.; Kabelitz, D.; et al. Comparative Characterization of Stroma Cells and Ductal Epithelium in Chronic Pancreatitis and Pancreatic Ductal Adenocarcinoma. *PLoS ONE* **2014**, *9*, e94357. [CrossRef]
141. Tjomsland, V.; Sandström, P.; Spångeus, A.; Messmer, D.; Emilsson, J.; Falkmer, U.; Falkmer, S.; Magnusson, K.-E.; Borch, K.; Larsson, M. Pancreatic adenocarcinoma exerts systemic effects on the peripheral blood myeloid and plasmacytoid dendritic cells: An indicator of disease severity? *BMC Cancer* **2010**, *10*, 87. [CrossRef] [PubMed]
142. Dallal, R.M.; Christakos, P.; Lee, K.; Egawa, S.; Son, Y.-I.; Lotze, M.T. Paucity of dendritic cells in pancreatic cancer. *Surgery* **2002**, *131*, 135–138. [CrossRef]
143. Hegde, S.; Krisnawan, V.; Herzog, B.H.; Zuo, C.; Breden, M.A.; Knolhoff, B.L.; Hogg, G.D.; Tang, J.P.; Baer, J.M.; Mpoy, C.; et al. Dendritic Cell Paucity Leads to Dysfunctional Immune Surveillance in Pancreatic Cancer. *Cancer Cell* **2020**, *37*, 289–307.e9. [CrossRef]
144. Murphy, T.L.; Murphy, K.M. Dendritic cells in cancer immunology. *Cell. Mol. Immunol.* **2021**, 1–11. [CrossRef]
145. Bronte, V.; Brandau, S.; Chen, S.-H.; Colombo, M.P.; Frey, A.B.; Greten, T.F.; Mandruzzato, S.; Murray, P.J.; Ochoa, A.; Ostrand-Rosenberg, S.; et al. Recommendations for myeloid-derived suppressor cell nomenclature and characterization standards. *Nat. Commun.* **2016**, *7*, 12150. [CrossRef]
146. Trovato, R.; Fiore, A.; Sartori, S.; Canè, S.; Giugno, R.; Cascione, L.; Paiella, S.; Salvia, R.; De Sanctis, F.; Poffe, O.; et al. Immunosuppression by monocytic myeloid-derived suppressor cells in patients with pancreatic ductal carcinoma is orchestrated by STAT3. *J. Immunother. Cancer* **2019**, *7*, 255. [CrossRef] [PubMed]
147. Choueiry, F.; Torok, M.; Shakya, R.; Agrawal, K.; Deems, A.; Benner, B.; Hinton, A.; Shaffer, J.; Blaser, B.W.; Noonan, A.M.; et al. CD200 promotes immunosuppression in the pancreatic tumor microenvironment. *J. Immunother. Cancer* **2020**, *8*, e000189. [CrossRef]
148. Siret, C.; Collignon, A.; Silvy, F.; Robert, S.; Cheyrol, T.; André, P.; Rigot, V.; Iovanna, J.; van de Pavert, S.; Lombardo, D.; et al. Deciphering the Crosstalk Between Myeloid-Derived Suppressor Cells and Regulatory T Cells in Pancreatic Ductal Adenocarcinoma. *Front. Immunol.* **2020**, *10*, 3070. [CrossRef]
149. Fujimura, T.; Mahnke, K.; Enk, A.H. Myeloid derived suppressor cells and their role in tolerance induction in cancer. *J. Dermatol. Sci.* **2010**, *59*, 1–6. [CrossRef]
150. Zhu, Y.; Herndon, J.M.; Sojka, D.K.; Kim, K.-W.; Knolhoff, B.L.; Zuo, C.; Cullinan, D.R.; Luo, J.; Bearden, A.R.; Lavine, K.J.; et al. Tissue-Resident Macrophages in Pancreatic Ductal Adenocarcinoma Originate from Embryonic Hematopoiesis and Promote Tumor Progression. *Immunity* **2017**, *47*, 323–338.e6. [CrossRef] [PubMed]
151. Lankadasari, M.B.; Mukhopadhyay, P.; Mohammed, S.; Harikumar, K.B. TAMing pancreatic cancer: Combat with a double edged sword. *Mol. Cancer* **2019**, *18*, 1–13. [CrossRef]
152. Mills, C.D. M1 and M2 Macrophages: Oracles of Health and Disease. *Crit. Rev. Immunol.* **2012**, *32*, 463–488. [CrossRef]
153. Mills, C.D.; Kincaid, K.; Alt, J.M.; Heilman, M.J.; Hill, A.M. M-1/M-2 Macrophages and the Th1/Th2 Paradigm. *J. Immunol.* **2000**, *164*, 6166–6173. [CrossRef]
154. Horwood, N.J. Macrophage Polarization and Bone Formation: A review. *Clin. Rev. Allergy Immunol.* **2016**, *51*, 79–86. [CrossRef] [PubMed]
155. Takahashi, H.; Sakakura, K.; Kudo, T.; Toyoda, M.; Kaira, K.; Oyama, T.; Chikamatsu, K. Cancer-associated fibroblasts promote an immunosuppressive microenvironment through the induction and accumulation of protumoral macrophages. *Oncotarget* **2016**, *8*, 8633–8647. [CrossRef] [PubMed]
156. Li, C.; Cui, L.; Yang, L.; Wang, B.; Zhuo, Y.; Zhang, L.; Wang, X.; Zhang, Q.; Zhang, S. Pancreatic Stellate Cells Promote Tumor Progression by Promoting an Immunosuppressive Microenvironment in Murine Models of Pancreatic Cancer. *Pancreas* **2020**, *49*, 120–127. [CrossRef] [PubMed]

157. Chang, Y.-T.; Peng, H.-Y.; Hu, C.-M.; Huang, S.-C.; Tien, S.-C.; Jeng, Y.-M. Pancre-atic Cancer-Derived Small Extracellular Vesical Ezrin Regulates Macrophage Polari-zation and Promotes Metastasis. *Am. J. Cancer Res.* **2020**, *10*, 12–37. [PubMed]
158. Nielsen, S.R.; Quaranta, V.; Linford, A.; Emeagi, P.; Rainer, C.; Santos, A.; Ireland, L.; Sakai, T.; Sakai, K.; Kim, Y.-S.; et al. Macrophage-secreted granulin supports pancreatic cancer metastasis by inducing liver fibrosis. *Nat. Cell Biol.* **2016**, *18*, 549–560. [CrossRef] [PubMed]
159. Yang, S.; Liu, Q.; Liao, Q. Tumor-Associated Macrophages in Pancreatic Ductal Adenocarcinoma: Origin, Polarization, Function, and Reprogramming. *Front. Cell Dev. Biol.* **2021**, *8*, 1–24. [CrossRef]
160. Mira, E.; Carmona-Rodríguez, L.; Tardáguila, M.; Azcoitia, I.; Gonzalez-Martin, A.; Almonacid, L.; Casas, J.; Fabrias, G.; Mañes, S. A lovastatin-elicited genetic program inhibits M2 macrophage polarization and enhances T cell infiltration into spontaneous mouse mammary tumors. *Oncotarget* **2013**, *4*, 2288–2301. [CrossRef]
161. Helm, O.; Held-Feindt, J.; Grage-Griebenow, E.; Reiling, N.; Ungefroren, H.; Vogel, I.; Krüger, U.; Becker, T.; Ebsen, M.; Röcken, C.; et al. Tumor-associated macrophages exhibit pro- and anti-inflammatory properties by which they impact on pancreatic tumorigenesis. *Int. J. Cancer* **2014**, *135*, 843–861. [CrossRef] [PubMed]
162. Hu, H.; Hang, J.-J.; Han, T.; Zhuo, M.; Jiao, F.; Wang, L.-W. The M2 phenotype of tumor-associated macrophages in the stroma confers a poor prognosis in pancreatic cancer. *Tumor Biol.* **2016**, *37*, 8657–8664. [CrossRef]
163. Knudsen, E.S.; Vail, P.; Balaji, U.; Ngo, H.; Botros, I.W.; Makarov, V.; Riaz, N.; Balachandran, V.; Leach, S.; Thompson, D.M.; et al. Stratification of Pancreatic Ductal Adenocarcinoma: Combinatorial Genetic, Stromal, and Immunologic Markers. *Clin. Cancer Res.* **2017**, *23*, 4429–4440. [CrossRef]
164. Kurahara, H.; Takao, S.; Maemura, K.; Mataki, Y.; Kuwahata, T.; Maeda, K.; Sakoda, M.; Iino, S.; Ishigami, S.; Ueno, S.; et al. M2-Polarized Tumor-Associated Macrophage Infiltration of Regional Lymph Nodes Is Associated With Nodal Lymphangiogenesis and Occult Nodal Involvement in pN0 Pancreatic Cancer. *Pancreas* **2013**, *42*, 155–159. [CrossRef]
165. Kurahara, H.; Shinchi, H.; Mataki, Y.; Maemura, K.; Noma, H.; Kubo, F.; Sakoda, M.; Ueno, S.; Natsugoe, S.; Takao, S. Significance of M2-Polarized Tumor-Associated Macrophage in Pancreatic Cancer. *J. Surg. Res.* **2011**, *167*, e211–e219. [CrossRef]
166. Bulle, A.; Lim, K.-H. Beyond just a tight fortress: Contribution of stroma to epithelial-mesenchymal transition in pancreatic cancer. *Signal Transduct. Target. Ther.* **2020**, *5*, 1–12. [CrossRef] [PubMed]
167. Kaneda, M.M.; Cappello, P.; Nguyen, A.V.; Ralainirina, N.; Hardamon, C.R.; Foubert, P.; Schmid, M.C.; Sun, P.; Mose, E.; Bouvet, M.; et al. Macrophage PI3Kγ Drives Pancreatic Ductal Adenocarcinoma Progression. *Cancer Discov.* **2016**, *6*, 870–885. [CrossRef] [PubMed]
168. Helm, O.; Held-Feindt, J.; Schäfer, H.; Sebens, S. M1 and M2: There is no "good" and "bad"—How macrophages promote malignancy-associated features in tumorigenesis. *OncoImmunology* **2014**, *3*, e946818. [CrossRef] [PubMed]
169. Chen, Q.; Wang, J.; Zhang, Q.; Zhang, J.; Lou, Y.; Yang, J.; Chen, Y.; Wei, T.; Zhang, J.; Fu, Q.; et al. Tumour cell-derived debris and IgG synergistically promote metastasis of pancreatic cancer by inducing inflammation via tumour-associated macrophages. *Br. J. Cancer* **2019**, *121*, 786–795. [CrossRef] [PubMed]
170. Halbrook, C.J.; Pontious, C.; Kovalenko, I.; Lapienyte, L.; Dreyer, S.; Lee, H.-J.; Thurston, G.; Zhang, Y.; Lazarus, J.; Sajjakulnukit, P.; et al. Macrophage-Released Pyrimidines Inhibit Gemcitabine Therapy in Pancreatic Cancer. *Cell Metab.* **2019**, *29*, 1390–1399.e6. [CrossRef] [PubMed]
171. Liu, Q.; Li, Y.; Niu, Z.; Zong, Y.; Wang, M.; Yao, L.; Lu, Z.; Liao, Q.; Zhao, Y. Atorvastatin (Lipitor) attenuates the effects of aspirin on pancreatic cancerogenesis and the chemotherapeutic efficacy of gemcitabine on pancreatic cancer by promoting M2 polarized tumor associated macrophages. *J. Exp. Clin. Cancer Res.* **2016**, *35*, 1–16. [CrossRef]
172. Weizman, N.; Krelin, Y.; Shabtayorbach, A.; Amit, M.; Binenbaum, Y.; Wong, R.J.; Gil, Z. Macrophages mediate gemcitabine resistance of pancreatic adenocarcinoma by upregulating cytidine deaminase. *Oncogene* **2013**, *33*, 3812–3819. [CrossRef] [PubMed]
173. Binenbaum, Y.; Fridman, E.; Yaari, Z.; Milman, N.; Schroeder, A.; Ben David, G.; Shlomi, T.; Gil, Z. Transfer of miRNA in Macrophage-Derived Exosomes Induces Drug Resistance in Pancreatic Adenocarcinoma. *Cancer Res.* **2018**, *78*, 5287–5299. [CrossRef] [PubMed]
174. Cheng, L.; Liu, J.; Liu, Q.; Liu, Y.; Fan, L.; Wang, F.; Yu, H.; Li, Y.; Bu, L.; Li, X.; et al. Exosomes from Melatonin Treated Hepatocellularcarcinoma Cells Alter the Immunosupression Status through STAT3 Pathway in Macrophages. *Int. J. Biol. Sci.* **2017**, *13*, 723–734. [CrossRef] [PubMed]
175. Deronic, A.; Nilsson, A.; Thagesson, M.; Werchau, D.; Smith, K.E.; Ellmark, P. The human anti-CD40 agonist antibody mitazalimab (ADC-1013; JNJ-64457107) activates antigen-presenting cells, improves expansion of antigen-specific T cells, and enhances anti-tumor efficacy of a model cancer vaccine in vivo. *Cancer Immunol. Immunother.* **2021**, 1–14. [CrossRef]
176. Vonderheide, R.H. CD40 Agonist Antibodies in Cancer Immunotherapy. *Annu. Rev. Med.* **2020**, *71*, 47–58. [CrossRef]
177. Beatty, G.; Chiorean, E.G.; Fishman, M.P.; Saboury, B.; Teitelbaum, U.R.; Sun, W.; Huhn, R.D.; Song, W.; Li, D.; Sharp, L.L.; et al. CD40 Agonists Alter Tumor Stroma and Show Efficacy Against Pancreatic Carcinoma in Mice and Humans. *Science* **2011**, *331*, 1612–1616. [CrossRef] [PubMed]
178. Byrne, K.T.; Betts, C.B.; Mick, R.; Sivagnanam, S.; Bajor, D.L.; Laheru, D.A.; Chiorean, E.G.; O'Hara, M.H.; Liudahl, S.M.; Newcomb, C.W.; et al. Neoadjuvant selicrelumab, an agonist CD40 antibody, induces changes in the tumor microenvironment in patients with resectable pancreatic cancer. *Clin. Cancer Res.* **2021**, *27*, 4574–4586. [CrossRef]
179. Morrison, A.H.; Diamond, M.S.; Hay, C.A.; Byrne, K.T.; Vonderheide, R.H. Sufficiency of CD40 activation and immune checkpoint blockade for T cell priming and tumor immunity. *Proc. Natl. Acad. Sci.* **2020**, *117*, 8022–8031. [CrossRef]

180. O'Hara, M.H.; O'Reilly, E.M.; Varadhachary, G.; Wolff, R.A.; Wainberg, Z.A.; Ko, A.H.; Fisher, G.; Rahma, O.; Lyman, J.P.; Cabanski, C.R.; et al. CD40 agonistic monoclonal antibody APX005M (sotigalimab) and chemotherapy, with or without nivolumab, for the treatment of metastatic pancreatic adenocarcinoma: An open-label, multicentre, phase 1b study. *Lancet Oncol.* **2021**, *22*, 118–131. [CrossRef]
181. O'Hara, M.H.; O'Reilly, E.M.; Wolff, R.A.; Wainberg, Z.A.; Ko, A.H.; Rahma, O.E.; Fisher, G.A.; Lyman, J.P.; Cabanski, C.R.; Karakunnel, J.J.; et al. Gemcitabine (Gem) and nab-paclitaxel (NP) ± nivolumab (nivo) ± CD40 agonistic monoclonal antibody APX005M (sotigalimab), in patients (Pts) with untreated metastatic pancreatic adenocarcinoma (mPDAC): Phase (Ph) 2 final results. *J. Clin. Oncol.* **2021**, *39*, 4019. [CrossRef]
182. Ho, T.T.B.; Nasti, A.; Seki, A.; Komura, T.; Inui, H.; Kozaka, T.; Kitamura, Y.; Shiba, K.; Yamashita, T.; Yamashita, T.; et al. Combination of gemcitabine and anti-PD-1 antibody enhances the anticancer effect of M1 macrophages and the Th1 response in a murine model of pancreatic cancer liver metastasis. *J. Immunother. Cancer* **2020**, *8*, e001367. [CrossRef]
183. Panni, R.Z.; Herndon, J.M.; Zuo, C.; Hegde, S.; Hogg, G.D.; Knolhoff, B.L.; Breden, M.A.; Li, X.; Krisnawan, V.E.; Khan, S.Q.; et al. Agonism of CD11b reprograms innate immunity to sensitize pancreatic cancer to immunotherapies. *Sci. Transl. Med.* **2019**, *11*, eaau9240. [CrossRef] [PubMed]
184. Pylayeva-Gupta, Y.; Das, S.; Handler, J.; Hajdu, C.H.; Coffre, M.; Koralov, S.; Bar-Sagi, D. IL35-Producing B Cells Promote the Development of Pancreatic Neoplasia. *Cancer Discov.* **2016**, *6*, 247–255. [CrossRef]
185. Minici, C.; Rigamonti, E.; Lanzillotta, M.; Monno, A.; Rovati, L.; Maehara, T.; Kaneko, N.; Deshpande, V.; Protti, M.P.; De Monte, L.; et al. B lymphocytes contribute to stromal reaction in pancreatic ductal adenocarcinoma. *OncoImmunology* **2020**, *9*, 1794359. [CrossRef] [PubMed]
186. Zheng, L.; Xue, J.; Jaffee, E.; Habtezion, A. Role of Immune Cells and Immune-Based Therapies in Pancreatitis and Pancreatic Ductal Adenocarcinoma. *Gastroenterology* **2013**, *144*, 1230–1240. [CrossRef]
187. Wörmann, S.M.; Diakopoulos, K.N.; Lesina, M.; Algül, H. The immune network in pancreatic cancer development and progression. *Oncogene* **2014**, *33*, 2956–2967. [CrossRef]
188. Ino, Y.; Yamazaki-Itoh, R.; Shimada, K.; Iwasaki, M.; Kosuge, T.; Kanai, Y.; Hiraoka, N. Immune cell infiltration as an indicator of the immune microenvironment of pancreatic cancer. *Br. J. Cancer* **2013**, *108*, 914–923. [CrossRef]
189. Fukunaga, A.; Miyamoto, M.; Cho, Y.; Murakami, S.; Kawarada, Y.; Oshikiri, T.; Kato, K.; Kurokawa, T.; Suzuoki, M.; Nakakubo, Y.; et al. CD8+ Tumor-Infiltrating Lymphocytes Together with CD4+ Tumor-Infiltrating Lymphocytes and Dendritic Cells Improve the Prognosis of Patients with Pancreatic Adenocarcinoma. *Pancreas* **2004**, *28*, e26–e31. [CrossRef]
190. Tewari, N.; Zaitoun, A.M.; Arora, A.; Madhusudan, S.; Ilyas, M.; Lobo, D.N. The presence of tumour-associated lymphocytes confers a good prognosis in pancreatic ductal adenocarcinoma: An immunohistochemical study of tissue microarrays. *BMC Cancer* **2013**, *13*, 436. [CrossRef]
191. Carstens, J.L.; de Sampaio, P.C.; Yang, D.; Barua, S.; Wang, H.; Rao, A.; Allison, J.; LeBleu, V.S.; Kalluri, R. Spatial computation of intratumoral T cells correlates with survival of patients with pancreatic cancer. *Nat. Commun.* **2017**, *8*, 15095. [CrossRef] [PubMed]
192. Hosein, A.N.; Brekken, R.A.; Maitra, A. Pancreatic cancer stroma: An update on therapeutic targeting strategies. *Nat. Rev. Gastroenterol. Hepatol.* **2020**, *17*, 487–505. [CrossRef]
193. Quaranta, V.; Rainer, C.; Nielsen, S.R.; Raymant, M.L.; Ahmed, M.S.; Engle, D.D.; Taylor, A.; Murray, T.; Campbell, F.; Palmer, D.H.; et al. Macrophage-Derived Granulin Drives Resistance to Immune Checkpoint Inhibition in Metastatic Pancreatic Cancer. *Cancer Res.* **2018**, *78*, 4253–4269. [CrossRef] [PubMed]
194. Saka, D.; Gökalp, M.; Piyade, B.; Cevik, N.C.; Sever, E.A.; Unutmaz, D.; Ceyhan, G.O.; Demir, I.E.; Asimgil, H. Mechanisms of T-Cell Exhaustion in Pancreatic Cancer. *Cancers* **2020**, *12*, 2274. [CrossRef]
195. Wherry, E.J.; Kurachi, M. Molecular and cellular insights into T cell exhaustion. *Nat. Rev. Immunol.* **2015**, *15*, 486–499. [CrossRef]
196. Russ, B.E.; Prier, J.; Rao, S.; Turner, S.J. T cell immunity as a tool for studying epigenetic regulation of cellular differentiation. *Front. Genet.* **2013**, *4*, 218. [CrossRef] [PubMed]
197. Huber, M.; Brehm, C.U.; Gress, T.M.; Buchholz, M.; Alhamwe, B.A.; Von Strandmann, E.P.; Slater, E.P.; Bartsch, J.W.; Bauer, C.; Lauth, M. The Immune Microenvironment in Pancreatic Cancer. *Int. J. Mol. Sci.* **2020**, *21*, 7307. [CrossRef] [PubMed]
198. Liao, W.; Lin, J.-X.; Leonard, W.J. Interleukin-2 at the Crossroads of Effector Responses, Tolerance, and Immunotherapy. *Immunity* **2013**, *38*, 13–25. [CrossRef]
199. Chen, S.; Crabill, G.A.; Pritchard, T.S.; McMiller, T.L.; Wei, P.; Pardoll, D.M.; Pan, F.; Topalian, S.L. Mechanisms regulating PD-L1 expression on tumor and immune cells. *J. Immunother. Cancer* **2019**, *7*, 1–12. [CrossRef]
200. De Monte, L.; Reni, M.; Tassi, E.; Clavenna, D.; Papa, I.; Recalde, H.; Braga, M.; Di Carlo, V.; Doglioni, C.; Protti, M.P. Intratumor T helper type 2 cell infiltrate correlates with cancer-associated fibroblast thymic stromal lymphopoietin production and reduced survival in pancreatic cancer. *J. Exp. Med.* **2011**, *208*, 469–478. [CrossRef]
201. Sica, A.; Schioppa, T.; Mantovani, A.; Allavena, P. Tumour-associated macrophages are a distinct M2 polarised population promoting tumour progression: Potential targets of anti-cancer therapy. *Eur. J. Cancer* **2006**, *42*, 717–727. [CrossRef]
202. Wynn, T.A. Fibrotic disease and the TH1/TH2 paradigm. *Nat. Rev. Immunol.* **2004**, *4*, 583–594. [CrossRef]
203. Formentini, A.; Prokopchuk, O.; Sträter, J.; Kleeff, J.; Grochola, L.F.; Leder, G.; Henne-Bruns, D.; Korc, M.; Kornmann, M. Interleukin-13 exerts autocrine growth-promoting effects on human pancreatic cancer, and its expression correlates with a propensity for lymph node metastases. *Int. J. Color. Dis.* **2008**, *24*, 57–67. [CrossRef] [PubMed]

204. Tassi, E.; Gavazzi, F.; Albarello, L.; Senyukov, V.; Longhi, R.; Dellabona, P.; Doglioni, C.; Braga, M.; Di Carlo, V.; Protti, M.P. Carcinoembryonic Antigen-Specific but Not Antiviral CD4+ T Cell Immunity Is Impaired in Pancreatic Carcinoma Patients. *J. Immunol.* **2008**, *181*, 6595–6603. [CrossRef]
205. Piro, G.; Simionato, F.; Carbone, C.; Frizziero, M.; Malleo, G.; Zanini, S.; Casolino, R.; Santoro, R.; Mina, M.M.; Zecchetto, C.; et al. A circulating TH2 cytokines profile predicts survival in patients with resectable pancreatic adenocarcinoma. *OncoImmunology* **2017**, *6*, e1322242. [CrossRef] [PubMed]
206. He, S.; Fei, M.; Wu, Y.; Zheng, D.; Wan, D.; Wang, L.; Li, D. Distribution and Clinical Significance of Th17 Cells in the Tumor Microenvironment and Peripheral Blood of Pancreatic Cancer Patients. *Int. J. Mol. Sci.* **2011**, *12*, 7424–7437. [CrossRef] [PubMed]
207. McAllister, F.; Bailey, J.M.; Alsina, J.; Nirschl, C.; Sharma, R.; Fan, H.; Rattigan, Y.; Roeser, J.C.; Lankapalli, R.H.; Zhang, H.; et al. Oncogenic Kras Activates a Hematopoietic-to-Epithelial IL-17 Signaling Axis in Preinvasive Pancreatic Neoplasia. *Cancer Cell* **2014**, *25*, 621–637. [CrossRef] [PubMed]
208. Hiraoka, N.; Onozato, K.; Kosuge, T.; Hirohashi, S. Prevalence of FOXP3+ Regulatory T Cells Increases During the Progression of Pancreatic Ductal Adenocarcinoma and Its Premalignant Lesions. *Clin. Cancer Res.* **2006**, *12*, 5423–5434. [CrossRef]
209. Tang, Y.; Xu, X.; Guo, S.; Zhang, C.; Tang, Y.; Tian, Y.; Ni, B.; Lu, B.; Wang, H. An Increased Abundance of Tumor-Infiltrating Regulatory T Cells Is Correlated with the Progression and Prognosis of Pancreatic Ductal Adenocarcinoma. *PLoS ONE* **2014**, *9*, e91551. [CrossRef]
210. Cinier, J.; Hubert, M.; Besson, L.; Di Roio, A.; Rodriguez, C.; Lombardi, V.; Caux, C.; Ménétrier-Caux, C. Recruitment and Expansion of Tregs Cells in the Tumor Environment—How to Target Them? *Cancers* **2021**, *13*, 1850. [CrossRef]
211. Lohr, J.; Knoechel, B.; Abbas, A.K. Regulatory T cells in the periphery. *Immunol. Rev.* **2006**, *212*, 149–162. [CrossRef]
212. Fu, S.; Zhang, N.; Yopp, A.C.; Chen, D.; Mao, M.; Chen, D.; Zhang, H.; Ding, Y.; Bromberg, J.S. TGF-beta Induces Foxp3 + T-Regulatory Cells from CD4 + CD25—Precursors. *Arab. Archaeol. Epigr.* **2004**, *4*, 1614–1627. [CrossRef] [PubMed]
213. Wang, X.; Lang, M.; Zhao, T.; Feng, X.; Zheng, C.; Huang, C.; Hao, J.; Dong, J.; Luo, L.; Li, X.; et al. Cancer-FOXP3 directly activated CCL5 to recruit FOXP3+Treg cells in pancreatic ductal adenocarcinoma. *Oncogene* **2017**, *36*, 3048–3058. [CrossRef] [PubMed]
214. Yang, M.-W.; Tao, L.-Y.; Yang, J.-Y.; Jiang, Y.-S.; Fu, X.-L.; Liu, W.; Huo, Y.-M.; Li, J.; Zhang, J.-F.; Hua, R.; et al. SFRP4 is a prognostic marker and correlated with Treg cell infiltration in pancreatic ductal adenocarcinoma. *Am. J. Cancer Res.* **2019**, *9*, 363–377. [PubMed]
215. Shen, T.; Jia, S.; Ding, G.; Ping, D.; Zhou, L.; Zhou, S.; Cao, L. BxPC-3-Derived Small Extracellular Vesicles Induce FOXP3+ Treg through ATM-AMPK-Sirtuins-Mediated FOXOs Nuclear Translocations. *iScience* **2020**, *23*, 101431. [CrossRef] [PubMed]
216. Grage-Griebenow, E.; Jerg, E.; Gorys, A.; Wicklein, D.; Wesch, D.; Freitag-Wolf, S.; Goebel, L.; Vogel, I.; Becker, T.; Ebsen, M.; et al. L1CAM promotes enrichment of immunosuppressive T cells in human pancreatic cancer correlating with malignant progression. *Mol. Oncol.* **2014**, *8*, 982–997. [CrossRef] [PubMed]
217. Jang, J.-E.; Hajdu, C.H.; Liot, C.; Miller, G.; Dustin, M.L.; Bar-Sagi, D. Crosstalk between Regulatory T Cells and Tumor-Associated Dendritic Cells Negates Anti-tumor Immunity in Pancreatic Cancer. *Cell Rep.* **2017**, *20*, 558–571. [CrossRef]
218. Chang, C.-H.; Pauklin, S. ROS and TGFβ: From pancreatic tumour growth to metastasis. *J. Exp. Clin. Cancer Res.* **2021**, *40*, 1–11. [CrossRef] [PubMed]
219. Himoudi, N.; Morgenstern, D.A.; Yan, M.; Vernay, B.; Saraiva, L.; Wu, Y.; Cohen, C.J.; Gustafsson, K.; Anderson, J. Human γδ T Lymphocytes Are Licensed for Professional Antigen Presentation by Interaction with Opsonized Target Cells. *J. Immunol.* **2012**, *188*, 1708–1716. [CrossRef]
220. Oberg, H.-H.; Peipp, M.; Kellner, C.; Sebens, S.; Krause, S.; Petrick, D.; Adam-Klages, S.; Röcken, C.; Becker, T.; Vogel, I.; et al. Novel Bispecific Antibodies Increase γδ T-Cell Cytotoxicity against Pancreatic Cancer Cells. *Cancer Res.* **2014**, *74*, 1349–1360. [CrossRef]
221. Viey, E.; Lucas, C.; Romagne, F.; Escudier, B.; Chouaib, S.; Caignard, A. Chemokine Receptors Expression and Migration Potential of Tumor-infiltrating and Peripheral-expanded Vγ9Vδ2 T Cells From Renal Cell Carcinoma Patients. *J. Immunother.* **2008**, *31*, 313–323. [CrossRef]
222. Matsuo, Y.; Ochi, N.; Sawai, H.; Yasuda, A.; Takahashi, H.; Funahashi, H.; Takeyama, H.; Tong, Z.; Guha, S. CXCL8/IL-8 and CXCL12/SDF-1α co-operatively promote invasiveness and angiogenesis in pancreatic cancer. *Int. J. Cancer* **2009**, *124*, 853–861. [CrossRef] [PubMed]
223. Gonnermann, D.; Oberg, H.-H.; Lettau, M.; Peipp, M.; Bauerschlag, D.; Sebens, S.; Kabelitz, D.; Wesch, D. Galectin-3 Released by Pancreatic Ductal Adenocarcinoma Suppresses γδ T Cell Proliferation but Not Their Cytotoxicity. *Front. Immunol.* **2020**, *11*, 1328. [CrossRef]
224. Song, S.; Ji, B.; Ramachandran, V.; Wang, H.; Hafley, M.; Logsdon, C.; Bresalier, R. Overexpressed Galectin-3 in Pancreatic Cancer Induces Cell Proliferation and Invasion by Binding Ras and Activating Ras Signaling. *PLoS ONE* **2012**, *7*, e42699. [CrossRef]
225. Jonescheit, H.; Oberg, H.-H.; Gonnermann, D.; Hermes, M.; Sulaj, V.; Peters, C.; Kabelitz, D.; Wesch, D. Influence of Indoleamine-2,3-Dioxygenase and Its Metabolite Kynurenine on γδ T Cell Cytotoxicity against Ductal Pancreatic Adenocarcinoma Cells. *Cells* **2020**, *9*, 1140. [CrossRef]
226. Daley, D.; Zambirinis, C.P.; Seifert, L.; Akkad, N.; Mohan, N.; Werba, G.; Barilla, R.; Torres-Hernandez, A.; Hundeyin, M.; Mani, V.R.; et al. γδ T Cells Support Pancreatic Oncogenesis by Restraining αβ T Cell Activation. *Cell* **2016**, *166*, 1485–1499.e15. [CrossRef]

227. Upadhrasta, S.; Zheng, L. Strategies in Developing Immunotherapy for Pancreatic Cancer: Recognizing and Correcting Multiple Immune "Defects" in the Tumor Microenvironment. *J. Clin. Med.* **2019**, *8*, 1472. [CrossRef]
228. Karamitopoulou, E. The Tumor Microenvironment of Pancreatic Cancer. *Cancers* **2020**, *12*, 3076. [CrossRef] [PubMed]
229. Hewitt, D.B.; Nissen, N.; Hatoum, H.; Musher, B.; Seng, J.; Coveler, A.L.; Al-Rajabi, R.; Yeo, C.J.; Leiby, B.; Banks, J.; et al. A Phase 3 Randomized Clinical Trial of Chemotherapy With or Without Algenpantucel-L (HyperAcute-Pancreas) Immunotherapy in Subjects with Borderline Resectable or Locally Advanced Unresectable Pancreatic Cancer. *Ann. Surg.* Publish Ah. **2020**. [CrossRef]
230. Middleton, G.; Silcocks, P.; Cox, T.; Valle, J.; Wadsley, J.; Propper, D.; Coxon, F.; Ross, P.; Madhusudan, S.; Roques, T.; et al. Gemcitabine and capecitabine with or without telomerase peptide vaccine GV1001 in patients with locally advanced or metastatic pancreatic cancer (TeloVac): An open-label, randomised, phase 3 trial. *Lancet Oncol.* **2014**, *15*, 829–840. [CrossRef]
231. Xie, C.; Duffy, A.G.; Brar, G.; Fioravanti, S.; Mabry-Hrones, D.; Walker, M.; Bonilla, C.M.; Wood, B.J.; Citrin, D.E.; Gil Ramirez, E.M.; et al. Immune Checkpoint Blockade in Combination with Stereotactic Body Radiotherapy in Patients with Metastatic Pancreatic Ductal Adenocarcinoma. *Clin. Cancer Res.* **2020**, *26*, 2318–2326. [CrossRef] [PubMed]
232. O'Reilly, E.M.; Oh, D.-Y.; Dhani, N.; Renouf, D.J.; Lee, M.A.; Sun, W.; Fisher, G.; Hezel, A.; Chang, S.-C.; Vlahovic, G.; et al. Durvalumab With or Without Tremelimumab for Patients With Metastatic Pancreatic Ductal Adenocarcinoma: A Phase 2 Randomized Clinical Trial. *JAMA Oncol.* **2019**, *5*, 1431–1438. [CrossRef]
233. Mahalingam, D.; Goel, S.; Aparo, S.; Arora, S.P.; Noronha, N.; Tran, H.; Chakrabarty, R.; Selvaggi, G.; Gutierrez, A.; Coffey, M.; et al. A Phase II Study of Pelareorep (REOLYSIN®) in Combination with Gemcitabine for Patients with Advanced Pancreatic Adenocarcinoma. *Cancers* **2018**, *10*, 160. [CrossRef]
234. Bockorny, B.; Semenisty, V.; Macarulla, T.; Borazanci, E.; Wolpin, B.M.; Stemmer, S.M.; Golan, T.; Geva, R.; Borad, M.J.; Pedersen, K.S.; et al. BL-8040, a CXCR4 antagonist, in combination with pembrolizumab and chemotherapy for pancreatic cancer: The COMBAT trial. *Nat. Med.* **2020**, *26*, 878–885. [CrossRef] [PubMed]
235. Tsujikawa, T.; Crocenzi, T.; Durham, J.N.; Sugar, E.A.; Wu, A.A.; Onners, B.; Nauroth, J.M.; Anders, R.A.; Fertig, E.J.; Laheru, D.A.; et al. Evaluation of Cyclophosphamide/GVAX Pancreas Followed by Listeria-Mesothelin (CRS-207) with or without Nivolumab in Patients with Pancreatic Cancer. *Clin. Cancer Res.* **2020**, *26*, 3578–3588. [CrossRef] [PubMed]
236. Wu, A.A.; Bever, K.M.; Ho, W.J.; Fertig, E.J.; Niu, N.; Zheng, L.; Parkinson, R.M.; Durham, J.N.; Onners, B.L.; Ferguson, A.K.; et al. A Phase II Study of Allogeneic GM-CSF–Transfected Pancreatic Tumor Vaccine (GVAX) with Ipilimumab as Maintenance Treatment for Metastatic Pancreatic Cancer. *Clin. Cancer Res.* **2020**, *26*, 5129–5139. [CrossRef] [PubMed]
237. Oberg, H.-H.; Kellner, C.; Gonnermann, D.; Sebens, S.; Bauerschlag, D.; Gramatzki, M.; Kabelitz, D.; Peipp, M.; Wesch, D. Tribody [(HER2)2xCD16] Is More Effective Than Trastuzumab in Enhancing γδ T Cell and Natural Killer Cell Cytotoxicity Against HER2-Expressing Cancer Cells. *Front. Immunol.* **2018**, *9*, 814. [CrossRef]
238. Oberg, H.-H.; Kellner, C.; Peipp, M.; Sebens, S.; Adam-Klages, S.; Gramatzki, M.; Kabelitz, D.; Wesch, D. Monitoring Circulating γδ T Cells in Cancer Patients to Optimize γδ T Cell-Based Immunotherapy. *Front. Immunol.* **2014**, *5*, 643. [CrossRef]
239. Kvarnhammar, A.M.; Veitonmäki, N.; Hägerbrand, K.; Dahlman, A.; Smith, K.E.; Fritzell, S.; Von Schantz, L.; Thagesson, M.; Werchau, D.; Smedenfors, K.; et al. The CTLA-4 x OX40 bispecific antibody ATOR-1015 induces anti-tumor effects through tumor-directed immune activation. *J. Immunother. Cancer* **2019**, *7*, 103. [CrossRef]
240. Zhang, Y.; Lazarus, J.; Steele, N.G.; Yan, W.; Lee, H.-J.; Nwosu, Z.C.; Halbrook, C.J.; Menjivar, R.; Kemp, S.B.; Sirihorachai, V.R.; et al. Regulatory T-cell Depletion Alters the Tumor Microenvironment and Accelerates Pancreatic Carcinogenesis. *Cancer Discov.* **2020**, *10*, 422–439. [CrossRef]
241. Chen, D.S.; Mellman, I. Elements of cancer immunity and the cancer–immune set point. *Nature* **2017**, *541*, 321–330. [CrossRef]
242. Barău, A.; Ruiz-Sauri, A.; Valencia, G.; Gómez-Mateo, M.D.C.; Sabater, L.; Ferrández, A.; Llombart-Bosch, A. High microvessel density in pancreatic ductal adenocarcinoma is associated with high grade. *Virchows Archiv.* **2013**, *462*, 541–546. [CrossRef]
243. Van Der Zee, J.A.; Van Eijck, C.H.; Hop, W.C.; Van Dekken, H.; Dicheva, B.M.; Seynhaeve, A.L.; Koning, G.A.; Eggermont, A.M.; Hagen, T.L.T. Angiogenesis: A prognostic determinant in pancreatic cancer? *Eur. J. Cancer* **2011**, *47*, 2576–2584. [CrossRef]
244. Wang, W.-Q.; Liu, L.; Xu, H.-X.; Luo, G.; Chen, T.; Wu, C.-T.; Xu, Y.-F.; Xu, J.; Liu, C.; Zhang, B.; et al. Intratumoral α-SMA Enhances the Prognostic Potency of CD34 Associated with Maintenance of Microvessel Integrity in Hepatocellular Carcinoma and Pancreatic Cancer. *PLoS ONE* **2013**, *8*, e71189. [CrossRef]
245. Yamakawa, M.; Liu, L.X.; Date, T.; Belanger, A.J.; Vincent, K.A.; Akita, G.Y.; Kuriyama, T.; Cheng, S.H.; Gregory, R.J.; Jiang, C. Hypoxia-Inducible Factor-1 Mediates Activation of Cultured Vascular Endothelial Cells by Inducing Multiple Angiogenic Factors. *Circ. Res.* **2003**, *93*, 664–673. [CrossRef]
246. Masamune, A.; Kikuta, K.; Watanabe, T.; Satoh, K.; Hirota, M.; Shimosegawa, T. Hypoxia stimulates pancreatic stellate cells to induce fibrosis and angiogenesis in pancreatic cancer. *Am. J. Physiol. Liver Physiol.* **2008**, *295*, G709–G717. [CrossRef]
247. Li, S.; Xu, H.-X.; Wu, C.-T.; Wang, W.-Q.; Jin, W.; Gao, H.-L.; Li, H.; Zhang, S.-R.; Xu, J.-Z.; Qi, Z.-H.; et al. Angiogenesis in pancreatic cancer: Current research status and clinical implications. *Angiogenesis* **2019**, *22*, 15–36. [CrossRef]
248. Carmeliet, P.; Jain, R.K. Angiogenesis in cancer and other diseases. *Nature* **2000**, *407*, 249–257. [CrossRef] [PubMed]
249. Dudley, A.C. Tumor Endothelial Cells. *Cold Spring Harb. Perspect. Med.* **2011**, 2, a006536. [CrossRef] [PubMed]
250. Lugano, R.; Ramachandran, M.; Dimberg, A. Tumor angiogenesis: Causes, consequences, challenges and opportunities. *Cell. Mol. Life Sci.* **2019**, *77*, 1745–1770. [CrossRef] [PubMed]

251. Hida, K.; Maishi, N.; Annan, D.A.; Hida, Y. Contribution of Tumor Endothelial Cells in Cancer Progression. *Int. J. Mol. Sci.* **2018**, *19*, 1272. [CrossRef] [PubMed]
252. Cheng, H.-W.; Chen, Y.-F.; Wong, J.-M.; Weng, C.-W.; Chen, H.-Y.; Yu, S.-L.; Chen, H.-W.; Yuan, A.; Chen, J.J. Cancer cells increase endothelial cell tube formation and survival by activating the PI3K/Akt signalling pathway. *J. Exp. Clin. Cancer Res.* **2017**, *36*, 1–13. [CrossRef] [PubMed]
253. Xiong, Y.-Q.; Sun, H.-C.; Zhang, W.; Zhu, X.-D.; Zhuang, P.-Y.; Zhang, J.-B.; Wang, L.; Wu, W.-Z.; Qin, L.-X.; Tang, Z.-Y. Human Hepatocellular Carcinoma Tumor–derived Endothelial Cells Manifest Increased Angiogenesis Capability and Drug Resistance Compared with Normal Endothelial Cells. *Clin. Cancer Res.* **2009**, *15*, 4838–4846. [CrossRef] [PubMed]
254. Hida, K.; Hida, Y.; Amin, D.N.; Flint, A.F.; Panigrahy, D.; Morton, C.C.; Klagsbrun, M. Tumor-Associated Endothelial Cells with Cytogenetic Abnormalities. *Cancer Res.* **2004**, *64*, 8249–8255. [CrossRef] [PubMed]
255. Ohga, N.; Ishikawa, S.; Maishi, N.; Akiyama, K.; Hida, Y.; Kawamoto, T.; Sadamoto, Y.; Osawa, T.; Yamamoto, K.; Kondoh, M.; et al. Heterogeneity of Tumor Endothelial Cells. *Am. J. Pathol.* **2012**, *180*, 1294–1307. [CrossRef]
256. Alessandri, G.; Chirivi, R.G.; Fiorentini, S.; Dossi, R.; Bonardelli, S.; Giulini, S.M.; Zanetta, G.; Landoni, F.; Graziotti, P.P.; Turano, A.; et al. Phenotypic and functional characteristics of tumour-derived microvascular endothelial cells. *Clin. Exp. Metastasis* **1999**, *17*, 655–662. [CrossRef]
257. Ruscetti, M.; Morris, J.P.; Mezzadra, R.; Russell, J.; Leibold, J.; Romesser, P.B.; Simon, J.; Kulick, A.; Ho, Y.-J.; Fennell, M.; et al. Senescence-Induced Vascular Remodeling Creates Therapeutic Vulnerabilities in Pancreas Cancer. *Cell* **2020**, *181*, 424–441.e21. [CrossRef]
258. Zhao, Q.; Eichten, A.; Parveen, A.; Adler, C.; Huang, Y.; Wang, W.; Ding, Y.; Adler, A.; Nevins, T.; Ni, M.; et al. Single-Cell Transcriptome Analyses Reveal Endothelial Cell Heterogeneity in Tumors and Changes following Antiangiogenic Treatment. *Cancer Res.* **2018**, *78*, 2370–2382. [CrossRef]
259. Hida, K.; Maishi, N.; Sakurai, Y.; Hida, Y.; Harashima, H. Heterogeneity of tumor endothelial cells and drug delivery. *Adv. Drug Deliv. Rev.* **2016**, *99*, 140–147. [CrossRef]
260. Maishi, N.; Hida, K. Tumor endothelial cells accelerate tumor metastasis. *Cancer Sci.* **2017**, *108*, 1921–1926. [CrossRef] [PubMed]
261. Adjuto-Saccone, M.; Soubeyran, P.; Garcia, J.; Audebert, S.; Camoin, L.; Rubis, M.; Roques, J.; Binétruy, B.; Iovanna, J.L.; Tournaire, R. TNF-α induces endothelial–mesenchymal transition promoting stromal development of pancreatic adenocarcinoma. *Cell Death Dis.* **2021**, *12*, 1–15. [CrossRef]
262. Choi, K.J.; Nam, J.-K.; Kim, J.-H.; Choi, S.-H.; Lee, Y.-J. Endothelial-to-mesenchymal transition in anticancer therapy and normal tissue damage. *Exp. Mol. Med.* **2020**, *52*, 781–792. [CrossRef]
263. Garcia, J.; Sandí, M.J.; Cordelier, P.; Binétruy, B.; Pouysségur, J.; Iovanna, J.L.; Tournaire, R. Tie1 deficiency induces endothelial–mesenchymal transition. *EMBO Rep.* **2012**, *13*, 431–439. [CrossRef]
264. Issa, Y.; Nummer, D.; Seibel, T.; Müerköster, S.S.; Koch, M.; Schmitz-Winnenthal, F.-H.; Galindo, L.; Weitz, J.; Beckhove, P.; Altevogt, P. Enhanced L1CAM expression on pancreatic tumor endothelium mediates selective tumor cell transmigration. *J. Mol. Med.* **2008**, *87*, 99–112. [CrossRef]
265. Sano, M.; Takahashi, R.; Ijichi, H.; Ishigaki, K.; Yamada, T.; Miyabayashi, K.; Kimura, G.; Mizuno, S.; Kato, H.; Fujiwara, H.; et al. Blocking VCAM-1 inhibits pancreatic tumour progression and cancer-associated thrombosis/thromboembolism. *Gut* **2021**, *70*, 1713–1723. [CrossRef]
266. Nummer, D.; Suri-Payer, E.; Schmitz-Winnenthal, H.; Bonertz, A.; Galindo, L.; Antolovich, D.; Koch, M.; Büchler, M.; Weitz, J.; Schirrmacher, V.; et al. Role of Tumor Endothelium in CD4+CD25+ Regulatory T Cell Infiltration of Human Pancreatic Carcinoma. *J. Natl. Cancer Inst.* **2007**, *99*, 1188–1199. [CrossRef] [PubMed]
267. Harjunpää, H.; Asens, M.L.; Guenther, C.; Fagerholm, S.C. Cell Adhesion Molecules and Their Roles and Regulation in the Immune and Tumor Microenvironment. *Front. Immunol.* **2019**, *10*, 1078. [CrossRef] [PubMed]
268. Klein, D. The Tumor Vascular Endothelium as Decision Maker in Cancer Therapy. *Front. Oncol.* **2018**, *8*, 367. [CrossRef]
269. Orozco, C.A.; Bosch, N.M.; Guerrero, P.E.; Vinaixa, J.; Dalotto-Moreno, T.; Iglesias, M.; Moreno, M.; Djurec, M.; Poirier, F.; Gabius, H.-J.; et al. Targeting galectin-1 inhibits pancreatic cancer progression by modulating tumor–stroma crosstalk. *Proc. Natl. Acad. Sci.* **2018**, *115*, E3769–E3778. [CrossRef]
270. Hotz, H. Angiogenesis inhibitor TNP-470 reduces human pancreatic cancer growth. *J. Gastrointest. Surg.* **2001**, *5*, 131–138. [CrossRef]
271. Kato, H.; Ishikura, H.; Kawarada, Y.; Furuya, M.; Kondo, S.; Kato, H.; Yoshiki, T. Anti-angiogenic Treatment for Peritoneal Dissemination of Pancreas Adenocarcinoma: A Study Using TNP-470. *Jpn. J. Cancer Res.* **2001**, *92*, 67–73. [CrossRef]
272. Martin, L.K.; Li, X.; Kleiber, B.; Ellison, E.C.; Bloomston, M.; Zalupski, M.; Bekaii-Saab, T.S. VEGF remains an interesting target in advanced pancreas cancer (APCA): Results of a multi-institutional phase II study of bevacizumab, gemcitabine, and infusional 5-fluorouracil in patients with APCA. *Ann. Oncol.* **2012**, *23*, 2812–2820. [CrossRef] [PubMed]
273. Gilles, M.-E.; Maione, F.; Cossutta, M.; Carpentier, G.; Caruana, L.; Di Maria, S.; Houppe, C.; Destouches, D.; Shchors, K.; Prochasson, C.; et al. Nucleolin Targeting Impairs the Progression of Pancreatic Cancer and Promotes the Normalization of Tumor Vasculature. *Cancer Res.* **2016**, *76*, 7181–7193. [CrossRef] [PubMed]
274. Viallard, C.; Larrivée, B. Tumor angiogenesis and vascular normalization: Alternative therapeutic targets. *Angiogenesis* **2017**, *20*, 409–426. [CrossRef] [PubMed]

275. Mazzone, M.; Dettori, D.; de Oliveira, R.L.; Loges, S.; Schmidt, T.; Jonckx, B.; Tian, Y.-M.; Lanahan, A.A.; Pollard, P.; de Almodovar, C.R.; et al. Heterozygous Deficiency of PHD2 Restores Tumor Oxygenation and Inhibits Metastasis via Endothelial Normalization. *Cell* **2009**, *136*, 839–851. [CrossRef] [PubMed]
276. Cartier, A.; Leigh, T.; Liu, C.H.; Hla, T. Endothelial sphingosine 1-phosphate receptors promote vascular normalization and antitumor therapy. *Proc. Natl. Acad. Sci.* **2020**, *117*, 3157–3166. [CrossRef] [PubMed]
277. Ivy, S.P.; Wick, J.Y.; Kaufman, B.M. An overview of small-molecule inhibitors of VEGFR signaling. *Nat. Rev. Clin. Oncol.* **2009**, *6*, 569–579. [CrossRef] [PubMed]
278. Ottaiano, A.; Capozzi, M.; De Divitiis, C.; De Stefano, A.; Botti, G.; Avallone, A.; Tafuto, S. Gemcitabine mono-therapy versus gemcitabine plus targeted therapy in advanced pancreatic cancer: A meta-analysis of randomized phase III trials. *Acta Oncol.* **2017**, *56*, 377–383. [CrossRef]
279. Kindler, H.L.; Niedzwiecki, D.; Hollis, D.; Sutherland, S.; Schrag, D.; Hurwitz, H.; Innocenti, F.; Mulcahy, M.F.; O'Reilly, E.; Wozniak, T.F.; et al. Gemcitabine Plus Bevacizumab Compared With Gemcitabine Plus Placebo in Patients With Advanced Pancreatic Cancer: Phase III Trial of the Cancer and Leukemia Group B (CALGB 80303). *J. Clin. Oncol.* **2010**, *28*, 3617–3622. [CrossRef]
280. Annese, T.; Tamma, R.; Ruggieri, S.; Ribatti, D. Angiogenesis in Pancreatic Cancer: Pre-Clinical and Clinical Studies. *Cancers* **2019**, *11*, 381. [CrossRef]
281. Miller, M.O.; Kashyap, P.C.; Becker, S.L.; Thomas, R.M.; Hodin, R.A.; Miller, G.; Hundeyin, M.; Pushalkar, S.; Cohen, D.; Saxena, D.; et al. SSAT State-of-the-Art Conference: Advancements in the Microbiome. *J. Gastrointest. Surg.* **2020**, *25*, 1–11. [CrossRef]
282. Thomas, H. Intra-tumour bacteria promote gemcitabine resistance in pancreatic adenocarcinoma. *Nat. Rev. Gastroenterol. Hepatol.* **2017**, *14*, 632. [CrossRef] [PubMed]
283. Gaiser, R.A.; Halimi, A.; Alkharaan, H.; Lu, L.; Davanian, H.; Healy, K.; Hugerth, L.W.; Ateeb, Z.; Valente, R.; Moro, C.F.; et al. Enrichment of oral microbiota in early cystic precursors to invasive pancreatic cancer. *Gut* **2019**, *68*, 2186–2194. [CrossRef] [PubMed]
284. Ciernikova, S.; Novisedlakova, M.; Cholujova, D.; Stevurkova, V.; Mego, M. The Emerging Role of Microbiota and Microbiome in Pancreatic Ductal Adenocarcinoma. *Biomedicines* **2020**, *8*, 565. [CrossRef]
285. Mitsuhashi, K.; Nosho, K.; Sukawa, Y.; Matsunaga, Y.; Ito, M.; Kurihara, H.; Kanno, S.; Igarashi, H.; Naito, T.; Adachi, Y.; et al. Association ofFusobacteriumspecies in pancreatic cancer tissues with molecular features and prognosis. *Oncotarget* **2015**, *6*, 7209–7220. [CrossRef]
286. Gopalakrishnan, V.; Spencer, C.N.; Nezi, L.; Reuben, A.; Andrews, M.C.; Karpinets, T.V.; Prieto, P.A.; Vicente, D.; Hoffman, K.; Wei, S.C.; et al. Gut microbiome modulates response to anti–PD-1 immunotherapy in melanoma patients. *Science* **2018**, *359*, 97–103. [CrossRef]
287. Matson, V.; Fessler, J.; Bao, R.; Chongsuwat, T.; Zha, Y.; Alegre, M.-L.; Luke, J.J.; Gajewski, T.F. The commensal microbiome is associated with anti–PD-1 efficacy in metastatic melanoma patients. *Science* **2018**, *359*, 104–108. [CrossRef]
288. Routy, B.; Le Chatelier, E.; DeRosa, L.; Duong, C.P.M.; Alou, M.T.; Daillère, R.; Fluckiger, A.; Messaoudene, M.; Rauber, C.; Roberti, M.P.; et al. Gut microbiome influences efficacy of PD-1–based immunotherapy against epithelial tumors. *Science* **2017**, *359*, 91–97. [CrossRef] [PubMed]
289. Kleeff, J.; Whitcomb, D.C.; Shimosegawa, T.; Esposito, I.; Lerch, M.M.; Gress, T.; Mayerle, J.; Drewes, A.; Rebours, V.; Akisik, F.; et al. Chronic pancreatitis. *Nat. Rev. Dis. Prim.* **2017**, *3*, 17060. [CrossRef] [PubMed]
290. Wei, M.-Y.; Shi, S.; Liang, C.; Meng, Q.C.; Hua, J.; Zhang, Y.-Y.; Liu, J.; Bo, Z.; Xu, J.; Yu, X.J. The microbiota and microbiome in pancreatic cancer: More influential than expected. *Mol. Cancer* **2019**, *18*, 97. [CrossRef] [PubMed]
291. Diakos, C.I.; Charles, K.A.; McMillan, D.C.; Clarke, S.J. Cancer-related inflammation and treatment effectiveness. *Lancet Oncol.* **2014**, *15*, e493–e503. [CrossRef]
292. Stone, M.L.; Beatty, G.L. Cellular determinants and therapeutic implications of inflammation in pancreatic cancer. *Pharmacol. Ther.* **2019**, *201*, 202–213. [CrossRef]
293. Pastushenko, I.; Blanpain, C. EMT Transition States during Tumor Progression and Metastasis. *Trends Cell Biol.* **2019**, *29*, 212–226. [CrossRef] [PubMed]
294. Hofman, P.; Vouret-Craviari, V. Microbes-induced EMT at the crossroad of inflammation and cancer. *Gut Microbes* **2012**, *3*, 176–185. [CrossRef]
295. Vergara, D.; Simeone, P.; Damato, M.; Maffia, M.; Lanuti, P.; Trerotola, M. The Cancer Microbiota: EMT and Inflammation as Shared Molecular Mechanisms Associated with Plasticity and Progression. *J. Oncol.* **2019**, *2019*, 1–16. [CrossRef]
296. Goebel, L.; Grage-Griebenow, E.; Gorys, A.; Helm, O.; Genrich, G.; Lenk, L.; Wesch, D.; Ungefroren, H.; Freitag-Wolf, S.; Sipos, B.; et al. CD4+T cells potently induce epithelial-mesenchymal-transition in premalignant and malignant pancreatic ductal epithelial cells–novel implications of CD4+T cells in pancreatic cancer development. *OncoImmunology* **2015**, *4*, e1000083. [CrossRef] [PubMed]
297. Rhim, A.D.; Mirek, E.T.; Aiello, N.M.; Maitra, A.; Bailey, J.M.; McAllister, F.; Reichert, M.; Beatty, G.L.; Rustgi, A.K.; Vonderheide, R.H.; et al. EMT and Dissemination Precede Pancreatic Tumor Formation. *Cell* **2012**, *148*, 349–361. [CrossRef]
298. Vétizou, M.; Pitt, J.M.; Daillère, R.; Lepage, P.; Waldschmitt, N.; Flament, C.; Rusakiewicz, S.; Routy, B.; Roberti, M.P.; Duong, C.P.M.; et al. Anticancer immunotherapy by CTLA-4 blockade relies on the gut microbiota. *Science* **2015**, *350*, 1079–1084. [CrossRef]

299. Tanoue, T.; Morita, S.; Plichta, D.R.; Skelly, A.N.; Suda, W.; Sugiura, Y.; Narushima, S.; Vlamakis, H.; Motoo, I.; Sugita, K.; et al. A defined commensal consortium elicits CD8 T cells and anti-cancer immunity. *Nature* **2019**, *565*, 600–605. [CrossRef] [PubMed]
300. Sivan, A.; Corrales, L.; Hubert, N.; Williams, J.B.; Aquino-Michaels, K.; Earley, Z.M.; Benyamin, F.W.; Lei, Y.M.; Jabri, B.; Alegre, M.L.; et al. Commensal Bifidobacterium Promotes Antitumor Immunity and Facilitates Anti-PD-L1 Efficacy. *Science* **2015**, *350*, 1084–1089. [CrossRef]
301. Froeling, F.; Casolino, R.; Pea, A.; Biankin, A.; Chang, D.; Precision-Panc, O.B.O. Molecular Subtyping and Precision Medicine for Pancreatic Cancer. *J. Clin. Med.* **2021**, *10*, 149. [CrossRef]
302. Ding, D.; Javed, A.A.; Cunningham, D.; Teinor, J.; Wright, M.; Javed, Z.N.; Wilt, C.; Parish, L.; Hodgin, M.; Ryan, A.; et al. Challenges of the current precision medicine approach for pancreatic cancer: A single institution experience between 2013 and 2017. *Cancer Lett.* **2021**, *497*, 221–228. [CrossRef] [PubMed]
303. Dreyer, S.; Jamieson, N.; Cooke, S.; Valle, J.; McKay, C.; Biankin, A.; Chang, D. PRECISION-Panc: The Next Generation Therapeutic Development Platform for Pancreatic Cancer. *Clin. Oncol.* **2020**, *32*, 1–4. [CrossRef]
304. Gore, J.; Korc, M. Pancreatic Cancer Stroma: Friend or Foe? *Cancer Cell* **2014**, *25*, 711–712. [CrossRef]
305. Jiang, H.; Torphy, R.J.; Steiger, K.; Hongo, H.; Ritchie, A.J.; Kriegsmann, M.; Horst, D.; Umetsu, S.E.; Joseph, N.M.; McGregor, K.; et al. Pancreatic ductal adenocarcinoma progression is restrained by stromal matrix. *J. Clin. Investig.* **2020**, *130*, 4704–4709. [CrossRef]
306. Dreyer, S.B.; Pinese, M.; Jamieson, N.B.; Scarlett, C.J.; Colvin, E.K.; Pajic, M.; Johns, A.L.; Humphris, J.L.; Wu, J.; Cowley, M.J.; et al. Precision Oncology in Surgery. *Ann. Surg.* **2018**, *272*, 366–376. [CrossRef] [PubMed]
307. Heredia-Soto, V.; Rodríguez-Salas, N.; Feliu, J. Liquid Biopsy in Pancreatic Cancer: Are We Ready to Apply It in the Clinical Practice? *Cancers* **2021**, *13*, 1986. [CrossRef] [PubMed]
308. Ho, W.J.; Jaffee, E.M.; Zheng, L. The tumour microenvironment in pancreatic cancer—Clinical challenges and opportunities. *Nat. Rev. Clin. Oncol.* **2020**, *17*, 527–540. [CrossRef] [PubMed]
309. Torphy, R.J.; Wang, Z.; True-Yasaki, A.; Volmar, K.E.; Rashid, N.; Yeh, B.; Johansen, J.S.; Hollingsworth, M.A.; Yeh, J.J.; Collisson, E.A. Stromal Content Is Correlated With Tissue Site, Contrast Retention, and Survival in Pancreatic Adenocarcinoma. *JCO Precis. Oncol.* **2018**, *2*, 1–12. [CrossRef]
310. Tripathi, A.; Kashyap, A.; Tripathi, G.; Yadav, J.; Bibban, R.; Aggarwal, N.; Thakur, K.; Chhokar, A.; Jadli, M.; Sah, A.K.; et al. Tumor reversion: A dream or a reality. *Biomark. Res.* **2021**, *9*, 1–27. [CrossRef]
311. Kocher, H.M.; Basu, B.; Froeling, F.E.M.; Sarker, D.; Slater, S.; Carlin, D.; Desouza, N.M.; De Paepe, K.N.; Goulart, M.R.; Hughes, C.; et al. Phase I clinical trial repurposing all-trans retinoic acid as a stromal targeting agent for pancreatic cancer. *Nat. Commun.* **2020**, *11*, 1–9. [CrossRef]

frontiers | Frontiers in Immunology

TYPE Original Research
PUBLISHED 28 June 2023
DOI 10.3389/fimmu.2023.1157397

OPEN ACCESS

EDITED BY
Sven Brandau,
University of Duisburg-Essen, Germany

REVIEWED BY
Changqing Xie,
Clinical Center (NIH), United States
Aristeidis E. Boukouris,
Red Cross Hospital, Greece

*CORRESPONDENCE
Susanne Sebens
susanne.sebens@email.uni-kiel.de

†These authors have contributed equally to this work and share first authorship

‡These authors have contributed equally to this work and share last authorship

RECEIVED 02 February 2023
ACCEPTED 09 June 2023
PUBLISHED 28 June 2023

CITATION
Daunke T, Beckinger S, Rahn S, Krüger S, Heckl S, Schäfer H, Wesch D, Pilarsky C, Eckstein M, Hartmann A, Röcken C, Wandmacher AM and Sebens S (2023) Expression and role of the immune checkpoint regulator PD-L1 in the tumor-stroma interplay of pancreatic ductal adenocarcinoma.
Front. Immunol. 14:1157397.
doi: 10.3389/fimmu.2023.1157397

Expression and role of the immune checkpoint regulator PD-L1 in the tumor-stroma interplay of pancreatic ductal adenocarcinoma

Tina Daunke[1†], Silje Beckinger[1†], Sascha Rahn[2], Sandra Krüger[3], Steffen Heckl[3,4], Heiner Schäfer[1], Daniela Wesch[5], Christian Pilarsky[6], Markus Eckstein[7], Arndt Hartmann[7], Christoph Röcken[3], Anna Maxi Wandmacher[1,4‡] and Susanne Sebens[1*‡]

[1]Institute for Experimental Cancer Research, Kiel University and University Hospital Schleswig-Holstein, Kiel, Germany, [2]Biochemical Institute, Kiel University, Kiel, Germany, [3]Institute of Pathology, University Medical Center Schleswig-Holstein, Kiel, Germany, [4]Department of Internal Medicine II, University Medical Center Schleswig-Holstein, Kiel, Germany, [5]Institute of Immunology, Kiel University and University Medical Center Schleswig-Holstein (UKSH), Kiel, Germany, [6]Translational Research Center, University Hospital Erlangen, Erlangen, Germany, [7]Institute of Pathology, University Hospital Erlangen, Friedrich-Alexander-Universität Erlangen-Nürnberg (FAU), Erlangen, Germany

Introduction: Immune checkpoint inhibitors (ICI), e.g., targeting programmed cell death protein 1-ligand 1 (PD-L1) or its receptor PD-1, have markedly improved the therapy of many cancers but so far failed in pancreatic ductal adenocarcinoma (PDAC). Macrophages represent one of the most abundant immune cell populations within the tumor microenvironment (TME) of PDAC being able to either support or restrain tumor progression depending on their phenotype. To better understand treatment failure of PD-L1/PD-1 inhibitors in PDAC, this study examined PD-L1 expression in the context of a dynamic TME in PDAC with a particular focus on the impact of macrophages.

Methods: Formalin-fixed and paraffin embedded tissue samples of primary PDAC tissues and corresponding liver metastases were used for immunohistochemical analyses. Serial sections were stained with antibodies detecting Pan-Cytokeratin, CD68, CD163, CD8, and PD-L1.To investigate whether the PD-1/PD-L1 axis and macrophages contribute to immune escape of PDAC cells, a stroma enriched 3D spheroid coculture model was established in vitro, using different PDAC cell lines and macrophages subtypes as well as CD8 + T cells. Functional and flow cytometry analyses were conducted to characterize cell populations.

Results: Immunohistochemical analyses revealed that PD-L1 is mainly expressed by stroma cells, including macrophages and not PDAC cells in primary PDAC tissues and corresponding liver metastases. Notably, high local abundance of macrophages and strong PD-L1 staining were commonly found at invasion fronts of tumoral lesions between CD8+ T cells and tumor cells. In order to investigate whether PD-L1 expressing macrophages impact the response of

10.3389/fimmu.2023.1157397

PDAC cells to treatment with PD-L1/PD-1 inhibitors, we developed a spheroid model comprising two different PDAC cell lines and different ratios of in vitro differentiated primary M1- or M2-like polarized macrophages. In line with our in situ findings, high PD-L1 expression was observed in macrophages rather than PDAC cells, which was further increased by the presence of PDAC cells. The effector phenotype of co-cultured CD8+ T cells exemplified by expression of activation markers and release of effector molecules was rather enhanced by PDAC macrophage spheroids, particularly with M1-like macrophages compared to mono-culture spheroids. However, this was not associated with enhanced PDAC cell death. ICI treatment with either Durvalumab or Pembrolizumab alone or in combination with Gemcitabine hardly affected the effector phenotype of CD8+ T cells along with PDAC cell death. Thus, despite strong PD-L1 expression in macrophages, ICI treatment did not result in an enhanced activation and cytotoxic phenotype of CD8+ T cells.

Conclusion: Overall, our study revealed novel insights into the interplay of PDAC cells and macrophages in the presence of ICI.

KEYWORDS

pancreatic cancer, immune checkpoint inhibitor, immune evasion, tumor microenvironment, macrophages, 3D co-culture

1 Introduction

In western countries, pancreatic ductal adenocarcinoma (PDAC) is the 4th leading cause of cancer-related deaths, with a low 5-year survival rate of 10% (1). PDAC is characterized by a pronounced immunosuppressive tumor microenvironment (TME) which plays a crucial role in tumor development and progression in the primary as well as in the secondary context (2). One of the most abundant stroma cell populations are tumor-associated macrophages (TAM) (3, 4) which can exhibit different phenotypes. Following a simplified model, an M1-like phenotype is associated with pro-inflammatory and anti-tumorigenic properties, while M2-like polarized macrophages exert anti-inflammatory and pro-tumorigenic effects (3). Macrophages are early recruited into precursor/tumoral lesions and, therefore, accumulate as one of the first immune cell populations (5). TAM's frequency and effector phenotype are highly variable and change during PDAC progression. However, most TAM exhibit M2-like characteristics (6, 7), a feature associated with poor prognosis and metastasis (8, 9). Of note, PDAC-derived TAM exhibit properties of both M2- and M1-like polarization and have been shown to promote epithelial-mesenchymal transition (EMT), a process that fosters invasion of PDAC and premalignant pancreatic ductal epithelial cells (PDEC) (10). As EMT is also associated with the acquisition of a drug resistant phenotype and immune evasive properties, TAM are potent drivers of drug resistance as well as immune escape and suppression at all stages of tumor development (11).

One mechanism of immunosuppression and immune evasion of cancers is the highly aberrant expression of immune checkpoint molecules such as programmed cell death protein 1-ligand 1 (PD-L1) or its receptor programmed cell death protein 1 (PD-1). Accordingly, engagement of PD-1 on T cells by its ligands PD-L1 or PD-L2 on antigen presenting cells or tumor cells leads to T cell exhaustion (12–14). Interfering with this inhibitory axis by treatment with immune checkpoint inhibitors (ICI) such as Pembrolizumab or Durvalumab revolutionized the therapeutic regimens for multiple cancer entities (15–17), but so far failed in PDAC (18, 19), although considerable PD-L1 expression levels in PDAC cell lines has been reported in PDAC (20–22). In this context, Rahn et al. demonstrated that in PDAC tissues staged T3N1M0, representing the most common resected PDAC stage, PD-L1 is expressed only in one third of the cases and stromal cells

Abbreviations: BSA, bovine serum albumin; ccK18, caspase-cleaved Keratin 18; CD, cluster of differentiation; EMT, epithelial-mesenchymal transition; EpCAM, epithelial cell adhesion molecule; FcR, Fc receptor; FCS, fetal calf serum; FoV, fields of view; Gem, Gemcitabine; GM-CSF, granulocyte-macrophage colony-stimulating factor; ICI, immune checkpoint inhibitors; ICOS, inducible T-cell costimulatory; IFNγ, interferon γ; IgG, immunoglobulin G; IHC, immunohistochemical; IL-2, interleukin-2; LAG3, lymphocyte-activation gene 3; MACS, magnetic activated cell sorting; M-CSF, macrophage colony-stimulating factor; MFI, median fluorescence intensity; Mϕ, macrophages; PBMC, peripheral blood mononuclear cells; PBS, phosphate-buffered saline; PD-1, programmed cell death protein 1; PDAC, pancreatic ductal adenocarcinoma; PD-L1, programmed cell death protein 1-ligand 1; PKM2, pyruvate kinase M2; TCM, T cell medium; TGF-β1, transforming growth factor-beta1; TIGIT, T cell immunoreceptor with Ig and ITIM domains; TIM3, T cell immunoglobulin and mucin domain-containing protein 3; TMB, tumor mutational burden; TME, tumor microenvironment.

10.3389/fimmu.2023.1157397

such as TAM predominantly exhibit PD-L1 expression (23, 24). Still, it is poorly understood whether PD-L1 expressing TAM with different polarization phenotypes contribute to immune evasion of PDAC cells, particularly when the latter themselves do not or only hardly express PD-L1.

In order to obtain further insight into PD-L1-mediated immune evasion during PDAC progression and the reasons for anti-PD-L1 treatment failure in this tumor entity, this study examined PD-L1 expression and its spatial distribution in primary PDAC tissues and corresponding liver metastases. To mimic this dynamic TME comprising different amounts and phenotypes of macrophages, one of the main immune cell populations impacting anti-tumor immunity during PDAC progression, a stroma enriched spheroid model with two different PDAC cell lines and different ratios of M1- or M2-like macrophages was used. Using this model the present study particularly focused on how the interplay of macrophages and PDAC cells affect the activation and effector phenotype of CD8+ T cells as well as PD-L1 expression of macrophages and PDAC cells. Finally, it was elucidated how these distinct stromal conditions impact treatment with ICI in monotherapy as well in combination with Gemcitabine. Combining a comprehensive *in situ* analysis of primary and metastatic PDAC tissues with 3D stroma enriched PDAC cell cultures, our study provides novel insights in the role of macrophages and the PD-L1/PD-1 axis in immune evasion of PDAC.

2 Material and methods

2.1 PDAC patient information and histological analysis

Immunohistochemical (IHC) stainings of whole mount serial sections from primary tumor and corresponding liver metastases of four PDAC patients were performed. All tissue samples were surgical resects. Three out of four cases were untreated at time point of surgical resection and one patient had obtained neoadjuvant therapy. The research was approved by the ethics committee of Kiel University (reference number: A110/99). Written consent was obtained from all patients. Patient characteristics are listed in Table 1. For IHC stainings following antibodies were used: PanCK (dilution 1:200, clone: AE1/AE3, NeoMarkers *via* Thermo Fisher Scientific, Waltham, USA), PD-L1 (dilution 1:100, clone: E1L3N, Cell signaling Technologies, Danvers, USA), CD68 (dilution 1:100, clone: 514H12, Leica Microsystems GmbH, Wetzlar, Germany), CD163 (dilution 1:100, clone: 10D6, Leica Microsystems GmbH) and CD8 (dilution 1:100, clone: C8144B, Leica Microsystems GmbH). Immunohistochemical staining was performed with the autostainer Bond™ RX System.

TABLE 1 Clinic-pathological characteristics of PDAC patients in analyzed cohort of this study.

Parameter	Number of cases
Patients	4
Median age (range)	71 (68-74)
Sex (male/female)	3/1
Tumor stage T1/T2/T3/T4	0/2/2/0
Nodal stage N0/N1	1/3
Metastasis stage M0/M1	0/4
Tumor grade 1 (well differentiated)	1
Tumor grade 2 (moderately differentiated)	0
Tumor grade 3 (poorly differentiated)	3

Furthermore, IHC double stainings of liver metastases were performed. The first step involved the staining of PD-L1 (dilution 1:100, clone: E1L3N, Cell Signaling Technologies). Antigen retrieval was achieved with ER2 (EDTA-buffer Bond pH 9.0; 20 minutes). The antigen retrieval step was modified for the PD-L1 staining of those slides, which were to be combined with an alpha-smooth muscle actin (αSMA) staining in the second step: In those cases, we decided to enhance PD-L1 visualization in relation to the naturally intense αSMA signal by prolonging ER2 antigen retrieval to 30 minutes. The immunoreaction was visualized with the Bond™ Polymer Refine Detection Kit (DS 9800, brown labeling, Novocastra; Leica Microsystems GmbH) resulting in a brown color. The second step involved the staining of either αSMA (dilution 1:400, clone: 1A4, NeoMarkers *via* Thermo Fisher Scientific), or CD68 (dilution 1:100; clone: 514H12, Leica Microsystems GmbH), or PanCK (dilution 1:200, clone: AE1/AE3, NeoMarkers *via* Thermo Fisher Scientific). Antigen retrieval was carried out with ER1 (citrate buffer Bond pH 6.0; 20 minutes for αSMA), or ER2 (EDTA-buffer Bond pH 9.0; 20 minutes for CD68). The immunoreaction was visualized with the BONDT™ Polymer Refine Red Detection Kit (DS9390, red labeling, Leica Microsystems GmbH) resulting in a red color.

Stained tissue sections were scanned using a Hamamatsu NanoZoomer 2.0 RS scanner (Hamamatsu Photonics Deutschland GmbH, Herrsching am Ammersee, Germany) at 400 times magnification and viewed with NDP.view2 software (Hamamatsu photonics). Analyses of the single IHC stainings were performed in two steps. To analyze the cellular and histoanatomical distribution of different stained markers, an overall evaluation of the tissue sections was first performed: the entire tissue section was screened at low magnification and the predominant distribution of immunopositive cells (tumor center and/or invasion front of primary tumor or liver metastases) was documented. In order to investigate more precisely the distribution and frequency of staining, ten representative fields of view (FoV) at the invasion front and tumor center (defined as at least one FoV away from invasion front at 200-fold magnification) of the primary tumor or metastasis were investigated. All tissue sections were studied with regard to the predominant areas of stained cells at 200-fold magnification (FoV: 0.48x0.85 mm), except those stained for PD-L1 which were analyzed at 400-fold magnification (FoV: 0.42x0.24 mm). Every tissue section was assessed by their predominant localization of immunopositive cells (at the invasion front, tumor/metastasis center or evenly distributed between invasion front and tumor center). For staining evaluation, a scoring system was established which rates the percentage of

immunopositive cells in the FoV. For scoring of highly abundant immunopositive cells (CD163+ as well as CD68+ macrophages), cell frequency was scored as 0%, <10%, 11-50% and >50% positively stained cells. As these categories were not suitable for less abundant immunopositive stained cells like CD8+ T cells and PD-L1 staining, PD-L1 and CD8 staining were graded into 0% (negative), <1% and > 1% positively cells stained. Furthermore, the PD-L1 staining intensity was graded as none, low and high. For each tissue section, areas with the highest frequency of immunopositive cells were documented to evaluate the main localization of cells stained for the respective markers within the tumor tissue. All stainings were evaluated independently by two examiners (SB and TD).

2.2 Generation of macrophages

Lymphocytes and monocytes were isolated from leukoreduction system chambers of healthy blood donors provided by the Institute of Transfusion Medicine in Kiel. Written informed consent from all donors was obtained. Isolation of peripheral blood mononuclear cells (PBMC) was done by density gradient centrifugation followed by counterflow centrifugation to separate lymphocytes from monocytes according to established protocols (10, 25). All lymphocyte fractions above 85% purity were frozen and only monocytes from fractions with a monocyte purity higher than 85% were polarized into M1- or M2-like macrophages as previously described (26). For this purpose, monocyte fractions were centrifuged and resuspended in M2 medium (RPMI-1640 medium, 1% FCS, 1% L-glutamine, 1% penicillin/streptomycin) and the cell number was determined. Then, $2x10^6$ monocytes per well were seeded into 12-well plates, stimulated either with 2.4 ng/ml GM-CSF (Biolegend, San Diego, USA) for M1-like macrophage polarization or 50 ng/ml M-CSF (Biolegend) for M2-like macrophage polarization and cultured for 6 to 7 days at 37°C, 5% CO_2 and 86% relative humidity. Culture medium for induction of M1-like polarization was supplemented with 5% fetal calf serum (FCS), while culture medium for induction of M2-like polarization was supplemented with only 1% FCS. Polarization into M1- and M2-like macrophages was verified according to established protocols with confirmed polarization markers (10, 27, 28).

2.3 Isolation of human CD8+ T cells

Frozen human lymphocytes derived from counterflow centrifugation were thawed in T cell medium (TCM) (RPMI-1640 medium, 10% FCS, 1% L-glutamine, 1% penicillin/streptomycin, 1% Sodium pyruvate and 2% HEPES). After centrifugation, cell count was determined. CD8+ T cells were isolated using the magnetic activated cell sorting (MACS) isolation kit (Miltenyi, Bergisch Gladbach, Germany) following modified manufacturer's instructions with reduced antibody and bead concentrations (50%) and extended incubation times (1.5-fold). After negative selection, CD8+ T cells were counted and analyzed for their purity *via* flow cytometry (MACSQuant X, Miltenyi) using immunofluorescence staining with the following antibodies: αβ-TCR-FITC (clone: IP26, Biolegend), CD4-APC (clone: RPA-T4, Biolegend) and CD8-PE (clone: RPA-T8, Biolegend). Only T cell populations with a purity higher than 90% were used for further experiments.

2.4 Activation of human CD8+ T cells

Prior to co-culture experiments, activation of isolated naïve CD8+ T cells was performed. For this purpose, a 24-well plate was coated by incubation for 2 h at 37°C with 200 µl of 1.5 µg/ml anti-CD3 antibody (clone: OKT3, Biolegend) in PBS. Before T cells were seeded, wells were washed 2-times with PBS. Then, 1.3 – $1.8x10^6$ naïve CD8+ T cells were seeded in 1 ml TCM supplemented with 1.5 µg/ml anti-CD28 antibody (clone: CD28.2, Biolegend) and 60 ng/ml IL-2 (Biolegend). CD8+ T cells were cultured for 3 days at 37° C, 5% CO_2 and 86% humidity.

2.5 Cultivation of human PDAC cell lines

Panc89 cells, derived from a lymph node metastasis of a 64-year-old caucasian male (29–31), were used as a PDAC cell line with low PD-L1 expression. Panc89 cells are described to be moderately differentiated and exhibit a mutation in *p53* (T220C) and depletion of *p16*, while the *k-ras* and *SMAD4* genes show a wildtype status (29, 30). PancTu1 cells, derived from the primary tumor of a caucasian female (29, 30), were used as a PDAC cell line with moderate PD-L1 expression. PancTu1 cells are described to be poorly differentiated and exhibit mutations in *k-ras* (G12V) and *p53* (C176S) and a depletion of *p16*. *SMAD4* have a wildtype status (29, 30). Both cell lines were cultivated in 75 cm^2 cell culture flasks with 10 ml medium (RPMI-1640 medium, 10% FCS, 1% L-glutamine, 1% Sodium pyruvate) at 37°C, 5% CO_2 and 86% humidity.

2.6 CellTracker labelling

In order to track and discriminate PDAC cells from macrophages during 3D co-culture, cell populations were labeled with different cell-trackers before seeding in mono- or co-culture spheroids. Tumor cells were labeled with CellTracker green (Invitrogen, Waltham, USA) and macrophages with CellTrace violet (Invitrogen) following the manufacturer's instructions. Visualization of the cells within spheroids was performed with a Lionheart FX microscope (Agilent BioTek, Santa Clara, USA).

2.7 Mono- and co-culture spheroids

For spheroid formation, a total cell number of $2x10^4$ cells per well was seeded in 96-well ultra-low attachment plates (Biofloat 96 well-plate, faCellitate, Mannheim, Germany). For mono-culture spheroids, $2x10^4$ PDAC cells were seeded. For co-culture spheroids with a 1:1 PDAC cell/macrophage ratio, $1x10^4$ PDAC cells and $1x10^4$ polarized macrophages were seeded. in case of a 3:1

10.3389/fimmu.2023.1157397

ratio, $1.5x10^4$ PDAC cells and $0.5x10^4$ polarized macrophages were seeded in a final volume of 150 µl TCM. After 72 h, PD-L1 levels on tumor cells and macrophages as well as the phenotype of macrophages were characterized *via* immunofluorescence staining and subsequent flow cytometric analysis. To assess PDAC cell death and the effector phenotype of CD8+ T cells, mono- or co-cultured spheroids were seeded as described above and after 24h spheroids were either left untreated or treated with 10 µg/ml Gemcitabine (Hexal, Holzkirchen, Germany) for further 24h. Afterwards, the medium was exchanged and spheroids either remained untreated or activated CD8+ T cells were added in a 1:10 target/effector cell ratio. In additional settings, spheroids were also treated with 10 µg/ml Durvalumab (Astra Zeneca, Cambridge, UK), Pembrolizumab (Merck/MSD pharma, Rahway, USA), or respective isotype controls (human IgG_1 or human IgG_4). After 24 h, supernatants were collected and CD8+ T cells were analyzed *via* flow cytometry.

2.8 LEGENDplex

LEGENDplex Human CD8/NK mix and match panel (BioLegend) was used to determine cytotoxic molecules and cytokines (Granzyme A, Granzyme B, Perforin, Granulysin, IFN-γ) in the supernatant of spheroid cultures according to the instructions of the manufacturer. For this purpose, supernatants were centrifuged at 15000xg, 4°C for 8 min to remove cell debris. For analysis, 12.5 µl of the supernatants were used. Measurement was performed using a BD FACSymphony A1 (Beckton Dickinson, East Rutherford, USA) and evaluation was performed with the LEGENDplex-data analysis software v8 (BioLegend).

2.9 M30 CytoDeath

For the cell-specific detection of cell death induction in PDAC cells, the M30 CytoDeath™ (PEVIVA®, Diapharma, West Chester, USA) ELISA was used. The assay detects caspase-cleaved Keratin 18 (ccK18) which is generated in the present culture settings exclusively by apoptotic PDAC cells. The ELISA was conducted according to the manufacturer's instructions and measured with a Tecan Infinite® 200 PRO Microplate Reader (Tecan, Männedorf, Switzerland). Resulting values were normalized to the respective PDAC cell count.

2.10 Immunofluorescence staining and flow cytometric analyses

Immunofluorescence staining was performed to characterize the phenotype of CD8+ T cells and macrophages as well as PD-L1 surface level of macrophages and PDAC cells. For this purpose, cells were washed with PBS and treated with FcR blocking reagent (human TruStain FcX, Biolegend) diluted 1:10 in MACS buffer (0.5% BSA, 2 mM EDTA in PBS). All following steps were conducted on ice in a 96-well v-bottom plate. After FcR blocking, cells were centrifuged, supernatants were discarded and cells were resuspended in MACS buffer supplemented with respective fluorochrome-conjugated antibodies. All antibodies were purchased from Biolegend. All isotype controls, if not other specified were clone MPOC-2: mIgG1-FITC, mIgG1-APC, mIgG1-PE, mIgG1-PeCy7, mIgG2a-PE (clone MOPC-173), mIgG2b-APC (clone MPC-11), specific antibodies: CD8-FITC (clone HIT8a), CD25-APC (clone BC96), CD69-PE (clone FN50), PD-1-PE (clone EH12.2H7), PD-L1-PeCy7 (clone MIH3), CD163-FITC (clone HGI/61), CD14-PE (clone M5E2), EpCAM-APC (clone 9C4). Cells were stained in antibody solutions for 30 min at 4°C in the dark. Afterwards, cells were washed twice and fixed with 1% PFA in MACS buffer. Immunofluorescence-stained cells were detected by a MACSQuant X flow cytometer and analyzed using the FlowJo software v10.7.1 (Becton Dickinson, Franklin Lakes, USA). Specific immunofluorescence staining was assessed by normalization of the staining intensity of the specific antibody to the staining intensity of the isotype control and is presented as median fluorescence intensity (MFI).

2.11 Relative quantification of PDAC cell and macrophage ratios after spheroid co-culture

After 72h spheroid cultivation, supernatants of co-culture samples containing macrophages were collected. Then, PDAC spheroids were dissociated by incubation in PBS supplemented with 1% trypsin (Biowest, Nuaillé, France) for 30 min at 37°C. Enzymatic dissociation was assisted by mechanical dissociation straining the cell suspension through a 30 G cannula every 10 min. Next, macrophage containing supernatants and dissociated respective spheroids were pooled and subjected to immunofluorescence staining and subsequent flow cytometric analysis using a MACSQuant X flow cytometer. For discrimination of PDAC cells and macrophages, cells were stained with EpCAM-APC and CD14-PE antibody, respectively. Analysis was performed using the FlowJo software v10.7.1 (Becton Dickinson, Franklin Lakes, USA).

2.12 Statistics

Statistical analysis was performed using GraphPad Prism Version 9.4.1 (GraphPad Software Inc., La Jolla, US). Gaussian distribution of data was tested by Shapiro-Wilk test. In case data sets passed the normality test, a one-way ANOVA followed by either Tukey`s multiple comparison or Dunnett's multiple comparison (for normalized data sets) test were performed. Parametrically distributed grouped data sets were analyzed by two way-ANOVA followed by multiple comparison Tukey test or Dunnett's multiple comparison test (for normalized data sets). Parametric data sets are presented by column bar graphs with mean and standard deviation, non-parametric data sets are depicted by bar graphs with median and interquartile ranges in both directions. Results were considered statistically significant for p-values < 0.05. Significance levels are indicated by asterisks: * = $p < 0.05$, ** = $p < 0.01$, *** = $p < 0.001$, **** = $p < 0.0001$.

10.3389/fimmu.2023.1157397

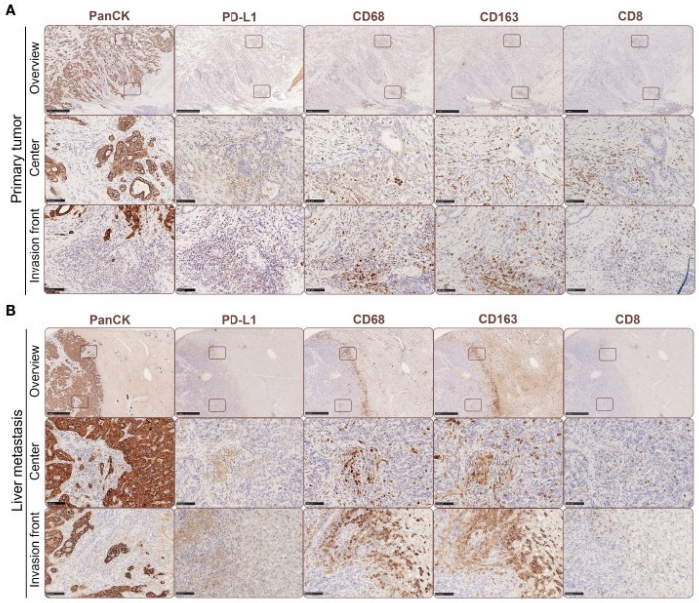

FIGURE 1
Spatial expression of PD-L1 in primary PDAC and corresponding liver metastases is associated with the presence of tumor-associated macrophages and CD8+ T cells. Representative immunohistochemical stainings for PanCK, PD-L1, CD68, CD163 and CD8 in primary tumors **(A)** and liver metastases of PDAC patients **(B)**. Scale bar overview pictures (above): 1000 µm, areas within tumor or invasion front (below): 100 µm.

3 Results

3.1 Spatial expression of PD-L1 in primary PDAC and corresponding liver metastases is associated with the presence of tumor-associated macrophages and CD8+ T cells

As previously reported, PD-L1 is predominantly expressed by stroma cells in primary PDAC (23). In order to examine potential correlations between PD-L1 expression, its spatial distribution and TME alterations during PDAC progression, we performed IHC stainings to detect PD-L1 expression in relation to tumor cells (pan-CK), macrophages (CD68) with an M2-like phenotype (CD163) and CD8+ T cells (CD8) in serial sections from primary tumor (Figure 1A) and corresponding liver metastases (Figure 1B) of four PDAC patients. We identified PD-L1 expression in all primary PDAC tissues, being evenly distributed within tumor center and the invasion front (Figures 1A, 2A). Of note, all corresponding liver metastases also showed PD-L1 expression with a similar localization pattern (Figures 1B, 2A). However, PD-L1 negative fields of view (FoV) were only observed in primary tumors but not in metastases and a higher proportion of PD-L1 positive FoV (>1% PD-L1+ cells in FoV) was detected in liver metastases (Figure 2B). Interestingly, PD-L1 expression was predominantly located at the invasion fronts of both, primary tumors and liver metastases within the group of FoV with highest PD-L1 frequency (<1% PD-L1+) (Figure 2C). In line, the frequency of FoV with strong PD-L1 staining intensity was significantly higher in liver metastases compared to primary tumors (Supplementary Figure 1). Similar to the expression pattern of PD-L1, CD68+ macrophages were found evenly distributed inside tumoral lesions and at the invasion fronts in both, the primary tumor and liver metastases (Figures 1A, B, 2D). These stainings also demonstrate that areas showing strong PD-L1 staining in primary tumors and liver metastases were characterized by a higher-than-average presence of macrophages, especially CD163+ macrophages (Figures 1A, B, Figures 2E–I). In over 50% of analyzed FoV, 11-50% of all cells were CD68+ and CD163+ (Figures 2E, H). Of note, within the group of FoV that showed the highest frequency of CD68 and CD163+ cells (> 50%), over 50% of these FoV were located at the invasion front of primary or metastatic lesions (Figures 2F, I). Similar to this, CD8+ cells were also associated with PD-L1+ areas (Figures 1A, B). In primary tumor tissues, CD8+ cells were found in two cases only at the invasion front and in the other two cases CD8+ cells were evenly distributed in the tumor. In liver metastases, CD8+ cells were found in 3 of 4 cases exclusively at the invasion front (Figure 2J). In more than 50% of FoV, more than 1% of all analyzed cells were CD8+ (Figure 2K). More precisely, most of these FoV enriched for CD8+

10.3389/fimmu.2023.1157397

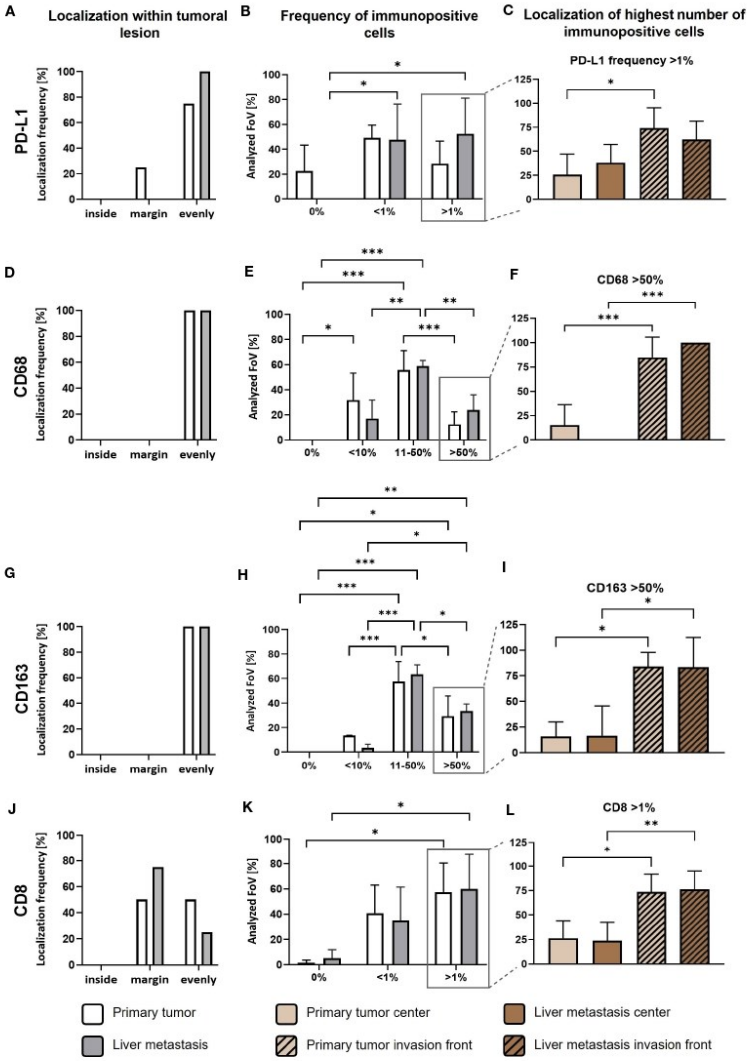

FIGURE 2
PD-L1 is predominantly expressed in tumor areas characterized by high infiltration of TAMs and CD8+ T cells in primary PDAC tissues and corresponding liver metastases. First, quantitative marker distribution of PD-L1 **(A)**, CD68 **(D)**, CD163 **(G)** and CD8 **(J)** in primary tumors (white) or liver metastases (grey) was assessed by considering localization of immunopositive cells in an overview picture of each tumoral lesion (inside, margin or evenly distributed between inside and margin). Then, percentage of PD-L1 **(B)**, CD68 **(E)**, CD163 **(H)** and CD8 **(K)** immunopositive cells within tumoral lesions was determined. Finally, localization of the highest frequencies (peak category) for PD-L1 **(C)**, CD68 **(F)**, CD163 **(I)** and CD8 **(L)** immunopositive cells was determined. For percentage of immunopositive cells, ten fields of view (FoV) at the invasion front and center (at least one FoV away from invasion front) of the primary tumor or metastasis were evaluated according to the following classification: PD-L1 and CD8: 0%, <1% and >1% immunopositive cells or CD68 and CD163: 0%, <10%, 11-50% or >50% immunopositive cells. Two-way ANOVA with Tukey's multiple comparison test and One-way ANOVA with Tukey's multiple comparison test. n=4. * = p<0.05; ** = p<0.01; *** = p<0.001.

10.3389/fimmu.2023.1157397

cells were located at the invasion front of primary and metastatic lesions (Figure 2L). Finally, double IHC stainings of liver tissues revealed that PD-L1 expression was more abundantly colocalized with macrophages (and also hepatic myofibroblasts) than PDAC cells (Supplementary Figure 2).

Overall, these data indicate that the presence of PD-L1 in primary PDAC seems to be associated with PD-L1 expression in liver metastases indicating that PD-L1 mediated immune evasion might operate during PDAC progression. As already shown in primary tumors (23, 24), PD-L1 is more frequently expressed by macrophages than PDAC cells and often found at the invasion fronts of tumoral lesions. This spatial PD-L1 expression is associated with the presence of CD8+ T cells, which however are mostly located at the margin/outside the tumoral lesions. Therefore, the question rises whether high PD-L1 expression on macrophages impairs the effector phenotype and killing activity of CD8+ T cells in PDAC.

3.2 Co-culture spheroids of PDAC cells and macrophages simulate PD-L1 expression and tumor stroma conditions observed in primary PDAC and liver metastases

To simulate the TME conditions in primary PDAC and liver metastases identified *in situ*, we set-up a PDAC co-culture spheroid model comprising PDAC cells with different status of driver mutations and PD-L1 expression as well as different ratios and types of macrophages to examine expression and role of PD-L1 in immune evasion of PDAC cells. During PDAC progression, the number of macrophages increases with the stage of disease (32) and a higher tumor infiltration by CD163+ macrophages correlates with shorter 5-year overall and recurrence-free survival (33). Therefore, we used a PDAC cell to macrophage ratio of 3:1 to mimic an infiltration by macrophages at primary site, whereas 1:1 ratio served as model for macrophage infiltration into liver metastasis. Figure 3A shows a schematic illustration of the experimental setup and Figure 3B depicts representative images of mono- and co-cultured spheroids of Panc89 and PancTu1 PDAC cells. After 72 h, both PDAC cell lines formed dense tumor spheroids and in co-cultured spheroids, macrophages were mostly located at the spheroid margin, being more pronounced in spheroids with higher amounts of macrophages (1:1). Flow cytometric analysis of PDAC cells and macrophages revealed that in co-culture spheroids the proportion of PDAC cells and macrophages remained almost stable over culture duration (Figure 3C). Next, it was investigated whether the presence of PDAC cells impacts macrophage polarization as macrophages exhibit a high plasticity and can change their phenotype due to surrounding microenvironment (6, 34, 35). Mono-cultured M2-like macrophages exhibited higher CD163 surface levels compared to M1-like macrophages. After 72 h co-culture with Panc89 or PancTu1 cells at either cell ratio, CD163 expression on M1-like macrophages was hardly affected compared to mono-cultured cells. In contrast, M2-like macrophages exhibited intensified CD163 surface levels after co-culture with either PDAC cell line (Figure 3D). These findings indicate that proportions of PDAC cells and macrophages as well as macrophage phenotypes remained stable in co-culture spheroids over a culture duration of 72h.

Furthermore, PD-L1 surface levels were analyzed in mono- and co-cultured Panc89 and PancTu1 cells as well as macrophages (Figure 3E). Mono-cultured Panc89 cells exhibited hardly any PD-L1 surface expression and this was almost not affected by either co-culture with macrophages (green bars, MFI ratio 1.2-1.69). Contrastingly, mono-cultured PancTu1 cells were characterized by considerable PD-L1 surface levels (dark green bar, MFI ratio 4.05), which, however, were not further increased by macrophages in either co-culture setting. In contrast, PD-L1 surface levels were detected at higher levels in both mono-cultured macrophage populations, albeit M1-like macrophages demonstrated higher expression levels compared to M2-like macrophages (blue bars, MFI ratio M1-like versus M2-like macrophages: 4.22 versus 2.1). Of note, co-culture with both PDAC cell lines clearly increased PD-L1 surface levels in both macrophage populations up to a similar level even if lower proportions of PDAC cells were present in the spheroids (1:1) (Figure 3E).

Overall, these results demonstrate that we established a stable PDAC cell spheroid model enriched with M1- or M2-like macrophages, that well reflects both cellular composition as well as PD-L1 expression levels identified in our *in situ* analyses of primary PDAC and liver metastases tissues. Moreover, higher PD-L1 expression was observed in macrophages rather than PDAC cells, being also in line with our *in situ* findings. Of note, the presence of PDAC cells further increased PD-L1 surface levels in either macrophage population.

3.3 PDAC spheroids comprising PD-L1 expressing M1- or M2-like polarized macrophages do not impair the effector phenotype of CD8+ T cells which is not associated with PDAC cell death induction

Next, we examined whether PD-L1 expressing macrophages in the different co-culture spheroids impact the effector phenotype and killing activity of CD8+ T cells. For this purpose, pre-activated CD8+ T cells were added to the mono- and co-culture spheroids (Figure 4A). Notably, after activation culture these pre-activated CD8+ T cells exhibited high cell surface expression levels of CD25 and the early activation marker CD69 along with considerable cell surface levels of PD-1 (Supplementary Figures 3A-C), pointing to an exhausted T cell phenotype often found in PDAC tissues (36–38). First, we investigated whether cell surface expression levels of CD69 and CD25 of pre-activated CD8+ T cells are altered by the different spheroid co-culture conditions. In comparison to mono-cultured pre-activated CD8+ T cells, CD8+ T cells cultured with PDAC mono-culture spheroids did not alter their CD69, CD25 and PD-1 surface expression (Supplementary Figures 4A-C). However, we observed that CD69 expression levels on CD8+ T cells were enhanced by trend after all macrophage co-culture conditions with both PDAC cell lines

10.3389/fimmu.2023.1157397

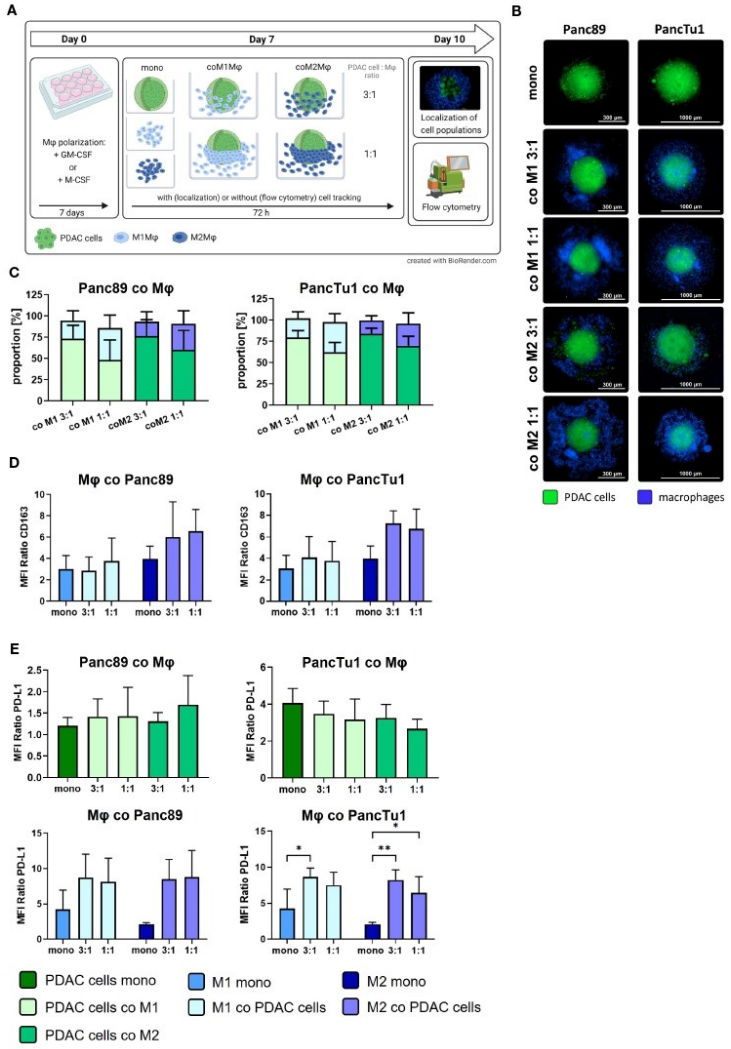

FIGURE 3
Co-culture spheroids containing PDAC cells and macrophages simulate PD-L1 expression and tumor stroma conditions in primary PDAC and liver metastases. PancTu1 and Panc89 cells were either mono- or co-cultured with M1Mφ or M2Mφ at ratios of 3:1 or 1:1 for 72 h in ultra-low attachment plates to form spheroids. **(A)** Schematic illustration of experimental set-up. **(B)** Representative fluorescence microscopy images of CellTracker green labeled Panc89 cells (left) or PancTu1 cells (right) and CellTrace violet labeled Mφ (violet) at indicated co-culture conditions. (Scale bar PancTu1: 1000 µm; Panc89: 300 µm). **(C)** Proportions of PDAC cells and Mφ in co-culture 72 h after seeding. To discriminate PDAC cells from Mφ, single cell suspension of spheroids was stained with EpCAM and CD14-targeting antibodies for flow cytometric analysis (light green: PDAC cells co-cultured with M1Mφ, dark green: PDAC cells co-cultured with M2Mφ, light blue: M1Mφ co-cultured with PDAC cells, dark blue: M2Mφ co-cultured with PDAC cells). Ratio 3:1: $1.5x10^4$ PDAC cells and $0.5x10^4$ Mφ; ratio 1:1: $1x10^4$ PDAC cells and $1x10^4$ Mφ. n=4. **(D)** Relative cell surface expression levels of CD163 on mono- or co-cultured Mφ. Data is presented as MFI ratio. n=3. **(E)** Relative cell surface expression levels of PD-L1 on mono- or co-cultured Panc89 (left, above) or PancTu1 cells (right, above) as well as Mφ in co-culture with Panc89 (left, below) or PancTu1 cells (right, below). Data is presented as MFI ratio. Two-way ANOVA with Tukey's multiple comparison test. n=5 (except mono-cultured Mφ n=3). * = p<0.05; ** = p<0.01.

10.3389/fimmu.2023.1157397

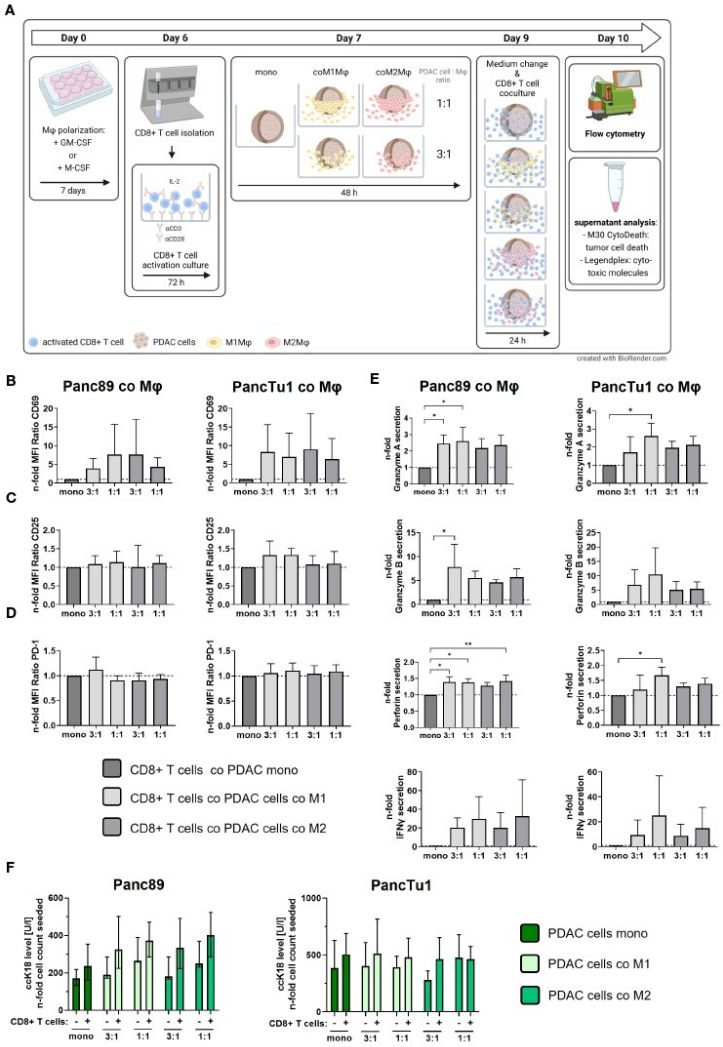

FIGURE 4
PDAC spheroids comprising PD-L1 expressing M1- or M2-like polarized macrophages do not impair the effector phenotype of CD8+ T cells but which is no associated with PDAC cell death. PancTu1 or Panc89 cells were mono- or co-cultured with either M1- or M2-like polarized Mϕ in ultra-low attachment plates to form spheroids. After 48 h, pre-activated CD8+ T cells were added to spheroids for 24 h. **(A)** Schematic illustration of experimental set-up. Immunofluorescence staining of activation markers **(B)** CD69, **(C)** CD25 and **(D)** PD-1 **(D)** on CD8+ T cells cultured with either mono-cultured Panc89 (left panel) or PancTu1 cells (right panel) or with the indicated co-cultures with M1- (light grey) or M2Mϕ (dark grey), measured *via* flow cytometer. Relative cell surface expression levels are normalized to the respective culture of CD8+ T cells with mono-cultured Panc89 or PancTu1 spheroids. Data is expressed as n-fold MFI ratio of specific staining. n=4. **(E)** Granzyme A, Granzyme B, Perforin and IFNγ concentration in supernatants of CD8+ T cells cultured with either mono-cultured Panc89 (left panel) or PancTu1 spheroids (right panel) or with the indicated co-culture spheroids with M1- (light grey) or M2Mϕ (dark grey). Concentrations were measured by multiplex assay and data is normalized to the respective cytokine concentrations of CD8+ T cells in culture with mono-cultured PDAC spheroids. One-way ANOVA using Dunnett's multiple comparison test comparing all samples with a control of 1. The dashed lines mark a concentration ratio of "1". n=3. **(F)** Supernatant levels of caspase-cleaved Keratin 18 (ccK18) in mono- or co-culture spheroids of Panc89 (left) or PancTu1 cells (right) and Mϕ without **(-)** or with CD8+ T cells (+). ccK18 levels were normalized to the respective PDAC cell count. Mono: $2x10^4$ PDAC cells; ratio 3:1: $1.5x10^4$ PDAC cells and $0.5x10^4$ Mϕ; ratio 1:1: $1x10^4$ PDAC cells and $1x10^4$ Mϕ. Not normally distributed data are depicted as median with interquartile range in both directions. Panc89: n=4; PancTu1: n=3. * = p<0.05.

10.3389/fimmu.2023.1157397

(Figure 4B), albeit its induction was more pronounced after co-culture with PancTu1 spheroids (n-fold MFI ratio 6,36 – 9.02) compared to Panc89 spheroids (n-fold MFI ratio 3.86 –7.68). Interestingly, co-culture with different ratios or polarizations of macrophages did not affect these elevated CD69 cell surface levels on CD8+ T cells. CD25 cell surface levels of CD8+ T cells were almost not affected by the different PDAC spheroid conditions (Figure 4C). Since PD-L1 cell surface expression levels were increased in macrophages after co-culture in PDAC spheroids (Figure 3E), we next examined whether PD-1 cell surface expression levels are altered in CD8+ T cells after the different co-culture conditions. However, PD-1 cell surface levels on CD8+ T cells were not affected by any spheroid co-culture setting (n-fold MFI ratio 0.91 – 1.12, Figure 4D).

Besides the expression of activation-associated marker proteins, the secretion of cytokines and cytotoxic effector molecules represents a hallmark of T cell activation and effector function. Therefore, we analyzed the levels of Granzyme A/B, Perforin and IFNγ in supernatants obtained from CD8+ T cells either cultured alone or cultured with mono- or co-culture spheroids. Compared to pre-activated mono-cultured CD8+ T cells, concentrations of Granzyme A and B, Perforin and IFNγ were clearly enhanced in supernatants of pre-activated CD8+ T cells in presence of mono-culture PDAC spheroids, an effect which was even more pronounced in culture with mono-culture PancTu1 spheroids (Supplementary Figures 5A-D). Thus, the presence of PDAC cells increased release of CD8+ T cell effector molecules. However, even more elevated levels of Granzyme A and B, Perforin as well as IFNγ (by trend) were detectable in supernatants derived from CD8+ T cells cultured with macrophage enriched PDAC spheroids compared to supernatants from CD8+ T cells cultured with mono-culture PDAC spheroids (Figure 4E). Overall, higher levels of all effector molecules were detected in supernatants of CD8+ T cells and co-culture spheroids containing an equal number of PDAC cells and macrophages, particularly M1-like polarized macrophages (1:1). Finally, we analyzed whether the observed alterations of the T cell effector phenotype correlate with PDAC cell death induction under the different stroma conditions. PDAC cell death was assessed by determination of an effector caspase-cleaved Keratin 18 fragment (ccK18) released in supernatants, indicative for epithelial cells undergoing apoptotic cell death (Figure 4F). Slightly increased ccK18 levels were detected in supernatants derived from CD8+ T cells cultured with mono- or co-cultured PDAC cell spheroids compared to supernatants from respective spheroid culture without CD8+ T cells (ΔccK18 level: Panc89 median (range): 136 (67-153), PancTu1 median (range): 122 (87-184)). However, no considerable effect by the different co-culture settings was observed.

In summary, these data indicate that the effector phenotype of CD8 + T cells exemplified by expression activation markers and release of effector molecules is not impaired in the presence of PD-L1 expressing macrophages particularly with an M1-like phenotype. In contrast, our findings rather suggest that the effector phenotype of CD8+ T cells is maintained or even promoted in presence of macrophages and PDAC cells independent of their PD-L1 expression, but which is not associated with increased PDAC cell death.

3.4 Blocking of PD-1 and PD-L1 does not enhance the effector phenotype of CD8+ T cells and does not increase PDAC cell death

Based on the fact that both macrophage populations as well as PancTu1 cells exhibit considerable PD-L1 expression (Figure 3E) and CD8+ T cells show marked PD-1 expression (Supplementary Figure 3), we next investigated whether antibody mediated blockade of PD-L1 (by Durvalumab) or PD-1 (by Pembrolizumab) impacts the effector phenotype of CD8+ T cells leading to increased PDAC cell death. Figure 5A shows a schematic illustration of the experimental set-up. Durvalumab treatment did neither impact CD69 expression (Figure 5B) nor CD25 expression (Figure 5C) of CD8+ T cells cultured under either mono- or co-culture PDAC spheroid conditions. Furthermore, PD-1 surface levels were not changed after Durvalumab treatment in comparison to respective IgG controls in all co-culture conditions with each PDAC cell line, but were significantly decreased on CD8+ T cells derived from all co-culture settings treated with Pembrolizumab (Figure 5D). This finding can be explained by the fact that Pembrolizumab bound to PD-1 blocks the PD-1 epitope recognized by the staining antibody. Therefore, these results confirmed successful inhibition of PD-1 in our experimental set-up. Successful inhibition of PD-L1 by Durvalumab could also be confirmed as PD-L1 was not detectable in Durvalumab treated macrophages and PDAC cells in all co-culture (Supplementary Figure 6). Next, the levels of cytotoxic effector molecules and IFNγ were investigated in supernatants from the different Durvalumab or Pembrolizumab treated spheroids. Overall, neither Granzyme A and B nor Perforin levels in supernatants of CD8+ T cells cultured with either mono- or co-culture spheroids were altered after Durvalumab or Pembrolizumab treatment (Figure 5E). Durvalumab treatment led to slightly increased secretion of IFNγ by trend into supernatants of CD8+ T cells co-cultured with PancTu1 spheroids at a ratio of 3:1 with either macrophage population, while Pembrolizumab slightly diminished IFNγ secretion under almost all co-culture conditions (Figure 5E). Finally, ccK18 levels of mono- and macrophage enriched PDAC cell spheroids after culture with CD8 + T cells and ICI treatment were measured in order to assess PDAC cell death induction under treatment of the different stromal conditions. In line with the findings regarding the effector phenotype of CD8+ T cells, no considerable effects were observed on PDAC cell death by either antibody treatment in all PDAC cell spheroid cultures (Figure 5F).

In summary, neither Durvalumab nor Pembrolizumab treatment impacted the effector phenotype of CD8+ T cells after co-culture with any PDAC cell spheroids and macrophages ratios. Moreover, none improvement of tumor cell death induction in both PDAC cell spheroid models was detected independently of the amount and subtype of macrophages and treatment with either Durvalumab or Pembrolizumab.

10.3389/fimmu.2023.1157397

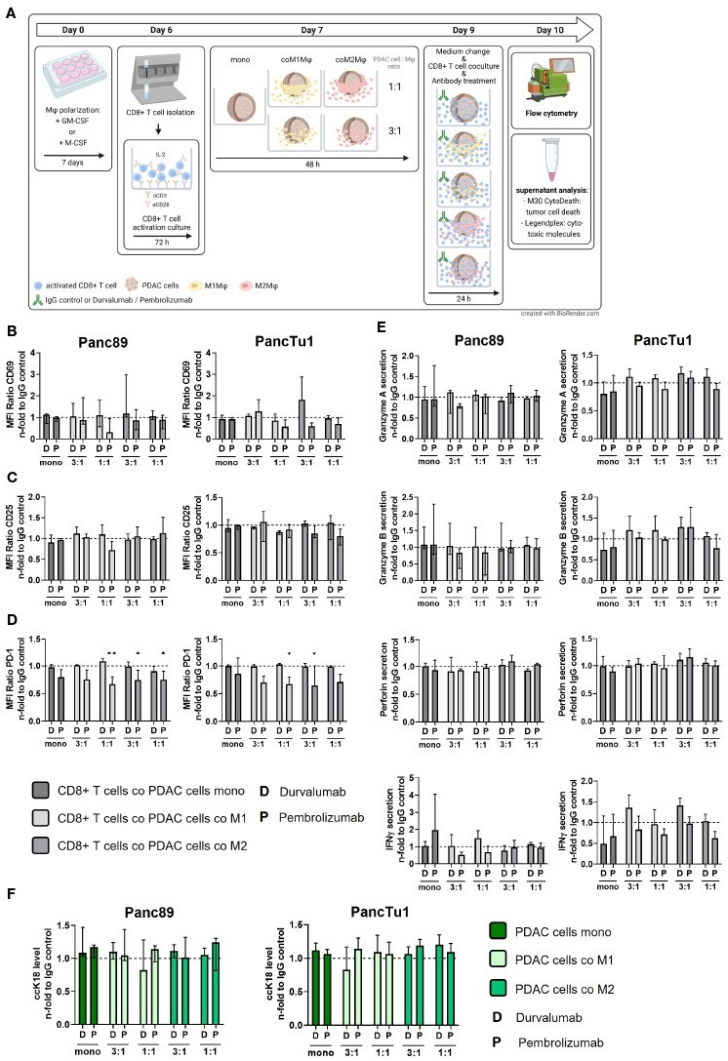

FIGURE 5
Blocking of PD-1 and PD-L1 only slightly affects the effector phenotype of CD8+ T cells and does not increase PDAC cell death. PancTu1 or Panc89 cells were mono- or co-cultured with either M1- or M2-like polarized Mφ in ultra-low attachment plates to form spheroids. After 48 h, medium was changed, mono- or co-cultures were treated with either Durvalumab (D) or Pembrolizumab (P) or their respective isotype controls (10 µg/ml) and CD8+ T cells were added for 24 h. **(A)** Schematic illustration of experimental set-up. Immunofluorescence staining of activation marker **(B)** CD69, **(C)** CD25 and **(D)** PD-1 on CD8+ T cells cultured with mono-cultured PDAC cell spheroids (dark grey) or co-cultured Panc89 (left panel) or PancTu1 (right panel) cell spheroids with M1Mφ (light grey) or M2Mφ (middle grey). Immunofluorescence staining was measured by flow cytometer and data is normalized to the respective IgG control samples of the indicated culture conditions. **(E)** Granzyme A, Granzyme B, Perforin and IFNγ concentration of supernatants of CD8+ T cells cultured with either mono-cultured (dark grey) Panc89 (left panel) or PancTu1 spheroids (right panel) or with the indicated co-cultures with M1- (light grey) or M2Mφ (middle grey) spheroids. Concentrations were measured by multiplex assay and data was normalized to the respective IgG control samples of the indicated culture conditions. **(F)** Levels of caspase-cleaved Keratin 18 (ccK18) in supernatants of CD8+ T cells cultured with mono-culture spheroids of Panc89 (left) or PancTu1 cells (right) or with the indicated Mφ co-culture conditions. ccK18 levels were normalized to the respective PDAC cell count and then to the respective IgG control samples of the indicated co-culture conditions. Mono: $2x10^4$ratio 3:1: $1.5x10^4$ PDAC cells and $0.5x10^4$ Mφ; ratio 1:1: $1x10^4$ PDAC cells and $1x10^4$ Mφ. Not normally distributed data are depicted as median with interquartile range in both directions. Two-way ANOVA with Dunnett's multiple comparison test comparing all samples with a control of 1. The dashed lines mark an MFI ratio of "1". n=3. * = $p<0.05$.

10.3389/fimmu.2023.1157397

3.5 Sequential treatment with Gemcitabine and immune checkpoint blockade does not lead to increased PDAC cell death

Standard chemotherapy agents can alter the expression of tumor-specific membrane antigens which can result in better antigen presentation *via* antigen-presenting cells and more effective cytotoxic T lymphocytes response (39) Thus, the modulation of tumor-specific membrane proteins as well the enhancement of T cell infiltration by (low dose) cytostatic drugs may serve as a promising strategy to improve the immunotherapy (39, 40). Furthermore, as most PDAC patients are treated with cytostatic drugs as first-line therapies (41), we investigated whether sequential therapy of low dose Gemcitabine followed by immune checkpoint blockade modulates the effector phenotype of CD8+ T cells and leads to elevated induction of PDAC cell death. For this purpose, mono- and macrophage co-cultured Panc89 and PancTu1 spheroids were treated with Gemcitabine for 24 h and then cultured with pre-activated CD8+ T cells and treated with Durvalumab, Pembrolizumab or respective isotype control (Figure 6A). Gemcitabine treatment led to slightly elevated ccK18 levels in supernatants of Panc89 spheroids and rather diminished levels in those of PancTu1 spheroids. However, overall Gemcitabine treatment hardly modulated ccK18 levels in supernatants of mono- and co-cultured PDAC spheroids, indicating that this dose does not lead to massive PDAC cell death under these conditions (Supplementary Figure 7A). Furthermore, Gemcitabine treatment did not impact PD-L1 expression of PDAC cells and either macrophage population (Figure 6B). To analyze whether Gemcitabine pretreatment of PDAC spheroids improves the efficacy of ICI treatment, the effector phenotype of CD8+ T cells and PDAC cell death was assessed compared to ICI treatment alone. To specifically outline the effects exerted by combined treatment, data shown in Figures 6C–F and 7 were derived only from Gemcitabine pretreated cultures with either additional treatment with ICI or isotype control antibody. Analyzing activation markers in CD8+ T cells under the different culture conditions revealed that combined treatment with Pembrolizumab enhanced CD69 surface levels in CD8+ T cells after culture with M1-like macrophage enriched spheroids of both PDAC cell lines, while it led to reduced CD69 levels in CD8+ T cells derived from PancTu1 spheroids comprising M2-like macrophages (1:1). In contrast, combined treatment with Durvalumab hardly impacted CD69 levels of CD8+ T cells cultured with either mono- or co-cultured PDAC spheroids (Figure 6C). No clear effects were detected for CD25 cell surface levels after either treatment (Figure 6D). PD-1 cell surface levels of CD8+ T cells were not altered after sequential treatment with Gemcitabine and Durvalumab after all culture conditions, while it was again reduced after treatment with Pembrolizumab (Figure 6E). In line with the marginal effects on the activation markers, release of Granzyme A and B, Perforin and IFNγ into supernatants of co-cultured CD8+ T cells was also hardly affected by sequential treatment with Gemcitabine and either immune checkpoint inhibitor (Figure 6F). Finally, PDAC cell death was not considerably increased after the different treatments reflected by the almost unaltered ccK18 levels measured in supernatants of the different spheroid cultures (Figure 7), while CD8+ T cell culture with either Gemcitabine pretreated PDAC cell spheroids resulted in slightly enhanced ccK18 levels (Supplementary Figure 7).

Overall, these data indicate that sequential treatment of PDAC with Gemcitabine and immune checkpoint inhibitors does not improve the effector phenotype of CD8+ T cells and PDAC cell death irrespective of the presence and subtype of macrophages.

4 Discussion

PDAC is mostly diagnosed at late stages of the disease due to the lack of specific symptoms and poor specificity of tumor markers. Further, it often metastasizes, especially to distant organs including liver (76-80% of patients), peritoneum (48%) or lung (45%) (42). To date, the only curative treatment option is resection but most of the patients are not eligible due to the late diagnosis or comorbidities. Even if the primary tumor is successfully surgical resected, the 5-year survival rate of these patients is only 27% (43). Therefore, improved therapeutic treatments are urgently needed. Several studies identified expression of the immune checkpoint molecule PD-L1 in PDAC patients (20–24). In patients without metastatic spread, most of these PD-L1 expressing cells are stromal cells (23). While ICI like Durvalumab and Pembrolizumab revolutionized the treatment of many solid malignancies even at advanced stages, e.g. NSCLC (44), single agent use of Durvalumab as well as other ICIs widely failed in PDAC (6, 19). Since the ICI failure in PDAC is still an unresolved issue, and given the role of CD163+ M2-like macrophages as a prominent cell population in the TME of PDAC (10, 24, 45), a better understanding of how stromal macrophages impact the PD-1/PD-L1 axis and activity of CD8+ T cells in this tumor entity is greatly needed.

To unveil whether PD-L1-mediated immune evasion might operate during PDAC progression, we first analyzed serial PDAC tumor tissues and their corresponding liver metastases concerning PD-L1 frequency and intensity as well as the abundance of macrophages and CD8+ T cells. A study by Rahn et al. already reported that in 69.6% of analyzed primary PDAC tissues (all stages T3N1M0) no or only low PD-L1 expression was detectable (23). In contrast, in our small collective of four PDAC patients all primary tumors as well as their corresponding liver metastases showed considerable PD-L1 expression. The higher frequency of PD-L1 expressing primary tumors in the present cohort might be explained by the fact that these patients mostly exhibited poorly differentiated tumors. The observation that poorly differentiated primary PDAC tumors express higher PD-L1 levels was also outlined in a previous study of Rahn et al. (24). Moreover, the fact that PD-L1 is expressed in the primary context as well as in metastases might indicate that PD-L1-mediated immune evasion is important for malignant progression and metastasis of PDAC. Interestingly, our histological analyses of PDAC tissues also revealed that PD-L1 expression was predominantly located in the TME at the tumor invasion fronts along with a high proportion of macrophages (CD68 + and CD163+ cells) supporting the view that the main source of PD-L1 are stromal cells. Double IHC stainings confirmed that PD-L1 is expressed to a much higher extent by macrophages than PDAC cells. This finding is in line with a former study demonstrating that in primary PDAC 76.5% of PD-L1 expressing cells are stromal cells (23).

10.3389/fimmu.2023.1157397

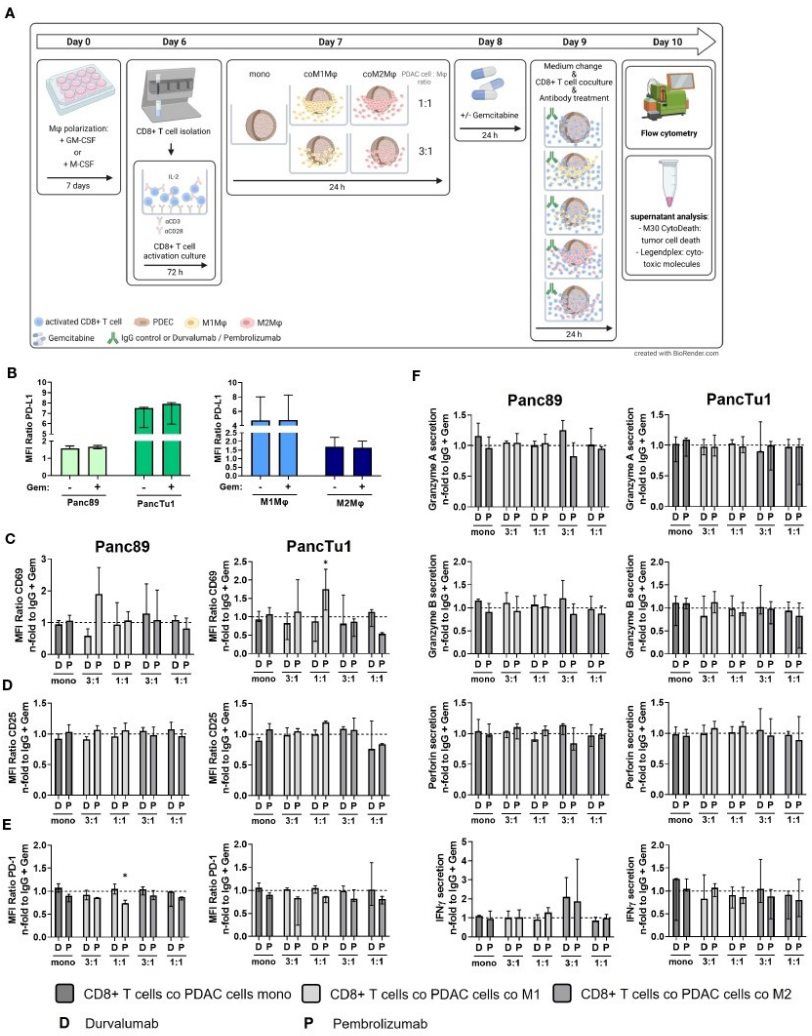

FIGURE 6
Sequential treatment with Gemcitabine and Durvalumab or Pembrolizumab does not improve CD8+ T cell effector phenotype. PancTu1 or Panc89 cells were mono- or co-cultured with either M1- or M2-like Mϕ for 24 h in ultra-low attachment plates to form spheroids. After 24 h, mono- or co-cultures were treated with Gemcitabine (Gem) (10 µg/ml) for 24 h. Afterwards, medium was changed, and cultures were treated with either Durvalumab (D) or Pembrolizumab (P) or their respective isotype controls (10 µg/ml) and simultaneous CD8+ T cell co-culture was started for 24 h. **(A)** Schematic illustration of experimental set-up. **(B)** PD-L1 staining of mono-cultured Panc89 or PancTu1 cells as well as M1- or M2-like Mϕ which were left untreated **(-)** or treated with Gemcitabine (+) for 24 h PD-L1 cell surface level was measured by flow cytometer and data is depicted as MFI ratio of specific staining. Immunofluorescence staining of activation marker **(C)** CD69, **(D)** CD25 and **(E)** PD-1 on cells surfaces of CD8+ T cells cultured with mono-cultured PDAC cell spheroids (dark grey) or co-cultured Panc89 (left panel) or PancTu1 (right panel) spheroids with M1Mϕ (light grey) or M2Mϕ (middle grey) after sequential treatment with Gemcitabine and ICI. Cell surface levels were measured by flow cytometer and data was normalized to the respective IgG control treated cells of the indicated Gemcitabine treated culture conditions. **(F)** Detection of Granzyme A, Granzyme B, Perforin and IFNγ in supernatants of CD8+ T cells cultured with either mono-cultured (dark grey) Panc89 (left panel) or PancTu1 spheroids (right panel) or with the indicated co-cultures with M1- (light grey) or M2Mϕ (middle grey) spheroids after sequential treatment with Gemcitabine and ICI. Concentrations were measured by multiplex assay and data is normalized to the respective IgG control samples of Gemcitabine treated culture conditions. Mono: $2x10^4$, ratio 3:1: $1.5x10^4$ PDAC cells and $0.5x10^4$ Mϕ; ratio 1:1: $1x10^4$ PDAC cells and $1x10^4$ Mϕ. Not normally distributed data are depicted as median with interquartile range in both directions. Two-way ANOVA with Dunnett's multiple comparison test comparing all samples with a control of 1. The dashed lines mark an MFI ratio of "1". * = $p<0.05$. n=3.

10.3389/fimmu.2023.1157397

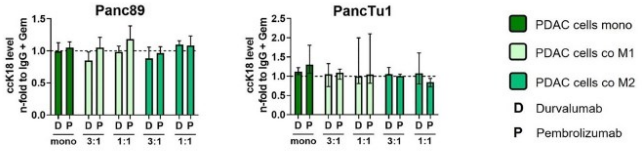

FIGURE 7
Sequential treatment with Gemcitabine and immune checkpoint blockade does not lead to increased PDAC cell death. PancTu1 or Panc89 cells were mono- or co-cultured with either M1- or M2-like Mϕ for 24 h in ultra-low attachment plates to form spheroids. After 24 h, mono- or co-cultures were treated with Gemcitabine (Gem) (10 µg/ml) for 24 h. Afterwards, medium was changed, and cultures were treated with either Durvalumab (D) or Pembrolizumab (P) or their respective isotype controls (10 µg/ml) and simultaneous CD8+ T cell co-culture was started for 24 h. Levels of caspase-cleaved Keratin 18 (ccK18) in supernatants of CD8+ T cells cultured with mono-culture spheroids of Panc89 (left) or PancTu1 cells (right) and with the indicated Mϕ co-culture conditions after sequential treatment with Gemcitabine and ICI. ccK18 levels were normalized to the respective IgG control samples of the indicated Gemcitabine treated culture conditions. Mono: $2x10^4$ratio 3:1: $1.5x10^4$ PDAC cells and $0.5x10^4$ Mϕ; ratio 1:1: $1x10^4$ PDAC cells and $1x10^4$ Mϕ. Not normally distributed data are depicted as median with interquartile range in both directions. Two-way ANOVA with Dunnett's multiple comparison test comparing all samples with a control of 1. The dashed lines mark an MFI ratio of "1".

CD8+ T cells could be detected at considerable frequencies in primary PDAC and in liver metastases, however, these cells were mainly located at the invasion fronts of the primary tumor or metastasis and thus separated from the tumor cells by PD-L1 expressing cells (macrophages). In another study analyzing biopsies of liver metastases from PDAC patients, metastatic tumor cells were also surrounded by CD68+ macrophages which was the most prominent immune cell population (46), underlining the results of our study. Moreover, it is known that M2 TAM can suppress immunotherapeutic efficacy of PD-1/PD-L1 inhibition by suppression of T cell activity and enhanced expression of PD-L1 in the TME. Particularly, the secretion of anti-inflammatory cytokines and exosomes can induce expression of immune checkpoint molecules (47). Our observation that especially macrophages are predominantly located at invasion fronts of primary PDAC as well as liver metastasis suggests a potent barrier impairing infiltration and tumor directed immunity of CD8+ T cells. Even taking into account the small size of the tissue cohort studied, the first comparative analysis of primary tumor and corresponding metastases from PDAC patients provides a unique insight into the potential role of PD-L1 and macrophages in immune evasion of PDAC.

To simulate the TME conditions in primary PDAC and liver metastases identified *in situ*, we established two PDAC co-culture spheroid models with different ratios and types of macrophages in order to investigate whether the presence and amount of different types of macrophages impact PD-L1 expression in PDAC cells as well as CD8+ T cell activity. Our 3D co-culture model well simulated the TME conditions detected *in situ*, as macrophages were mostly located at high frequencies at the margin of tumor spheroids. Additionally, the M2-like phenotype of macrophages, indicated by expression of CD163, was further promoted by both PDAC cell spheroid co-cultures. This observation is supported by several studies reporting high abundance of M2 macrophages in the TME of human and murine PDAC (8, 24, 48). Moreover, either macrophage population exhibited considerable PD-L1 expression being in line with our *in situ* analysis which revealed PD-L1 expression more on stromal cells/macrophages rather than tumor cells. Accordingly, we chose PancTu1 cells exhibiting moderate PD-L1 expression and Panc89 cells lacking PD-L1 expression as PDAC cell models for our *in vitro* studies in order to reflect tumor heterogeneity regarding PD-L1 expression in PDAC. While PD-L1 expression was not altered in both PDAC cell lines due to the attendance of either macrophage subtype, it was clearly enhanced in both macrophage populations after co-culture with either PDAC cell line. In contrast to our results, Xia et al. showed a PD-L1 increase on PDAC cells due to the attendance of M2-like macrophages (21). One explanation for this discrepancy might be that in this study a higher macrophage to PDAC cell ratio was used. Moreover, they identified Transforming growth factor-beta1 (TGF-β1) as a main inducer of PD-L1 expression (21), which seemed not be the inducer of PD-L1 expression in our model system, as TGF-β1 was not detectable or only in small amounts in the culture supernatants (data not shown). Thus, our findings support the view that macrophages are a superior source of PD-L1 expression in PDAC, however, the identification of the inducing factors in our PDAC 3D model system is subject of future investigation.

Next, it was investigated whether the attendance of PD-L1 expressing macrophages impacts the effector phenotype of CD8+ T cells. Interestingly, the effector phenotype of CD8+ T cells was rather promoted by either co-culture with macrophages reflected by an increase of the early activation marker CD69 and the release of Granzyme A/B, Perforin and IFNγ. Of note, the release of effector molecules was more increased in the presence of higher number of (M1) macrophages indicating a relationship between the T cell effector phenotype and the abundance of macrophages. In PDAC patients, a high density of CD8+ T cells in tumor areas is associated with better survival outcome (49, 50). Further, several therapy approaches targeting phenotype switch from M2 to M1 macrophages and thereby induce CD8+ T cell response, T cell recruitment and IFN responses (4, 51, 52) underlie our results of enhanced CD8+ T cell effector phenotype in presence of M1 macrophages. Although macrophages showed higher PD-L1 expression in co-culture with PDAC cells, the effector phenotype of CD8+ T cells was rather intensified, but which was not associated with elevated PDAC cell death. Here, it can be speculated whether infiltration of CD8+ T cells into the spheroids is impaired not allowing a further increase in PDAC cell death induction. To this end, we cannot make any reliable conclusion on this issue because our available imaging modalities which do not properly decipher whether CD8+ T cells are infiltrated

into the spheroids or whether they are attached at the margin. However, the latter would be in line with our findings *in situ* where CD8+ T cells were also separated from the tumor cells. As high tumoral PD-L1 expression is correlated with poor survival of PDAC patients (21, 53), the concept of inhibiting the PD-1/PD-L1 axis to enhance T cell cytotoxicity is promising. However, single agent immunotherapy with Durvalumab or Pembrolizumab has still failed in clinical trials for PDAC (6). In order to elucidate whether different ratios and phenotypes of macrophages may impact treatment efficacy of Durvalumab or Pembrolizumab, we treated mono- and co-culture spheroids with either antibody. Despite considerable expression of PD-L1 and PD-1 in macrophages and CD8+ T cells, respectively, ICI treatment did not lead to enhanced PDAC cell death in either mono- or co-culture model. These findings are in line with the above-mentioned clinical situation. Another determinant for ICI responses is the tumor mutational burden (TMB). In other malignancies including melanoma, non-small-cell lung cancer and urothelial cell carcinoma, patients with high TMB clearly more benefit from ICI therapy compared to patients with low TMB (54). One explanation for this is that tumors with high TMB exhibit more immunogenic neoantigens, which can be recognized by T cells thereby fostering ICI therapy (54). In PDAC, only 1.1% of patients show a high TMB, supporting the low response rate towards ICI treatment. However, preliminary results of anti-PD-1 treatment in the subgroup of PDAC patients with high TMB revealed promising effects (55). As monotreatment with Durvalumab and Pembrolizumab failed in our 3D co-culture model and Gemcitabine has been identified as inducer of PD-L1 expression (56, 57), we investigated whether sequential treatment with Gemcitabine and ICI showed superior effects on the effector phenotype of CD8+ T cells and induction of PDAC cell death. This concept was further supported by data from a murine model of pancreatic cancer liver metastasis, where the combination of Gemcitabine treatment and anti-PD-1 antibody was associated with infiltration of CD8+ T cells and M1 macrophages along with prolonged survival of the mice (58). However, Gemcitabine treatment did not increase PD-L1 expression in PDAC cells and the combination of Gemcitabine pretreatment and ICI did neither impact the CD8+ T cell activation status nor increased PDAC cell death. Nevertheless, several clinical studies evaluating different combinational treatments are ongoing, e.g., an open label, single arm, multicenter clinical trial investigates the combination of AZD0171 and Durvalumab as well as standard-of-care chemotherapy in metastatic PDAC (NCT04999969). Another randomized multicenter phase Ib/II clinical trial study investigates efficacy of a combination of neoadjuvant chemoradiation therapy with Pembrolizumab treatment in PDAC (NCT02305186).

Besides the PD-L1/PD-1 axis several other mechanisms might operate in PDAC impairing CD8+ T cell mediated tumor reactivity and limiting the effects of PD-1/PD-L1 blockade. Although PD-1/PD-L1 axis is a major player in regulating T cell functions and was efficiently blocked in our *in vitro* experiments, several other co-inhibitory interactions can restrain the anti-tumor function of CD8+ T cells in the TME (59). These co-inhibitory molecules include Inducible T cell costimulator (ICOS), T cell immunoreceptor with Ig and ITIM domains (TIGIT), PD-1 and lymphocyte-activation gene 3 (LAG3) were identified at elevated levels on CD8+ T cells in PDAC tissues (60), suggesting that the TIGIT-CD155 or LAG3-MHC interaction are more potent immunosuppressive mechanisms in PDAC. Especially TIGIT, which is expressed on tumor-infiltrating cytotoxic T cells in multiple malignancies and its ligand CD155, often expressed by tumor-infiltrating myeloid cells and upregulated on cancer cells, provide a promising target to overcome the local suppression of immune surveillance. As CD155-TIGIT interaction is associated with cancer resistance to PD-1 blockade, targeting this interaction might be a promising strategy to increase the efficacy of PD-1 inhibition (59). Accordingly, Pearce et al. could recently show that CD8+ tissue-resident memory T cells in PDAC patients co-express PD-1 and TIGIT on their surfaces and blocking of both molecules enhanced IFNγ secretion and T cell proliferation, suggesting a promising route to improve ICI efficacy (61). In line with this hypothesis, Freed-Pastor et al. showed that targeting the TIGIT-CD155 axis in combination with CD40 agonists and anti-PD-1 treatment elicits profound anti-tumor responses in pancreatic cancer mouse models *in vivo* (62). Furthermore, Gulhati et al. demonstrated an enhanced expression of *LAG3, Tnfrsf9* (41BB) and *Havcr2* (TIM3) in genetically engineered PDAC mouse model under anti-PD-1 monotherapy (48), supporting the view that combined targeting of different immune regulatory mechanisms might be an efficient strategy to induce a potent tumor directed immunity in PDAC. Preclinical and clinical studies underscore this hypothesis as co-blockade of PD-1 and a second co-inhibitory molecule such as CTLA-4 augment the antitumor immunity compared to single PD-1 blockade in different solid malignancies (59). Taken together, these findings support the view that the interplay of several co-inhibitory mechanisms rather than the PD-L1/PD-1 axis alone lead to PDAC immune evasion. Accordingly, targeting only one co-inhibitory axis by antibody blocking is not effective in improving tumor elimination and thereby the clinical situation of PDAC patients, rather than combinational targeting approaches of different co-inhibitory receptors or ligands.

Our stroma-enriched 3D co-culture systems well reflect several conditions in PDAC and its liver metastases regarding PD-L1 expression in PDAC and stromal cells as well as TME composition regarding macrophages and the effector phenotype of CD8+ T cells. However, it cannot fully mimic the complete spatial composition and dynamic changes in PDAC TME, e.g. several other determinants of immune evasion were not considered, e.g., the presence of ECM or additional immunosuppressive stromal cells such as myofibroblasts. Furthermore, it has to be critically mentioned that we cannot provide any reliable information on whether and to which extent CD8+ T cells and macrophages infiltrate into PDAC spheroids and whether ICI treatment impacts on it. For obtaining clear information regarding the spatial distribution of immune and PDAC cells in our spheroids, studies are planned to generate FFPE sections from spheroids for immunohistochemical stainings as performed with patient derived tissues. Additionally, T cells and macrophages were isolated and generated from PBMCs of healthy donors, thus being from another donor as the used PDAC cell lines. Accordingly, well defined time periods of co-cultures of CD8+ T cells and mono- and co-culture spheroids had to be used in order to avoid allogeneic T cell reactions. Furthermore, PBMCs of healthy donors might exhibit a different composition and activation status compared to PBMCs of PDAC patients (60). To overcome these limitations and to validate the

findings obtained by this model system, future studies are planned to use PDAC cells and tumor associated macrophages from PDAC tissues as well as and PBMCs/CD8+ T cells from the same PDAC patient. However, here the challenge will be to obtain sufficient cell numbers of all cell populations analyzed. Furthermore, it would be interesting to analyze whether and how ICI treatment impacts polarization and effector phenotype of macrophages as well as plasticity of PDAC cells in order to get a comprehensive insight into ICI mediated effects on the entire TME. Finally, the results of the IHC stainings of matching primary tumors and liver metastases provided already valuable and unique insight into PD-L1 expression and the tumor stroma interplay during malignant progression of PDAC. Of note, metastases are not routinely resected and especially matched samples of primary tumors and metastases are very rare, so that this small collective has be considered very valuable but a validation of these findings with more matching tissue samples is certainly needed. Despite these limitations, our study revealed novel insights into the interplay of PDAC cells and macrophages in the presence of ICI treatment.

Conclusion

Our study revealed that PD-L1 expression in primary PDAC correlates with PD-L1 expression in liver metastases with macrophages being a main source of PD-L1 expression. These cells can be predominantly found at the invasion fronts in primary tumors as well as in liver metastases presenting a barrier for CD8+ T cells which were also mainly detectable at the invasive fronts. This *in situ* condition was well mimicked by a 3D co-culture spheroid model using two PDAC cell lines with different PD-L1 expression status as well as different ratios and types of macrophages. In line with the *in situ* findings, macrophages were the main source of PD-L1 expression, however, the effector phenotype of CD8+ T cells was not impaired which was not associated with PDAC cell death induction. Despite the considerable PD-L1 and PD-1 expression in the different spheroid models, treatment with PD-1 and PD-L1 inhibitors Pembrolizumab and Durvalumab, respectively, as well as pre-treatment with Gemcitabine did neither boost the CD8+ T cell effector phenotype nor increased PDAC cell death. Despite its limitations, our study is in line with the view that the PD-1/PD-L1 axis may not be the main immunosuppressive mechanism of T cell mediated tumor immunity in PDAC.

Data availability statement

The original contributions presented in the study are included in the article/Supplementary Material. Further inquiries can be directed to the corresponding author.

Ethics statement

The studies involving human participants were reviewed and approved by Ethics committee of the Medical Faculty of Kiel University, Schwanenweg 20, 24105 Kiel, Germany and the ethics committee of the Friedrich-Alexander Universität Erlangen-Nürnberg, Krankenhausstr. 12 91054 Erlangen, Germany. The patients/participants provided their written informed consent to participate in this study.

Author contributions

Conceptualization: TD, SB and SS; methodology: TD, SB, SR, SK and SH; resources: DW, CP, ME, AH, CR, HS, SS; writing—original draft preparation: TD, SB and SS; writing—review and editing: SR, SK, SH, HS, DW, CP, ME, AH, CR and AW; visualization: TD; funding acquisition: AMW, SS. All authors contributed to the article and approved the submitted version.

Funding

This work was supported by the Stiftung für Krebsentstehung und Immunologie (SS), the Deutsche Krebshilfe (AZ 70112935, SS) and the Deutsche Forschungsgemeinschaft (Projektnummer 413490537, AW). We acknowledge financial support by DFG within the funding program Open Access-Publikationskosten.

Acknowledgments

We thank Astra Zeneca for providing Durvalumab. The TriBanK (formerly BMB-CCC), providing clinical data and patient material, is a member of the PopGen 2.0 Biobanking Network (P2N) Kiel and was funded by the German Federal Ministry of Education and Research (BMBF grant 01EY1103). We also thank Sandra Ussat for excellent technical assistance.

Conflict of interest

The authors declare that the research was conducted in the absence of any commercial or financial relationships that could be construed as a potential conflict of interest.

Durvalumab was kindly provided by Astra Zeneca, which did play neither a role in the conceptualization and conduction of the study nor in the interpretation of the data.

Publisher's note

Supplementary material

The Supplementary Material for this article can be found online at: https://www.frontiersin.org/articles/10.3389/fimmu.2023.1157397/full#supplementary-material

References

1. Siegel RL, Miller KD, Fuchs HE, Jemal A. Cancer statistics, 2021. *CA Cancer J Clin* (2021) 71(1):7–33. doi: 10.3322/CAAC.21654

2. Pandey V, Storz P. Targeting the tumor microenvironment in pancreatic ductal adenocarcinoma. *Expert Rev Anticancer Ther* (2019) 19(6):473–82. doi: 10.1080/14737140.2019.1622417

3. Lankadasari MB, Mukhopadhyay P, Mohammed S, Harikumar KB. TAMing pancreatic cancer: combat with a double edged sword [Internet]. *Mol Cancer BioMed Cent Ltd* (2019) 18:1–13. doi: 10.1186/s12943-019-0966-6

4. Yang S, Liu Q, Liao Q. Tumor-associated macrophages in pancreatic ductal adenocarcinoma: origin, polarization, function, and reprogramming. *Front Cell Dev Biol* (2020) 8:607209. doi: 10.3389/FCELL.2020.607209

5. Liu Q, Li Y, Niu Z, Zong Y, Wang M, Yao L, et al. Atorvastatin (Lipitor) attenuates the effects of aspirin on pancreatic cancerogenesis and the chemotherapeutic efficacy of gemcitabine on pancreatic cancer by promoting M2 polarized tumor associated macrophages. *J Exp Clin Cancer Res* (2016) 35(1):1–16. doi: 10.1186/s13046-016-0304-4

6. Wandmacher AM, Mehdorn AS, Sebens S. The heterogeneity of the tumor microenvironment as essential determinant of development, progression and therapy response of pancreatic cancer. *Cancers (Basel)* (2021) 13(19):4932. doi: 10.3390/cancers13194932

7. Sica A, Schioppa T, Mantovani A, Allavena P. Tumour-associated macrophages are a distinct M2 polarised population promoting tumour progression: potential targets of anti-cancer therapy. *Eur J Cancer* (2006) 42(6):717–27. doi: 10.1016/J.EJCA.2006.01.003

8. Kurahara H, Shinchi H, Mataki Y, Maemura K, Noma H, Kubo F, et al. Significance of M2-polarized tumor-associated macrophage in pancreatic cancer. *J Surg Res* (2011) 167(2):e211–9. doi: 10.1016/J.JSS.2009.05.026

9. Kurahara H, Takao S, Maemura K, Mataki Y, Kuwahata T, Maeda K, et al. M2-polarized tumor-associated macrophage infiltration of regional lymph nodes is associated with nodal lymphangiogenesis and occult nodal involvement in pn0 pancreatic cancer. *Pancreas* (2013) 42(1):155–9. doi: 10.1097/MPA.0b013e318254f2d1

10. Helm O, Held-Feindt J, Grage-Griebenow E, Reiling N, Ungefroren H, Vogel I, et al. Tumor-associated macrophages exhibit pro- and anti-inflammatory properties by which they impact on pancreatic tumorigenesis. *Int J Cancer* (2014) 135(4):843–61. doi: 10.1002/IJC.28736

11. Poh AR, Ernst M. Tumor-associated macrophages in pancreatic ductal adenocarcinoma: therapeutic opportunities and clinical challenges. *Cancers (Basel)* (2021) 13(12):2860. doi: 10.3390/CANCERS13122860

12. Amarnath S, Mangus CW, Wang JCM, Wei F, He A, Kapoor V, et al. The PDL1-PD1 axis converts human Th1 cells into regulatory T cells. *Sci Transl Med* (2011) 3(111):111ra120. doi: 10.1126/SCITRANSLMED.3003130

13. Sun C, Mezzadra R, Schumacher TN. Regulation and function of the PD-L1 checkpoint. *Immunity* (2018) 48(3):434–52. doi: 10.1016/j.immuni.2018.03.014

14. Davis AA, Patel VG. The role of PD-L1 expression as a predictive biomarker: an analysis of all US food and drug administration (FDA) approvals of immune checkpoint inhibitors. *J Immunother cancer* (2019) 7(1). doi: 10.1186/S40425-019-0768-9

15. Nguyen CM, Jacob SE. Pembrolizumab. *J Dermatol Nurses Assoc* (2022) 9(2):95–7. doi: 10.1097/JDN.0000000000000264

16. Alvarez-Argote J, Dasanu CA. Durvalumab in cancer medicine: a comprehensive review. *Expert Opin Biol Ther* (2019) 19(9):927–35. doi: 10.1080/14712598.2019.1635115

17. Twomey JD, Zhang B. Cancer immunotherapy update: FDA-approved checkpoint inhibitors and companion diagnostics. *AAPS J* (2021) 23(2):1–11. doi: 10.1208/S12248-021-00574-0/FIGURES/2

18. O'Reilly EM, Oh DY, Dhani N, Renouf DJ, Lee MA, Sun W, et al. Durvalumab with or without tremelimumab for patients with metastatic pancreatic ductal adenocarcinoma. *JAMA Oncol* (2019) 5(10):1431. doi: 10.1001/jamaoncol.2019.1588

19. Brahmer JR, Tykodi SS, Chow LQM, Hwu WJ, Topalian SL, Hwu P, et al. Safety and activity of anti–PD-L1 antibody in patients with advanced cancer. *N Engl J Med* (2012) 366(26):2455–65. doi: 10.1056/NEJMoa1200694

20. Principe DR, Underwood PW, Kumar S, Timbers KE, Koch RM, Trevino JG, et al. Loss of SMAD4 is associated with poor tumor immunogenicity and reduced PD-L1 expression in pancreatic cancer. *Front Oncol* (2022) 12:806963/FULL. doi: 10.3389/FONC.2022.806963/FULL

21. Xia Q, Jia J, Hu C, Lu J, Li J, Xu H, et al. Tumor-associated macrophages promote PD-L1 expression in tumor cells by regulating PKM2 nuclear translocation in pancreatic ductal adenocarcinoma. *Oncogene* (2022) 41(6):865. doi: 10.1038/S41388-021-02133-5

22. Wang X, Li X, Wei X, Jiang H, Lan C, Yang S, et al. PD-L1 is a direct target of cancer-FOXP3 in pancreatic ductal adenocarcinoma (PDAC), and combined immunotherapy with antibodies against PD-L1 and CCL5 is effective in the treatment of PDAC. *Signal Transduct Target Ther* (2020) 5(1). doi: 10.1038/S41392-020-0144-8

23. Rahn S, Krüger S, Röcken C, Helm O, Sebens S. Response to: "Patterns of PD-L1 expression and CD8 T cell infiltration in gastric adenocarcinomas and associated immune stroma.". *Gut* (2019) 68(1):179–80. doi: 10.1136/gutjnl-2017-315843

24. Rahn S, Krüger S, Mennrich R, Goebel L, Wesch D, Oberg HH, et al. POLE score: a comprehensive profiling of programmed death 1 ligand 1 expression in pancreatic ductal adenocarcinoma. *Oncotarget* (2019) 10(16):1572–88. doi: 10.18632/oncotarget.26705

25. Banfalvi G. Cell cycle synchronization of animal cells and nuclei by centrifugal elutriation. *Nat Protoc* (2008) 3(4):663–73. doi: 10.1038/NPROT.2008.34

26. Walter F, Winter E, Rahn S, Heidland J, Meier S, Struzek AM, et al. Chitosan nanoparticles as antigen vehicles to induce effective tumor specific T cell responses. *PloS One* (2020) 15(9). doi: 10.1371/JOURNAL.PONE.0239369

27. Verreck FAW, de Boer T, Langenberg DML, Hoeve MA, Kramer M, Vaisberg E, et al. Human IL-23-producing type 1 macrophages promote but IL-10-producing type 2 macrophages subvert immunity to (myco)bacteria. *Proc Natl Acad Sci* (2004) 101(13):4560–5. doi: 10.1073/pnas.0400983101

28. Krausgruber T, Blazek K, Smallie T, Alzabin S, Lockstone H, Sahgal N, et al. IRF5 promotes inflammatory macrophage polarization and TH1-TH17 responses. *Nat Immunol 2011 123.* (2011) 12(3):231–8. doi: 10.1038/ni.1990

29. Moore PS, Sipos B, Orlandini S, Sorio C, Real FX, Lemoine NR, et al. Genetic profile of 22 pancreatic carcinoma cell lines: analysis of K-ras, p53, p16 and DPC4/Smad4. *Virchows Arch* (2001) 439(6):798–802. doi: 10.1007/s004280100474

30. Sipos B, Möser S, Kalthoff H, Török V, Löhr M, Klöppel G. A comprehensive characterization of pancreatic ductal carcinoma cell lines: towards the establishment of an *in vitro* research platform. *Virchows Arch* (2003) 442(5):444–52. doi: 10.1007/s00428-003-0784-4

31. Heckl SM, Mau F, Senftleben A, Daunke T, Beckinger S, Abdullazade S, et al. Medical sciences programmed death-ligand 1 (PD-L1) expression is induced by insulin in pancreatic ductal adenocarcinoma cells pointing to its role in immune checkpoint control. *Med Sci* (2021) 2021:48. doi: 10.3390/medsci9030048

32. Zuo C, Baer JM, Knolhoff BL, Belle JI, Liu X, Alarcon De La Lastra A, et al. Stromal and therapy-induced macrophage proliferation promotes PDAC progression and susceptibility to innate immunotherapy. *J Exp Med* (2023) 220(6):e20212062. doi: 10.1084/jem.20212062

33. Atanasov G, Pötner C, Aust G, Schierle K, Dietel C, Benzing C, et al. TIE2-expressing monocytes and M2-polarized macrophages impact survival and correlate with angiogenesis in adenocarcinoma of the pancreas. *Oncotarget* (2018) 9(51):29715–26. doi: 10.18632/ONCOTARGET.25690

34. Horwood NJ. Macrophage polarization and bone formation: a review. *Clin Rev Allergy Immunol* (2016) 51(1):79–86. doi: 10.1007/s12016-015-8519-2

35. Locati M, Curtale G, Mantovani A. Diversity, mechanisms and significance of macrophage plasticity. *Annu Rev Pathol* (2020) 15:123. doi: 10.1146/ANNUREV-PATHMECHDIS-012418-012718

36. Wherry EJ. T Cell exhaustion. *Nat Immunol* (2011) 12(6):492–9. doi: 10.1038/ni.2035

37. Saleh R, Taha RZ, Toor SM, Sasidharan Nair V, Murshed K, Khawar M, et al. Expression of immune checkpoints and T cell exhaustion markers in early and advanced stages of colorectal cancer. *Cancer Immunol Immunother* (2020) 69(10):1989–99. doi: 10.1007/S00262-020-02593-W/FIGURES/4

38. Yi JS, Cox MA, Zajac AJ. T-Cell exhaustion: characteristics, causes and conversion. *Immunology* (2010) 129(4):474. doi: 10.1111/J.1365-2567.2010.03255.X

39. Szlasa W, Janicka N, Sauer N, Michel O, Nowak B, Saczko J, et al. Chemotherapy and physical therapeutics modulate antigens on cancer cells. *Front Immunol* (2022) 13:889950. doi: 10.3389/FIMMU.2022.889950

40. Zheng X, Kuai J, Shen G. Low-dose metronomic gemcitabine pretreatments overcome the resistance of breast cancer to immune checkpoint therapy. *Immunotherapy* (2023). 15(6):429–42 doi: 10.2217/IMT-2022-0254

41. Hidalgo M. Pancreatic cancer. *N Engl J Med* (2010) 362(17):1605–17. doi: 10.1056/NEJMra0901557

42. Yachida S, White CM, Naito Y, Zhong Y, Brosnan JA, Macgregor-Das AM, et al. Clinical significance of the genetic landscape of pancreatic cancer and implications for identification of potential long-term survivors. *Clin Cancer Res* (2012) 18(22):6339–47. doi: 10.1158/1078-0432.CCR-12-1215/273485/AM/CLINICAL-SIGNIFICANCE-OF-THE-GENETIC-LANDSCAPE-OF

43. McGuigan A, Kelly P, Turkington RC, Jones C, Coleman HG, McCain RS. Pancreatic cancer: a review of clinical diagnosis, epidemiology, treatment and outcomes. *World J Gastroenterol* (2018) 24(43):4846. doi: 10.3748/WJG.V24.I43.4846

44. Vansteenkiste J, Wauters E, Reymen B, Ackermann CJ, Peters S, De Ruysscher D. Current status of immune checkpoint inhibition in early-stage NSCLC. *Ann Oncol Off J Eur Soc Med Oncol* (2019) 30(8):1244–53. doi: 10.1093/ANNONC/MDZ175

45. Helm O, Mennrich R, Petrick D, Goebel L, Freitag-wolf S, Ro C, et al. Comparative characterization of stroma cells and ductal epithelium in chronic pancreatitis and pancreatic ductal adenocarcinoma. *Pancreatology* (2014) 9(5):e94357. doi: 10.1371/journal.pone.0094357

46. Nielsen SR, Quaranta V, Linford A, Emeagi P, Rainer C, Santos A, et al. Macrophage-secreted granulin supports pancreatic cancer metastasis by inducing liver fibrosis. *Nat Cell Biol* (2016) 18(5):549–60. doi: 10.1038/ncb3340

47. Pu Y, Ji Q. Tumor-associated macrophages regulate PD-1/PD-L1 immunosuppression. *Front Immunol* (2022) 13:2004. doi: 10.3389/fimmu.2022.874589

48. Gulhati P, Schalck A, Jiang S, Shang X, Wu CJ, Hou P, et al. Targeting T cell checkpoints 41BB and LAG3 and myeloid cell CXCR1/CXCR2 results in antitumor immunity and durable response in pancreatic cancer. *Nat Cancer* (2022). doi: 10.1038/s43018-022-00500-z

49. Masugi Y, Abe T, Ueno A, Fujii-Nishimura Y, Ojima H, Endo Y, et al. Characterization of spatial distribution of tumor-infiltrating CD8+ T cells refines their prognostic utility for pancreatic cancer survival. *Mod Pathol* (2019) 32(10):1495–507. doi: 10.1038/s41379-019-0291-z

50. Kiryu S, Ito Z, Suka M, Bito T, Kan S, Uchiyama K, et al. Prognostic value of immune factors in the tumor microenvironment of patients with pancreatic ductal adenocarcinoma. *BMC Cancer* (2021) 21(1):1–13. doi: 10.1186/S12885-021-08911-4/FIGURES/5

51. Zhu Y, Knolhoff BL, Meyer MA, Nywening TM, West BL, Luo J, et al. CSF1/CSF1R blockade reprograms tumor-infiltrating macrophages and improves response to T cell checkpoint immunotherapy in pancreatic cancer models. *Cancer Res* (2014) 74 (18):5057. doi: 10.1158/0008-5472.CAN-13-3723

52. Jones KI, Tiersma J, Yuzhalin AE, Gordon-Weeks AN, Buzzelli J, Im JH, et al. Radiation combined with macrophage depletion promotes adaptive immunity and potentiates checkpoint blockade. *EMBO Mol Med* (2018) 10(12):1–16. doi: 10.15252/emmm.201809342

53. Hussain SM, Kansal RG, Alvarez MA, Hollingsworth TJ, Elahi A, Miranda-Carboni G, et al. Role of TGF-β in pancreatic ductal adenocarcinoma progression and PD-L1 expression. *Cell Oncol* (2021) 44(3):673–87. doi: 10.1007/S13402-021-00594-0/FIGURES/7

54. Ning B, Liu Y, Wang M, Li Y, Xu T, Wei Y. The predictive value of tumor mutation burden on clinical efficacy of immune checkpoint inhibitors in melanoma: a systematic review and meta-analysis. *Front Pharmacol* (2022) 13:748674/FULL. doi: 10.3389/FPHAR.2022.748674/FULL

55. Lawlor RT, Mattiolo P, Mafficini A, Hong SM, Piredda ML, Taormina SV, et al. Tumor mutational burden as a potential biomarker for immunotherapy in pancreatic cancer: systematic review and still-open questions. *Cancers (Basel)* (2021) 13(13):3119. doi: 10.3390/CANCERS13133119/S1

56. Del Re M, Vivaldi C, Rofi E, Salani F, Crucitta S, Catanese S, et al. Gemcitabine plus nab-paclitaxel induces PD-L1 mRNA expression in plasma-derived microvesicles in pancreatic cancer. *Cancers (Basel)* (2021) 13(15):3738. doi: 10.3390/CANCERS13153738

57. Du B, Wen X, Wang Y, Lin M, Lai J. Gemcitabine and checkpoint blockade exhibit synergistic anti-tumor effects in a model of murine lung carcinoma. *Int Immunopharmacol* (2020) 86(April):106694. doi: 10.1016/j.intimp.2020.106694

58. Ho TTB, Nasti A, Seki A, Komura T, Inui H, Kozaka T, et al. Combination of gemcitabine and anti-PD-1 antibody enhances the anticancer effect of M1 macrophages and the Th1 response in a murine model of pancreatic cancer liver metastasis. *J Immunother Cancer* (2020) 8(2):1–12. doi: 10.1136/jitc-2020-001367

59. Ge Z, Peppelenbosch MP, Sprengers D, Kwekkeboom J. TIGIT, the next step towards successful combination immune checkpoint therapy in cancer. *Front Immunol* (2021) 12:699895. doi: 10.3389/FIMMU.2021.699895

60. Steele NG, Carpenter ES, Kemp SB, Sirihorachai VR, The S, Delrosario L, et al. Multimodal mapping of the tumor and peripheral blood immune landscape in human pancreatic cancer. *Nat cancer* (2020) 1(11):1097. doi: 10.1038/S43018-020-00121-4

61. Pearce H, Croft W, Nicol SM, Margielewska-Davies S, Powell R, Cornall R, et al. Tissue-resident memory T cells in pancreatic ductal adenocarcinoma co-express PD-1 and TIGIT and functional inhibition is reversible by dual antibody blockade. *Cancer Immunol Res* (2023). doi: 10.1158/2326-6066.CIR-22-0121

62. Freed-Pastor WA, Lambert LJ, Ely ZA, Pattada NB, Bhutkar A, Eng G, et al. The CD155/TIGIT axis promotes and maintains immune evasion in neoantigen-expressing pancreatic cancer. *Cancer Cell* (2021) 39(10):1342–60.e14. doi: 10.1016/j.ccell.2021.07.007